Lime-based construction materials: effect of novel additives on physical and chemical properties

Westgate, Paul

Award date:
2020

Awarding institution:
University of Bath

Lime-based construction materials: effect of novel additives on physical and chemical properties

Paul Westgate

A thesis submitted for the degree of Doctor of Philosophy

University of Bath
Faculty of Engineering and Design
Department of Architecture and Civil Engineering

August 2019

ACKNOWLEDGEMENTS

The work in this thesis was carried out in the Department of Architecture and Civil Engineering at the University of Bath between August 2013 and July 2019.

Firstly, I would like to thank Dr R J Ball and Dr K Paine for their continued guidance and support throughout this work. I would also like to thank the staff in the Microscopy and Spectroscopy Suite for their helpful advice. Thanks also go to Singleton Birch and 2DTech for help with advice and materials.

Finally, I would like to thank my children Jacqueline, Sammy and Bradley for keeping me going through the difficult times.

ABSTRACT

A lower environmental impact and the realisation that modern cementitious materials are incompatible with older buildings has led to a revival in the use of lime over the last 40 years, for both conservation and new build.

This research investigated the use of novel additive materials that have the potential to improve the physical properties of lime based construction materials, reduce their environmental impact and promote their use.

Five experimental lime based mixes were prepared: an insulating lime plaster incorporating aerogel granules and polypropylene monofilament fibres, mortar containing olivine sand aggregate, 'hot lime' mortars with slate and granite aggregate, lime putty and sand mortar with nanosilica and nanolime with graphene oxide. Physical and chemical properties of the mixes containing novel additives were compared with lime containing standard sand as a reference.

The insulating plaster achieved thermal conductivity approximately 75% lower than gypsum plasters, and the addition of fibres imparted a high degree of flexibility. The use of olivine aggregate increased the level of carbonation by 10.4%, which also had the effect of increasing compressive strength. The investigation of 'hot lime' mixes did not discover any significant difference compared with lime putty binder, but the use of slate and granite aggregate was found to improve the interconnectedness of the pore structure and increase 91 day compressive strength by 45.7%. compared with silica sand. The addition of nanosilica to the lime putty and sand mortar had the unexpected effect of significantly reducing compressive strength. The effect of graphene oxide appeared to have a positive effect on early carbonation but the evidence was inconclusive.

This work has demonstrated there is significant potential for improving the properties of lime-based construction materials and to reduce the environmental impact associated with their use; however, there is still much further research that should be carried out.

DISSEMINATION

Elements of this thesis have been published in the following peer-reviewed journals:

Westgate, P., Paine, K., Ball, R.J., 2018. Physical and mechanical properties of plasters incorporating aerogel granules and polypropylene monofilament fibres. *Construction and Building Materials,* 158(2018), pp.472-480

Westgate, P., Paine, K., Ball, R.J., 2019. Olivine as a reactive aggregate in lime mortars. *Construction and Building Materials,* 1095(2019), pp.115-126

Fasihnikoutalab, M.H., Westgate, P, Huat, B.B.K., Asadi, A., Ball, R.J., Nahazanan, H., Singh, P., 2015. New Insights into Potential Capacity of Olivine in Ground Improvement, *Electronic Journal of Geotechnical Engineering,* 20(2015), pp.2137-2148

Fasihnikoutalab, M.H., Asadi, A., Huat, B.K., Westgate, P., Ball, R.J., Pourakbar, S., 2016. Laboratory-scale model of carbon dioxide deposition for soil stabilisation. Journal of Rock Mechanics and Geotechnical Engineering, 8(2016), pp.178-186

Contents

LIST OF FIGURES

CHAPTER 2

CHAPTER 3

CHAPTER 4

CHAPTER 5

CHAPTER 6

CHAPTER 7

CHAPTER 8

LIST OF TABLES

CHAPTER 2

CHAPTER 3

CHAPTER 4

CHAPTER 5

CHAPTER 6

LIST OF ABBREVIATIONS

$CaCO_3$	Calcium carbonate
CaO	Calcium oxide
$CaMg(CO_3)_2$	Dolomite
$Ca(OH)_2$	Calcium hydroxide
CO_2	Carbon dioxide
C-S-H	Calcium silicate hydrate
GO	Graphene oxide
$MgCO_3$	Magnesium carbonate
OPC	Ordinary Portland cement
$(Mg,Fe)_2SiO_4$	Olivine
Fe_2SiO_4	Fayalite
Mg_2SiO_4	Forsterite
rGO	Reduced graphene oxide
SiO_2	Silica

CHAPTER 1 INTRODUCTION

Lime is an important material in construction and civil engineering. Knowledge relating to the use and application of lime-based construction materials is important for conservation work and the maintenance and repair of older residential property. In recent years, there has also been a resurgence in the use of lime for new build construction due to its reputation as an environmentally friendly material, especially in comparison with cement, its main rival.

The use of lime does, as with all materials, have its limitations and disadvantages. Throughout the history of construction, a variety of different additives has been used to help control and enhance the physical properties of lime-based construction materials. Materials such as animal hair, straw, brick dust and volcanic ash have all been utilised to improve the adhesion, strength or durability of lime-based mortars, plasters and renders. Modern construction faces new challenges, however. Carbon dioxide emissions, efficient use of resources and pollution are now high on the list of concerns, and both political and legal pressure has been brought to bear on the construction industry to address these issues. One way in which these stricter criteria will be met is through the development and use of new and innovative construction materials.

The importance of addressing the environmental impact of construction related activities cannot be underestimated. There has been a significant amount of research carried out into improving the energy efficiency of cement usage; however, there is comparatively little similar new research into lime-based materials. This work will seek to contribute new knowledge relating to the use of lime in construction and particularly how the properties of this traditional material might be enhanced through the development of previously untested composite mixes.

This research investigates five different novel additive materials that have the potential to enhance the physical properties of lime-based construction materials and lower their environmental impact. Each of the five materials being investigated here takes fundamentally different approaches. The first material, aerogel, is a modern, man-made material that has unique insulating properties with the potential to reduce energy consumption in buildings. The second material, by contrast, is a naturally

occurring mineral: olivine. This material is of great interest due to its potential to sequester atmospheric carbon dioxide. The third area of research is graphene oxide. This is a nanomaterial, which has been shown to confer significant strength increases in cementitious materials, potentially reducing material consumption, but its use has not been extensively investigated in conjunction with lime. Lastly, the effects of using different recycled aggregates with hot lime are investigated with the objective of assessing the potential to reduce material wastage.

As the literature review will explain in detail, there exists different forms of lime as used in construction. This work has been predominantly carried out using non-hydraulic lime putty. This is considered the most appropriate form for this research due its properties of permeability, low compressive strength and long storage life. In the 'Hot Lime Mortars' chapter', quicklime (CaO) is investigated. This is mixed with water and sand at the point of use to produce a non-hydraulic lime and is used in this section of the work to compare its properties with lime putty. This area of research was suggested as a subject of interest by Historic England. Also, in the 'Lime and Nanosilica' chapter, a natural hydraulic lime (NHL2) was introduced as a comparison material.

1.1 Aims and objectives

This work aims to investigate the potential of novel additive materials to improve the physical and chemical properties of lime-based construction materials. The overarching aim is to assess whether enhancing the properties of these materials, through the incorporation of novel additive materials, could potentially be utilised as a means of improving the thermal efficiency of buildings, reducing the carbon footprint of construction materials or reduce wastage or materials.

The specific objectives of this research are:

- To investigate the physical and chemical properties of different experimental lime/additive mixes through a schedule of tests to examine strength, water vapour permeability, thermal conductivity and resistance to shrinkage and cracking.

- To investigate, using thermodynamic modelling, the extent to which the various mixes will form carbonate phases and consume atmospheric CO_2.
- To investigate the potential for aerogel particles to be incorporated into lime binders for the purpose of reducing thermal conductivity of plasters and renders.
- To investigate the interaction between polypropylene fibres and lime binders and the influence of interfacial properties on strength.
- To investigate the potential for using slate and granite as aggregate materials with hot lime mortars.

1.2 Structure of this thesis

The first chapter introduces the report and outlines the focus of the research and the reasons that it was undertaken. The main part of the thesis starts in Chapter two with a review of the relevant literature relating to the production, use, properties and pathology of lime-based construction materials and additives. The third chapter provides details of the experimental methods that have been used during the course of this research and the reason for their use. The fourth, fifth, sixth, seventh and eighth chapters detail the experimental work carried out, with each chapter covering a specific area of research. Because each area of research deals with fundamentally different materials, the details of these materials have been included in the relevant chapter rather than together in a materials chapter. In Chapter nine, a general overview of the work is given with comments on the findings with explanations about the limitations of the research. In Chapter ten general conclusions are drawn and Chapter eleven provides general comments on further work. Copies of academic papers published during the course of this work are included in the Appendices at the end of the thesis.

CHAPTER 2 LITERATURE REVIEW

2.1 History of lime as a construction material

The use of lime as a construction material, as used in mortar, plaster and render, dates back thousands of years. Lime was used extensively by the Romans in the construction of buildings over two thousand years ago, and some examples, such as the Pantheon, are still standing today. The earliest use of lime probably goes back much further even than this; in Israel, evidence has been discovered of a possible lime kiln dating from 10,400-10,000 BC (Carran et al., 2011, pp.117-118).

For several hundred years leading up to the industrial revolution, builders would obtain lime for construction work in the form of quicklime (calcium oxide) to be slaked either at the building yard or on site as required. It would either be mixed with sand and water to form a 'hot mix' mortar or slaked with an excess of water to form a lime putty for use later after it had been aged for several months. Use of these materials was associated with frequent quality problems. The high cost of fuel for lime burning lead to economising, which often resulted in limes that were underburnt. It was common practice to screen slaked lime for unburnt lumps, but the proportion of unburnt lime could be so high as to make the lime unusable. Further problems arose during transportation. Transporting lime from kiln to site as quicklime was seen as a way of reducing costs, as lime in this form was significantly lower in weight than lime putty. However, this often resulted in lime that was partially carbonated due to air slaking (Brocklebank, 2012b, pp.1-18).

John Smeaton significantly advanced the knowledge of lime mortars 1756 when he carried out experimental work with hydraulic lime. Just prior to this work, Smeaton had been on a study tour of the low countries where he studied the design of water engineering, drainage and canal structures. During this tour he discovered the use of trass-based mortars for hydraulic engineering works. The knowledge he gained served as a reference for his future work in the design of harbours, bridges, and canals. Smeaton had some reservations about the use of trass, so he imported material from Pozzuoli in Italy, which he considered to have more long-term predictable behaviour. He then carried out a series of laboratory trials with numerous domestically available

limes, establishing the impact of the proportion of clay in the parent material (Brocklebank, 2012a, pp.73-104).

Lime technology was further advanced by the French engineer Louis Vicat. He studied lime for over thirty years and carried out a comprehensive study of hydraulic limes from around France. In 1818, Vicat established beyond doubt that 'the seizing of hydraulic mortars and their hardening were determined by the combination of lime with silica'. It was Vicat who developed the classification system for lime. Depending on the amount of clay present, the lime was classified as either feebly, moderately or eminently hydraulic. During his investigations, he prepared an artificial hydraulic lime by calcining chalk limestone, and clay ground together in a wet mill. This was considered the forerunner of Portland cement (Bergoin, 2012, pp.33-52).

Information relating to the historic use of these lime-based construction materials is often contradictory. Brocklebank (2012c, pp.21-31) states that a CaO to SiO_2 ratio of 1:3 would normally be used for a base coat of lime plaster and a ratio of 1:2 for a finish coat. Artis (2012, pp.144-154), however, recommends a ratio of 1:2 for base coats and 1:2.5-3 for finishes. Artis also makes no allowance for the form of lime being used, despite acknowledging that calcium hydroxide tends to be used in either 'powder or putty form'. Gibbons (1997), when recommending appropriate mix ratios, does identify the need to differentiate between lime powder and lime putty, however, equating one part lime powder to two parts lime putty.

The way in which lime materials are prepared for use has changed over the years, and this fact is often overlooked. The common use of a 1:3 mix, whilst correctly based on the requirement to fill the voids between aggregate particles with binder, fails to take into account the type of lime being used. The skilled tradesmen of the past would mix up mortar in a typical ratio of 1:3; however, the lime they used would have most likely have been quicklime (calcium oxide) and not slaked lime (calcium hydroxide). As quicklime increases in volume after slaking, a set mortar will have a more lime-rich composition than the original specified ratio. Analysis of historic lime mortars has revealed that the typical ratio in finished mixes in fact varies between 1:1.5 and 1:2 (Lynch, 2012, pp.221-228).

Use of lime as a construction material began to fall into decline with the introduction of Portland cement in 1845. The fast setting time and high strength of Portland cement

were seen as significant advantages over lime, particularly in speeding up construction times. These advantages over lime became particularly important when rapid construction was needed after the large-scale destruction of buildings suffered during the Second World War (Brocklebank 2012c, pp.1-18).

In recent years, the use of lime in construction has undergone a revival. In the 1970s it started to become apparent that the use of cementitious construction materials was causing damage to older buildings. This discovery has led to the increased use and interest in lime, not only for conservation work, but for new-build applications also (Building Limes Forum, 2014). Despite the obvious advantages of using cement, it became apparent that in many cases the use of cementitious materials in traditionally built mass masonry structures can create latent defects (Forster and Carter, 2011, p.374). Cement mortar has lower permeability than lime mortar, which can result in moisture entrapment within building structures. The more porous nature of lime mortar, by contrast, facilitates moisture evaporation from masonry, a process often referred to as 'breathability'. Also, cement is a much stronger binder than lime. Excessive strength in mortars results in a building that is inflexible and unable to accommodate building movement, a situation that can result in fracturing of the softer and more porous masonry materials found in older buildings.

In recent years the construction industry has undergone significant change and development. Widespread criticism of its poor performance has prompted the UK government to embark on a series of initiatives to encourage 'new ways of working and thinking'. Offsite production has been cited by large construction companies as 'the future of the UK construction industry', due to its environmental performance, reduced dependence on skilled labour and predictability of delivery timescales (Nadim& Goulding, 2010, pp.181-202). Notwithstanding the potential benefits of offsite production, there remains concerns and uncertainties.

2.2 Lime and the environment

The construction industry has an unavoidably significant impact on the environment. In the UK, the construction industry annually consumes 170 million tonnes of primary materials and products, 125 million tonnes of quarry products and 70 million tonnes of

secondary recycled and reclaimed products (Holmes, 2019). This consumption is of great concern in relation to global warming and consumption of natural resources.

The problem of high consumption of resources by construction activities is compounded by high levels of waste. In the UK approximately 13% of material delivered to a construction site goes in the skip without being used. Of the 400 million tonnes of waste produced in the UK each year 72 million tonnes comes from the construction industry (Bradley, 2019). This makes construction one of the highest waste generating industries, being responsible for 32% of landfill waste and a further 29% of landfill waste is generated by mining and quarrying (Network Waste, 2019). Of specific relevance to this research is the high level of waste generated from mineral sources (Figure 2.1). Lime mortar is less wasteful of resources because masonry items can be recycled due to the lower binding strength of lime mortars (Ibstock, 2005).

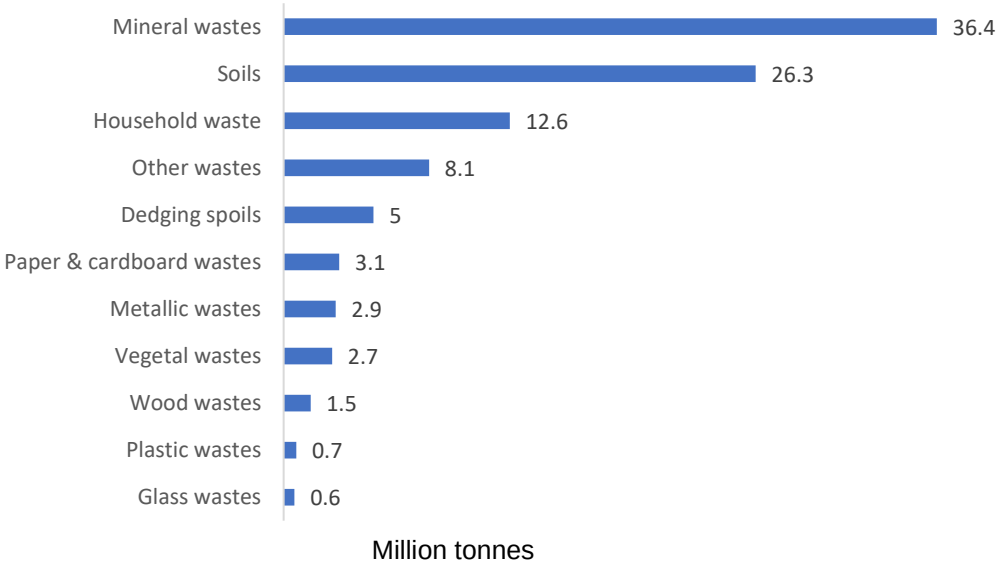

Figure 2.1: Waste generation in the UK by waste material (Defra Statistics, 2016).

Global warming also continues to be one of the most challenging environmental problems we face today. Despite greenhouse gas emissions in the UK falling significantly since 1990 (Figure 2.2), there is still significant pressure to reduce emissions further. The government announced this year that the UK will commit to reaching a legally binding net zero target by 2050. In the UK, the government is putting special emphasis on retrofitting and refurbishment of the existing housing stock in an effort to tackle this problem, as this offers the greatest potential for CO_2 reduction in the short to medium term. This will be an enormous challenge, with approximately 25 million homes requiring upgrading by the end of 2050 if carbon reduction targets are to be met (Edwards, J & Townsend, A., 2011).

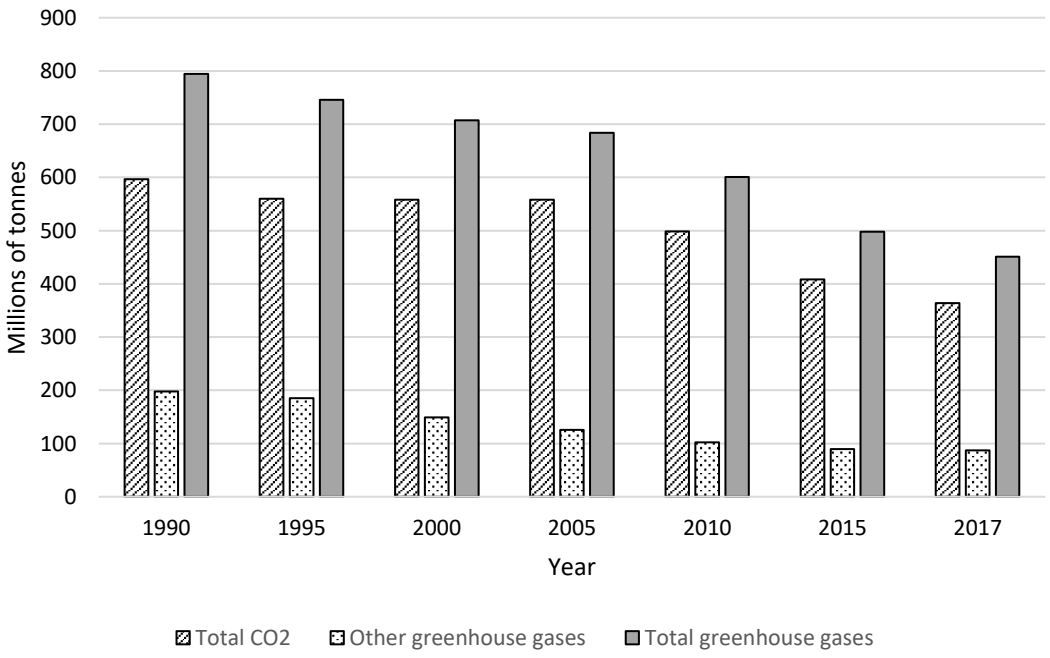

Figure 2.2: UK Greenhouse Gas Emissions
(Department for Business, Energy & Industrial Strategy, 2019).

A significant factor in the resurgence of lime-based materials in construction is that they are considered more environmentally friendly than alternative cementitious materials, their main competition. The production of lime and cement for construction materials consumes vast amounts of fuel, adding significantly to CO_2 emissions. Lime requires a firing temperature of around 900-1100ºC to produce, whereas cement requires temperatures in the range 1200-1500ºC. Additionally, lime construction materials will reabsorb CO_2 throughout the setting process, as the calcium hydroxide reacts with water and atmospheric CO_2 to form $CaCO_3$, further reducing their environmental impact (Pritchett, 2003, p.84).

The cement industry is making concerted efforts to reduce its CO_2 emissions. Strategies such as employing more efficient processes, reducing heat loss during pyro-processing and recovering energy from exhaust streams are all being investigated. Whilst it has been recognised that these strategic processes have potential to reduce CO_2 emissions, 'technical, economic and legal challenges still play as remarkable obstacles against widespread implementation of such approaches' (Benhelal et al., 2013, pp.142-161). The lime industry is also implementing measures to reduce CO_2 emissions. Large-scale investment has been made into new technologies such as switching from horizontal to vertical kilns to increase fuel efficiency and installing heat exchangers to recover some of the heat from flue gases. A range of other measures are also being considered such as 'efficient kiln insulation, optimised combustion processes, improved process and input control, optimal change-over and further improved maintenance procedures (Stork et al., 2014).

It is not possible to calculate extremely precise values for the embodied carbon for a general category of construction material. Materials vary in form and type; however, published figures are considered to be a good benchmark for calculating the lifecycle performance of construction materials. Values published by Hammond & Jones (2008, pp.87-98) show that the embodied carbon of a mortar mix decreases with increasing lime content (Table 2.1).

Table 2.1: Embodied energy and carbon of mortars containing cement and lime.

Mortar mix cement:lime:sand	Binder/Aggregate ratio	% Lime content	Embodied energy (Mj/kg)	Embodied carbon (kgC/kg)
1:0:3	1:3	0	1.5	0.058
1:1:6	1:3	12.5	1.18	0.044
1:2:9	1:3	16.7	1.09	0.039

To fully assess the CO_2 emissions associated with a building, additional factors must be taken into consideration other than just the materials used. Construction methods, operational use, maintenance cycles and building service life all have a bearing on the carbon footprint of a building over its operational life. It is possible in certain applications that the use of cementitious materials might have a higher initial impact but 'result in a much lower impact across the building service life' (Bras & Faria, 2017, pp.523-528).

2.3 Types of lime materials used in construction

Cement and lime construction materials are often treated as completely different materials. 'In reality, however, pure lime and modern Portland cement lie at the two extremes of a broad spectrum of materials (Table 2.2) with essentially allied characteristics' (Brocklebank, 2012c, pp.21-31). Although cement is often considered a completely different material than lime, it is also comprised largely of CaO. The main distinction between the different lime-based materials can be made with respect to their chemical composition and physical properties.

Table 2.2: Overview of physical properties of lime-based construction materials.

	← Porosity Strength →					
Type of lime	**Non-hydraulic lime**	**NHL 2**	**NHL 3.5**	**NHL 5**	**Natural cement**	**Cement**

2.3.1 Non-hydraulic lime

Non-hydraulic lime is produced from the purest limestone. Since it requires the presence of carbon dioxide to set, or 'carbonate', it is often referred to as 'air lime'. Due to this requirement for carbon dioxide, non-hydraulic lime will not set under water, unlike the hydraulic category of limes. The extraction, processing and end use of lime as a construction material can be described by the well-known 'lime cycle' (Figure 2.3).

In the first stage of this process, limestone is extracted from lime quarries. In the case of non-hydraulic lime, the limestone should have a calcium carbonate ($CaCO_3$) content of 95% or higher. The calcium carbonate is then burnt in kilns at a temperature of around 900ºC. This burning process, also known as 'calcining', causes CO_2 to be driven off in a thermal decomposition reaction, leaving calcium oxide (CaO) – commonly known as quicklime. Water is then added to the quicklime to produce 'slaked lime'. This is a highly exothermic process, during which a considerable quantity of heat is generated. The result of this hydration process is the more stable calcium hydroxide ($Ca(OH)_2$).

$Ca(OH)_2$ can be produced in two basic forms: hydrated lime and lime putty. Hydrated lime is produced by adding a controlled quantity of water to the CaO; just sufficient to produce a powder that is stable. Lime putty, by contrast, is produced by adding an excess of water. This results in a plastic putty material that is then stored under water in order to prevent carbonation prior to use. Lime putty can then be mixed with aggregate to form a mortar or plaster without the need to add additional water, whereas hydrated lime powder must be mixed with water and aggregate to form a workable mortar.

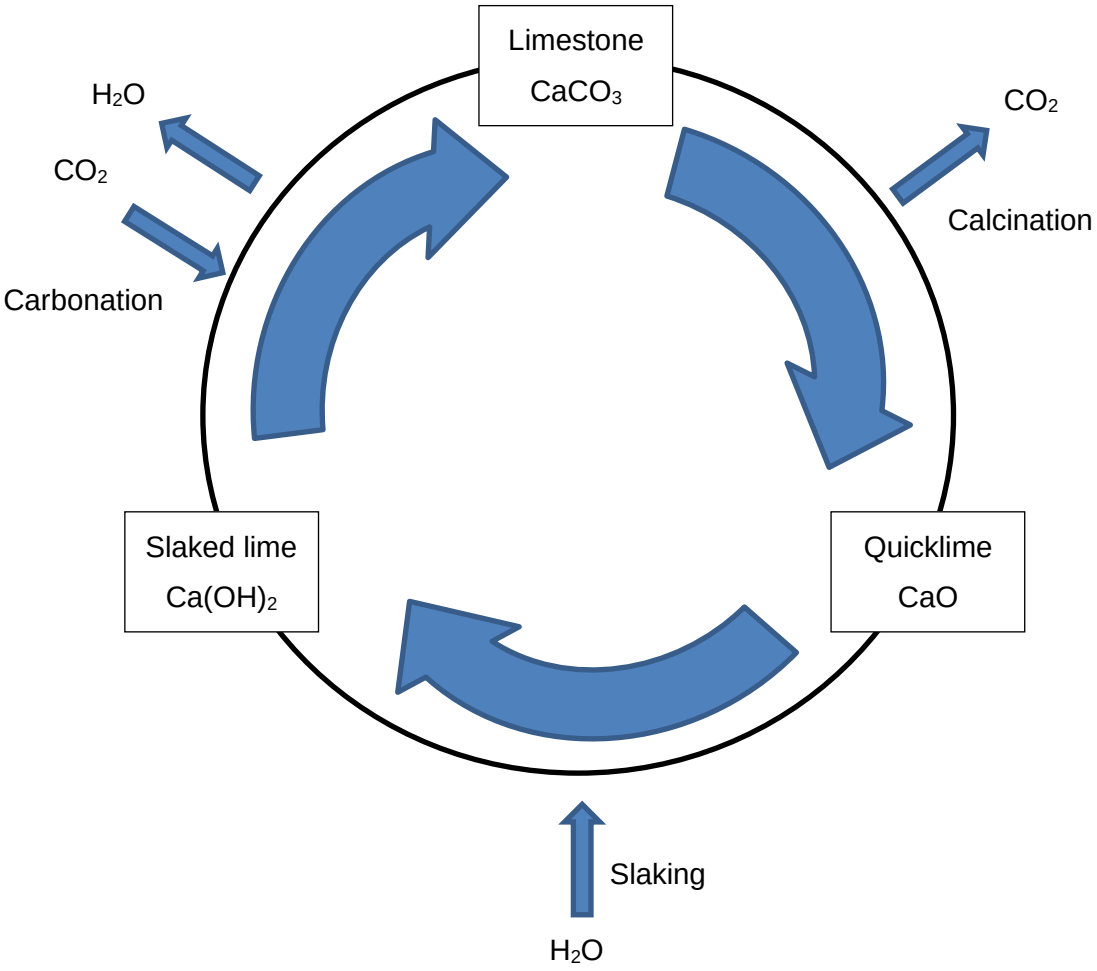

Figure 2.3: The Lime Cycle.

Prior to the introduction of hydraulic cements, non-hydraulic lime putty was routinely used as the binder material for mortars, plasters and renders in building construction and has proved to be durable over many centuries (Ingham, 2012, pp.155-173). It has a significantly lower environmental impact than that of the more commonly used Portland cement due to the lower kiln temperatures required during production and hence lower CO_2 output. Portland cement is produced in kilns operating at a temperature of approximately 1450˚C (Karstensen, 2008), whereas lime kilns operate at approximately 1,000˚C (BLA, 2019). But the case for lime as a low carbon material

is strengthened further by the fact that it actually reabsorbs CO_2 whilst setting; a non-hydraulic lime putty can absorb nearly its own weight in CO_2 (Greenspec, 2017).

A further advantage of non-hydraulic lime is its long shelf life. It is common for manufacturers to recommend that, once opened, bags of hydrated lime are used within a specified time or discarded. In practice, practitioners may keep lime from a few days to one year depending on the storage conditions and risk of excessive hydration and carbonation within the bag. Non-hydraulic lime putty, however, can be stored for significantly longer due to the effectiveness of the milk-of-lime layer on the surface of the putty at preventing carbonation. The carbonation rate and plasticity of lime putty have been found to be still improving after storage periods in excess of five years (Margalha et al., 2013, pp. 1524-1532).

The use of a lime as a binder is also advantageous for the recycling of materials. Hardened lime binder can be removed from masonry relatively easily, whereas the high strength bonding of cement mortars and renders can prevent recycling of materials, as it cannot be removed easily from brick and stone without causing damage.

2.3.2 Hydraulic limes

Hydraulic lime is produced in the same way as non-hydraulic lime, but the limestone from which it is produced contains impurities. These impurities may be present in the form of naturally occurring clay, in which case the product is called ‘natural hydraulic lime’. Alternatively, impurities (including various other chemicals in addition to clay) may be added manually, and limes produced in this way are not permitted to be classified as ‘natural’.

Hydraulic limes cover a wide range of physical properties depending on their chemical composition. For this reason, they have been classified according to their strength. Until the demise of the lime industry in the UK, they were classified as ‘feebly’, ‘moderately’ or ‘eminently’ hydraulic. This system has now been superseded by the natural hydraulic lime classifications NHL2, NHL3.5 and NHL5 according to the European standard BS EN 459-1:2015. It should be noted, however, that the two systems are not equivalent. A modern NHL2 lime is most closely equivalent to a traditional ‘moderately hydraulic’ lime, whilst an NHL3.5 lime is closer to an ‘eminently

hydraulic' lime and an NHL5 lime can easily attain strength levels equivalent to those of natural cements (Brocklebank, 2012c, pp.21-31). The modern standard classification is based on specific compressive strength values as tested at 28 days. The designations of NHL2, NHL3.5 and NHL5 imply strengths of 2, 3.5 and 5 MPa respectively, but in practice the values normally fall within a fairly wide range:

NHL2	2 - 7 MPa
NHL3.5	3.5 – 10 MPa
NHL5	5 – 15 MPa

The usefulness of such a classification system is questionable, however. Bergoin (2012, pp.33-52) argues that the emphasis on strength at 28 days is derived from the cement industry and of limited value for natural hydraulic limes. He states that studies have proven that the true performance of these materials is more accurately measured over a much longer timescale, usually several months. This criticism of the NHL specification system is backed up by Figueiredo et al., (2016), who have pointed out that the system does not provide a consistent representation of the properties of mortars produced from specific NHL limes because different limes with the same classification can possess very different properties and behaviour.

Although their strength comes mostly from hydration of calcium silicates, hydraulic limes also benefit from a degree of carbonation. The more permeable mortars carbonate the quickest and 'textured surfaces encourage carbonation to a greater depth and at a faster rate than smooth or heavily worked surfaces' (Allen et al., 2003, p.24)

2.3.3 Quicklime and hot lime

As already mentioned, the production of lime binders begins with the process of calcining limestone in a lime kiln. This causes thermal decomposition of the limestone to leave CaO and CO_2 as shown in the reaction below:

$$CaCO_3\,(s) + \text{heat} \Rightarrow CaO\,(s) + CO_2\,(g) \qquad (2.1)$$

The CaO resulting from this process is commonly referred to as ‘quicklime’. CaO is sometimes delivered to the point of use without being slaked first, to be used in a ‘hot lime’ mix. The term ‘hot lime’ refers to mortars that are mixed using CaO, water and aggregate. The resultant mix is a non-hydraulic lime mortar, the difference being that the quicklime is slaked at the same time as mixing with the aggregate. The mixing process generates a considerable amount of heat, and this is where the term ‘hot lime’ comes from.

Slaking CaO is a highly exothermic reaction (Equation 2.2) due to the relatively low specific heats of CaO (0.226 cal/g) and $Ca(OH)_2$ (0.286 cal/g). The reaction is capable of raising the ambient temperature by 730˚C (Hocking, 2005). For this reason, it is considered dangerous to store large quantities of CaO in combustible bags if there is any risk of contact with water.

$$CaO\ (s) + H_2O\ (l) \Leftrightarrow Ca(OH)_2\ (aq) \qquad (2.2)$$

CaO is available in two forms: ‘kibbled’ and powdered. Kibbled quicklime is granular and comprises particles 1mm and larger. Both forms are chemically identical, but kibbled lime is denser than powdered and expands to approximately 2.7 times its original volume, compared to powdered lime which expands to approximately 2.1 times (Brown, 2019). There are advantages and disadvantages associated with using either form of quicklime (Table 2.3).

The use of hot lime mortars requires more preparation than with other types of lime, and there are two main methods of preparation. The first method involves adding the quicklime to the sand and water in the specified amounts and thoroughly mixing together. It is important that the correct amount of water is added to the mix; too little and the mix can overheat but too much and the mortar will be over-wetted. This method is typically used for building or pointing rubble masonry and harling. In the alternative method, quicklime is added to damp sand measured to specified proportions (typically 1:3) and left to slake, which produces a dry mix of sand and hydrated lime. Water is then added and it is mixed to the required consistency. The mortar made in this way can be used straight away or left covered to mature for use later on (Snow, 2014).

Table 2.3: Advantages and Disadvantages of Powdered Versus Kibbled Quicklime (Brown, 2017).

Powdered Quicklime	Kibbled Quicklime
Reacts faster than kibbled – a quicker reaction can be harder to control and mix as it stiffens	Reacts a little more slowly than powder
No hotspots – as a powder it is all of similar granulometry	Hotspots – larger pebbles can reach higher temperatures during slaking causing spitting
Plumes – powdered quicklime can be thrown into the air during mixing, posing significant health and safety issues (eyes, inhalation, skin)	No plumes – granules and pebbles are heavier and denser than the powder
Limited pop outs – less prone to latent expansion after the mortar has been placed as almost all of it converts to lime	Pop outs – some larger pebbles can be slow to slake, causing delayed expansion, which can disrupt the mortar face

The length of time that a hot lime mix is left to mature before using has been shown to have an influence on the physical properties of the cured mortar. Margalha et al. (2011, pp.796-804) compared hot lime mixes that had been kept wet for 1, 7, 45 and 90 days before moulding. It was found that the maturation time had a ‘very positive effect on flexural and compressive strength, cracking susceptibility and water absorption by capillarity’. The work did concede, however, that a longer maturation period would require more care and be more time consuming.

Although still an area of uncertainty and ongoing investigation, it has been hypothesised that the use of hot limes has certain benefits compared to pre-slaked lime. It has been claimed that the heat generated during mixing has a positive effect on the bond characteristics between the binder and aggregate. Another claim is that the development of steam during mixing creates an altered pore structure within the binder (Forster, 2012, pp.251-269). Work carried out by Lawrence et al. (2014, pp.7-33) comparing different types of non-hydraulic lime and siliceous and calcareous aggregate did not support this theory. Mortars were prepared with dry hydrate, ‘hot

lime' and lime putty and containing siliceous or calcareous aggregate. The type of aggregate was found to affect strength to a greater degree than the type of binder (Figure 2.4).

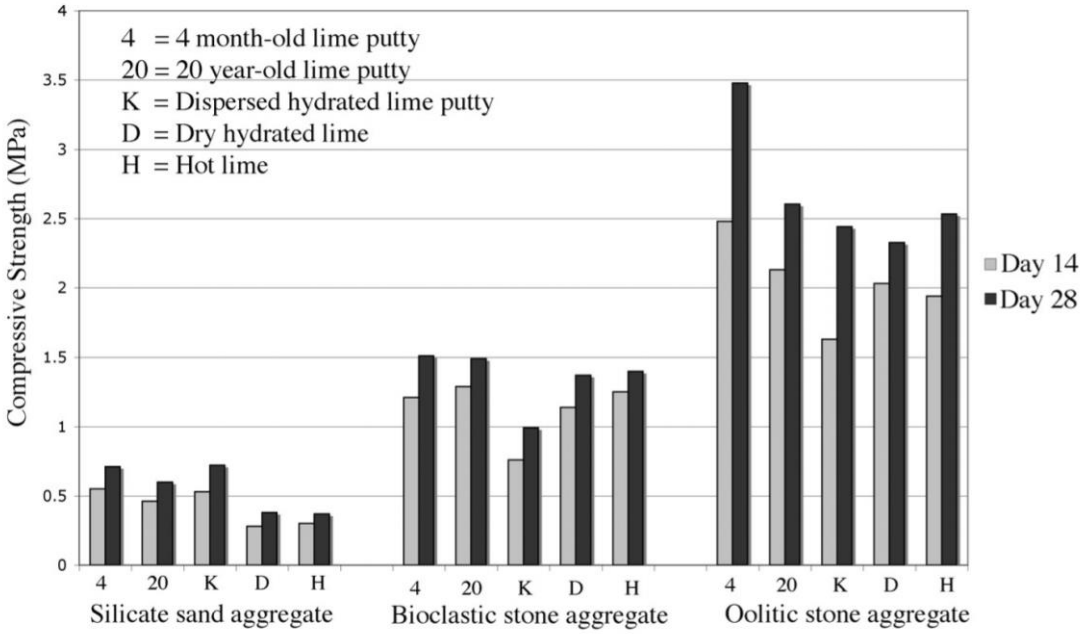

Figure 2.4: 14 and 28 day strength of mortars prepared using hydrated lime, lime putty and hot lime and siliceous and calcareous aggregate.

2.3.4 Dolomitic lime

Dolomitic lime is obtained from limestone that contain more than about 35% magnesium carbonate. It is an anhydrous mineral comprising carbonates of both calcium and magnesium and has the chemical formula $CaMg(CO_{3)2}$. Dolomite is normally found as a substituting mineral in calcareous limestone. Dolomitic limestone can contain varying amounts of dolomite and can also contain magnesium carbonate ($MgCO_3$) and calcium carbonate ($CaCO_3$) separately (Chever et al., 2010, pp.283-296).

Dolomitic limes were used extensively in the Italy, India and the United States during the nineteenth and early twentieth centuries. They were also used in areas of the United Kingdom where they were readily available.

Dolomitic limestone is calcined to produce both calcium oxide (CaO) and magnesium oxide (MgO). These two oxides are then hydrated to produce calcium hydroxide ($Ca(OH)_2$) and ($Mg(OH)_2$). Whilst the carbonation of calcium hydroxide to calcium carbonate (predominantly calcite) is somewhat predictable, the carbonation of magnesium hydroxide occurs at a slower rate and can result in varying ratios of magnesium oxide, magnesium hydroxide, magnesium carbonate and a variety of hydroxycarbonates (Hartshorn, 2012).

Dolomitic lime also differs from high calcium lime with respect to calcining temperature. Whilst the recommended upper temperature limit for calcining high calcium limes is around 1,300˚C, the figure for dolomitic limes can be as low as 900˚C, depending on the proportion of impurities present.

2.3.5 Lime composites

There are premixed composite lime-based construction materials on the market designed for specific situations. Hemp lime is a popular composite plaster for use where insulation is a priority. Hemp is a plant grown specifically for industrial uses. It can be spun into fibres, which are very strong and can be added to a lime binder and either formed into boards or blocks or used as a light weight insulating plaster. The hemp fibres are between 5 and 25 mm long, have a density between 110 and 150 kg/m^3 and have a thermal conductivity of 0.05 W/m.K (St. Astier, 2019). Suppliers claim that the addition of hemp fibres offers superior flexural strength compared to traditional lime plasters and that its thermal properties can help to improve the insulation performance of walls. Hemp is also a natural, renewable plant that absorbs carbon dioxide whilst it grows (Ty-Mawr, 2019).

Fibrelime is another popular lime composite plaster. This product is a proprietary plaster/render promoted as a one-coat plaster that has excellent adhesion to almost any surface. It is comprised of non-hydraulic lime plaster that has been seeded with chalk and mixed with polypropylene monofilament fibres. The product is supplied in 24kg tubs in a ready to use form. There is no requirement to add aggregate or water. The chemical analysis for Fibrelime, provided by the supplier is shown in Table 2.4. The polypropylene monofilament fibres are added to this mix in the proportion of 3kg per tonne.

Table 2.4: Fibrelime composition.

Sample	%LOI 575	%LOI 1000 CO_2	% $CaCO_3$	% $Ca(OH)_2$	% SiO_2	% CaO
Fibrelime	2.47	38.04	86.45	10.17	2.10	1.28
Fibrelime	2.16	38.37	87.2	8.89	1.95	1.96
Fibrelime	2.08	38.24	86.91	8.54	2.27	2.28
Average	2.24	38.22	86.85	9.20	2.11	1.84

2.3.6 Restoration mortars

Restoration mortars are proprietary mortars developed for masonry repair. There are many different products on the market, but they can generally be categorised as: cement-based restoration mortars, lime-based restoration mortars or hybrid-mix restoration mortars. They are available as ready to use mortars comprising binder, aggregate, additives, binders and fillers (Torney, 2016). The use of restoration mortars is a controversial subject. The composition can vary significantly from one product to another and in many cases, they are unsuitable (Saint Astier, 2019). Work carried out by Torney et al., 2014, pp.1-12) highlighted the importance of knowledge of compatibility between repair mortars and the substrate to which they are being bonded.

2.3.7 Nanolime

Nanolime is comprised of nano-size, plate-like calcium hydroxide crystals suspended in an alcohol-based medium. There is a number of types of alcohol that can be used in lime dispersions including ethanol, n-propanol and isopropanol. Originally, water was used, but it was discovered by Giorgi et al. (2000) that using alcohol enabled concentrations of calcium hydroxide up to three times higher than in water. The use of nanolime then became widespread in the early 2000s, when it was developed and manufactured for use as a stone consolidant.

The theory when using nanolime for consolidation is that the nanolime is drawn into the stone and penetrates the pore network. The alcohol then evaporates, depositing calcium hydroxide within the stone. For optimum consolidation, the calcium hydroxide must be deposited at sufficient depth to treat the entire zone of deterioration. The calcium hydroxide will then carbonate when exposed to atmospheric carbon dioxide and moisture (Historic England, 2017).

2.3.8 Roman cement

Roman cement was invented by Rev. James Parker and patented in 1796. In contrast to limes, Roman cement required grinding rather than slaking prior to use. It was also different from lime in that it was brown in colour and was very reactive, typically setting in approximately fifteen minutes. The term 'Roman cement' refers to a range of natural cements containing 25% or more of clay. These materials were classed as 'natural' because all of the required oxides (lime, silica, alumina etc.) are contained in the source material rather than being blended, as in the production of Portland cement. The use of Roman cement was short-lived compared to other binder materials and went into decline following the introduction of Portland cement, patented in 1824.

2.4 Chemistry of lime-based construction materials

2.4.1 Carbonation

Carbonation is the process whereby non-hydraulic limes gain their strength. Calcium hydroxide reacts with water vapour and atmospheric carbon dioxide resulting in the formation of precipitated calcium carbonate. The physical and mechanical properties of lime-based construction materials are determined by the microstructural characteristics of the calcium carbonate. The process involves a complex sequence of ion interactions (Lawrence, 2006):

1. Diffusion of atmospheric CO_2 through the pores in the mortar/plaster

2. Dissolution of $Ca(OH)_2$ in the pore water

$$Ca(OH)_2 \Leftrightarrow Ca^{2+} + OH^- \quad (2.3)$$

3. Dissolution of CO_2 in the pore water

$$CO_2 + OH^- \Leftrightarrow HCO^-_3 \quad (2.4)$$

4. Chemical equilibration of dissolved CO_2 in the pore water

$$HCO^-_3 + OH^- \Rightarrow CO^{2-}_3 + H_2O \quad (2.5)$$

5. Precipitation of $CaCO_3$

Carbonation is a diffusion related process and is therefore dependent upon the appropriate level of moisture within the material. If it is allowed to dry out, there is no transport mechanism for the carbon dioxide through the pore system of the lime. If, however, the material is saturated, carbon dioxide diffusion through the water filled pores will be severely restricted. If the pores are blocked by water, carbonation is effectively halted, as diffusion of CO_2 through water is approximately 10,000 times lower than through air (Richardson, 1988). The optimum water content for carbonation is the water content that corresponds to maximum adsorption on the surface of the pores before capillary condensation. For 100% of the pore surface to be available for carbonation, relative humidity should be between about 40% and 80%. At 90% and above, less than 50% of the pore surface is available and below 20%, the lack of pore water prevents carbonation from occurring at all (Van Balen and Van Gemert, 1994, pp.393-398).

The carbonate formed by the carbonation process results in an increase in weight of approximately 35% compared to the calcium hydroxide from which it is formed. There is also a corresponding 11.8% increase in solids volume (Moorhead, 1986, p.701). This increase in volume is accommodated by the internal pore structure, which has the effect of making the mortar less permeable to atmospheric CO_2 as carbonation proceeds, slowing down the reaction. Pore blocking may not be the only limiting factor during carbonation. It has been hypothesised that the heat generated during the $Ca(OH)_2 \Rightarrow CaCO_3$ conversion is sufficient to evaporate the capillary water and/or decrease CO_2 solubility (Cultrone et al., 2004, pp.2278-2289). Another theory is that

during carbonation, portlandite crystals become covered in calcium carbonate, which has low porosity and therefore slows down the reaction (Dheilly, 1998, pp.789-795).

The limiting factors during carbonation mean that lime based construction materials do not completely carbonate. Mortar samples up to a thousand years old have been found to still contain portlandite (Despotou et al., 2014). The degree of carbonation will depend upon the application i.e. thickness of plaster or thickness of wall in the case of mortars. It has been shown that a sharp boundary is normally found to exist between carbonated and uncarbonated material and that a carbonation front progresses through the material as carbonation progresses (Moorehead, 1986).

There have been a number of efforts to model the carbonation process mathematically. A simple method for expressing the progress of carbonation is given by:

$$X = k \sqrt{t} \qquad (2.6)$$

or

$$x = e + k \sqrt{t} \qquad (2.7)$$

Where x is the carbonation depth, k is a factor, t is time and e is a constant. The k factor can be determined by experimental methods based on one of the above equations (van Balen & van Gamert, 1994).

2.4.2 Hydraulicity

Hydraulicity is the chemical process by which a binder sets in contact with water. Hydraulic lime is produced by burning limestone that either contains impurities such as silica, alumina and iron oxides or has additive materials added to it prior to firing. These materials will combine, totally or partially, with the calcium oxide and water at certain temperatures to produce silicates, aluminates and ferrites, giving hydraulic properties to the lime.

There are two main forms of hydraulic calcium silicate compound: alite and belite. Alite is comprised of tricalcium silicate, while belite is mainly dicalcium silicate. Both forms of hydraulic compound can be formed from the same raw material, but the

composition of the end material depends on the firing temperature. Belite is formed at between approximately 900˚C and 1200˚C, whilst alite is produced at temperatures in excess of 1260˚C. Alite sets harder and faster than belite and is the predominate calcium silicate compound in cement. The calcium silicate in hydraulic lime is almost entirely belite.

There are five polymorphs of belite: β, γ, α, α_H and α_L. The α polymorphs are all formed at temperatures higher than are used during the production of the CaO for lime binders and are therefore not found in these materials.

Hydration involves a reaction between anhydrous compounds and water to produce a hydrate and does not require contact with air; consequently, hydraulic limes are capable of setting under water. The reaction involves the hydration of dicalcium silicate (belite) to form calcium silicate hydrate (C-S-H). The ratio of calcium to silica can vary significantly, but a simplified version of the reaction is shown in the equation below:

belite + water ⇨ C-S-H (2.8)

$$2(2CaOSiO_2) + 4H_2O \Rightarrow 3CaO.2SiO_2.3H_2O + Ca(OH)_2 \quad (2.9)$$

2.4.3 pH of lime materials

Lime prior to setting has a very high pH level in solution. Hydrated lime and lime putty have a pH level of around 12, which makes them very caustic when wet and somewhat hazardous to work with. After carbonation, the pH level can decrease to around 8.6. This change in pH is a chemical property that can easily be exploited to assess the degree of carbonation in lime mortar or plaster, using a phenolphthalein spray indicator.

2.4.4 Crystallinity

The crystal structure of non-hydraulic lime before carbonation (calcium hydroxide) and after carbonation (calcium carbonate) are significantly different, which can be a useful aid in microscopy analysis of mortar specimens.

Calcium hydroxide adopts a polymeric structure in the form of easily identifiable plate like hexagonal crystals. The size of the crystals diminishes considerably upon aging (Figure 2.5), resulting in a much larger surface area available for carbonation. This has been hypothesised as a possible reason for the quality improvement of aged lime putties (Rodriguez-Navarro et al., 1998, pp.3032-3034).

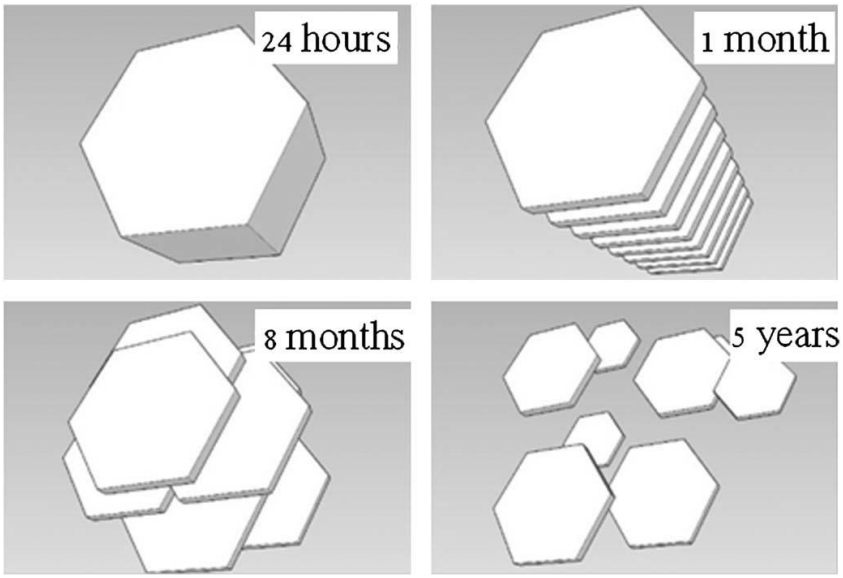

Fig. 2.5: Evolution of lime putty portlandite morphology determined from ESEM observations: (a) 24 h, large portlandite crystal; (b) 1 month, weak van der Waals bonds cause separation of plates; (c) 8 months, plate sliding; (d) 5 years, reduction in plate size from reprecipitation. (Margalha, M. G. et al, 2013).

It was reported by Margalha et al. (2013) that the free water content of lime putty decreases over time. This causes a decrease in the space between the crystals and a corresponding increase in the forces between them, which was cited as confirmation of the hypothesis that water retention increases with slaking time, improving plasticity.

Calcium carbonate has three hydrous polymorphs: monohydrocalcite, ikaite and amorphous calcium carbonate (ACC) and three anhydrous polymorphs: hexagonal calcite, orthorhombic aragonite and hexagonal vaterite. Experiments have shown that hydrous amorphous calcium carbonate forms at the initial stage of carbonation but is

unstable at ambient conditions and freely converts into vaterite and/or the more stable calcite (Cizer et al., 2012, pp.6151-6155).

2.4.5 Solubility

The carbonation process depends on calcium hydroxide dissolving in the pore water of mortars and plasters during the setting phase. Calcium hydroxide is sparingly soluble in water, however, having a solubility product K_{sp} of 5.5×10^{-6} , and unlike many salts, its solubility decreases with increase in temperature (Table 2.5).

Table 2.5: Solubility of lime at different temperatures (Forster, 2012).

Temperature (˚C)	**$Ca(OH)_2$ (g/100g)** saturated solution
0	0.185
10	0.176
20	0.165
30	0.153
40	0.140
50	0.128
60	0.116
70	0.104
80	0.092
90	0.081
100	0.071

The dissolution process is exothermic, which facilitates the elimination of heat and increases the equilibrium constant, thereby increasing the solubility at low temperature (Lohninger, 2019).

Calcium carbonate has a very low solubility in water and, like calcium hydroxide, its solubility decreases with increase in temperature but increases with increased acidity, which can be caused by carbon dioxide and sulphur dioxide dissolved in rainwater.

2.5 Physical properties of lime-based construction materials

2.5.1 Strength

Compressive and flexural strength are important considerations in the specification of lime-based mortars, plasters and renders. The strength values for these materials can vary considerably depending on a number of factors including (Walker & Zhou Z, 2012, pp.53-63):

- the binder to aggregate ratio
- the water to binder ratio
- the characteristics of the aggregate
- the environmental conditions during hardening
- Potential dewatering through layering with dry bricks
- Age

It has been shown that for a given mortar mix, the strength will generally increase the higher the binder to aggregate ratio. A study by Lanas (2003, pp.1867-1876) found that compressive strength in non-hydraulic lime mortars at 360 days increased with increased lime content in an approximately linear relationship.

The type of aggregate also has a significant impact on strength. It has been established that greater strength can be achieved with limestone aggregate compared to silicate aggregate, although the reasons for this are not fully understood. A study by Lawrence (2006) compared the compressive strength of four different non-hydraulic lime mortars containing limestone aggregate. All four mortars prepared with limestone aggregate achieved significantly higher strength levels than specimens containing 'standard sand'. This could be at least partly explained by the angular nature of the limestone aggregate compared to the more rounded silica sand, although it was proposed by Lawrence that that it is possible for calcitic aggregate to act as a nucleation site for calcite crystal formation. Another explanation proposed was that siliceous aggregates provide small radius pores that hinder the diffusion of CO_2 through the mortar, causing decreased carbonation. Calcitic aggregates, by contrast, increase the amount of medium and large radius pores thereby facilitating better carbonation and hence improved strength (Lanas, 2003, pp.1867-1876).

A different study by Pavia & Toomey (2008, pp.559-569) reported conflicting results to those of Lawrence. Their work suggested that compressive and flexural strength decreased with increasing calcite content of the aggregate. A significant factor in these two studies might be the aggregate morphology. In the work by Lawrence, standard sand was used, which is comprised of mainly spherical particles, whereas the sand used in the study by Pavia and Toomy was angular.

Compressive strength of a mortar will be influenced by both the shape and size of the aggregate. It is recommended that aggregates be well graded, as a suitable particle size distribution will facilitate higher mortar strengths. Also, angular particles having been shown to improve strength compared to rounded particles.

The effect of the water to binder ratio of a concrete mix is defined by Abram's rule, which states that strength is inversely related, although not linear, to the mass ratio of water to cement. The applicability of this rule to lime-based mixes is less certain, however. A study by Schaefer & Hisldorf (1993 pp.605-612) found that the rule held true for hydraulic and semi-hydraulic mortars, but that non-hydraulic mortars did not obey the rule.

Considering the number of factors affecting strength, it is not surprising that empirical evidence shows a wide range of strength values for different lime mortars. A comparison of the strength development of different non-hydraulic lime mortars carried out by Lawrence (2006) is shown in Figure 2.6. Interestingly, variation of strength values during the early stages of carbonation was ±30% but only ±6% after six months.

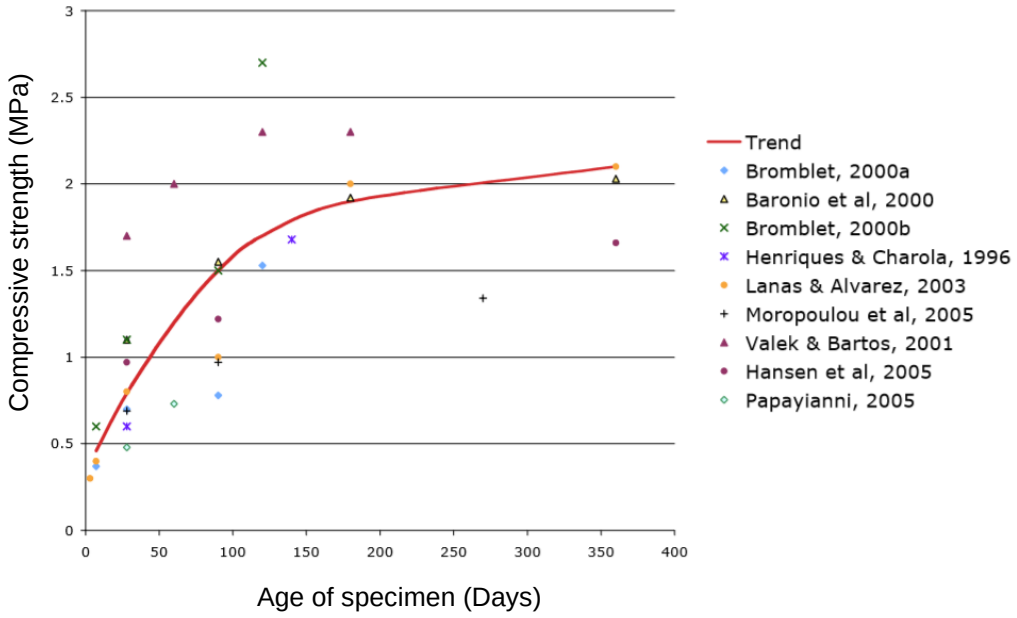

Figure 2.6: Compressive strength of lime mortars (Lawrence, 2006).

2.5.2 Autogenous healing

An often cited beneficial property of lime-based constructional materials is that of autogenous healing. This occurs when small movements of a building cause fine cracks to develop. Water penetration into these cracks then dissolves free lime and transports it to the surface where the water evaporates, leaving precipitated calcium carbonate to heal the cracks.

The healing of cracks prevents further water penetration and the damage to masonry that this results in after repeated freeze thaw cycles. In mortar, autogenous healing has also been shown to restore compressive strength. A study by Nardi et al. (2017) found that samples pre-damaged to 70% of normal compressive strength regained strength similar to undamaged samples after 14 days immersed in water. This work also concluded that micro-cracks, macro-cracks and fissures can all be healed by autogenous healing.

Migration of $Ca(OH)_2$ throughout lime binders is not beneficial in all circumstances, however. Where masonry structures experience prolonged periods of saturation, this can result in $Ca(OH)_2$ leaching out of the structure to the extent that the mortar becomes 'weak and friable and is easily lost from joints by washing out or compressive extrusion' (Forster et al., 2012, pp.199-207). Resistance of mortar to leaching is related to the type of lime and increases with increasing hydraulicity. A similar phenomenon was identified with carbonated mortars, with 'the resistance to deterioration increased in the order NHL2<NHL3.5<NHL5 binder, in line with the increasing hydraulicity of the binder' (Banfill et al., 2016, pp.182-190).

2.5.3 Porosity

An understanding of pore structure is important in the analysis of lime based construction materials as it has an effect on the diffusion of carbon dioxide within the material and hence the carbonation rate, and it also effects the ability of the material to allow evaporation of moisture from its pores and hence its long-term durability. The porosity of a mortar is defined as the total volume of open spaces within the structure and may include pores and cracks generated during the later stages of curing and will therefore be affected by the conditions during curing such as temperature and humidity. Porosity is further subdivided into open porosity, where pores are interconnected, and closed porosity, where pores are not connected to each other. Pore size distribution is another important factor in porosity analysis and is defined as the fraction of total pore volume that falls within a stated size range.

A study by Papayianni & Stefanidou (2005, pp.700-705) determined that the water to binder ratio was the most important factor in determining porosity in lime mortars with larger pores found in water rich mixes. There was also found to be an inverse relationship between porosity and strength and the most widely known definition of this relationship is given by the formula:

$$S = S_0 e^{-kp} \qquad (2.10)$$

where S is the strength, S_0 is the strength at zero porosity, P is the porosity and k is the rate constant.

This relationship between porosity and strength was also reported by Schaefer et al. (1993, pp.605-612.) who showed that as the amount of hydraulic material in a mortar increases, the porosity decreases and compressive strength increases. The situation may be different for non-hydraulic lime mortars, though. Lanas & Alvarez (2003, pp.1867-1876) studied the effect of porosity on strength and found that larger amounts of binder increased the porosity of the mortar, due to the high porosity of the binder compared with the aggregate (Figure 2.7), and this resulted in increased strength. It was hypothesized that the larger binder content allows for a good interlocked continuous structure, whereas larger amounts of aggregate cause discontinuities in the structure owing to the increase in interfaces. Thomson et al (2004) did not make this distinction between hydraulic and non-hydraulic mortars in their study of historic mortars. They found that progressive carbonation in all lime mortars results in a decrease in porosity with an associated increase in strength.

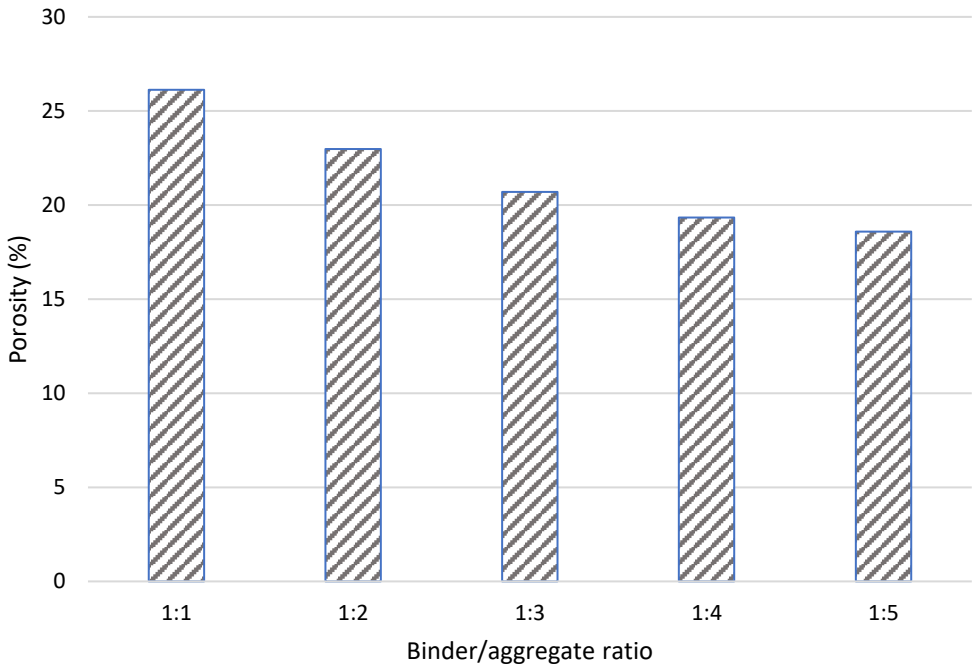

Figure 2.7: Open porosity in mortars tested after 365 days (Lanas & Alvarez).

The porosity of a mortar will change during the carbonation process. As the lime changes state from portlandite to calcite, ‘there is an increase in the volume of pores at around 0.1 μm in diameter’. This involves a reduction of pores larger than 0.1 μm

which is significant because ‘pores below 0.1 µm are not involved in the carbonation process’ and is ‘therefore evidence of the self-limiting nature of the carbonation process (Lawrence et al., 2007, pp.1059-1069).

The mode of diffusion of gas molecules through porous media depends on the size of the pores and the mean free path of the gas molecules (Figure 2.8) and is often divided into three different categories. Ordinary molecular diffusion occurs when the where molecule-molecule collisions dominate the diffusion process and the mean free path of the gas molecules is smaller than the pore diameter. Knudsden diffusion occurs when the mean free path of the gas molecules is larger than the pore diameter and the process is dominated by molecule-pore wall collisions. The third mode of diffusion, surface diffusion, is normally neglected as it is an assumption that is not based on empirical evidence. As the mean free path of carbon dioxide is 0.045µm, ordinary molecular diffusion will occur in pores of diameter greater than 0.045µm, both ordinary and Knudsden diffusion will occur where pores diameters are between 0.045µm and 0.45µm, and Knudsden diffusion will occur where pore diameters are smaller than 0.045µm (Lawrence, 2006).

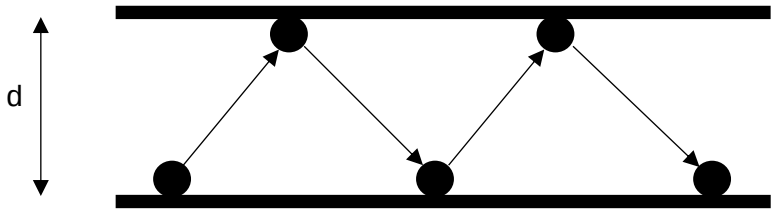

Knudsden diffusion

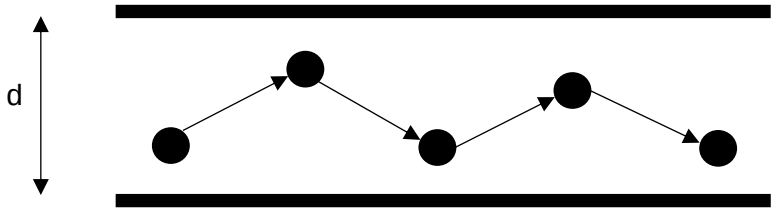

Ordinary molecular diffusion

Figure 2.8: Modes of diffusion in mortar.

2.5.4 Water vapour permeability

Water vapour permeability is an important physical property for construction materials. This is especially true for older properties, where the masonry is significantly more porous than that found in modern buildings.

Lime plasters and mortars have the advantage of possessing superior water vapour permeability compared to modern commercial plasters (Straube, 2000, p.3). When used as a render, the higher permeability of lime plaster helps moisture to escape from within the walls, preventing freeze thaw damage (El-Turki et al., 2010, pp.1392-1397). When used as a plastering material, its ability to release moisture also helps to prevent mould formation and reduction in thermal resistance.

The diffusion rate of water vapour through a mortar is also a useful method of assessing its water transport characteristics. A low value of water vapour permeability will limit access to dissolved CO_2 and consequently show poor carbonation progress. It was shown by van Balen & van Gembert (1994, pp393-398) that the optimal level of relative humidity at which carbonation occurs is approximately 60%. Moisture transport, or permeability, of a mortar or plaster is dependent upon the nature of its pore structure and only occurs within interconnected pores. Pore size, also, has an effect on permeability: 'capillary pores range from approximately 0,1 to 100 micrometres and contribute to the capillary water transfer. Water present in finer pores is bound more tightly to the material and these pores provide no moisture transfer contribution. Pores coarser than 100 micrometres contribute to the water permeability through gravity or wind driven water ingress' (Thomson et al., 2007, pp75-103).

Although there is little published data on the permeability of aerogel plasters, one study by Ibrahim et al (2014, p.243) reported a figure of 5.1×10^{-11} kg/s m Pa for an experimental aerogel based external render. This figure is significantly higher than was found in a study by Wang et al (2011, p.854) where five commercially available gypsum plasters were found to possess values of between 1.62 and 2.53×10^{-12} kg/s m Pa.

The type of lime is an important factor in determining water vapour permeability. It was determined by Forster (2002) that there is a correlation between water vapour permeability and hydraulicity, at least with binary mortars, with permeability decreasing with increasing hydraulicity.

2.5.5 Thermal conductivity

Thermal conductivity is the measurement of a materials ability to transfer heat. The chemical composition and molecular structure of a material have a significant influence on thermal conductivity. Materials with a simple chemical composition and molecular structure have higher thermal conductivity than more complex materials. The porosity of a material is another determining factor. As the thermal conductivity of solid matter is higher than that of air, the higher the porosity of a material is, the lower its thermal conductivity will be. This property is the reason for the extremely low thermal conductivity found in aerogel materials.

Ambient conditions will also affect thermal conductivity independently from a material's physical composition. Thermal conductivity will rise with increasing humidity because the thermal conductivity of water is twenty times greater than that or air. The practical problems associated with this can be seen in buildings where the external walls have become damp, resulting in a lowering of the thermal efficiency of the wall and leading to condensation on the internal surface. If trapped moisture within a material freezes, the problem becomes more serious still, as the thermal conductivity of ice is eighty times greater than that of air. The effect of increasing temperature is also to increase thermal conductivity. As temperature increases, thermal motion in the material becomes more active and the heat conduction of the air within the material's pores is increased (Zhang, 2011).

Heat flows from higher temperature to lower temperature. In the UK this usually means from inside a building to outside. To conserve heat energy within a building the walls, floors and ceilings are insulated using low thermal conductivity materials. Insulating materials can be broadly divided into two groups: organic and inorganic. Organic insulation materials include foamed plastics, vegetable fibre insulation board, wood fibre board, Celotex and perforated plate. Inorganic insulating materials can be either: fibrous, such as glass wool, mineral cotton and relative products; granular, such as expanded vermiculite and relative products or porous, such as foamed concrete, aerated concrete, diatomite, micro-porous sodium silicate and foam glass. A comparison of the properties of common building insulation materials is given in Table 2.6.

Table 2.6: Technical Parameters of Common Heat Insulating Materials (Zhang, 2011).

Name	Surface density (kg/m^3)	Strength (MPa)	Thermal conductivity [W/(m*K)]	Uses
Expanded Perlite	40 - 300		Normal Temperature 0.02 ~ 0.044 High Temperature 0.06 ~ 0.17 Low Temperature 0.02 – 0.038	High-efficient filling material Heat insulation Cold insulation
Cement Expanded Perlite	300 - 400	fc 0.5 ~ 1.0	Normal Temperature 0.05 ~ 0.081 Low Temperature 0.081 ~ 0.12	Heat Preservation Heat Insulation
Water Glass Expanded Perlite	200 ~ 300	fc 0.6 ~ 1.2	Normal Temperature 0.056 ~ 0.065	Heat Preservation Heat Insulation
Asphalt Expanded Perlite	400 ~ 500	fc 0.2 ~ 1.2	0.093 ~ 0.12	Used in normal temperature or negative temperature
Cement Expanded Vermiculite	300 ~ 500	fc 0.2 ~ 1.0	0.076 ~ 0.105	Heat Preservation Heat Insulation
Micro Porous Calcium Silicate Product	250	fc > 0. ft > 0.3	0.041	Heat insulation of exterior protected construction and pipeline
Foamed Concrete	300 ~ 500	fc ≥ 0.4	0.081 ~ 0.19	Exterior protected construction
Aerated Concrete	400 ~ 700	fc ≥ 0.4	0.093 ~ 0.16	Exterior protected construction

Wood Fibre Board	300 ~ 600	fv 0.4 ~ 0.5	0.11 ~ 0.26	Ceiling, Partition Board, Wall Panel
Soft Fibre Board	150 ~ 400		0.047 ~ 0.093	Ditto Smooth surface
Reed Board	250 ~ 400		0.093 ~ 0.13	Ceiling Partition Board
Cork Board	150 ~ 350	fv 0.15 ~ 2.5	0.052 ~ 0.70	Low water absorption non-corrosion non-combustion Heat insulation
Polystyrene Foamed Plastics	20 ~ 50	fv = 0.15	0.031 ~ 0.047	Heat insulation of roof and wall
Hard Polyurethane Foamed Plastics	30 ~ 40	fc ≥ 0.2	0.037 ~ 0.055	Heat preservation of roof and wall Heat insulation of cold storage
Glass Fiber Product	120 ~ 150		0.035 ~ 0.041	Heat preservation of exterior protected construction and pipeline
Soft Calcified Plastic Board	100 ~ 150	fc 0.1 ~ 0.3 ft 0.7 ~ 0.11	0.047	Heat preservation Heat insulation Water resistance decoration
Foamed Glass	150 ~ 200	fc 0.55 ~ 1.6	0.042	Wall construction Heat insulation of cold storage

The actual thermal performance of a building element (wall, floor, roof etc) will depend on the combined effect of all materials used in its construction such as bricks, tiles, blocks, render, membranes and the insulating material. The combined effect of these materials is used to calculate the thermal transmittance, commonly known as a 'U-value', which is a measure of the amount of heat energy lost through a square metre (m^2) of the building element for every degree (K) difference in temperature between the inside and the outside of the building. For insulation purposes, the lower the U-value, the better. In the UK, the minimum thermal performance of buildings is controlled by the Building Regulations Part L1(a)(i), which requires residential buildings to meet the U-values as shown in Table 2.7.

Table 2.7: Standards for new thermal elements (Building Regulations).

Element	**Standard W/(m^2*K)**
Wall	0.28
Pitched roof – insulation at ceiling level	0.16
Pitched roof – insulation at rafter level	0.18
Flat roof or roof with integral insulation	0.18
Floors	0.22
Swimming pool basin	0.25

Calculating the U value can become quite complex given the number of different materials that are used in modern construction. A typical wall construction, for example, might include a brick outer leaf, lightweight block inner leaf, insulation batts, a vapour control layer, a breathable membrane, plasterboard and render. The formula for calculating a U-value is given below, but there are a number of online calculators available to make the task easier.

$$U = \frac{1}{R_{Se}+\frac{d_1}{\lambda_1}+\frac{d_2}{\lambda_2}+\frac{d_3}{\lambda_3}+R_{Si}} \quad (2.11)$$

Where:

U =heat transfer coefficient (W / (m^2 K)

R_{se} = external heat transfer resistance (m^2 K) / W

R_{si} = internal heat transfer resistance (m^2 K) / W

λ = specific thermal conductivity of that layer W / (K m)

d_i = thickness of layer number i (m)

2.5.6 Pathology and durability

Non-hydraulic lime has been used in many buildings, dating back as far as Roman times, that are still standing today. Problems encountered with loss of structural integrity are more likely to have been the result of poor workmanship than with the material. The porosity of lime is a major contributor to its durability. This 'breathability' makes a significant contribution to the longevity of old buildings (Hughes, 1986) and, in spite of the apparent poor structural quality of air lime mortars, there is still a place for them in the continuum of structural binders (Bromblet, 2000a, 2000b).

The climate in the UK is generally favourable for the use of lime mortars and renders in terms of temperature and humidity. These materials are vulnerable during the setting phase, however. It is important that appropriate humidity levels are maintained during this period. If the pore structure is allowed to become saturated, the mortar or render will be susceptible to damage in freezing conditions. When water freezes it expands in volume, which will impart hydraulic forces on the pore walls (Livesy, 2012, pp.241-250). The effect of temperature during the setting phase is both important and complex. Increased temperature has the effect of accelerating the setting process and increasing early strength. However, it also causes a dense phase to form on the surface of lime grains, which inhibits further reaction and therefore results in lower final strength. Low temperatures, by contrast, result in a slower reaction and lower early strength. This also has the effect of increasing porosity and later strength. To achieve a durable mortar or render, the optimum temperature is approximately 15˚C (Livesy, 2012, pp.241-250).

The main agent of decay in lime-based construction materials is water. Being porous, these materials absorb water, albeit slowly. Calcium carbonate has very low solubility in pure water but will result in loss of material by dissolution over long time periods. Water is also an efficient solvent of electrolytes, which enables ionic compounds to be transported into the lime mortar from other building elements such as bricks or cement floors or pointing. This can result in damaging chemical reactions, especially from sulfates from Portland cement, which can cause sulfate attack or lead to the formation of gypsum (calcium sulfate hydrate). Sulfate attack occurs when mono calcium aluminate hydrate from the Portland cement is converted to ettringite (calcium sulfoaluminate hydrates), which takes up greater volume. The formation of gypsum is also deleterious due to its expansive nature. Lime mortars gauged with Portland cement that also contain limestone aggregate are also susceptible to the thaumasite form of sulphate attack (TSA). This is a reaction in which cement hydrates are replaced by thaumasite (calcium carbonate silicate sulfate hydroxide hydrate). Such a reaction requires the presence of carbonate and sulphates and cold, wet conditions (Ingham, 2012).

Water is capable of transporting pollutants into construction materials not only from other materials but also from the atmosphere. Rainwater is very different from pure water and can contain dissolved carbon dioxide, sulphur dioxide, nitrogen oxides and other atmospheric pollutants. Carbon dioxide is produced by industrial, commercial and residential activities and animals, whilst sulphur dioxide and nitrogen oxides are produced by automotive exhaust fumes and industrial processes. Lime materials are much more vulnerable to this acidified water than to pure water. Carbon dioxide dissolved in rainwater produces carbonic acid with a pH of about 5.6. This is a relatively weak acid. The reactions with sulphur dioxide and nitrogen oxides produce more acidic, and therefore damaging, rainfall. Sulphur dioxide reacts with rainwater to form sulphurous acid (H_2SO_3), more commonly known as ‘acid rain’, and can have a pH as low as 3.5 in extreme cases. Nitrogen oxides form nitric acid and have a similar effect on the pH of rainwater (Inkpen, 2004) (Nuno et al., 2015).

Rainwater is not the only means by which building elements can be impregnated with moisture. Where porous building materials are in contact with damp soil, groundwater can enter the fabric of a building through capillary suction. This is commonly known as ‘rising damp’ and can cause serious damage to masonry.

2.5.7 Shrinkage cracking

Shrinkage cracking is a common problem with lime-based construction materials and can occur for a number of reasons. This can negatively impact the durability of mortar or render, as it allows water to enter the building fabric where it can cause damage by bringing with it contaminants and salts or by freeze thaw action. Mostly the causes are the result of not tending the mortar during the or lack of knowledge about working with lime.

Lime mortars and renders require care after their application. It is usual to cover the newly applied mortar or render with hessian to prevent it drying out too quickly. Misting is regularly carried out for the same reason. If the lime dries out before sufficient carbonation has taken place this can cause cracking, as the mortar has not gained sufficient strength at this time to resist the tensile stresses imposed upon it. The use of limestone aggregate has been shown to produce large and medium size pores that assist carbonation and thereby reduce stress during the drying and crystallisation process (Alvarez, 2003).

Cracking can also be caused by unequal contraction between two layers of render or plaster (differential drying). This happens if the second coat is applied too soon and the layer underneath has not been allowed to achieve a sufficient set.

The choice of appropriate aggregate materials should be given careful consideration if shrinkage and cracking are to be avoided. Sands should not contain a high proportion of fines. The higher surface area of the fines increases water demand, and this has a negative effect on strength and can result in cracking during drying as the loss of water reduces the volume of the mortar. In lime mortars, the proportion of aggregate in the mix also has an effect on shrinkage, with the highest binder to aggregate mixes suffering the greatest shrinkage (Stewart et al., 2001).

2.6 Traditional aggregate materials

The basic constituents of a mortar or plaster are the binder, fine aggregate (sand) and water. There is sometimes confusion over the difference between the terms ‘fine aggregate’ and ‘sand’, but there is no difference and the words may be used interchangeably. The specification for a mortar mix is based on the principle that the

binder fills the voids in the fine aggregate, which will usually be in the range of 25 – 40%. If the voids are not completely filled, there is a risk that the mortar will suffer from poor durability. The main purpose of the aggregate is to act as a bulk filler material and can often comprise as much as 75% of the volume of a mortar. It may be inert or reactive. The aggregate material also reduces shrinking cracking, gives colour and texture and contributes to compressive strength (Gibbons, 2003).

A distinction is normally made between primary and secondary aggregate. Primary aggregates are obtained from naturally occurring mineral deposits and are extracted from quarries by drilling and blasting bedrock specifically to be crushed and sized for use as aggregate. Alternatively, naturally occurring aggregate can be obtained by dredging rivers or the seabed. Aggregates obtained from the seabed are similar in geological and mineral composition to land-based sources and their chemical and physical properties are identical. Secondary aggregates are classed as by-products of other quarrying and mining operations and include blast furnace and steel slag, coal-fired power station ash and spent foundry sand (Natural Environmental Research Council, 2019).

2.6.1 Types of aggregate material

Traditionally, aggregate materials were sourced locally and were often very different to those commercially available today. Historic sources of aggregate materials would have been seashore sand, riverbed sand, naturally occurring sand and gravel pits. The colour, texture and performance of these aggregate materials varied widely according to the geology at the source. They mainly consist of limestone, quartz, feldspar and other rock fragments (Artis, 2012, pp.144-154).

The most commonly used aggregate material is silicate sand. It is hard, chemically inert and less porous than limestone aggregate. It is normally recommended that sands for use in mortar be sharp, clean and well graded (having a good distribution of particle sizes), with most particles falling within the 2mm to 0.3mm size range, although sands for use in plaster would be somewhat smaller. (Artis, 2012, pp.144-154).

Limestone is also often used as an aggregate material. Limestone is a sedimentary rock comprised mainly of calcite, the most stable polymorph of calcium carbonate

($CaCO_3$). All limestones contain at least small amounts of other materials such as quartz, feldspar, clay minerals, pirite, siderite and other minerals. There are different varieties of limestone used as aggregate. Chalk is soft, white limestone that has been formed from the calcareous remains of microscopic marine organisms. Oolitic limestone is comprised of calcium carbonate 'oolites', which are small spheres of precipitate formed on a grain of sand or shell fragment. Bioclastic limestone are formed from skeletal fossil fragments from land or marine organisms.

The sand often used in experimental work is 'standard sand'. As there is no natural sand that fulfils the particle size distribution of BS EN 196-1 (Methods of testing cement. Determination of strength), 'Standard Sand' is an artificial product comprising several different types of sand. This sand is produced to a fixed specification, which permits consistency, repeatability and comparison of experimental work. Particle size ranges from 0.08 to 2mm and the maximum moisture content is 0.2%.

2.6.2 Particle size

The particle size distribution of an aggregate will have an effect on the water requirement and shrinkage of a mortar. It was demonstrated by Sanchez et al. (1997, pp.17-28) that in lime mortars the larger the maximum dimension of the aggregate, the smaller the shrinkage. By contrast, the greater the amount of fines below 0.08mm, the greater was the extent of the shrinkage.

The aggregate particle size also has a significant effect on mortar strength. Work carried out by Stefanidou & Paayianni (2005, pp.914-919) compared binders prepared with sand aggregate in the following size ranges: 0-2mm, 0-4mm, 0-8mm and 0-16mm. It was found that even for different binder aggregate ratios, the highest strength values were achieved with particle sizes in the 0-4mm range.

Aggregates will normally be required to be 'graded', which refers to the particle size distribution. An aggregate that consists mainly of similarly sized particles is said to be 'poorly graded'. An aggregate consisting of a wide range of particle sizes is said to be 'well graded'. A well graded sand will typically have particles ranging in size from 0.125mm to 4mm with the majority of particles at the mid-point sieve fractions. The actual particle size specified will depend on the intended use of the material. Mortars

containing the larger particle sizes are more suited to building and pointing, with the largest particle size being no more than one third the width of the mortar joint. Ordinary builders' sand is not suitable for most lime work because it is poorly graded and contains more rounded particles. Very fine sand is more appropriate for ashlar work (Snow & Torney, 2014).

2.6.3 Particle morphology

As well as chemical composition and size, the shape of aggregate particles has an effect on the physical properties of a mortar. Angular sands are normally chosen in preference to rounded sands because the particles interlock together well, rather than rounded particles, which tend to roll over each other and can result in a poorly bonded mortar having greatly reduced compressive strength (Artis, 2012, pp.144-154).

The shape of aggregate particles can vary considerably (Figure 2.9) depending on their origin and processing. Rounded aggregates are those occurring naturally in the sea or riverbeds and have been worn down by erosion and abrasion. Rounded particles possess the minimum surface area for the same mass compared to other shapes of aggregate and thus require less binder for bonding. Angular aggregates are the result of crushing rocks and have well-defined edges at the intersection of roughly planar faces. These require more binder than rounded particles. Flaky aggregates are generally angular but have a small thickness compared to their width and length.

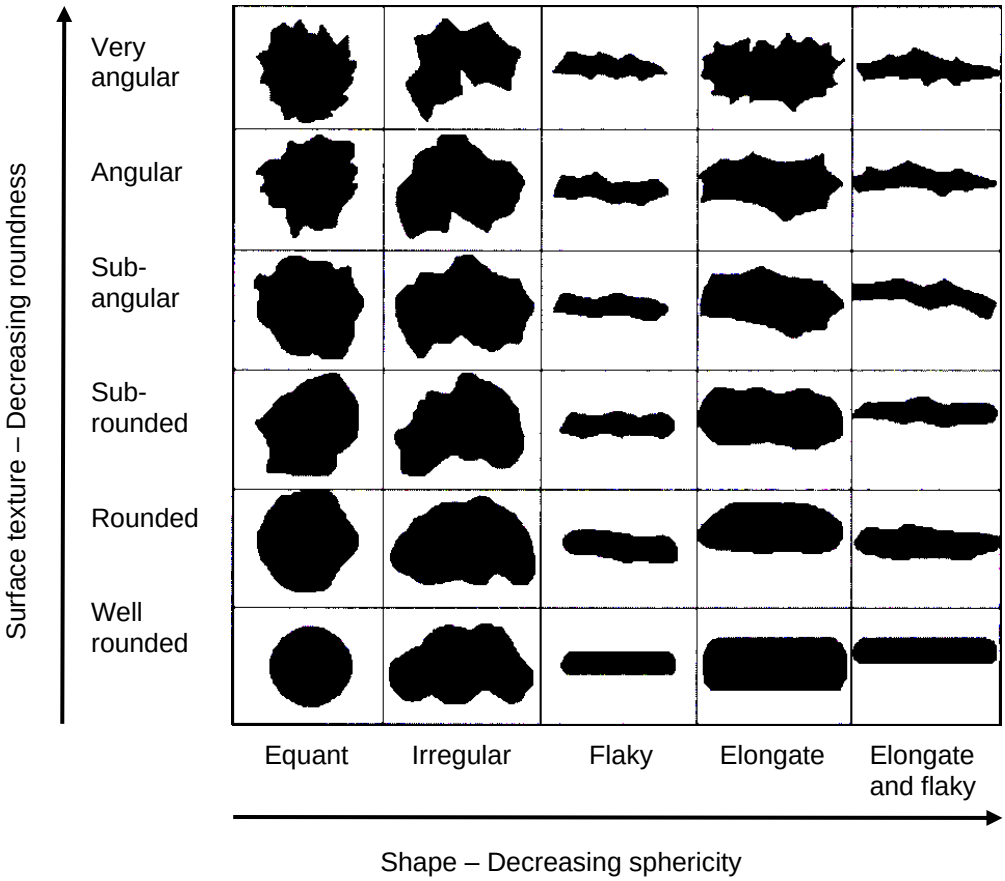

Figure 2.9: Classification of aggregate particle shape and surface texture (Ingham, 2012).

2.6.4 Aggregate impurities

There exists different and sometimes conflicting requirements when selecting aggregate materials. Artis (2012) recommends that aggregate materials do not contain significant proportions of fine-grained material, salts, organic (plant) material, wood fragments, coal gypsum or other sulphates and iron sulphides. However, in conservation work it is normally recommended that materials match the original structure as closely as possible, which may well contain one or more of the above. For this reason, when using original specification materials, the work may not conform to British Standards.

The standard for aggregates is BS EN 13139 (Aggregates for mortar), which covers aggregates for masonry mortars, exterior wall coverings, grouting, construction

materials, interior wall coverings masonry cement and plasters and provides guidance on the effects of some chemical constituents found in mortars. This is of importance because even small quantities of some impurities can have a significant effect on the properties of mortar or render and should be avoided where possible.

Fines are particles passing a 63 µm sieve and due to their small size and large surface area they increase water demand, which can increase shrinkage. The quantity that is permitted depends on the size of the aggregate and the intended end use. A summary of the limits for each type of application is detailed in Table 2.8.

Table 2.8: Percentage fines permitted in aggregate (BS EN 13139).

	Application	**The limits permitted to pass a 0.063mm sieve**
Category 1	Floor screeds, sprayed repair mortar and grouts (all aggregates)	3%
Category 2	Rendering and plastering mortars (all aggregates)	5%
Category 3	Masonry mortars (all aggregates except crushed rock)	8%
Category 4	Masonry mortars (crushed rock)	30%

It is essential that sands are cleaned before use. They should not contain appreciable amounts of ‘clay minerals, organic matter, compounds which reduce the durability of the mortars, for example: oxidisable iron sulphides (pyrites, marcasites); mica particles, shales with laminar or scaly structures in sufficient quantities that can affect the finish of the mortar, and its mechanical strength and hardness.’ (ANCADE, 2019).

2.6.5 Recycled aggregate

The construction industry generates a vast amount of aggregate waste material each year, and concerns Environmental concerns are forcing the industry to address this problem, and all construction companies have a duty of care when managing their waste under section 34 of the Environmental Protection Act.

The production of slate is an extremely wasteful process. It was reported by Arup (2001) that more than 90% of blasted virgin slate is classed as waste material. This is largely due to the size and shape requirements for its use in roofing. The slate that is not used is stockpiled as waste. Slate is officially classified as a recycled material by the British Standards Institution (BSI) and is potentially a viable source of recycled primary aggregate. Work carried out by Oti et al. (2010) determined that it is possible to produce concrete incorporating slate waste aggregates. They found that the compressive strength of concrete containing slate waste aggregate was lower than concrete containing limestone aggregate (although still acceptable) but the tensile splitting strength was approximately the same. Watson (1980).

The cutting of granite rock also produces a vast amount of waste material. As with slate, there has been a significant amount of research into using recycled granite waste for use in concrete but not with lime-based mortars. The research generally indicates that granite has potential as a replacement aggregate for concrete. Singh et al. (2016) investigated using granite cutting waste (GCW) as a substitute for sand in high strength concrete. They substituted sand with up to 70% GCW, and they found that at up to 40% substitution, compressive and flexural strength were similar or improved. Interestingly, at higher proportions of GCW replacement (25 – 40%), the carbon dioxide intrusion and carbonation were found to Increase with increasing GCW content. Similar results were achieved by Vijayalakshm, (2013), who found that mixes Containing recycled granite waste aggregate were stronger than those prepared with limestone aggregate.

2.7 Novel aggregate materials

When considering new materials for use as aggregate in mortars and renders, it is necessary to take certain factors into consideration. The large quantities of aggregate demanded by the construction industry each year mean that transportation costs, and

hence location of the source, are significant factors. CO_2 emissions associated with transportation are also an important consideration for an industry that is striving to halve emissions in the built environment by 2025 (EDIE, 2017). Furthermore, a sustainable source of supply is required that is not wasteful of natural resources. Consideration is given here to two materials that could have the potential to meet these requirements.

2.7.1 Slate

Slate is a fine-grained metamorphic rock composed mainly of clay minerals or micas. It is formed by metamorphosis of shale, whereby the original clay minerals transform into micas with increasing levels of heat and pressure. Slate can also contain large amounts of quartz and smaller amounts of feldspar, calcite, pyrite, hematite and some other minerals. It is formed when shales and mudstones are subjected to compressive force and heat, which causes foliation perpendicular to the direction of the force. This foliation is responsible for the well-known cleavage found in slate, which enables it to be split into slates for roofing (Geology.com). It is important to distinguish between shale and slate because the two names are often used interchangeably, but shale is a lightly compacted, sedimentary rock and possesses much lower strength than slate.

Slate has been used as a construction material for hundreds of years. It is well known as a roofing material but has also been used to make floor tiles and has even found use as a damp proof course material in some older buildings. It has long been a popular choice for roofing due to its durability. Its extremely low water absorption rate makes it waterproof and therefore it does not suffer from freeze thaw damage like some other construction materials.

Despite its many advantages, a major disadvantage of working with slate is the large amount of waste generated during cutting and machining operations in roofing slate production. Thousands of tonnes of slate waste are produced worldwide, and the consequential environmental impact has driven research into the potential for recycling. However, utilisation of slate waste is still low due to the distance of slate stockpiles in Wales from the main aggregate markets. In an effort to reduce

transportation costs, the UK government has promised to invest in rail infrastructure in the area (J E Oti, 2010).

Whilst there appears to be a dearth of information relating to the use of slate aggregate in lime construction materials, research has been carried out into incorporating slate aggregate in concrete. Work carried out by Oti et al. (2007, 2010) compared the physical properties of mixes comprising different proportions of slate waste aggregate. The results confirmed that all mixes were workable and within the recommended range for slump. Furthermore, the 28 day compressive strength showed only a 'slight variation' with increased proportion of slate. The mix comprising 100% slate waste aggregate did display the lowest strength value, and this was attributed to the flaky nature of the slate.

Labib (2019) in a study of slate waste aggregate in cement highlighted three potential constraints. The particle shape, being smooth and flaky, might cause problems with workability and strength. Rough surface texture is associated with a stronger binder to aggregate bond than smooth surfaces. This problem can be overcome, however, during processing. Butter (2000) used grid rollers to improve the shape of slate waste and make it acceptable for use in concrete mixes. The second potential problem highlighted was the possibility of Alkali-silica reaction (ASR). This would be a problem if the slate contains quantities of finely divided silica and mica. A further issue could be the presence of pyrite. Not all forms of pyrite are unstable and small quantities will not normally cause a problem, but the material would require analysis to check this.

2.7.2 Granite

Granite is a coarse-grained, crystalline igneous rock comprising mainly of quartz and feldspar with smaller amounts of mica, amphiboles and other minerals. It forms when magma from below the earth's surface slowly crystallises. The mineral composition gives granite its colour, which can be a red, pink, grey or white colour with dark mineral grains clearly visible throughout the rock (Geology.com).

Granite is the best-known and most common igneous rock found at the earth's surface. In the UK, granite is found in a number of locations and they vary in colour

and texture according to geological age and origin. There are numerous granite quarries throughout England (mainly in Devon and Cornwall), Scotland and Wales. Production of granite dimension stone has almost completely ceased, and these quarries now produce mainly crushed rock aggregate, roadstone and other bulk products. In recent years there has been a resurgence in the of popularity of granite for decorative interiors and cladding, although this is mostly imported from overseas.

Granite has been widely used in construction for many years, and there are many examples of buildings and monuments in the UK made from granite. Because of its strength and durability, granite has been used for a wide range of purposes from structural and engineering foundations to decorative building interiors. It was particularly favoured in the Victorian era and regarded as a prestigious material. For this reason, it was often used for commercial buildings such as banks, offices and entrances to major ecclesiastical and public buildings (Hyslop & Lott, 2007).

2.8 Traditional lime additive materials

It is common practice to include additives in lime-based construction materials and there are different reasons for doing this. Additive materials can be used to increase strength, improve durability, reduce shrinkage and cracking or to accelerate the setting process. The way in which these additive materials are incorporated into lime binders and plasters is also varied. Pozzolans and cement are used as a binder replacement, whereas animal hair is used as a reinforcement.

2.8.1 Pozzolans

The earliest use of pozzolanic materials was probably in Mediterranean countries where volcanic material was readily available such as volcanic ash, tuff and pumice. The term ‘pozzolan’ originates from the historic use of crushed pumice from Pozzuoli near Naples. The Romans added this pozzolanic material to lime putty to produce a lime with greater strength and lower porosity (Sanchez-Moral et al., 2005, pp.1555-1565). Today, however, the term pozzolan covers a much broader range of materials, both natural and manufactured. The main categories of pozzolanic materials are (Gibbons, 1997):

- Natural, very finely divided, highly reactive materials of volcanic origin
- Low temperature calcined clay products in various forms
- Clay or kaolin products specifically manufactured as pozzolans
- Mineral slag
- Ashes of organic origin
- Certain natural sands and crushed rock products

A pozzolan is ‘a siliceous or siliceous and aluminous material which, in itself, possesses little or no cementitious value but which will, in finely divided form and in the presence of water, react chemically with calcium hydroxide at ordinary temperature to form compounds possessing cementitious properties' (ASTM 2007). The reactivity of a pozzolanic material is influenced by a number of factors including its chemical and mineralogical composition, the type and proportion of its active phases, the particle’s specific surface area, the ratio of lime to pozzolan, water content, curing time and the temperature.

A pozzolanic material will react with calcium hydroxide to form calcium silicate hydrate and calcium aluminate hydrate, which possess cementitious properties. This process increases binding of the aggregate as evidenced by an increase in compressive strength. The initial setting rate may or may not increase as a result. Some porous additive materials can speed up the carbonation process by introducing entrained air and by improving capillary action for removal of water, but these materials are not necessarily pozzolanic (Boffey, 1999, pp.34-42).

When matching historical materials, it is important to carry out a comprehensive analysis of the original material, as mixes varied considerably. Traditionally, with non-hydraulic lime mixes, the proportions in a pozzolanic mix would have been one part lime powder (or two parts lime putty) to one of sand and one of pozzolan, or one part of lime powder (or two parts lime putty) to up to two and a half of pozzolan or trass, but without the addition of sand. In the case of natural hydraulic limes, however, the relative proportions of pozzolanic material were reduced. The material used could also vary. Brick dust was widely used (in varying proportions), but lime-ash is known to have been used in conjunction with sand and gypsum for floors (Gibbons, 1997).

2.8.2 Animal hair

Animal hair has been used for centuries as a means of reinforcing plasters. Traditionally, animal hair from goats, cows or horses has been added to lime plasters to improve their strength and to reduce shrinkage cracking. The hair needs to be strong, soft and evenly distributed throughout the binder. The quantity added should be 4-8 kg/m^3, and the lengths should be varied between 25mm and 100mm. Hairs from goat and cattle are considered to be the most suitable because they are coarse and covered with tiny barbs that hold hairs in place within the lime binder. Horse hair has a smooth surface and can consequently be pulled away from the hardened mortar by hand (Ingham, 2012, pp.155-173).

Despite being used for centuries, degradation of hair in external renders and internal plasters has been noticed in recent years. It has been reported by The Building Lime Forum (2015) that degradation of hair in lime does appear to be more common nowadays. The organisation suggests that this problem is caused by the modern practice of cleaning and sterilising the hair, making it less resistant to the high pH of the lime and more susceptible to mechanical damage.

2.8.3 Cement

Although most often referred to as a primary binder material, cement has also been widely used as an additive in lime binders. The practice of adding cement to non-hydraulic lime probably developed from the use of Portland cement / lime hybrid mortars used in the twentieth century. The mix ratios for these mortars were typically 1:1:6 or 1:2:9 cement:lime:sand (Brocklebank, 2012b).

The addition of cement to lime imparts a chemical set, which accelerates setting time. This property provides protection from the rain before carbonation has been completed, a distinct advantage for construction work in Britain. Also, the chemical set occurs before full shrinkage occurs, reducing the risk of cracking. Furthermore, cement is a well understood material. It is manufactured in controlled conditions and is predictable and reliable in use unlike some of the pozzolanic materials (O'Hare, 1995).

Despite the undoubted advantages that cement can offer, its use is not appropriate in all situations, particularly in older buildings. Traditionally, lime mortar was used in

conjunction with masonry that was softer and more porous than that found in modern construction. The lime mortar was relatively soft and flexible, which could accommodate building movement without damaging the masonry. The use of cement, in contrast, is brittle and inflexible, which can result in a build-up of stress and consequent cracking and spalling on the face of softer masonry (Taylor, 2003).

Cement mortar is also less permeable than lime. Lime mortars allow buildings to 'breathe'; moisture escapes the structure by evaporating through the porous mortar. Cement mortar traps moisture within the masonry where it can freeze and expand causing the brick or stone to deteriorate (Taylor, 1998).

A further problem associated with the use of cement in lime mortars is the introduction of soluble salts. Portland cement is a potential source of sulphates, which can cause extensive decay in porous building materials, with limestone being particularly susceptible. Damage is caused when salts are dissolved in pore water and subsequently crystallise out of solution as drying and evaporation takes place. Crystals forming on the face of masonry are known as efflorescence and, whilst quite dramatic in appearance, are relatively harmless. However, crystallisation within the pores below the masonry surface, known as cryptoflorescence, cannot easily be accommodated by the fine pores and causes microcracks within the material (Woolfitt, 2000).

2.8.4 Gypsum

Gypsum is a naturally occurring compound comprising calcium sulphate and water ($2CaSO_4.2H_2O$). When used as a plaster, gypsum is very vulnerable to moisture due to having a high porosity, over 50 per cent by volume. For this reason, gypsum plasters are not suitable for external applications or in areas where dampness occurs (Greenspec, 2019).

Although often considered as a modern material, gypsum has been in use as a construction material for hundreds of years. Gypsum plaster is widely used in modern construction but normally considered too hard and brittle for conservation work. As an additive material, gypsum is often added to lime plaster, known as 'gauging', to accelerate the setting time. This practice can reduce the setting time from weeks to a matter of hours (Ratcliffe, 1997).

2.9 Novel lime additive materials

2.9.1 Graphene Oxide

A relatively new nanomaterial, graphene was first isolated in 2004. It is an allotrope of carbon comprising a one (or few) atom thick layer of carbon atoms arranged in a hexagonal lattice. Graphene is 200 times stronger than steel, is an excellent electrical conductor and is chemically stable. Although nominally a sheet of graphene is one layer thick, bi-layer and few-layer graphene has properties similar to mono-layer graphene (2-dtech, 2018).

Graphene oxide is produced by oxidation of graphite. Whilst pure graphene is comprised solely of carbon atoms, graphene oxide consists of the graphene structure with several different oxygen-containing functional groups attached, which are typically carboxylic acid, hydroxyl, epoxide and carbonyl groups (Figure 2.10) (Furukawa, K, 2013,pp.1-5) (Mater, J., 2012, pp.23374-23379). This functionalisation significantly modifies the electrical and mechanical properties of the original graphene. The oxygen-containing functional groups make the material hydrophilic, enabling graphene oxide to be easily dispersed in water and organic solvents. Also, oxidisation transforms highly conductive graphene into an insulator (Graphenea, 2015).

There are several different methods in use for producing graphene oxide, the main four main processes being: Staudenmaier, Hofmann, Brodie and Hummers. Variations to these methods are being constantly investigated in attempts to improve the production process, with the effectiveness of the process often being assessed by the carbon to oxygen ratio of the graphene oxide produced (Graphene-info, 2018).

Several studies have been carried out confirming that graphene oxide can be utilised to significantly improve the compressive and flexural strength of concrete (Lu, 2017, pp.1-14) (Lia, 2017) (Shenghau, 2013, pp.121-127). Whilst there is less information currently available on the use of graphene oxide with lime mortars, one study by Faria et al did achieve modest improvements in the mechanical and physical characteristics of hydraulic lime mortars to which graphene oxide had been added at 0.1%wt. The form of graphene oxide proved to be significant in this investigation, as better results were obtained with water dispersed rather than powdered graphene oxide (Faria et al., 2017, pp.1150-1157).

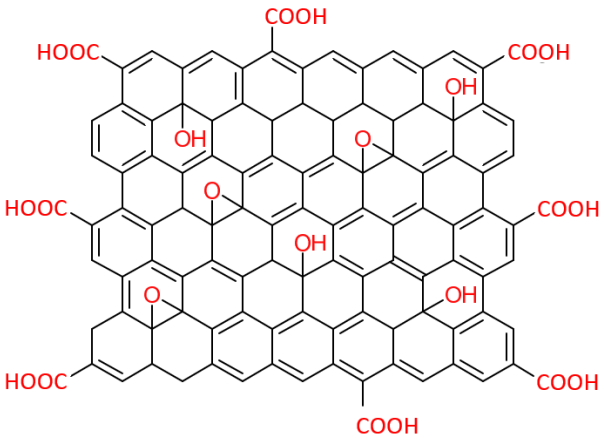

Figure 2.10: Chemical structure of graphene oxide.

2.9.2 Nanosilica

Nanomaterials are particles that have at least one dimension under 1000nm (some authors place the upper limit at 100nm), or 1µm (Buzea, et al., 2007). Owing to their extremely small size and high surface to volume ratio, these particles possess unique mechanical, optical, electronic and magnetic properties (Gonsalves et al., 2000).

Within the construction industry, the advantages of nanotechnology have been exploited for use in various applications such as insulation materials, antimicrobial coatings, scratch-resistant coatings, nano composites for use in roofing and flooring, stronger and corrosion-resistant steel, solar cells and as nano based binders for paints, mortars, renderings, plasters and concrete (Gill, 2012). The majority of literature relating to the use of nano materials in construction relates to its incorporation in cement. As there are chemical and physical aspects common to both cement and 'lime' construction materials, the information should have a high degree of relevance to this research.

Nano silica has been shown to improve the hydration and setting time of concrete. A recent review of the role of nanosilica in cement based materials found that "the

pozzolanic reaction of nanosilica with $Ca(OH)_2$, which is formed during the hydration of cement, produces additional C–S–H, which is the main constituent for strength and density in the hardened cementitious system. At the same time $Ca(OH)_2$, which hardly contributes to strength development, is consumed" (Singh et al., 2013, pp.1069-1077). This study also identified that the nanosilica "filling the pores to give higher packing density" resulted in "higher strength with lesser porosity". This study, whilst identifying the potential for reducing cement consumption, highlighted the need for further research on the dispersion mechanism of nanosilica in cement and the optimum quantity, particle size and type (dry powder, colloidal etc) of nanosilica used.

Another similar study, specifically using nanosilica in colloidal form, also identified strength gains and lower porosity resulting from pozzolanic and filler effects on the cementitious matrix (Said et al., 2012, pp.833-844). The choice of the colloidal form of nanosilica was significant in this study, as it was stated that dry nanosilica requires special treatment to ensure adequate dispersion, whilst colloidal nanosilica requires no special treatment before use.

In a direct comparison between colloidal and powdered nano silica it was found that both forms improve the properties of concrete, but with slightly different results. Tests carried out on self-compacting concrete with the addition of 3.8% of nano silica (based on the mass of the cement), produced similar flow and viscosity behaviour to a mix containing no nano silica. However, the addition of both types of nano silica brought about improvements in compressive and tensile strength. Interestingly, it was found that the colloidal form gave the greatest increase in compressive strength, whilst the powdered form produced the greatest improvement in tensile strength (Quercia, 2014).

The strength enhancing effect of adding nanosilica to mortar mixes has been attributed to different mechanisms. When properly dispersed throughout the matrix, the nano-sized particles have a particle packing effect, which can result in increased strength, durability and chemical resistivity. However, as the particle size gets smaller, the water demand increases and achieving the optimum mix proportions can prove to be a challenge (Vandenberg, A., Willie, K., 2015). Pozzolanic activity is also credited with imparting strength. The amorphous nature and high surface area of nanosilica promote a reaction with calcium hydroxide to form calcium silicate hydrates (C-S-H), resulting in a denser matrix (Lazaro, A., Brouwers, H.J.H., 2016). Yet another reason

for the increase of strength in mortars containing nanosilica is that in hydraulic compounds the nano particles act as nucleation sites for hydration reactions (Said, A.M. et al., 2012, pp.838-844). The increased strength in mortars containing nanosilica is achieved at the cost of reduced water vapour permeability. However, these two material properties have to be taken into account depending upon the end use of the material.

2.9.3 Silica Aerogel

Aerogels are a special class of extremely low density, amorphous, mesoporous materials with a nanostructure. In the case of aerogels, the 'nano' designation refers to the size of the pores within the material rather than the actual particle size. Pore sizes in aerogels are generally between 5 and 70 nm and have a pore density of between 85 and 99.8% by volume (Baetens et al., 2011, p.764) resulting in a very low thermal conductivity, a low gaseous conductivity and a low radiative infrared transmission, making them an extremely efficient insulating material. Aerogel is normally available in monolithic sheet form or as granules (Figure 2.11).

Figure 2.11: Aerogel granules.

Aerogel is produced by removing the liquid from a gel. Initial attempts at removing the liquid from gel pores resulted in significant shrinkage, which caused profound damage to the structure of the material. This problem was overcome by Kistler (1931, p.741), who successfully experimented with replacing the liquid with gas and then allowing the gas to escape.

Aerogel possesses a very high strength to mass ratio and can support up to 1600 times its own mass (Haranath, 1996, p.64); however, as manufactured, it is a brittle material, having a fracture toughness of only ~0.8 kPa m^2. Although easily crushed, this does not destroy its porous structure; aerogel that has been ground into a powder occupies approximately the same space as the original sample, demonstrating that the pore structure of the material does not change significantly when damaged (Kistler, 1931, p.58). In addition to its low weight and lower space requirements, silica aerogel's higher durability makes it an attractive alternative to organic fibre and foam insulation materials that may be susceptible to damp-induced decay. (Canaday, 2016).

An important property of aerogel for use in construction materials is its behaviour in the presence of water. There are several methods of manufacturing an aerogel, and the method used determines whether the finished product is hydrophilic or hydrophobic. Hydrophilic aerogels possess a large number of surface hydroxyl groups, making them extremely hygroscopic. When liquid water enters the pore structure of hydrophilic aerogel the surface tension of the water exerts strong capillary forces on the pore walls, causing collapse. This problem can be easily solved, however, by converting the surface hydroxyl groups (-OH) to non-polar (-OR) groups, where R is typically a methyl group (Ayers, 2016). It is only necessary to transform 30% of the polar -OH groups into non-polar groups in order to make the struts of the aerogel repel water. This makes the aerogel capable of floating on water indefinitely without wicking water into the poe structure, which would result in the aerogel shrivelling up (aerogel.org, 2019).

There has been much interest in exploiting the properties of aerogel to develop insulating products for the construction industry. One experimental aerogel product developed by Stahl et al (2012), comprising a mineral and cement free binder and hydrophobised granular aerogel at up to 90% by volume, has achieved a thermal conductivity value of 0.025 W/mK. Another, similar investigation by Buratti et al. (2014) tested more simple composites, comprising just granular silica aerogel and natural plaster. The plasters under test had an aerogel content ranging from 80 to 99% by volume, with 80% being proposed by the authors as a viable commercial solution. This investigation reported thermal conductivity values of between 0.014 and 0.050 for the proportions of aerogel used in the tests, compared to a value of 0.5 for a natural plaster containing no aerogel. Interestingly, this work also highlighted the importance of using

granules that are not too small, as the binder properties decrease due to the plaster becoming hydrophobic. The granules detailed in the work were irregular in shape and had an original size of 3-4mm, which reduced to 0.1-2mm in the final mix.

To date, there is only one known commercially available plaster that incorporates aerogel granules as the insulating element: the Fixit 222 Aerogel Insulating Plaster System. Fixit 222 is a highly developed product, comprising aerogel granules, light weight mineral aggregate, natural hydraulic lime, white cement and calcium hydroxide. Despite the use of cement and mineral aggregate, it still claims to achieve a thermal conductivity value of 0.028 W/mK. A potential disadvantage with this product is the amount of labour required in its application. The recommended procedure involves applying a layer of insulating plaster to a depth of at least 30mm, followed by a mineral-based undercoat stabiliser, a special embedding mortar with coarse mesh reinforcement fabric, a mineral-based final coating layer and then a mineral-based topcoat (Fixit, 2016). All of these aerogel-based plasters have significantly better thermal insulation performance than traditional cement or gypsum plasters with sand aggregate, which typically have thermal conductivity values of between 0.22 and 0.72 W/mK (The Engineer, 2006).

Interestingly, though, there appears to be little published information relating to strength or flexibility for any of these new insulating lime plaster materials. Two studies, involving cementitious mortars incorporating aerogel, which did investigate strength, however, reported compressive strength, flexural strength and thermal conductivity all reducing with increased aerogel content (Jelle, 2016, p.645) (Julio, 2016, p.493). Work has been carried out to investigate ways of improving the mechanical properties of aerogel plasters by incorporating fibres into the actual aerogel structure (rather than into the binder) to produce fibre-reinforced aerogel composites. It was found that composites could be produced that had a higher strength compared to non-reinforced aerogel, but sacrificed little thermal performance (Yang, 2011, pp.4830–4836).

Although principaly known for its impressive insulating properties, silica aerogel has another highly desirable property: fire resistance. Silica is inorganic and nonflammable, making it a suitable material where fire safety is a high priority. There are silica aerogel based products on the market that provide thermal insulation and fire protection in one product. Aspen Aerogels in America have produced a product called Pyrogel, which

comprises up to sixty percent silica aerogel and is used in high temperature industrial environments such as refineries and gas processing plants (Aspen Aerogels, 2019).

Compared to other insulation materials such as glass and natural fibre, aerogel is still significantly more expensive. However, it should be noted that it is still a relatively new material for construction applications. As its use becomes more widespread, higher production quantities and economies of scale will help lower the cost (Ibrahim, 2015, p.186). It is also noteworthy that over the service life of a building a reduction in operational costs associated with better insulation can be realised. Iddon and Firth (2013, p,479) report that for a typical building between 74-80% of the total energy in the first 60 years of service is consumed during operation and use. The remainder is the embodied energy and energy used during the construction process.

2.9.4 Polypropylene fibres

Polypropylene fibres have been used extensively in cementitious building materials, and are considered one of the most effective and relatively inexpensive methods to reduce plastic shrinkage and cracking in mortars (Filho, 1999, pp.1597-1604). Much investigative work has been carried out in relation to improving concrete, particularly its poor tensile strength. Due to concretes relatively high modulus of elasticity, it is difficult to achieve improvements in this area; however, research has indicated that improvements in strain capacity, toughness, impact resistance and crack control is possible even with low modulus fibres (Zheng. Z., 1995).

A study by Stefanidou et al. (2016) compared the effect of adding five different types of fibre to a non-hydraulic lime binder: Cellulose, wood, cannabis, nano-carbon and polypropylene fibres were added at 1% by weight to a 1:3 ratio mix of lime to sand. The sample containing polypropylene fibres was found to possess the highest fracture of all the samples and, compared to a reference sample containing no fibres, a compressive strength increase of 61%. The carbon fibre sample achieved a compressive strength increase of 71%; however, it was necessary to sonicate these fibres for thirty minutes prior to use in order to de-agglomerate them.

The effects of the volume fraction of polypropylene fibre on the mechanical properties of concrete was investigated by Rajguru R. S. et al. This work found that the

flexural strength of test beams increased significantly with increased fibre content from 0.25% to 0.5%, but the rate of strength increase achieved by increasing fibre content from 0.5% to 1% was marginal.

Kennedy et al. (2015) have stated that natural animal hair, having a much rougher texture, is more suitable for historic buildings than modern synthetic fibres, which were developed for use with cement, although they have also been used successfully with lime. A good example of polypropylene fibres being successfully incorporated into lime is the proprietary plaster/render 'Fibrelime'. This highly adhesive, breathable lime putty is suitable for new build, sustainable building and historic building and can be applied in a single coat to a variety of building materials, internally or externally (Fibrelime, 2015).

2.9.5 Olivine

Olivine is a naturally occurring mineral having the composition $(Mg, Fe)_2 SiO_4$,. The name Olivine refers to a range of iron/magnesium silicate minerals, with the composition varying from pure fosterite (Mg_2SiO_4) to pure fayalite (Fe_2SiO_4). Most Olivine falls somewhere between these two extremes, and the Mg and Fe content can be in any ratio. Olivine is a nesosilicate or orthosilicate mineral, having a structure comprised of isolated silica tetrahedra. In comparison to other minerals, olivine has a very high crystalisation temperature, which makes it one of the first minerals to crystallise from magma. Minerals that form at higher temperatures are less stable and are more prone to undergo weathering than minerals formed at lower temperatures (Goldich, 1938).

Olivine has gained much attention in recent years regarding its potential to sequester carbon dioxide from the atmosphere. The process by which this may be achieved involves converting the magnesium rich mineral into a carbonate. The most efficient form of olivine for this process is the magnesium-rich form of olivine: fosterite (Hangx, 2009). One method being investigated to achieve CO_2 sequestration is 'coastal spreading', whereby olivine is quarried, and milled to reduce the particle size (referred to as activation) and then spread over beaches to weather naturally.

The process of carbon sequestration involves a complex sequence of reactions, comprising three general reactions, as shown in the following chemical equations:

$$CO_2 + H_2O \leftrightarrow H_2CO_3 \leftrightarrow HCO_3^- + H^+ \leftrightarrow CO_3^{2-} + H^+ \quad (2.12)$$

$$Mg_2SiO_4 + 4H^+ \rightarrow 2Mg^{2+} + H_4SiO_4 \quad (2.13)$$

$$Mg^{2+} + CO_3^{2-} \leftrightarrow MgCO_3 \quad (2.14)$$

The first step involves the dissolution of atmospheric carbon dioxide in water, forming carbonic acid, which in turn dissociates and lowers the pH of the system (equation 1). The next reaction (equation 2) shows the dissolution of the magnesium-rich olivine by acid consumption. The third reaction is the precipitation of magnesium carbonate (equation 3) (Tove, 2010).

Once this process is complete, CO_2 can be stored indefinitely within the magnesite rock; as magnesite is stable, it is unlikely to rerelease the bound CO_2. This process is exothermic and thermodynamically favourable and occurs naturally over geologic timescales; however, to be of benefit in the current efforts to reduce the amount of CO_2 in the atmosphere, the process must be accelerated. It is possible to increase the reaction rate by raising the reaction temperature, increasing pressure, using a catalyst or decreasing the particle size (Demirbas, 2006, pp.59-65).

Decreasing the particle size of olivine is accomplished through ‘mechanical activation’ by high energy milling. This process changes the character of the olivine beyond reducing the particle size and increasing the surface area, however. “During and after activation, the crystal lattice is not in equilibrium and the excess energy caused by disordering contributes to lowering the activation energy of any further reaction of the material” (Tkacova, 1989).

Olivine is used in construction materials, but its use is normally limited to environments where fire safety is a high risk factor or where high temperatures are present, such as in foundries. Research has also been recently carried out involving the use of olivine as an aggregate in shotcrete mixtures for use as a protective layer in areas such as tunnels. The research found that “The replacement of limestone with olivine led to concrete superior in terms of strength at all temperatures of strain,

indicating that the utilization of olivine-based shotcrete enables production of a fire resistant shotcrete at temperatures up to 850°C" (Papayianni, 2013, pp. 246-252).

2.10 Summary and conclusions from the literature review

The construction industry is under pressure to improve the thermal efficiency of buildings and reduce the energy consumption and CO_2 emissions associated with its activities. In many construction applications, lime is a viable alternative to the more commonly used cement and can offer certain advantages. It emits lower levels of CO_2 during production and its lower strength accommodates building movement without causing cracking and facilitates the recycling of masonry. Furthermore, the porous nature of lime mortars and plasters permits moisture to escape from the building fabric and avoid damage that might otherwise be caused by freeze thaw cycles.

The large amount of waste generated by the construction industry is another issue that was highlighted as a major concern. Some building components from natural mineral sources that require cutting to size, such as roofing slates, kitchen worktops and floor tiles, generate a large amount waste material. Investigation is warranted into whether this waste could potentially be used as aggregate to produce a lime based mortar in which both binder and aggregate have a reduced environmental impact compared to traditional mortar mixes.

In recent years, new opportunities have presented themselves with the development of nanomaterials. These modern synthesised materials possess unique physical properties and have been incorporated into material composites to enhance properties such as strength and insulation capability. New working methods are also changing the way the construction industry operates. Off-site production is seen as an opportunity to reduce waste and transportation and mitigate the problem of the skills shortage associated with conventional construction methods. Research needs to establish whether lime-based construction materials incorporating novel additives can be developed that are compatible with these modern materials and processes.

The literature highlights emerging materials and technologies that present potential opportunities for the use of lime-based materials in construction. There are, however, gaps in the knowledge, and more research is required to investigate the potential for

these materials and methods to be used with lime-based materials. Work needs to be carried out to investigate how lime will react with these materials that possess completely different chemical and morphological characteristics compared with to traditional aggregate and additive materials.

It is evident that lime in its many different forms is a very versatile material. Non hydraulic lime is porous and relatively weak, making it compatible with many older buildings and conservation work. At the other end of the scale, hydraulic lime can be specified that has physical properties closer to cement. The adoption of the novel additive materials researched here has the potential to broaden the range of applications for this material still further whilst also contributing to reducing CO_2 production, improving the thermal efficiency of buildings and reducing material wastage.

2.11 References

2-dtech, 2018. *High Purity Low Defect Graphene* [online]. Manchester. Available from: https://www.2-dtech.com/wp-content/uploads/2018/04/Graphene-Datasheet-v1.2.pdf [accessed 29 June 2018].

Allen, G., Allen, J., Elton, N., Farey, M., Holmes, S., Livesey, P., 2003. *Hydraulic Lime Mortar for Stone, Brick, Block Masonry,* Donhead Publishing, Shaftsbury.

ANCADE, 2019. *Practical Guide to Lime Mortars.* University of Madrid

Artis, R., 2012. Sands and Aggregates for Conservation Mortars. In: I. Brocklebank ed. *Building Limes in Conservation*. Shaftsbury: Donhead, pp.144-154

ARUP. *Slate Tips – Sustainable Source of Secondary Aggregate*, 2001, ARUP, Cardiff, Report for the National Assembly for Wales, Cardiff.

Aspen Aerogels, 2019. *Flexible Insulation for High Temperature Applications* [online]. Northborough: Aspen Aerogels Inc. Available from: https://www.aerogel.com/products-and-solutions/pyrogel-xte/ [Accessed 12 January 2019]

Ayers, M., 2016. *Science of aerogels* [online]. California: E. O. Lawrence Berkely National Laboratory. Available from: http://energy.lbl.gov/ecs/aerogels/sa-chemistry.html [accessed 9th May 2016.

Baetens, R., Jelle, B.P. and Gustavsen., A, 2011. Aerogel insulation for building applications: A state of the art review. *Energy and buildings*, 43(4), p.764

Banfill, P.FG., Szadurski, E.M., Forster, A.M., 2016. Deterioration of natural hydraulic lime mortars, II: Effects of chemically accelerated leaching on physical and mechanical properties of carbonated materials. *Construction and Building Materials.* 111(2016), pp.182-190

Benhelal, E., Zahedi, G., Shamsael, E., and Bahadori, A., 2013. Global strategies and potentials to curb CO_2 emissions in cement industry. *Journal of Cleaner Production,* 51(2013), pp.142-161

Bergoin, P., 2012. Life After Vicat. In: I. Brocklebank, ed. *Building Limes in Conservation.* Shaftsbury: Donhead Publishing, pp.33-52

Boffey, G., Hirst, E. (1999) The Use of Pozzolans in Lime Mortars. *Journal of Architectural Conservation*, 5:3, pp.34-42

Bradley, J. *Sustainable construction* [online]. Available from: http://www.orbee.org/teaching-learning-resources.html?view=oerareas&expand=3%3A25 [Accessed 5 May 2019].

Bras, A., & Faria, P., 2017. Effectiveness of mortars composition on the embodied carbon long-term impact. Energy and Buildings, 154(2017), pp.523-528

British Lime Association, 2019. *How lime is made* [online]. Available from: https://britishlime.org/education/how_lime_is_made.php. [accessed 11 July 2019].

Brocklebank, I., 2012a. Developments in the Use of lime in London. In: I. Brocklebank, ed. *Building Limes in Conservation.* Shaftsbury: Donhead Publishing, pp.73-104

Brocklebank, I., 2012b. The Decline of Lime. In: I. Brocklebank, ed. *Building limes in conservation.* 1st ed. Shaftsbury: Donhead Publishing pp.1-18

Brocklebank, I., 2012c. The Lime Spectrum. In: I. Brocklebank, ed. *Building Limes in Conservation.* Shaftsbury: Donhead Publishing, pp.21-31

Bromblet, P, 2000a. Evaluation of the durability and compatibility of traditional repair lime-based mortars on three limestones. *International Journal for Restoration of Buildings and Monuments,* 6 (5), pp.513-528.

BROMBLET, P, 2000b. Properties and durability of air lime-based mortars for limestone repairs on monuments. In: Bartos, P., Groot, C., & Hughes, J.J., eds. *International RILEM Workshop on Historic Mortars: Characteristics and Tests*, Cachan, France: RILEM Publications s.a.r.l., pp.327-337.

Brown, A., 2018. *Hot-mixed mortars Advantages and limitations* [online]. Cathedral Communications. Available from: http://www.buildingconservation.com/articles/hot-mixed-mortars/hot-mixed-mortars.htm (accessed 18 March 2019].

BS EN 13139 – Annex D. Aggregates for mortar

Building Limes Forum, 2014. *About lime* [online]. Available from: http://www.buildinglimesforum.org.uk/about-lime [Accessed 25 January 2014].

Buratti, C., Moretti, E., Belloni, E., and Agosti, F., 2014. Development of Innovative Aerogel Based Plasters: Preliminary Thermal and Acoustic Performance Evaluation. *Sustainability*, 6, pp.5839-5852

Butter, A., Leek, D. and Johnson, R., Nov 2000, The potential for using some alternative aggregates in structural concrete, The Structural Engineer, v.78, No.22, pp.22-25.

Buzea, C., Pacheco, I.I., and Robbie, K., 2007. Nanomaterials and nanoparticles: Sources and toxicity. *Biointerphases*, 2(4), p.6

Canaday, H., 2016. *Aerogels look promising for lightweight insulation*. AviationWeek.com [online]. Available from: http://aviationweek.com/advanced-machines-aerospace-manufacturing/aerogels-look-promising-light-weight-insulation [accessed 21 August 2017].

Carran, D., Hughes, J., Leslie, A. and Kennedy, C., 2011. A Short History of the Use of Lime as a Building Material Beyond Europe and North America. *International Journal of Architectural Heritage*, 6(2), pp.117-118

Chever, L., Pavia, S., Howard, R., 2010. Physical properties of magnesian lime mortars, *Materials and structures,* 2020(43), pp.283-296

Cizer, Ö., Rodriguez-Navarro, C., Ruiz-Agudo, E., Elsen, J., Van Gemert, D., Van Balen, K, 2012. Phase and morphology evolution of calcium carbonate precipitated during carbonation of hydrated lime pastes. *Journal of Material Science*, 47(16), pp.6151−6165.

Cultrone G., Sebatian E., Ortega Huertas M., 2005. Forced and natural carbonation of lime based mortars with and without additives: Mineralogical and textural changes. *Cement and Concrete Research* 35, pp. 2278–2289

DEFRA, 2019. *UK Statistics on Waste*. Government Statistical Service

Demirbas, A., 2006. Carbon Dioxide Disposable via Carbonation. *Energy Sources, Part A: Recovery, Utilisation and Environmental Effects,* 29(1) pp.59-65

Despotou, E., Schlegel, T., Shtiza, A., Verhelst, F., 2014. Literature study on the rate and mechanism of carbonation of lime in mortars. *9th International Conference 2014 in Guimaraes.* 7-9 July 2014 Guimaraes.

Dheilly, R. M., Tudo, J., Queneudec, M., 1998. Influence of Climatic Conditions on the Carbonation of Quicklime. *Journal of Materials Engineering and Performance,* 7(6), pp.789-795

Edwards, J & Townsend, A., 2011. Buildings under Refurbishment. *Carbon Action 2050 White Paper.* Chartered Institute of Building: Englemere

El-Turki, A., Ball, R. J., Holmes, S., Allen, W. J. and Allen, G. C., 2010. Environmental cycling and laboratory testing to evaluate the significance of moisture control for lime mortars. *Construction and Building Materials*, 24 (8), pp. 1392-1397.

Faria, P., Duarte, P., Barbosa, D., Ferreira, I., 2017. New composite of natural hydraulic lime mortar with graphene oxide. *Construction and Building Materials, 156(2017), pp.1150-1157).*

Fibrelime, 2015. Product website [online]. Available from: www.fibrelime.co.uk [accessed 1 April 2015].

Figueiredo, C., Ball, R. J., M. Lawrence. 2016. Is BS EN 459-1:2015 fit for purpose in the context of conservation?. *The Journal of the Building Limes Forum,* 23, pp.46-52

Filho, R.D., Toledo, Sanjuan, M.A., 1999. Effect of low modulus sisal and polypropylene fibre on the free and restrained shrinkage of mortars at an early age. *Cement and Concrete Research,* 1999, Vol.29(10), pp.1597.

Fixit, 2016. *Aerogel Insulating Plaster System* [online]. Available from: http://www.fixit.ch/aerogel/pdf/Fixit_222_Aerogel_Verarbeitungsrichtlinien_A4_EN.pdf [accessed 7 August 2016].

Forster, A.M. and Carter, K., 2011. A framework for specifying natural hydraulic lime mortars for masonry construction. *Structural survey,* 29(5), p.374

Forster, A.M., 2002. *An assessment of the relationship between the water vapour permeability and hydraulicity of lime based mortars with particular reference to building conservation materials science.* Thesis (PhD). Heriot-Watt University

Forster, A.M., Szadurski, E., Banfill, P.F.G., 2014. Deterioration of natural hydraulic lime mortars, I: Effects of chemically accelerated leaching on physical and mechanical properties of uncarbonated materials. *Construction and Building Materials*, 72(2014), pp.199-207

Forster, A. 2012. Hot Lime Mortars. In: I. Brocklebank, ed. *Building Limes in Conservation.* Shaftsbury: Donhead Publishing, pp.251-269

Furukawa, K., Ueno, Y., 2013. Biosensing on a Graphene Oxide Surface. *NTT Technical Review,* 11(8), pp.1-5

Gibbons, P., 1997. Pozzolans for Lime Mortars, *The Conservation and Repair of Ecclesiastical Buildings.* Cathedral Communications

Gibbons, P. (2003), The Preparation and Use of Lime Mortars: *Technical Advice Note 1*, Historic Scotland, HMSO, Edinburgh.

Gill, T., 2012, Application of Nano Technologies in the Built Environment. USA: Nanotechnology KTN.

Giorgi, R., Dei, L., Baglioni, P., 2000. A new method for consolidating wall paintings based on dispersions of lime in alcohol, *Studies in Conservation*, 45 (3), pp.154–161

Goldich, S. S., 1938. A study in Rock Weathering. *Journal of Geology,* 46.

Gonsalves, K.E., Rangarajan, S.P. and Wang, L., 2000. Chemical synthesis of nanostructured metals, metal alloys and semiconductors. In: *Nanostructured materials and nanotechnology*. London: Academic Press, p1

Graphene-info, 2018. Graphene oxide: *Information and Market News* [online]. Available from: https://www.graphene-info.com/graphene-oxide [Accessed 20 July 2018].

Greenspec, 2019. *Plaster and Render* [online]. Available from: http://www.greenspec.co.uk/building-design/plaster-and-render/#gypsum [accessed 12 February 2019]

Greenspec, 2017, *Lime mortar, render and plaster* [online]. Available from: http://www.greenspec.co.uk/building-design/lime-mortar-render/ [acessed 18th January 2017].

Hammond, G.P. & Jones C.I., (2008). Embodied energy and carbon in construction materials. *Proceedings of the Institution of Civil Engineers.* Energy 161(EN2), pp.87-98.

Hangx, S. J. T., Spiers, C. J., 2009. Coastal spreading of olivine to control atmospheric CO2 concentrations. *International Journal of Greenhouse Gas Control,* 3(2009), pp.757-767

Haranath, D., 1996. Aerogel The Lightest Solid Known. *Resonance,* November 1996, pp.64-68

Hartshorn, H., 2012. *Dolomitic Lime Mortars: Carbonation Complications and Susceptibility to Acidic Sulphates*. Dissertation (MSc). Columbia University

Historic England, 2017. *Nanolime A Practical Guide to its Use for Consolidating*

Weathered Limestone.

Hocking M. B., 2005. Industrial Bases by Chemical Routes. *Handbook of Chemical Technology and Pollution Control.* (3).

Holmes, J. and Capper, G., LOW CARBON DESIGN, Northumbria University http://www.orbee.org/teaching-learning-resources.html?view=oerareas&expand=3%3A25 Accessed 21st March

Hughes, P, 1986. The need for old buildings to breathe. London: Society for the Protection of Ancient Buildings.

Hyslop, E., Lott, G., 2007. Rock of Ages. *The Building Conservation Directory*

Ibrahim, M., Wurtz, E., Biwole, P.H., Achard, P., Sallee, H., 2014. Hygrothermal performance of exterior walls covered with aerogel-based insulating rendering, *Energy and Buildings*, 84(2014) pp.241-251

Ibrahim, M., Biwole, P. H., Achard, P. & Wurtz, E., 2015. Aerogel-based Materials for Improving the Building Envelope's Thermal Behaviour: A Brief Review with a focus on a New Aerogel-Based Rendering, *Energy Sustainability Through Green Energy*. New Delhi Heidelberg New York Dordrecht London: Springer, p.186

Ibstock, 2005. *Ibstock Dzine Magazine* [online], June 2005. Available from: http://www.ibstock.com/pdfs/dzine/autumn-2005.pdf. [Accessed 5 January 2014]

Iddon, C. R. & Firth, S. K. 2013. Embodied and operational energy for new-build housing: A case study of construction methods in the UK. *Energy and Buildings*, 67 (2013), p.479

Ingham, J., 2012. Laboratory Investigation of Lime Mortars, Plasters and Renders. In: I. Brocklebank , ed. *Building Limes in Conservation*. Shaftsbury: Donhead Publishing, pp.155-173

Inkpen, R., 2004. Pollution, Climate Change and Historic Buildings. *The Building Conservation Directory*

Jelle, B. P., Zhen, Y., Wallevik, O, H., 2016. Effect of storage and curing conditions at elevated temperatures on aerogel-incorporated mortar samples based on UHPC

recipe. *Construction and Building Materials,* 106(2016), p.645.

Julio, M. F., Soares, A., Ilharco, L. M., Flores-Cohen, I., Brito, J., 2016. Aerogel-based renders with lightweight aggregates: Correlation between molecular/pore structure and performance. *Construction and Building Materials,* 124(2016) p.493

Karstensen, K. H., 2008. Formation, release and control of dioxins in cement kilns, Chemosphere, 70(2008), pp.543-560.

Kennedy, C.J., Revie, W.A., Troalen, L., Wade, M., Wess, T.J., 2013. Studies of hair for use in lime plaster: Implications for conservation and new work. *Polymer Degradation and Stability,* 98(2013), pp.894-898

King, H. M., 2019. *Granite* [online]. Available from: https://geology.com/rocks/granite.shtml [accessed 9 May 2019]

Kistler, S. S., 1931. Coherent Expanded Aerogels and Jellies. *Nature*, 3211(127), p.741

Kistler, S.S., 1931. Coherent expanded aerogels. *The Journal of Physical Chemistry*, 01/1931, Vol.36(1), pp.58.

Labib, W., Eden, N., 2019. An Investigation Into The Use of Slate Waste Aggregate in Concrete [online]. Available from: https://www.irbnet.de/daten/iconda/CIB10676.pdf

Lanas J., Alvarez, J., 2003. Masonry repair of lime-based mortars: Factors affecting the mechanical behaviour. *Cement and Concrete Research,* 2003(33), pp.1867-1876

Lawrence, R.M.H., 2006. *A Study of Carbonation in Non-hydraulic Lime Mortars.* Thesis (PhD). University of bath

Lawrence, R.M., Mays, T.J., Rigby, S.P., Walker, P., and D'Ayala, D.D., 2007. Effects of carbonation on the pore structure of non-hydraulic lime mortars. *Cement and Concrete Research,* 37(2007), pp.1059-1069

Lawrence, M., Walker, P., & D'Ayala,D., (2006) Non-Hydraulic Lime Mortars. *Journal of Architectural Conservation*, 12(1), pp.7-33

Lazaro, A., Brouwers, H.J.H., 2016. Nanotechnologies for sustainable construction. *Sustainability of Construction Materials,* 2(2016). pp.55-78

Lia, X., Lia, C., Liu, Y., Chen, S. J., Wang, C. M., Sanjayan, J. G., and Duan, W. H., 2017. Improvement of mechanical properties by incorporating graphene oxide into cement mortar. *Mechanics of Advanced Materials and Structures,* DOI: 10.1080/15376494.2016.1218226

Lohninger, H., 2019. *Calcium Hydroxide* [online]. Available from: http://www.vias.org/genchem/inorgcomp_calcium_hydroxide.html [accessed 18 March 2019]

Lu, L and Ouyang, D., 2017. Properties of Cement Mortar and Ultra-High Strength Concrete Incorporating Graphene Oxide Nanosheets. *Nanomaterials*, 7(187), pp.1-14.

Lynch,G., 2012. Lime Mortars: The Myth in the Mix. In: I. Brocklebank ed. *Building Limes in Conservation*. Shaftsbury: Donhead, pp.221-228

Margalha, G., Veiga, R., Silva, A.S. and De Brito, J., 2011. Traditional methods of mortar preparation: The hot lime mix method. *Cement and Concrete Composites,* 33(8), pp.796-804*.*

Margalha, M. G., Silva, A. S., Do Rosário Veiga, M., De Brito, J., Ball, R. J. and Allen, G. C., 2013. Microstructural changes of lime putty during aging. *Journal of Materials in Civil Engineering*, 25 (10), pp. 1524-1532.

Mater, J., 2012. Fingerprinting photoluminescence of functional groups in graphene oxide. *Journal of Materials Chemistry,* 22, pp.23374-23379.

Moorhead, 1986. Cementation by the Carbonation of Hydrated Lime. *Cement and Concrete Research,* 16(5), p.701

Nadim, W., Goulding, J.S., 2010. Offsite production in the UK: the way forward? A UK construction industry perspective. *Construction Innovation,* 10(2), pp.181-202

Nardi, C. D., Cecchi, A., Ferrara, L., Benedetti, A., Cristofori, D., 2017. Effect of age and level of damage on the autogenous healing of lime mortars. *Composites Part B*, 124(2017), pp.144-157

Natural Environmental Research Council, 2013.

Network Waste, 2019. *Construction Waste Statistics* [online]. Available from: http://www.networkwaste.co.uk/network-news/construction-waste-statistics [accessed 7 May 2019].

Ng, S., Jelle, B. P., Zhen, Y., Wallevik, O, H., 2016. Effect of storage and curing conditions at elevated temperatures on aerogel-incorporated mortar samples based on UHPC recipe. *Construction and Building Materials,* 106(2016), p.645.

Nuno, M., Pesce, G. L., Bowen, C. R., Xenophontos, P., Ball, R. J., 2015. Environmental performance of nano-structured Ca(OH)/TiO_2 photocatalytic coatings for buildings, *Building and Environment*, 92(2015) pp.734-742

O'Hare, G., 1995. The Relative Merits of Adding Cement. *The Building Conservation Directory.* Cathedral Communications

Oti J. E., Bai J, Delpak R, Kinuthia J. M., Snelson DG. A preliminary investigation into tensile strength and elastic modulus of concrete made with slate aggregates. 2007a, *Proceedings of the 6th Research and Innovation Conference*, London, 31–38.

Oti, J. E., Kinuthia, J. M., Snelson, D. G., Bai, J., 2010. Applications of slate waste material in the UK. *Proceedings of the Institution of Civil Engineers – Waste and Resource Management,* 163(1), pp.9-15

Oti, J. E., Kinuthia, J. M., Bai, J., Delpak, R., Snelson, D. G., 2010. Engineering properties of concrete made with slate waste. *Construction Materials,* 163(CM3), pp.131-142

Papayianni, I., Papachristoforou, M., Patsiou, V., Petrohilou, V, 2013. *Development of fire resistant shotcrete with olivine aggregates*. IABSE Symposium, May 6 2013 Rotterdam 2013: Assessment, Upgrading and Refurbishment of Infrastructures, pp. 246-252

Papayianni, I., Stefanidou, M., 2005. Strength-porosity relationships in lime pozzolan mortars. *Construction and Building Materials,* 20(2006) pp.700-705

Pavia, S., & Toomey, B., 2007. Influence of the aggregate quality on the physical properties of natural feebly-hydraulic lime mortars. *Materials and Structures,* 41(2008), pp.559-569

Pritchett, I., 2003. Lime versus cement: traditional methods for today's buildings. *Proceedings of the Institution of Civil Engineers,* June 2003, London: ICE, p.84

Rajguru, R. S., Ghode A. R., Pathan M. G., Rathi M. K., 2014. Effect of volume fraction of polypropylene fiber on the mechanical properties of concrete, *Int. Journal of Engineering Research and Applications, Vol. 4, Issue 6(Version 1), June 2014,* pp.67-69

Ratcliffe, 1997. The Use of Gypsum Plaster. *The Building Conservation Directory.* Cathedral Communications

Richardson, M., 1988. Carbonation of Reinforced Concrete. Its Causes and Management, Citis, Dublin.

Rodriquez-Navarro, C., Hansen, E., Ginell, W. S., 1998. Calcium Hydroxide Crystal Evolution upon Aging of Lime Putty. *Journal of American Ceramics,* 81(11), pp.3032-3034.

Sanchez, J.A., Barrios, J., Barrios, A., Agudo, A.R.D.. 1997. The shrinkage in lime mortars, *Materiales de Construction*, 47 (245), pp.17-28.

Sanchez-Moral, S., Luque, L., Canaveras, J-C., Soler, V., Garciaguinea, J., Aparicio, A., 2005. Lime pozzolana mortars in Roman catacombs: composition, structures and restoration. *Cement and Concrete Research*, 35, pp.1555-1565

Said, A.M., Zeidan, M.S., Bassuoni, M.T., Tian, Y., 2012. Properties of concrete incorporating nano-silica. *Construction and Building Materials, 36(2012).* pp.838-844

Schafer, J., Hilsdorf, H.K., 1993. Ancient and new lime mortars - the correlation between their composition structure and properties. In: M.J. THIEL ed., Conservation of Stone and other Materials, London: E. & F.N. Spon, pp.605-612.

Schandl, H., Krausmann, F., 2019. *20th century saw a 23-fold increase in natural resources used for building* [online]. Available from: http://theconversation.com/the-

20th-century-saw-a-23-fold-increase-in-natural-resources-used-for-building-73057 [accessed 5 May 2019].

Shenghua Lv, S., Ma, Y., Qiu, C., Sun, T., Liu, J., and Zhou, Q., 2013. Effect of graphene oxide nanosheets of microstructure and mechanical properties of cement composites. *Construction and Building Materials,* 49(2013), pp.121-127

Singh L.P., Karade S.R., Bhattacharyya S.K., Yousuf M.M. and S. Ahalawat S., 2013. Beneficial role of nanosilica in cement based materials. *Construction and Building Materials,* 47, p.1071

Singh, S., Nagar, R., Agrawal, V., Rana, A., Tiwari, A., 2016. Sustainable utilization of granite cutting waste in high strength concrete. *Journal of Cleaner Production,* 116(2016), pp.223-235.

Snow, J. H., 2016. *Hot-mixed lime mortars.* Edinburgh: Historic Environment Scotland

Snow, J., Torney, C., 2014. *Lime Mortar in Traditional Buildings.* Edinburgh: Historic Scotland

Stahl, S., Brunner, S., Zimmermann, M., Ghazi Wakili, K., 2012. Thermo-hygric properties of a newly developed aerogel based insulation rendering for both exterior and interior applications, *Energy and Buildings,* 44(2012), pp.114-117

St. Astier, 2019. *Hemp Mortars using St. Astier Natural Hydraulic Limes and Products* [online]. Available from: http://www.stastier.co.uk/nhl/guides/hempconstruction.htm [accessed 9 July 2019].

St. Astier, 2019. *Restoration and Conservation Mortars.* [online]. Available from: http://www.stastier.co.uk/nhl/testres/restorationconservationmortars.php [accessed 30 October 2019]

Stefanidou, M., Papachristoforou, M., Kesikidou, F., 2016. Fibre reinforced lime mortars. *4th Historic Mortars Conference.* 10-12 October 2016 Santorini. Laboratory of Building Materials, Civil Engineering Department, Greece. pp.422-430

Stefanidou, M., Papayianni, I., 2007. The role of aggregates on the structure and properties of lime mortar. *Cement & Concrete Composites,* 27, pp.914-919

Stewart, J., Glover, R., Houston, J., Seeley, N., Proudfoot, T., 2001. Field and laboratory assessment of lime-based mortars. *Journal of Architectural Conservation*, 7 (1), pp.7-41.

Stork, M., Meindertsma, W., Overgaag, M & Neelis, M, 2014. A competitive and efficient lime industry cornerstone for a sustainable Europe, European Lime Association (EuLA)

Straube, J., 2000. Moisture Properties of Plaster and Stucco for Strawbale Buildings, *Research Highlight,* Technical Series 00-132, p.3

Taylor, J., 2003. Window Head Details in Exterior Brick Walls, *The Building Conservation Directory.* Cathedral Communications

Taylor, J., 1998. 10 Ways to Ruin an Old Building, *The Building Conservation Directory.* Cathedral Communications

The Engineer, 2006. Thermal Conductivity, *The Engineer,* October 2006

Thomson, M. L., Lindqvist, J. E., Elsen, J., Groot, C.J.W.P, 2004. Porosity of Historic Mortars. *13th International Brick and Block Masonry Conference.* 4-7 July 2004 Amsterdam

Thomson, Margaret & Lindqvist, Jan & Elsen, Jan & Groot, Caspar. 2007. *Characterisation of Old Mortars with Respect to their Repair*. RILEM publications SARL, pp.75-103

Torney, C., 2016. *Restoration Mortars for Masonry Repair*. Edinburgh: Historic Environment Scotland.

Torney, C., Forster, A.M., Szadurski, M., 2014. Specialist 'restoration mortars' for stone elements: a comparison of the physical properties of two stone repair materials. *Heritage Science,* 2(1), pp.1-12

Tove, A.H. 2010. *Dissolution and carbonation of mechanically activated olivine.* Thesis (PhD). Norwegian University of Science and Technology, Trondheim.

Tkacova, K., 1989. *Mechanical activation of minerals.* Amsterdam: Elsever Science Publishers

Ty-Mawr, 2019. *Lime Hemp Plaster (Non Hydraulic)* [online]. Available from: https://www.lime.org.uk/lime-hemp-plaster-non-hydraulic.html [accessed 11 February 2019].

Van Balen, K. & Van Gemert, D., 1994. Modelling lime mortar carbonation. *Materials and Structures,* 27, pp393-398

Vandenberg, A., Willie, K., 2015. Understanding the Dispersion Mechanisms of Nanosilica in Ultra High Performance Concrete. *Nanotechnology in Construction: Proceedings of NICOM5.* 24-26 May 2015 Chicago. Springer. Pp.311-316

Vijayalakshmi, M., Shekar, A. S. S., Ganesh, G., 2013. Strength and durability properties of concrete made with granite industry waste. *Construction and Building Materials,* 46(2013), pp.1-7.

Walker, P. & Zhou, Z., 2012. Structural Properties of Lime-Mortared Masonry. In: I. Brocklebank, ed. *Building Limes in Conservation.* Shaftsbury: Donhead Publishing, pp.53-63

Wang, Q., Liu, H., 2011. The Experimental Research on the Water Vapour Permeability of Construction Gypsum Plaster Materials. *International Conference on Materials for Renewable Energy & Environment,* May 2011, Vol. 1, pp.854

Woolfitt, C., 2000. Soluble Salts in Masonry. *The Building Conservation Directory,* Cathedral Communications.

Yang, X., Sun, Y., Shi, D., Liu, J., 2011. Experimental investigation on mechanical properties of a fiber-reinforced silica aerogel composite. *Materials Science and Engineering A*, 528 pp.4830–4836

Zhang, H., 2011. Heat-insulating Materials and Sound-absorbing Materials. In: H. Zhang ed.. *Building Materials in Civil Engineering.* Woodhead Publishing, pp.304-423

Zheng, Z, Feldman. D., 1995. *Synthetic reinforced concrete* [online], 20. Available from: http://ac.els-cdn.com.ezp1.bath.ac.uk/0079670094000306/1-s2.0-0079670094000306-main.pdf?_tid=62cd4044-b30d-11e3-bb13-00000aacb35d&acdnat=1395635762_719c6cc6cc86b1db223c2c926a783af5 [accessed 20th March 2014]

CHAPTER 3 EXPERIMENTAL METHODS

3.1 Thermodynamic modelling

3.1.1 Introduction

Thermodynamic modelling allows the user to investigate the chemical reactions and phase assemblages of mortars with different mix proportions and varying temperature and atmospheric pressure. Thermodynamic modelling has been used extensively to model cement compositions and has proven a reliable predictor of physical and chemical properties in practice (Bolte et al., 2019) (Lothenbach, 2008). There is a lack of information relating to the use of this this software with lime-based materials; however, the chemical composition of lime is simpler than that of cement and the elements comprising lime-based materials are all to be found in cement. It is reasonable to conclude that thermodynamic modelling is a viable technique for this study.

3.1.2 Background theory

The thermodynamic modelling software used in this study is designed to quantify the effects of equilibrium on a system at specific values of temperature, pressure and bulk composition. It is based around the theory of chemical equilibrium. A chemical system will tend towards equilibrium by minimising its Gibbs free energy in a spontaneous reaction. Chemical reactions are spontaneous because they either give off heat energy or they result in an increase in the disorder of the system. The change in Gibbs free energy can therefore be calculated using the formula:

$$\Delta G^0 = \Delta H^0 - T\Delta S^0 \qquad (3.1)$$

where ΔG is the change in Gibbs free energy, ΔH is the change in heat energy, ΔS is the change in entropy and T is temperature.

3.1.3 Software

The thermodynamic modelling software GEM-Selektor v.3 (GEMS3) was used as an initial stage in this investigation to help predict the phase assemblages resulting from different lime/aggregate mixes. GEMS3 is a geochemical modelling programme, which uses an “advanced convex programming method of Gibbs energy minimisation implemented as an efficient Interior Points Method (IPM)” (Paul Scherrer Institut 2015).

The programme requires the user to input a ‘recipe’ of components, which can be selected from the in-built database of independent components, dependent components, compositions or equilibrium phases. Additionally, there are several third-party databases available that can be downloaded and incorporated into GEMS3 software. For this investigation, the third-party database ‘CEMDAT07’ was employed in addition to the default database. This database was developed specifically for modelling cement based reactions; however, it contains several components not available from the default database, but which are essential for modelling lime-based construction materials.

The software can model a single reaction, or a series of reactions, and results can be plotted as absolute values in ‘Lines/Symbols’ mode, or can be plotted as cumulative values in ‘Cumulative’ mode (Figure 3.1).

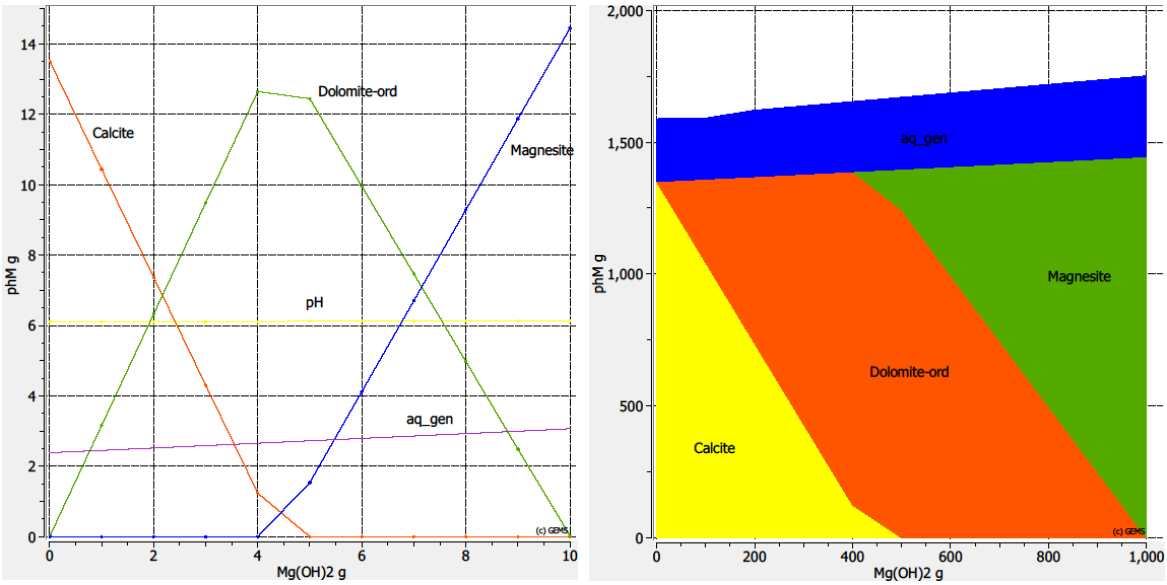

Figure 3.1: Typical thermodynamic modelling plotted results.

3.2 Mechanical strength testing

3.2.1 Introduction

Compressive and flexural strength are not necessarily the most important physical properties for lime mortars. It is, however, important to test for strength in conjunction with testing for other properties such as porosity, granulometry and carbonation in order to obtain a full understanding of the material. There is no specified time intervals at which testing should be carried out, and various studies of lime mortars have included testing at intervals from 3, 7, 28, 60, 90, 120, 140, 180, 270, 360, 540 and 720 days from the date of manufacture (Lawrence, 2006).

3.2.2 Equipment

Mechanical strength testing was carried out to test both the flexural and compressive strength of the experimental materials in accordance with BSEN 1015-11:1999. The tests were conducted using a 50kN Instron 3369 Universal motorised load frame as shown in Figure 3.2. The load frame was connected to a PC running Bluehill 3 software, which monitored and recorded the applied force on the specimen as a function of strain. The maximum force was then used to calculate the compressive stress (equation 3.2) and flexural strength (equation 3.3).

$$\text{Compressive stress} = \frac{F\ (N)}{a\ (mm^2)} \qquad (3.2)$$

where:
F = compressive force, a = cross sectional area of specimen

$$\text{Flexural stress} = \frac{3FL}{2bd^2} \qquad (3.3)$$

where:

F=force

L=distance between supports

b=specimen width

d=specimen thickness

Figure 3.2: Flexural and compressive strength testing of Fibrelime specimens.

The flexural tests were carried out first, and then the compressive tests were completed afterwards using the two halves of the prisms that resulted from the flexural test.

3.3 Phenolphthalein staining

3.3.1 Introduction

The chemical Phenolphthalein ($C_{20}H_{14}O_4$) is the chemical indicator most commonly used to identify areas of carbonation in lime mortars and plasters (Rilem, 1998). Unlike most alternative test procedures, which can only test very small sample sizes, such as TGA, phenolphthalein staining has the advantage that a large area can be sampled in a single test, making it an ideal method for testing the progress of carbonation in a specimen.

3.3.2 Background theory

Phenolphthalein solution is colourless in acidic conditions but turns pink in alkaline solutions, and this property is used to identify carbonation within a specimen. The uncarbonated zone within the specimen (calcium hydroxide) is highly alkaline and appears pink upon spraying with phenolphthalein solution, whereas the carbonated zone (calcium carbonate) is neutral and remains uncoloured (Figure 3.3).

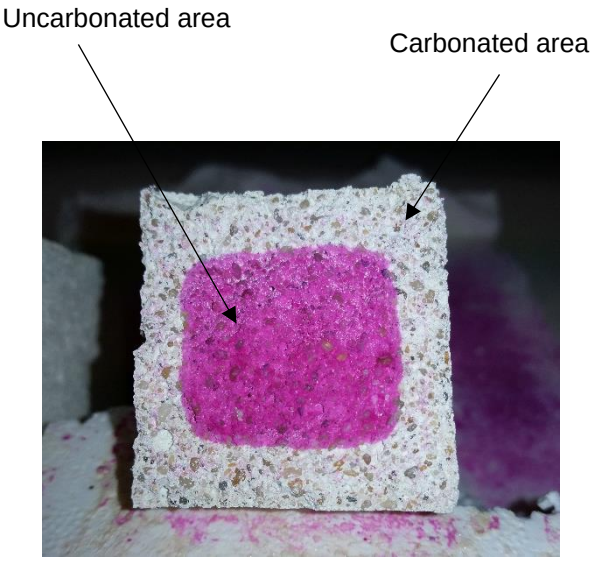

Figure 3.3: Phenolphthalein staining of lime putty.

Phenolphthalein does not change colour at a specific pH level, but over a narrow range. It begins to turn colourless at a pH of about 8.2 and changes colour completely at a pH of about 9.8. One limitation is that the phenolphthalein has a level of inaccuracy due to the fact that it does not change colour sharply at alkaline pH levels (Despotou et al., 2014).

A useful feature of phenolphthalein staining is the ability to observe Liesegang patterns. These are patterns of concentric rings of stained and unstained binder, showing variations in the degree of carbonation at different distances from the surface (Figure 3.4). A study by Rodriguez-Navarro (2001) reported that well developed Liesegang patterns only occur in mortars prepared from aged lime putty and that the

carbonation of these mortars was found to be faster than that of mortars not displaying Liesegang patterns. The smaller portlandite particles in the aged putty enhance dissolution, increase the ion concentration and creates a higher volume of pores with r<0.1µm. The small pores facilitate higher nucleation rates due to the very high supersaturation rates with respect to calcium carbonate, which is a crucial factor in pattern development.

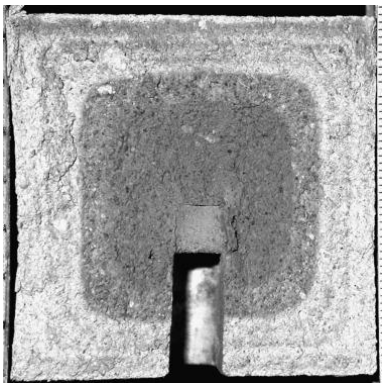

Figure 3.4: Lime mortar specimen showing Liesegang pattern (Lawrence).

3.4 Fourier Transform Infra-Red Spectroscopy (FTIR)

3.4.1 Introduction

Infra-red spectroscopy is a commonly used materials characterisation technique, whereby the chemical composition of a specimen is identified by wavelengths absorption of infra-red energy. It is a useful, non-destructive technique that is often used to provide information about crystalline and amorphous phases present in cementitious materials. It is also very sensitive to the presence of carbonates, and so is a useful technique for the analysis of lime-based materials.

3.4.2 Background theory

The technique is carried out using a spectrometer, which irradiates the specimen with an infra-red beam over a range of wavelengths, typically between 400 and 4,000

cm^{-1}. Some of the radiation will pass through the sample (transmittance) and some will be absorbed by the sample (absorption). Absorption occurs when the infra-red frequency of the beam matches the vibrational frequencies of the chemical bonds within the sample. All chemical bonds vibrate at different frequencies and this can be used to identify the composition of the specimen. Absorption in the infra-red region is plotted against wavenumber to produce a characteristic 'spectrum'.

Different regions of the spectrum provide specific information about the test specimen. The region from 0 to 1450 cm^{-1} is known as the fingerprint region and usually contains a complicated arrangement of peaks which are unique for each different compound. The region between 1450 cm^{-1} and 4000 cm^{-1} is the functional group region, which typically contains relatively few peaks. In the spectrum shown in Figure 3.5, the clear peak at around 3300 cm^{-1} is an O-H peak characteristic of calcium hydroxide.

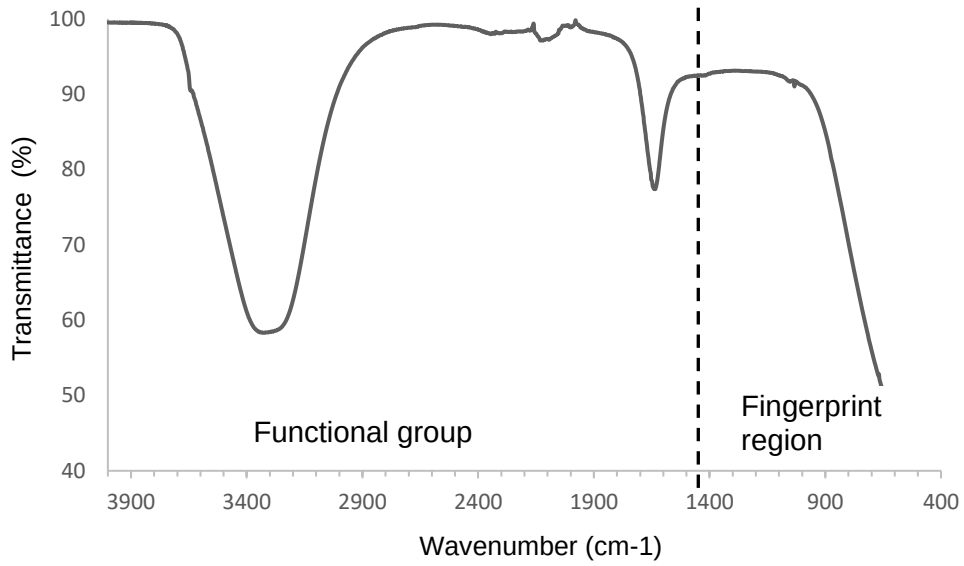

Figure 3.5: FTIR spectrum for a typical lime putty.

The infra-red beam can induce either stretching or bending vibrations in the molecule and this is dependent on the frequency (and hence the energy) of the infra-red source. Generally, it takes less energy to bend a bond than to stretch (or compress) it, and for this reason, bending vibrations typically occur in the fingerprint region of the

spectrum, whilst stretching vibrations are normally associated with the functional group region (Figure 3.5). Stretching vibrations involve a change in bond length, whilst in bending vibrations it is the bond angle that changes. When bonds stretch in-phase it is termed ‘symmetrical stretching’ and when bonds stretch out-of-phase this is called ‘asymmetric stretching’.

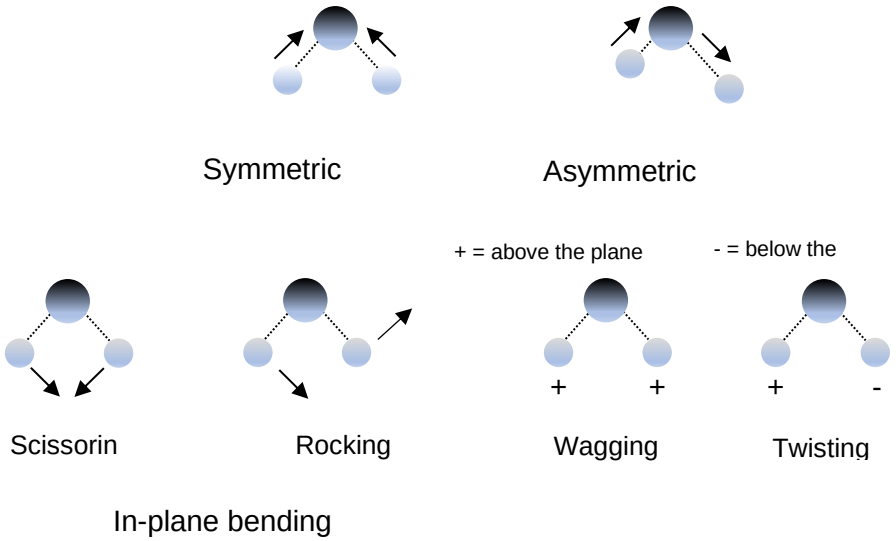

Figure 3.6: Vibrational modes in a molecule.

There is a finite number of ways in which a molecule or ion can move. These are known as ‘degrees of freedom’. For an atom moving in 3-dimensional space, its translational movement can be described using 3 coordinates, so its degree of freedom is 3. If the molecule has N atoms, the value will be 3N. In addition to translational movement, the movement can also include rotation and vibration. For a non-linear molecules, therefore, the degrees of vibrational modes can be calculated using the formula:

$$3N - 5 \qquad (3.4)$$

For a linear molecule, rotation around its own axis is not taken into account because it does not change the molecule. The degrees of freedom for non-linear molecules is calculated using the formula:

$$3N - 6 \qquad (3.5)$$

A limitation of infra-red spectroscopy is that it is not effective on all molecules. For a substance to be IR active, the vibrations induced by the Infra-red energy must cause a net change in the dipole moment of the molecule. For this reason, the vibrations of symmetrical molecules (i.e. N_2, O_2) will not be IR active. By contrast, Raman spectroscopy is only effective on symmetrical molecules, and is therefore considered a good complimentary technique to use in conjunction with infra-red spectroscopy.

3.4.3 Equipment

The equipment used to carry out the FTIR analysis for this work was a PerkinsElmer Frontier model (Figure 3.7). The spectrometer was connected to a computer running PerkinElmer Spectrum 10 Spectroscopy software, which plots the results and can automatically label all the peaks in the spectrum to aid analysis.

Figure 3.7: PerkinElmer FTIR spectrometer.

Figure 3.8 shows a simplified schematic of a two-beam absorption spectrometer. The beam of infrared light is generated at the infra-red source and travels through the interferometer and then split into two separate beams. One beam travels through the specimen and the other travels through a reference. Both beams are then reflected back to an optical chopper, which alternates the beams entering the monochromator. The two beams then travel on to the infra-red detector where the beams are compared and the results are plotted by the software.

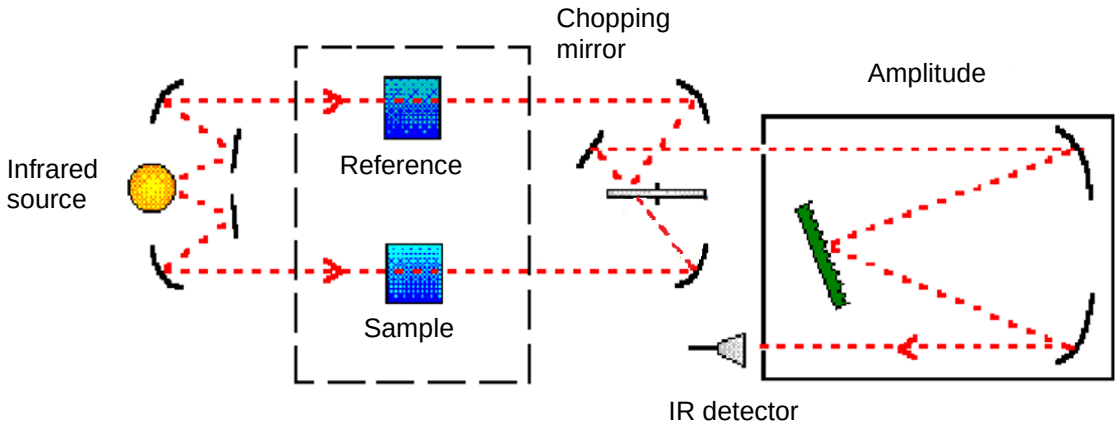

Figure 3.8: Schematic drawing of the operation of a PerkinElmer Frontier FTIR spectrometer (Abihuynh).

3.5 Raman spectroscopy

3.5.1 Introduction

Raman spectroscopy is a technique that analyses the molecular vibrations of a sample material for identification. It is based on the principle of inelastic scattering of light. It is a non-contacting, non-destructive, works on almost all materials and typically requires no sample preparation.

3.5.2 Background theory

The technique involves irradiating the specimen surface with a laser and then analysing the inelastically scattered light that is emitted. Most of the light photons from the laser are absorbed and promote the sample molecule momentarily to a higher vibrational state (virtual state) before being instantly scattered elastically back to the initial energy level (ground state). However, a very small number of photons lose or gain energy and are scattered inelastically and return to a vibrational state that is higher, called an excited state (Anti-stokes scattering) or lower (Stokes scattering) than their original state (Figure 3.9). The Raman effect is very weak; only about 1 part in a million of the scattered photons are scattered inelastically.

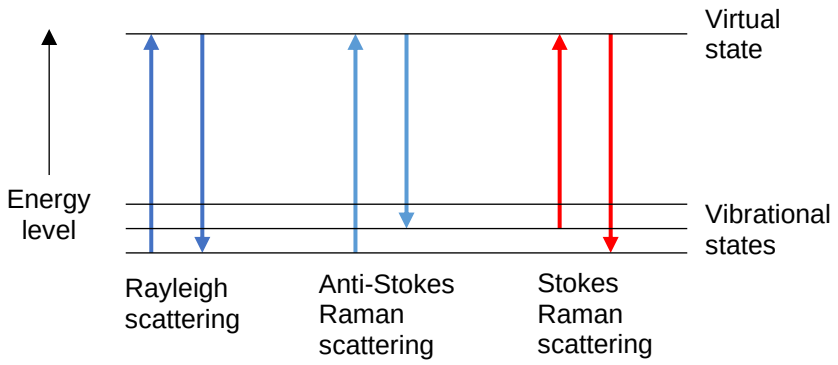

Figure 3.9: Different types of light scattering possible in a polarisable molecule.

It is possible for a small number of molecules in a sample to exist in an excited state at normal ambient temperature. Anti-stokes scattering is therefore much weaker than Stokes scattering as the intensity is reduced by molecules relaxing to their ground state. If the sample is heated, the opposite effect is seen, with Anti-stokes scattering increasing relative to Stokes scattering. It is normally Stokes scattering that is detected, but detecting Anti-stokes scattering may be preferable in systems where fluorescence is a concern. Fluorescence occurs when a molecule is excited to a higher electronic state, as distinct from a higher vibrational state. The molecule will usually remain in this excited state for a period of 0.5 – 20ns, known as the resonance lifetime; however, the excitation of virtual states in Raman microscopy requires the molecule to

immediately emit a photon rather than remaining in this excited resonance state. Fluorescence can become a problem when its high background signal swamps the weaker Raman bands (Edwards, 2009).

Data obtained from Raman spectroscopy is used to plot a spectrum of the material under test, where the frequency of the incident beam is plotted on the x axis and the intensity of the output signal (inelastically scattered photons) is plotted on the y axis (Figure 3.10).

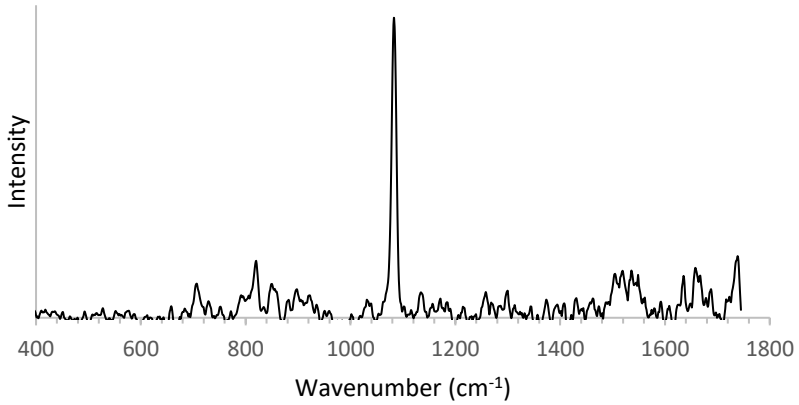

Figure 3.10: Raman spectrum of calcite.

Not all materials can be analysed using Raman spectroscopy. The molecules of the material under test must be polarisable for the required inelastic scattering to take place. The polarizability of a material relates to how easily the molecular orbit can be deformed to create an induced dipole moment. This effect is most noticeable on relatively neutral atomic bonds such as C-C, C-H and C=C. In contrast, Infra-red spectroscopy is based on detecting changes in the dipole moment of a molecule. In general, molecular vibrations that are Raman active are not Infra-red inactive and vice versa. Raman and Infra-red spectroscopy are thus considered to be complimentary techniques.

Raman spectroscopy is a very versatile technique for material analysis, as it requires minimal sample preparation, is non-destructive and can be carried out on both solids and liquids. It can be used to determine whether materials are the same or

different by comparing their Raman spectra and can distinguish between polymorphs of the same chemical. It is a particularly valuable technique for identifying different phases of lime materials within a sample mortar or plaster. $CaCO_3$ produces a strong peak at around 1085 cm^{-1} and its polymorphs (calcite, vaterite and aragonite) all display distinctive peaks in the 700 – 800 cm^{-1} region (Kontoyannis & Vagenas, 2000). $Ca(OH)_2$ can be identified by a strong peak at 3620 and 3640 cm^{-1} (Dawson et al, 1973). Also, due to its sensitivity to the local environment, Raman spectroscopy can be used to obtain spectra from samples that do not have any long range structural order. The advantage of this is that materials such as C-S-H can be analysed, which would not be possible with X-ray diffraction.

A disadvantage of the technique is that the laser spot size is typically in the order of microns and therefore provides very localised information about the sample. The minimum laser spot size is determined by the choice of aperture used and is given by:

$$D = \frac{1.22 * \lambda}{NA} \qquad (3.6)$$

Where λ is the wavelength used and NA is the numerical aperture of the focusing objective. The shorter the wavelength and the higher the numerical aperture used, the smaller the spot size. This can be a disadvantage for non-homogenous samples but can be mitigated by carrying out a scan whereby an area of the sample is scanned by the laser and a map of the different phases is produced. The depth to which the laser penetrates the sample is determined by the wavelength of the laser used and the type of material and is given by:

$$h = 2.53 * \lambda (f / D)^2 \qquad (3.7)$$

where h is the depth of penetration, λ is the wavelength, f is the focal length of the microscope and D is the effective laser beam diameter. Figure 3.11 provides an overview of the effect that wavelength has on sample penetration (Lewandowska, 2010).

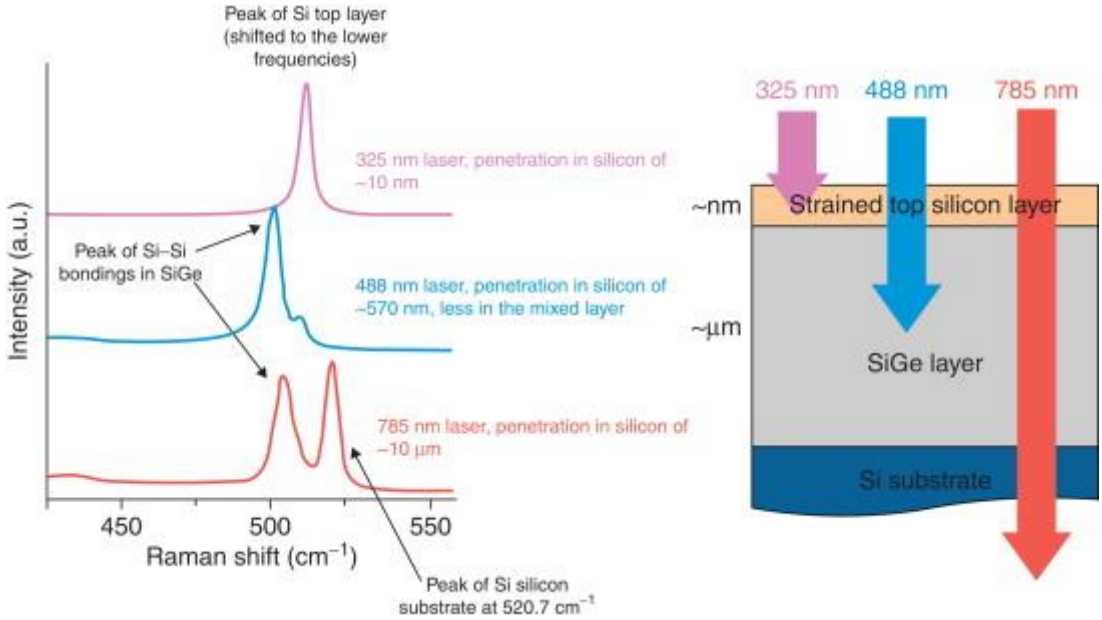

Figure 3.11 An example of the application of the UV excitation to analyse a thin silicon cap layer. The figure on the right shows schematically the depth penetration of different wavelengths; on the left, one can see the Raman spectra recorded using the respective wavelengths (Lewandowska, 2010).

3.5.3 Equipment

For the work carried out during this study, a Renishaw InVia Raman Spectrometer was used. A self-collimated, highly monochromatic laser beam in the ultraviolet (UV), visible (Vis) or near infra-red (NIR) range is used to irradiate the sample. The light scattered by the sample is collected with a lens and is directed through an interference filter or spectrophotometer to obtain the Raman spectrum (Figure 3.12).

Figure 3.12: Renishaw InVia spectrometer.

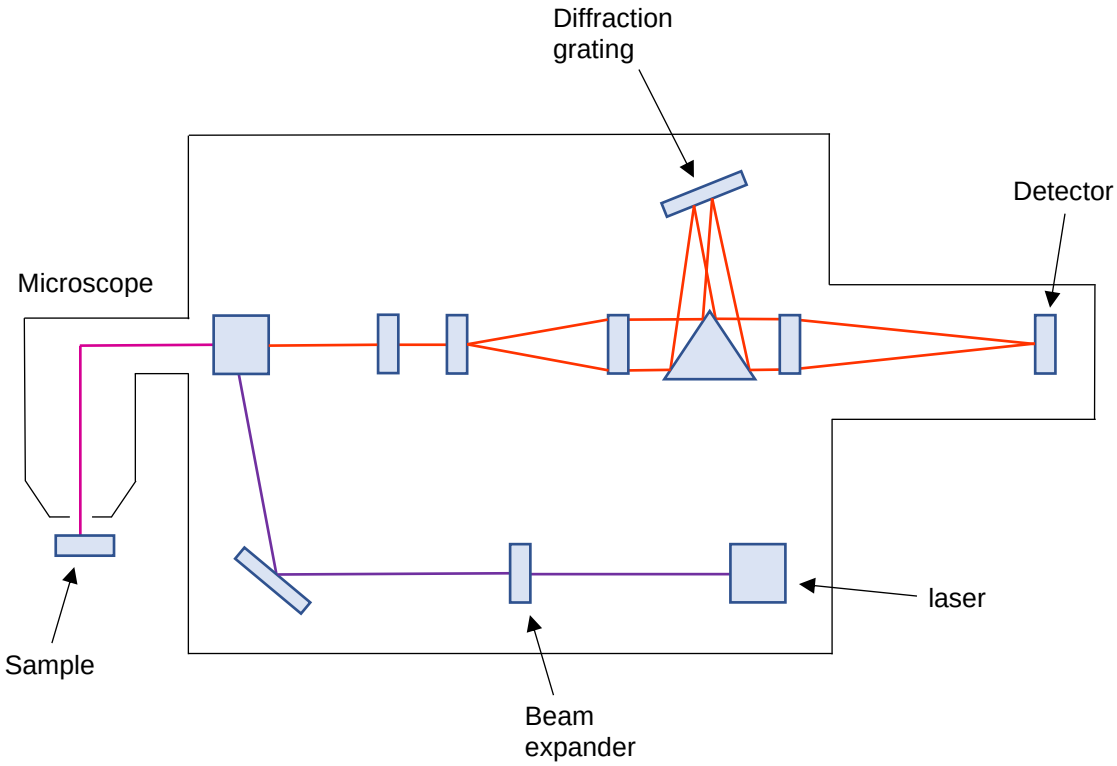

Figure 3.13: Schematic of Raman microscope.

3.6 X-Ray Diffraction (XRD)

3.6.1 Introduction

X-ray diffraction is a technique used to determine information about the crystal phases present in materials. XRD exploits the fact that the extremely small distances between atoms in a crystal lattice causes it to act as a diffraction grating for X-ray wavelengths similar to the spacings between planes in a crystal lattice. The extremely small distances between rows of atoms, in the order of a few nanometres, makes them natural diffraction gratings for X-rays.

3.6.2 Background theory

The operation of XRD is most often explained using a geometric explanation based the theoretical reflection of X-rays and their interpretation using Bragg's law. In this explanation of XRD, incident X-rays are reflected from atoms in different rows of a crystal lattice (see Figure 3.14), resulting in constructive interference when the reflected rays from different rows in the lattice are in phase with each other. The reflected rays are collected by an X-ray detector and the signal is plotted against the angle of incidence, with the points of constructive interference appearing as characteristic peaks in the 'diffraction pattern' (Figure 3.15).

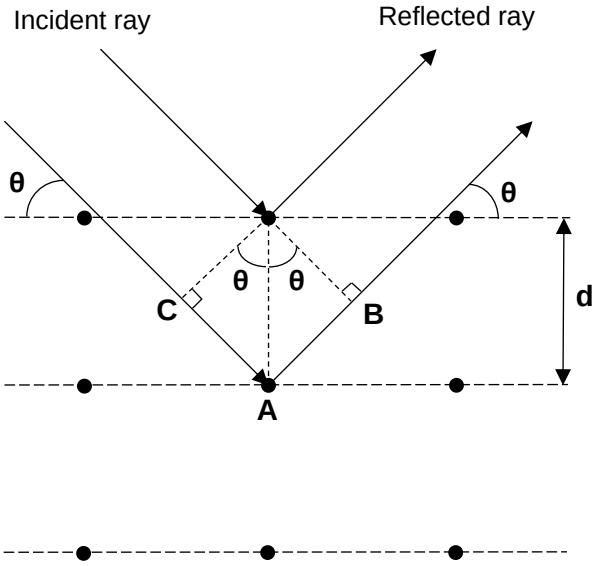

Braggs law: maximum constructive interference when $n\lambda=2d\sin\theta$

Where:
n = a positive integer
d = the distance between lattice planes
θ = angle of incident X-ray

Figure 3.14: X-rays diffracted in a crystal lattice and Braggs Law.

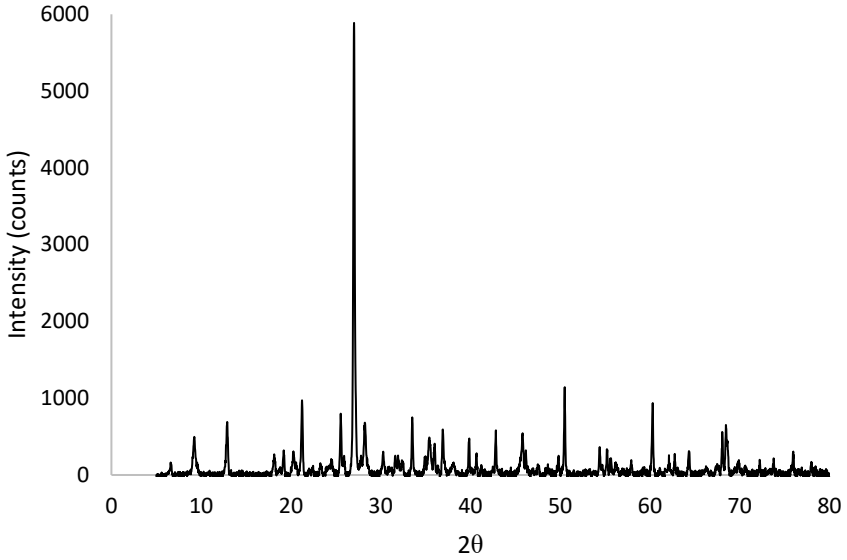

Figure 3.15: XRD pattern for slate.

The incident X-ray beam has a wavelength λ and an angle θ to the crystal lattice. The distance between the rows of atoms is d. The X-ray diffracted from the second row of atoms in the lattice travels a distance of CA + AB farther than the X-ray diffracted by the first row. For constructive interference to occur, this difference in the distance travelled by the two X-rays must be equal to an integer number of wavelengths. Using trigonometry, it can be seen that CA and AB are both equal to dsinθ, which leads to the Bragg equation:

$$2d\sin\theta = n\lambda \qquad (3.8)$$

When the wavelength of the X-rays and the angle θ are known quantities, the Bragg equation can be used to calculate the spacing between crystal planes.

The X-rays are produced by colliding electrons with a metal target. A filament provides a source of electrons, which are accelerate by a high voltage towards a metal anode. The anode must be metallic so that it conducts the electrons and have a high melting point, which limits the choice to chromium (Cr), iron (Fe), cobalt (Co), copper (Cu), molybdenum (Mo) and a number of other less commonly used materials. The high energy incoming electrons can dislodge one or more K shell electrons from atoms

in the anode (Figure 3.16). Removal of a K shell electron ionises the atom and makes it unstable. Electrons from the outer shells then move to the K shell to fill the vacancy and stabilise the atom. As an electron moves to the k shell it emits an x-ray of energy equivalent to the difference in energy levels of the two shells involved. The X-ray emission is named after the shell from which the electron is ejected and the number of shells higher from which it is filled. So, an electron falling from the L shell to the K shell is K α radiation and an electron falling from the M shell down to the K shell would be K β radiation.

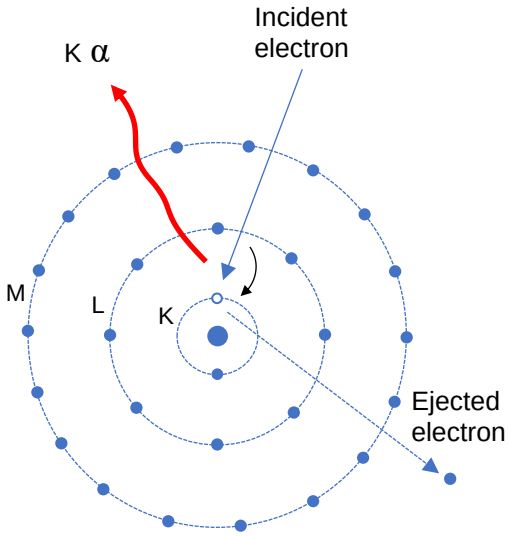

Figure 3.16: Generation of X-rays.

XRD is normally used for the study of crystal materials. It requires minimal sample preparation, other than grinding the sample material into a powder if it is not flat, and data interpretation is relatively straight forward. However, overlapping of peaks can make it difficult to identify multi-phase materials. A typical XRD pattern for slate is shown in Figure 3.15. The 2θ position of each peak on the x axis is used to identify the minerals within the sample and the height of each peak represents the relative proportions present within the sample.

XRD is a very useful tool to help identify the phases in lime-based construction materials. Data relating to characteristic peaks for these chemical compounds is readily available. The XRD peaks for the main lime compounds encountered in this work is shown in Table 3.1.

Table 3.1: XRD data of relevant compounds (Mineraldata).

	Chemical formula	**2θ**	**I (%)**	**2θ**	**I (%)**	**2θ**	**I (%)**
Lime	CaO	37.36	100	53.85	45	32.20	34
Portlandite	$Ca(OH)_2$	34.09	100	18.09	74	47.12	42
Calcite	$Ca(CO_3)$	29.40	100	43.14	18	39.40	18
Aragonite	$Ca(CO_3)$	26.22	100	45.86	65	27.22	52
Vaterite	$Ca(CO_3)$	32.78	100	27.00	100	24.85	100
Quartz	SiO_2	26.65	100	20.85	22	50.14	14
Chamosite	$(Fe^{++},Mg,Fe^{+++})_5 Al(Si_3Al)O_{10}(OH,O)_8$	25.28	100	12.55	100	35.60	90
Muscovite	$KAl_2(Si_3Al)O_{10}(OH,F)_2$	26.83	100	8.88	95	34.88	55

3.7 Scanning Electron Microscopy (SEM)

3.7.1 Introduction

SEM can be used to obtain detailed images of samples at far greater magnifications than is possible with optical microscopy. Of particular benefit is the ability to identify crystal habits and to visually analyse the interface between binder and aggregate. Additionally, SEM can be used for elemental analysis.

3.7.2 Background theory

The technique involves scanning a sample in a vacuum with a focussed beam of electrons. The incident electrons interact with the surface of the sample being imaged and may cause the emission of elastically and inelastically scattered electrons, secondary electrons, backscattered electrons or generation of X-rays (Figure 3.17). These emitted electrons can be detected and used to compute an image or provide elemental analysis of the sample.

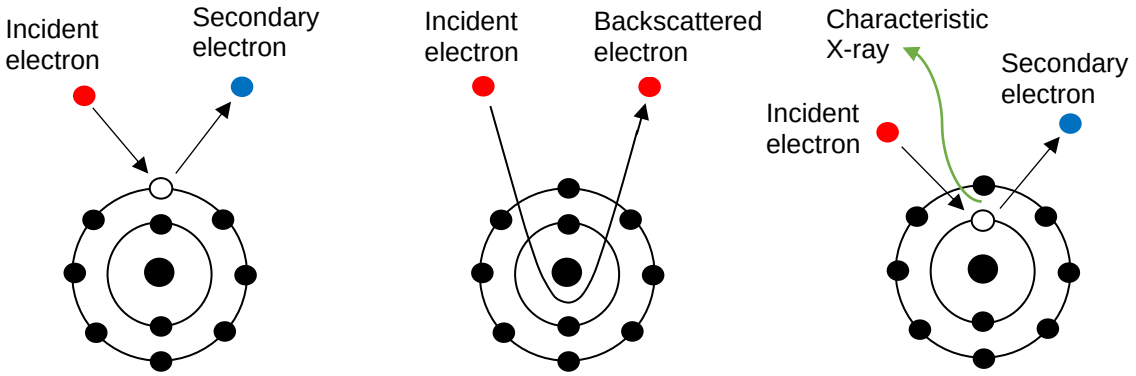

Figure 3.17: Incident electron interaction with sample.

. Secondary electrons originate from the surface of the sample, and for this reason they are best for imaging the topography of a sample. They are caused by incident electrons ejecting valence electrons from the surface of the sample. Secondary electrons are low energy, and therefore any electrons ejected from a deep region within the sample are quickly reabsorbed. Only electrons from the top surface of the sample are emitted out from the specimen. The negatively charged electrons are easily collected by a positively charged detector. The attraction force between electrons and the detector facilitates detection of electrons from a wide area and from around corners, giving secondary electron images a 3-dimensional look (Iowa State University, 2019). Also, the amount of secondary electron emission is greater when the incident electron beam enters the sample obliquely (Figure 3.18).

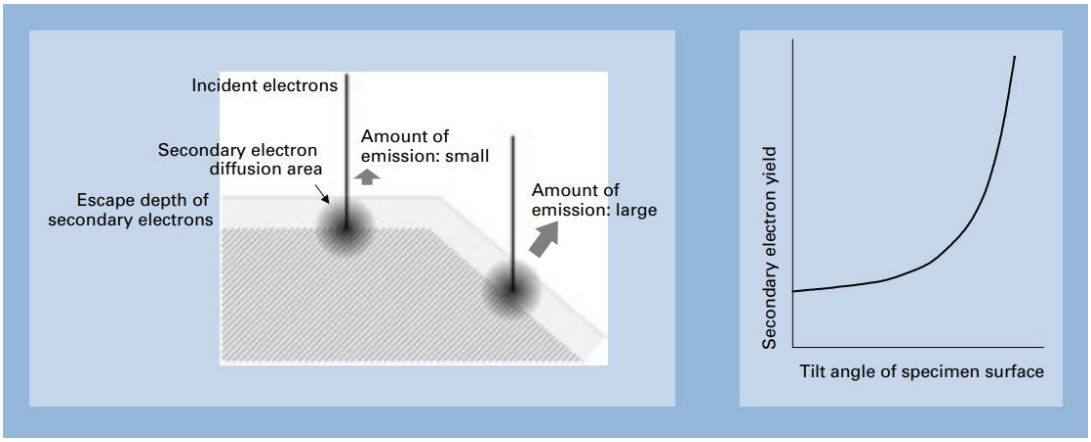

Figure 3.18: Relationship between the incidence angle of the electron probe and the secondary electron. (JEOL).

Backscattered electrons occur when incident electrons are attracted to the nucleus of the sample, but rather than being captured by the positively charged nucleus, they circle the nucleus and exit back out of the sample without losing any energy. Backscattered electrons possess more energy than secondary electrons and therefore provide information from a relatively deep region of the sample. Backscattered electrons are sensitive to the chemical composition of the sample, with the number of electrons increasing with increasing atomic size. This characteristic can be exploited to identify the different elements in a sample. Differences in the number of electrons produces differences in the brightness within an image, with brightness increasing with increasing electron density. This produces contrast between different atomic weight elements and is a useful feature to help identify the different phases and pore structure within a sample, although the images have lower resolution compared to secondary electrons (Diamond, 2004, p.920).

When a primary beam electron interacts with an inner shell electron in the sample, this can cause the electron to be ejected from that shell (Figure 3.6). This leaves the atom with a missing inner shell electron, which is filled by an electron dropping down

from an outer shell. The electron dropping from an outer shell to an inner shell releases energy in the form of an X-ray. The energy levels of each shell are specific to each element and so the emitted X-ray will have a specific and unique value, allowing elemental composition to be identified. These X-rays are thus called Characteristic X-rays. The high energy of characteristic X-rays means that, in comparison to secondary and backscattered electrons, they can travel long distances and can be generated at a greater depth within the sample.

Electromagnetic radiation can also be generated when incident electrons undergo deceleration as they interact with the Coulombian field of the sample electrons. This is known as 'bremsstrahlung'. As the electrons decelerate, they lose energy, which is emitted in the form of X-rays. These X-rays, however, can have any energy value from zero up to the original energy of the incident electron and cannot therefore be used for elemental analysis.

Each type of signal generated originates from a specific emission volume within the sample (Figure 3.19). The depth and volume of penetration in the sample by the incident electron beam depends on the energy of the electron beam and the chemical composition of the sample. The electron beam will penetrate further into a sample of low atomic number than it will in a sample having a high atomic number and increasing the accelerating voltage of the primary electron beam will also increase penetration. The energy spectrum of the emitted electrons falls into three distinct regions:

i Elastically scattered electrons with energies similar to those of the primary electron beam

ii Multiply scattered electrons with energies in between 50eV and the energy of the primary electron beam

iii Low energy electrons of less than 50eV

Secondary electrons are in group iii and backscattered electrons should be in group i, although a significant proportion of backscattered electrons fall within group ii due to slight inelastic effects (Lloyd, 1987).

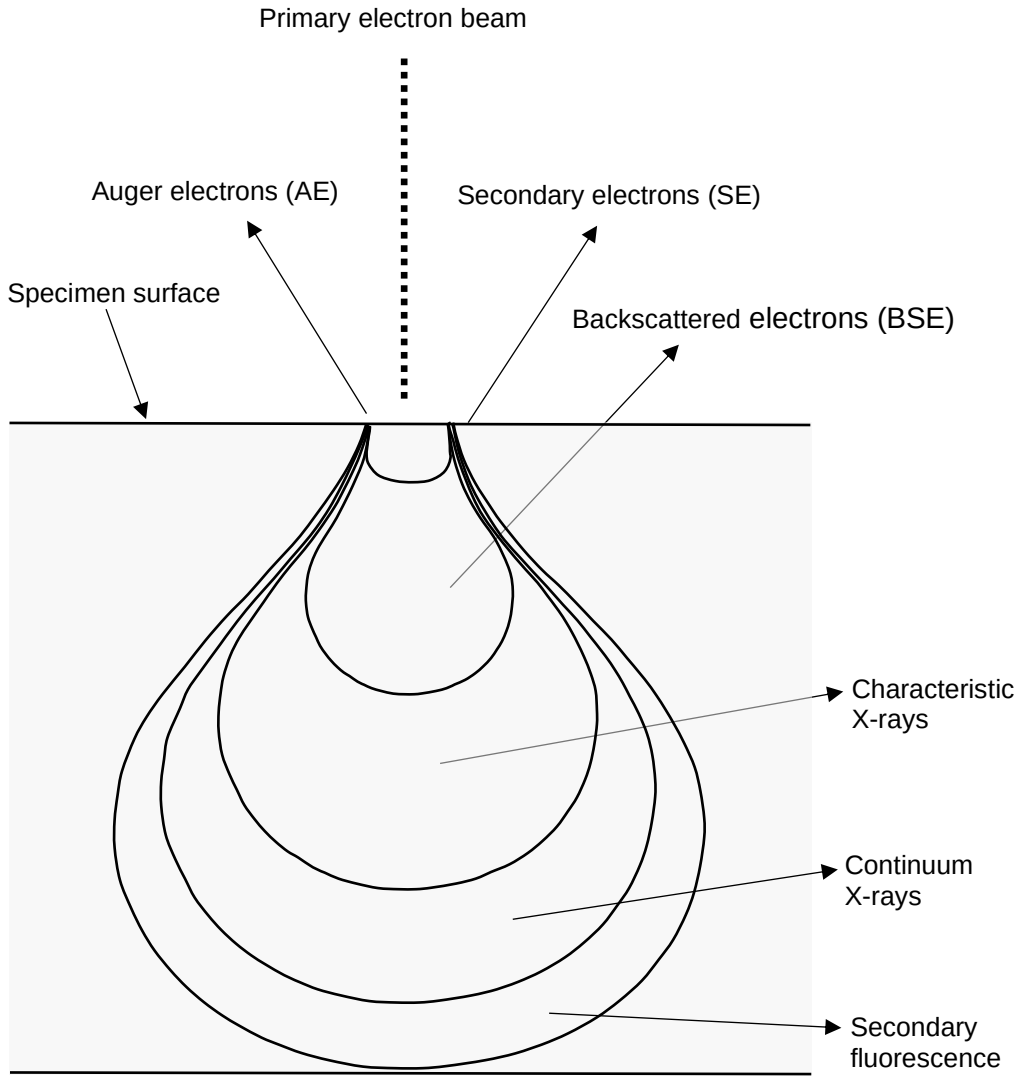

Figure 3.19: Electron penetration of sample.

3.7.3 Equipment

A schematic of a scanning electron microscope is shown in Figure 3.20. The electron gun comprises a tungsten filament that is heated up to lower the work function of the tungsten and make it easier for the electrons to be drawn off. Electrons are then accelerated towards the positively charged anode. Some of the electrons hit the anode, but some of the electrons pass through an opening and carry on down the column towards the sample under test. The voltage of the anode determines the velocity at

which the electrons are accelerated down the column. The condenser lenses are circular magnets that focus the electrons into a small diameter beam, the diameter of which can be adjusted according to the resolution required. The electron beam then passes through the scanning coil, which scans the beam over the surface of the sample. The scan of the coil is synchronised with the scan of the viewing screen to produce the image.

The chamber in which the electron gun, electron beam and sample are housed is maintained at a high vacuum during operation. This is because any gas remaining in the chamber could interact with the electron beam or emitted electrons.

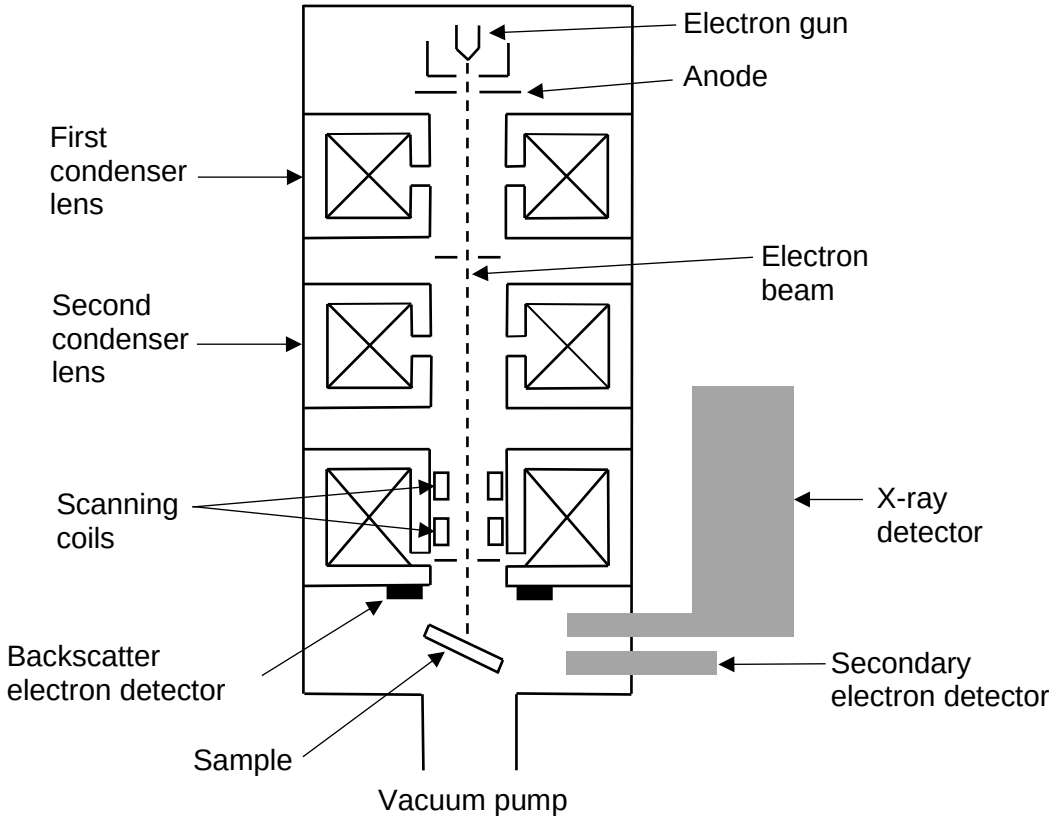

Figure 3.20: Schematic diagram of a scanning electron microscope.

Specimen preparation is very important for successful results. The specimen must meet certain requirements before it is loaded into the microscope:

- The sample surface must be exposed
- The specimen must be fixed firmly to the specimen mount
- The specimen must be conductive

Powdered specimens such as the olivine and lime mortar investigated during this work, had to be dusted onto conductive double-sided adhesive tape, ensuring they are dispersed as much as possible across the tape.

Non-conductive specimens require surface coating with a thin film of a metallic substance in order to make them conductive. Typical methods to achieve this are by vacuum evaporation and ion sputtering. The specimens in this work were prepared using ion sputtering. Alternatively, the specimens can be mounted on a carbon disc.

A problem that is sometimes encountered during scanning electron microscopy is charging of the specimen. Electrons entering a specimen lose their energy and are absorbed by the specimen. In conductive specimens the electrons pass through the specimen to ground. If the path to ground is broken, though, even conducting specimens will rapidly accumulate charge causing a rise in surface potential. Charging is more often encountered with specimens that are partially or completely non-conductive. The electrons hitting the specimen cannot easily disperse to ground, resulting in charge accumulation, which alters the surface potential of the specimen. Incoming electrons will then be repelled by the negatively charged specimen. This results in distorted images that suffer from drift, blur and low contrast.

3.8 Transmission electron microscopy (TEM)

3.8.1 Introduction

Transmission electron microscopy offers the most powerful magnification of the electron microscopes, at a maximum of around five million times, and is used in a number of different fields including materials science, metallurgy, life science, biology,

nanotechnology, forensic analysis, geoscience and in the semiconductor industry (Wen, 2014).

3.8.2 Background theory

Transmission electron microscopy (TEM), like scanning electron microscopy, utilises a focussed beam of electrons directed at a specimen to provide morphologic, compositional and crystallographic information about a sample.

EM is a very useful characterisation tool for use with nanomaterials due to the high magnification achievable. It can help in determining structure, composition and in some cases bonding information. No other technique is capable of analysing the nanoscale heterogeneity of aerogel and aerogel composite materials (Stroud et al., 2004).

TEM was used in this investigation for materials having nano dimensions: aerogel particles and colloidal nanosilica. The equipment used for this work was a JEOL JEM1200EXII transmission electron microscope operating at 120 kV.

3.8.3 Equipment

A schematic of a transmission electron microscope is shown in the schematic drawing in Figure 3.21. The electron beam is produced by the electron gun comprising a filament, normally of tungsten, which is heated in order to activate the electrons and then these electrons are accelerated by applying a high voltage (TEM working voltage). The beam of electrons is controlled by the condenser lenses. The first condenser lens controls the beam size and the second condenser lens controls the beam intensity. The condenser aperture is adjustable and controls the image resolution: a smaller condenser aperture produces a higher resolution image, whilst a larger aperture is normally used for general observations. The objective lens is the most important lens, as it forms the first image and diffraction pattern of the specimen, which are then further magnified by the intermediate and project lenses. If there are any distortions in the first image or diffraction pattern, these will become severe after the higher magnification. The viewing screen is coated with phosphorescent powders, and these emit visible

light upon irradiation with high energy electrons. The images produced can be captured by a CCD camera and saved as digital files (Luo, 2016)

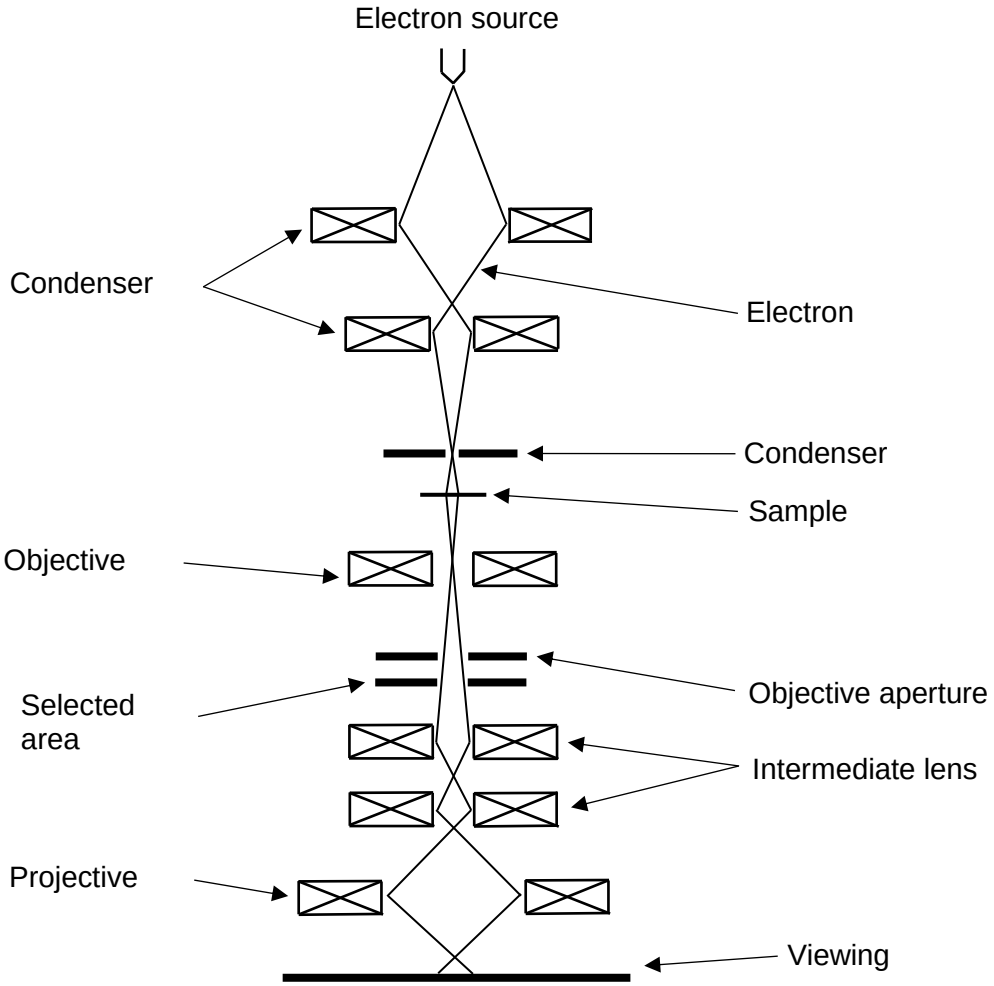

Figure 3.21: Schematic diagram of a transmission electron microscope.

3.9 Optical microscopy (Polarised light microscopy)

3.9.1 Introduction

Polarised light microscopy is an investigative technique used in the earth sciences for examining rocks and minerals. These types of material are visible in a polarising microscope primarily due to their optically anisotropic nature. Specimens are viewed in 'thin section' and the technique cannot, therefore, be used to analyse surface topography.

3.9.2 Background theory

Polarised light microscopy involves illuminating a thin section of the sample material with polarised light. This has the effect of enhancing contrast in birefringent materials, which have varying optical properties depending on the orientation of the incident light with the crystallographic axes.

The thin section sample is a specially prepared thin slice of the material 0.03mm thick. The thin slice is cut from a larger sample using a diamond saw and is then mounted on a glass slide and ground smooth using progressively finer abrasive grit. As lime mortars are relatively friable, they need to be consolidated with epoxy resin before grinding. Also, as lime samples are sensitive to heat and water, the drying and resin curing stages of preparation need to be carried out at low temperature (<60˚C) and the coolants used during cutting and grinding need to be oil and alcohol based rather than water.

Thin section petrography is a particularly valuable technique for analysing lime mortars and plasters. Hughes et al. (2012) claimed that the technique is the 'most suitable analytical technique' for identifying Roman cement and Ingham (2012) rates petrographic examination as the 'most useful technique for the investigation of lime mortars'. Examination of thin section slides provides a large amount of information about materials in the sample, their relative proportions, texture, porosity and condition. This is particularly beneficial when investigating for evidence of decay as a result of leaching, salt attack, freeze thaw damage and, where Portland cement is present, sulphate attack (Ingham, 2012).

3.9.3 Equipment

A polarising microscope is equipped with a polariser, which must be positioned in the light path between specimen and the illuminator, and an analyser (second polariser), which must be positioned in the optical path between the objective aperture and the camera. Polarisation of the light is achieved by using a synthetic film into which tiny crystals of iodoquinine sulphate are embedded, oriented in the same direction. Two separate light waves are produced, polarised in mutually perpendicular planes. The light waves pass through the specimen and are recombined at the analyser with both constructive and destructive interference. The images produced can be viewed through the binocular eyepiece or with a suitable digital single lens reflex (DSLR) camera and software they can be recorded digitally on a computer.

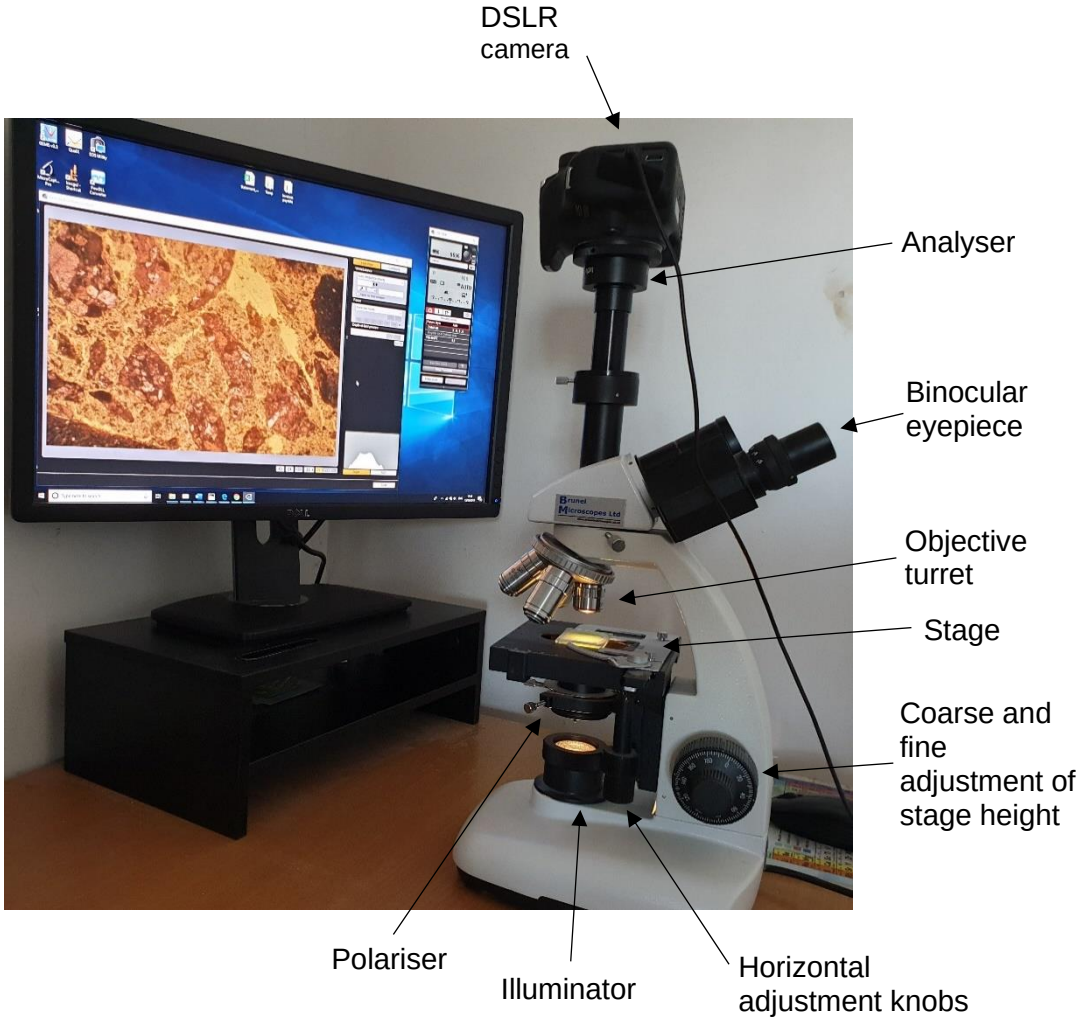

Figure 3.22: Petrographic microscope.

3.10 Stereo microscopy

3.10.1 Introduction

Stereo microscopy has been in use for hundreds of years, but the first stereo microscope as we know them today was introduced in 1957 by the American Optical Company. The stereo microscope is used for lower magnification work than compound microscopes, typically up to 100X. Unlike compound microscopes, the stereo microscope uses reflected light to illuminate the sample being viewed. This allows examination of thicker samples that cannot be viewed by compound microscopy, making it a valuable tool for studying samples with complex surface topography.

3.10.2 Equipment

The stereo microscope (Figure 3.23) generates a three-dimensional image of the specimen. It is able to achieve this because it has separate objective lens and eyepieces for each eye. As the user looks into a stereo microscope, the two light paths image the specimen from slightly different angles, which the user interprets as stereo vision.

Figure 3.23: Leica M 205 C Stereo microscope.

The schematic shown in Figure 3.24 shows the two separated light paths in a stereo microscope (a) that are required to achieve true stereo vision. Example (a) shows the arrangement that might be found in a more conventional stereo microscope, which would achieve a moderately large working distance. Example (b) shows a stereo microscope with an extremely long working distance. This type of microscope is typical of those used in medical applications.

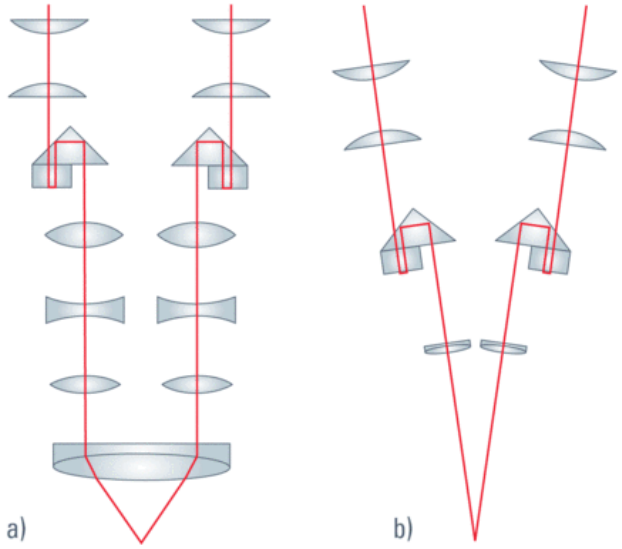

Figure 3.24: Separated light paths in two different stereo microscopes (Leica).

3.11 Particle size analysis

3.11.1 Introduction

Determination of particle size can be a very important tool in analysing aggregate materials. This is particularly true for any material that might have a pozzolanic effect because the reactivity of these materials is determined not just by their chemical composition but also by their particle size and hence surface area, with finely ground pozzolans being substantially more reactive than coarse ones (Moropoulou et al, 2004).

3.11.2 Equipment

Particle size distribution of aggregates for use in mortars and renders is normally carried out by sieve analysis in accordance with BS EN 933 – Part 1. Sieving divides the material into size fractions by passing the material through a column of progressively smaller mesh sieves and then weighing the amount of material that passes through each sieve as a percentage of the total mass of aggregate being tested. Typical mesh sizes are 0.063, 0.125, 0.25, 0.5, 1, 2, 4mm.

For this work particle size analysis was also carried out using the Malvern Mastersizer system to analyse the fine olivine sand. This was necessary because the olivine sand tended to agglomerate and clog up the small mesh size sieves. This equipment consists of an optical unit, a sample preparation accessory and a computer system. The sample preparation accessory is used to prepare the sample before delivery to the optical unit. In this case, this involved mixing the olivine granules in distilled water and passing the sample through the optical unit. The optical unit then directs a laser light at the sample and collects the light scattered from it. This data is collected and fed to the computer system, which calculates the particle sizes using the Malvern software. The equipment can be fitted with a range of different lens sizes, according to the size of particles being measured. For this test work, the 300mm lens was used.

3.12 Thermal conductivity testing

3.12.1 Introduction

The ability to investigate accurately the thermal properties of construction materials is essential. The thermal efficiency of buildings in the UK is highly regulated and controlled by building regulations. The range of thermal conductivities can vary considerably depending on the structure, density and porosity of the material. Values as low as 0.01 W/mK can be seen in loose powders with low interstitial gas pressure, whilst the thermal conductivity of dense crystals may be as high as 10,000 W/mK or higher. Because of this large variation in thermal conductivities, a number of different experimental techniques have been used for different materials.

3.12.2 Equipment

Thermal conductivity measurements for this work were obtained using the transient hot strip method (Figure 3.25). This method is particularly suitable for thermal conductivity measurement of porous substances and has previously been used on plasters (Singh, 1984). The method works by measuring the temperature rise at a known distance from a linear heat source. The linear heat source and a temperature sensor (thermocouple) are incorporated, at a known distance, within the sensing strip. To take the measurements, the sensing strip is placed between two similar specimens. Upon commencing the measurement process, a constant direct current is passed through the strip causing its temperature to rise and generate a stable temperature within the test specimens. The temperature increase will cause a corresponding change in voltage across the strip. Temperature data are recorded at regular intervals and for a predetermined period as programmed by the user. The variation in voltage is used to obtain precise information about the heat flow between the strip and the test specimens (Log, 1992).

Figure 3.25: Thermal conductivity test using the ‘hot strip method’.

3.13 Thermogravimetric analysis (TGA)

3.13.1 Introduction

Thermogravimetric analysis is used to provide useful information about the chemical composition of a material by measuring changes in physical and chemical properties at increasing temperature. There are two modes of thermal analysis used: ‘differential thermal analysis’ (dTG), which measures changes in heat content as a function of increasing temperature and ‘thermogravimetric analysis’ (TG), which measures changes in weight as a function of increasing temperature. The two techniques can provide information relating to physical and chemical phenomena such as: chemisorption, desolvation, decomposition, oxidative degradation, solid state reactions and solid – gas redox reactions (Coats et al., 1963).

3.13.2 Background theory

The analysis is carried out by plotting the resultant data on a graph with temperature on the x-axis and the corresponding sample mass on the y-axis for thermogravimetric analysis or the differential of weight change with respect to time for differential thermal analysis (Figure 3.26). A horizontal portion of the DT curve indicates a constant weight. The curved portions indicate that the sample is losing weight and the steepness of the curve is related to the rate of weight loss. The weight loss is occurring fastest where the slope of the DT curves is the steepest, and this corresponds to the peaks on the dTG curves.

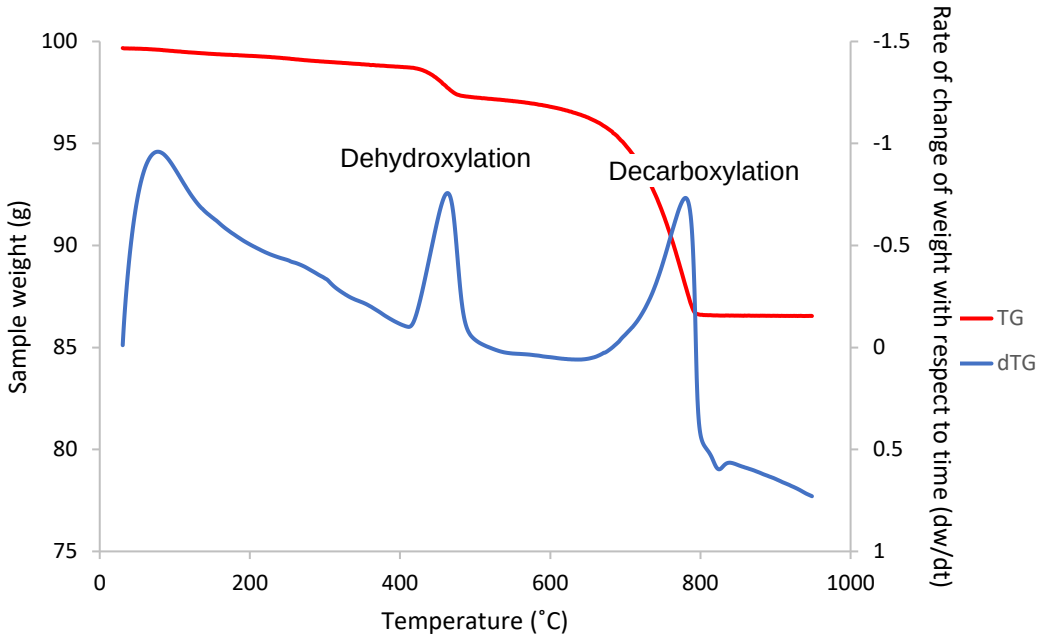

Figure 3.26: Typical TGA graph for a non-hydraulic lime.

Thermogravimetric analysis can be used with lime mortars to assess the bound water, calcium hydroxide and calcium carbonate content. The technique is not, however, capable of differentiating between the different polymorphs of calcium carbonate that might be present in a sample, the most likely of which would be calcite and aragonite. These two polymorphs have nearly identical specific heats. In a study by Faust (1950) in which ten aragonite samples and nine calcite samples from different geological locations were analysed by thermogravimetric analysis, it was found that the thermal decomposition of the aragonite samples ranged from 870˚C to 959˚C, whilst the calcite samples thermally decomposed (decarboxylation) at temperatures ranging from 914˚ to 972˚C. A different study Montoya et al. (2003), experimentally established thermal decomposition of calcite as occurring at approximately 860˚, whilst a further paper by Villagran-Zaccardi et al (2017) recorded the thermal decomposition of calcite occurring at a lower temperature: between 600˚C and 800˚C. The identification of magnesium containing mortars (dolomite) is also of importance in mortar analysis. The thermal decomposition of dolomitic lime can be distinguished from

that of calcium carbonates due to its occurrence at lower temperature, approximately 700˚C. The thermal decomposition of portlandite (dehydroxylation) is easy to distinguish from the carbonates, occurring at approximately 460˚C (Montoya, 2003).

3.13.3 Equipment

The technique is carried out using a thermogravimetric analyser, which comprises a furnace with a programmable temperature controller. Inside the furnace is a crucible, in which the sample is contained, connected to a precision balance. During operation, the furnace temperature is increased at a uniform rate in steps of temperature increase programmed by the user. Temperature and sample weight are recorded throughout the process by and saved to a computer. The SETSOFT 2000 software that controls the operation can also be used to carry out analysis of the data obtained.

3.14 Mercury intrusion porosimetry (MIP)

The pore structure of lime-based construction is a very important characteristic, affecting carbonation, strength and water vapour permeability. Mercury intrusion porosimetry is a technique that can provide important data about pore size distribution, total pore volume, porosity and specific area of the sample. A particularly useful feature is the ability to obtain information over a very large range of pore sizes including from 0.01 to 100mm, which is the pore size range involved in the carbonation process (Moropoulou et al., 2005).

The technique involves placing the sample into a container and then evacuating the container to remove contaminant gases and vapours. The container is then filled with mercury and pressure is increased incrementally, forcing mercury into the pores. Low pressure porosimetry at up to 400KPa is used to analyse the large pores, and pressures up to 400 MPa are used to analyse the very small pores. The volume of mercury that enters the sample due to the increase in pressure is equal to the volume of the pores in the associated size range. Data obtained are analysed using the Washburn equation (1921):

$$P = \frac{-2\gamma\cos\theta}{R} \qquad (3.9)$$

where γ is the surface tension of mercury and θ is the contact angle between mercury and the surface of the sample. Pores are assumed to be cylindrical and, although rarely the case, the Washburn equation is widely accepted as a practical method for the analysis of complex pore structures (Lawrence, 2006, p.159).

Mercury is used as the intrusion material due to its non-wetting property. The high surface tension of mercury causes it to form a bead rather than spreading out on the contact surface, thus it must be forced into the pores using pressure. The smaller the pore size, the greater the pressure required.

3.15 Water vapour permeability testing

3.15.1 Introduction

The virtues of lime as a 'breathable' construction material have already been well documented elsewhere in this thesis. The term 'breathability' can be misleading, though, because the term actually refers to moisture transport, not air movement. Breathability, more correctly termed water vapour permeability, is a measure of the ability of a material to allow water vapour to diffuse through its structure.

3.15.2 Background theory

There are two commonly used methods of testing this property: the 'wet cup method' and the 'dry cup method'. The two methods are set up in similar fashion, but the results are in no way comparable. In the dry cup method, a test specimen is sealed on the open moth of a test dish containing a desiccant. The permeability of the test specimen is determined by measuring the increase in weight of the test dish as the water vapour that has diffused through the test specimen is absorbed by the desiccant. In the wet cup method, the test specimen is sealed on the open mouth of a dish containing a saturated solution of potassium nitrate (KNO_3). Permeability with this method is determined by measuring the weight loss of the dish as water vapour diffuses out of the dish through the test specimen. The dry cup method is designed to simulate moisture being driven into a heated dry building during heavy rain. The wet

cup method simulates the movement of water vapour out of a building. The wet cup method was used for this work.

3.15.3 Equipment

Water vapour permeability is carried out in accordance with BS EN 1015-19:1999. A circular mortar specimen of thickness 15mm is sealed on the open mouth of a test dish and sealed around the edge with silicon sealer (Figure 3.27). In the bottom of the dish is a saturated solution of potassium nitrate. Between the top of the potassium nitrate solution and the underside of the test specimen there should be an air gap of 10mm ± 5mm. The dish and specimen are then placed on a precision balance in a climate controlled environment at a temperature of 20 ˚C ± 2˚C and relative humidity of 50 % ± 5 %. The balance is connected to a data logger that records the weight of the dish and specimen at five minute intervals on a PC. The weight loss is plotted on a graph against time and when three points can be plotted on a straight line the water vapour diffusing through the specimen is constant.

The water vapour flux, $\Delta G/\Delta t$ (kg/s), is determined from the experimental results and then the mean water vapour permeance is calculated using the formula:

$$\Lambda = \frac{1}{A\Delta_p/(\Delta G/\Delta t) - R_A} \quad \text{in kg/m}^2\,\text{s Pa} \qquad (3.10)$$

where Λ is water vapour permeance, A is the open mouth area of the test dish, R_A is the water vapour resistance of the air gap between the underside of the specimen and the surface of the potassium nitrate solution ($0{,}048 \times 10^9$ Pa m^2s/kg per 10 mm air gap) and Δ_p is the difference in water vapour pressure between ambient air and the potassium nitrate solution. The water vapour permeability is calculated by multiplying the value for water vapour permeance by the thickness of the test specimen.

$$W_{vp} = \Lambda t \qquad (3.11)$$

where W_{vp} is water vapour permeability (kg m^{-1} s^{-1} Pa^{-1}) and t is the thickness of the test specimen (m).

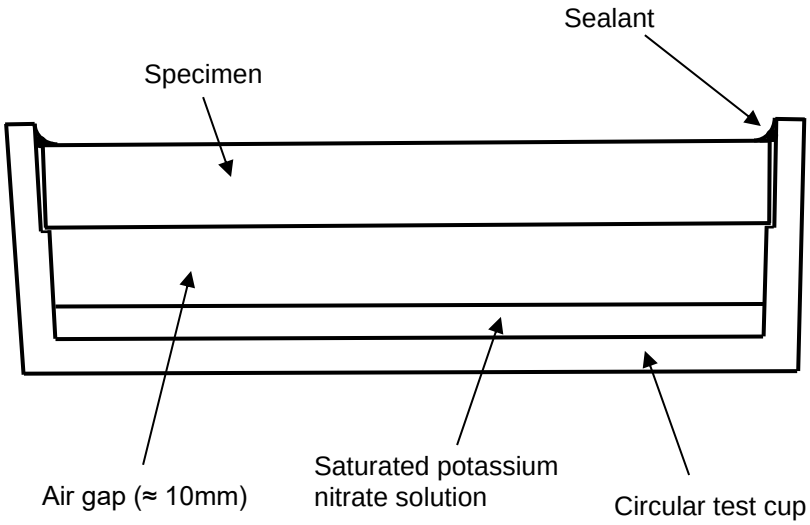

Figure 3.27: Schematic diagram of water vapour permeability testing set up.

Figure 3.28: Sample mortar disc prepared for water vapour permeability testing.

3.16 X-ray tomography

3.16.1 Introduction

X-ray tomography is a non-destructive bulk technique that allows the internal structure of a sample to be analysed and imaged. The technology used is similar to that used for medical imaging, except that in X-ray tomography a large number of images are taken from very slightly different angles, which are then mathematically used to construct a 3-dimensional image. Each image taken is commonly referred to as a ‘slice’, and the computed image is constructed from a contiguous set of slices. The technique has proved to be a capable technique for quantifying macro voids in mortar specimens (Birgul, 2008).

3.16.2 Background theory

The technique is based on the ability of X-rays to penetrate the sample under test. As the X-ray radiation passes through the sample being imaged it interacts with it; this is known as attenuation. The degree of attenuation is determined by the density and atomic number of the material and the energy of the X-rays. In composite samples, each individual material will attenuate the X-rays to a different degree. The X-ray radiation that passes through the sample is captured by an X-ray detector as a 2-dimensional radiographic image.

The X-rays travel in a straight line, known as a beam path, so each beam that hits the detector has passed through a different part of the sample and the attenuation and intensity at each point will depend on the structure of the sample. The energy of the X-rays is controllable and should be chosen according to the size and composition of the sample material. Higher energy X-rays will pass through a greater thickness of denser material.

3.16.3 Equipment

The equipment basically comprises an X-ray source, X-ray detectors and a means of rotating the sample (Figure 3.29). Most machines use X-ray tubes as the source of monochromatic X-rays, but a synchrotron or gamma-ray emitter can also be used. X-ray detectors normally utilise scintillators. Smaller detectors provide better resolution

but reduced count rates due to their smaller area. This is compensated for by using longer acquisition times to reduce noise levels.

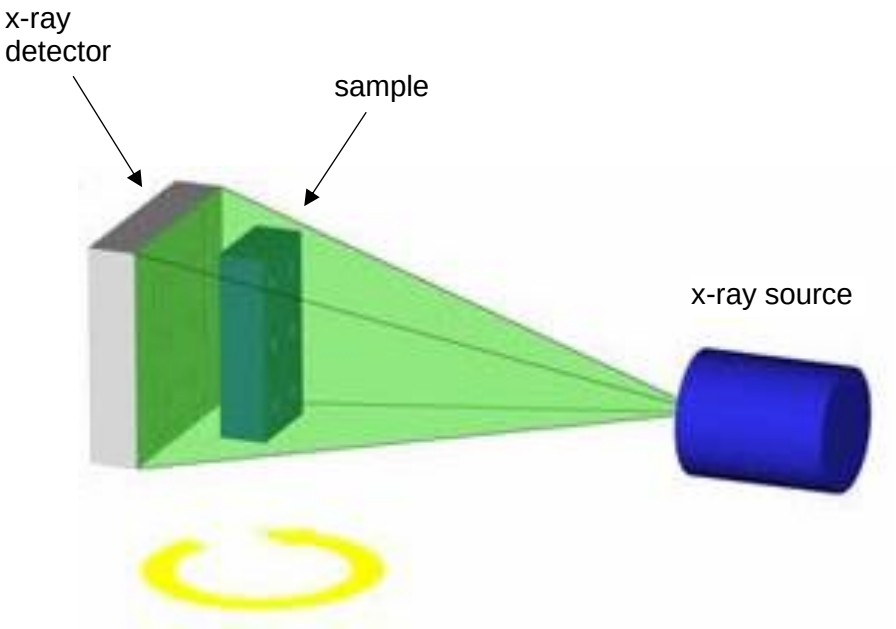

Figure 3.29: Basic schematic of an x-ray tomography machine.

3.17 References

Birgul, R., 2008. Monitoring macro voids in mortar by X-ray computed tomography. *Nuclear Instruments and Methods in Physics Research.* 596(2008), pp.459-466

Bolte, G., Zajac, M., Skocek, J., Haha, M. B., 2019. Development of composite cements characterised by low environmental footprint. *Journal of Cleaner Production.* 226(2019), pp.503-514

BS EN 933- Part 1: Determination of particle size distribution - Sieving method

BS EN 1015-19 Methods of test for mortar for masonry - Part 19: Determination of water vapour permeability of hardened rendering and plastering mortars

Coats, A. W. and Redfern, J. P., 1963. Thermogravimetric Analysis. *Analyst,* 88, pp. 906-924

Despotou, E., Schlegel, T., Shtiza, A., Verhelst, F., 2014. Literature study on the rate and mechanism of carbonation of lime in mortars. *9th International Conference 2014 in Guimaraes.* 7-9 July 2014 Guimaraes.

Diamond, S., 2004. The microstructure of cement paste and concrete – a visual primer. *Cement and Concrete Composites*, 26, pp.919-933.

Edwards, D. D., 2009. *Sustainable Lime Mortars.* Thesis. University of Bristol

Faust, G. T., 1950. Thermal analysis studies on carbonates. *American Mineralogist,* 35 (3-4)

Hughes, D., Swann, S., Gardner, A., 2012. The History, Use and Analysis of Roman Cements. . In: I. Brocklebank, ed. *Building Limes in Conservation.* Shaftsbury: Donhead Publishing, p.123

Iowa State University, 2019. Secondary Electrons and detection [online]. Available from: http://www.mse.iastate.edu/research/laboratories/sem/microscopy/how-does-the-sem-work/high-school/how-the-sem-works/secondary-electrons-and-detection/ [accessed 19 January 2019].

Ingham, J., 2012. Laboratory Investigation of Lime Mortars, Plasters and Renders. In:

I. Brocklebank , ed. *Building Limes in Conservation*. Shaftsbury: Donhead Publishing, pp.155-173

Lewandowska, R., 2010. Raman Microscopy: Analysis of Nanomaterials, Encyclopaedia of Materials Science and Technology. ScienceDirect

Lloyd, G. E., 1987. Atomic number and crystallographic contrast images with the SEM: a review of backscattered electron techniques. *Mineralogical Magazine,* 51, pp.3-19

Lothenbach, B., Matschei, T., Moeschner, G., Glasser, F. P. Thermodynamic modelling of the effect of temperature on the hydration and porosity of Portland cement, *Cement and Concrete Research,* 38(2008), pp.1-18

Luo, Z., 2016. *A Practical Guide to Transmission Electron Microscopy.* New York: Monument Press

Montoya, C., Lanas, J., Aandigoyen, M., Navarro, I., Casado, P. J., Alvarez, J. I., 2003. Study of ancient dolomitic mortars of the church of Santa Maria de Zamarce in Navarra (Spain): comparison with simulated standards. Thermochimica Acta, 398 (2003) pp.107-122.

MOROPOULOU, A., BAKOLAS, A., AGGELAKAPOULOU, E., 2004. Evaluation of pozzolanic activity of natural and artificial pozzolans by thermal analysis. *Thermochimica Acta*, 420, pp.135-140.

Moropoulou, A., Bakolas, A., Moundoulas, P., Aggelakopoulou, E., Anagnostopoulou, S., 2005. Strength development and lime reaction in mortars for repairing historic masonries. *Cement and Concrete Composites*, 27, pp.289-294.

Paul Scherrer Institut, 2015. *GEM-Selektor overview* [online]. Available from: http://gems.web.psi.ch/overview.html

Rilem Committee TC56, 1998. Measurement of hardened concrete carbonation depth. Draft RILEM recommendation CPC-118. *Materials and Structures*, 21 (126), 1998, pp.453-455.

Rodriguez-Navarro, C., Cazalla, O., Elbert, K., Sebastian, E., 2001. *Liesegang pattern development in carbonating traditional lime mortars.* Royal Society Publishing

Singh, R., 1984. Simultaneous measurement of thermal conductivity and thermal diffusivity of some building materials using the transient hot strip method, *J. Phys. D: Appl. Phys*. 18

Wen J.G. (2014) Transmission Electron Microscopy. In: Sardela M. (eds) *Practical Materials Characterization*. Springer, New York, NY

CHAPTER 4 INSULATING AEROGEL PLASTER

4.1 Introduction

This phase of the thesis investigates the potential to utilise the insulating properties of aerogel in lime plasters. Aerogels are one of the most promising insulating materials being investigated for use in construction, and although discovered over seventy years ago, there are currently only a very limited number of commercially available construction products that employ aerogel as the insulating material. Aerogel 'blankets' are available for retrofitting areas such as lofts, pipework and soffits and are produced in a range of thicknesses (Passivhouse.Homes Ltd, 2019). Alternatively, walls and floors can be retrofitted with rigid blocks comprising aerogel blankets mounted on a magnesium oxide board (Proctor Group Ltd, 2019). Another approach being developed is to incorporate aerogel granules into plaster or render, and this is the method used in this investigation (Buratti et al., 2014).

It is not surprising that the bulk of the research work being carried out regarding the use of aerogel in construction products relates to cementitious materials. The use of lime-based construction materials is tiny in comparison to cement-based products. However, the resurgence in lime usage and the lower environmental impact of lime justifies its choice here as the binder material, in line with the objective of creating a plaster with a low environmental impact.

Initial attempts during this investigation to incorporate aerogel granules with lime plasters resulted in high shrinkage and extensive cracking of the lime matrix. The decision to include polypropylene fibres in this investigation was taken in an attempt to mitigate these problems.

4.2 Materials

4.2.1 Lime putty

The binder material used for this work was a lime putty supplied by J J Sharpe, which was matured for at least 6 months. The lime putty was weighed before and after drying in an oven to remove the water content and was found to have a solids content,

assumed to be calcium hydroxide of 51%. This allowed accurate batching of the mix constituents.

4.2.2 Aerogel granules

The silica aerogel was supplied by Aerogel UK. The material comprised open cell, hydrophobic aerogel granules ranging in size from 125µm to 5mm. The physical properties claimed by the manufacturer are shown in Table 4.1. The most important property regarding this work is that the aerogel is hydrophobic; unless functionalised, aerogel is hydrophilic and will catastrophically collapse when in contact with water.

Table 4.1: Physical properties of aerogel (data from Aerogel UK).

Property	Data
Density	80-100kg/m^3
	100-120kg/m^3
Particle size range	0.5 – 5mm
Surface area	500-650m^2/g
Porosity	90% +
Pore diameter	20-100 nm
Hydrophobicity	Hydrophobic
Thermal resistance	0.013 W/m/K
Sound speed	100m/sec

4.2.3 Standard sand

The sand used in this investigation was a dry siliceous natural sand conforming to BS EN 196-1 and ISO 679: 2009. This grade of sand comprises particles that are generally isometric and rounded in shape and having a particle size distribution as shown in Figure 4.1. This type of sand was specified for this investigation to facilitate consistency and repeatability of experimental conditions.

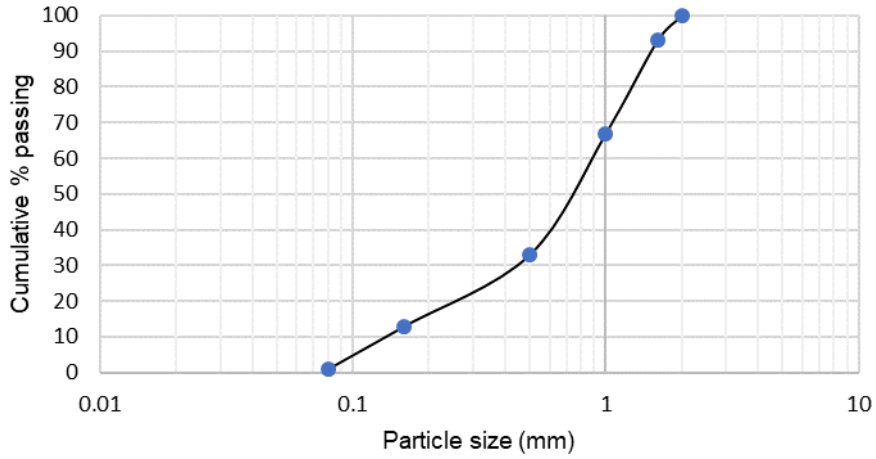

Figure 4.1: Particle size distribution for standard sand used.

4.2.4 Polypropylene fibres

Polypropylene monofilament fibres from Adfil (2016) having lengths 12 and 18mm and a diameter of 20µm were added to the experimental plaster mixes at 0.5% by volume, to help reduce shrinkage and cracking. The fibres had been treated with a surfactant for optimum dispersion and bonding. No details of the surface treatment were provided by the manufacturer.

The volume fraction was kept at 0.5%, as it was considered that higher proportions of fibres might negatively affect the rheology of the plaster and that strength per se was not the most important physical property for a plaster, as it is more important for a plaster to be flexible; plaster that is too strong can result in delamination (Ingham, 2012).

4.3 Initial investigation

4.3.1 Aerogel granules

An initial investigation was carried out in which the aerogel granules were mixed in a 2:1 ratio by volume of aerogel to lime putty binder. The aerogel granules were mixed in by hand to ensure that the particles did not get crushed, as it was of interest to see how the binder reacted with particles over the complete size range. It was intended to solely investigate the aerogel/binder interaction at this stage, so no other aggregate materials were used. The purpose of this was to assess how well the granules mixed with the binder and in particular how the porous aerogel would affect carbonation. The lime putty/aerogel mix was used to prepare 40 x 40 x 160mm prisms using polystyrene prism moulds. The moulds were left uncovered.

The specimens were wrapped in clingfilm to maintain high humidity around the specimens (approximately 90%) and then stored in a climate controlled chamber at 20ºC ± 2ºC and relative humidity of 65% ± 5%. After 7 days the cling film was removed and they were stored under the same conditions for a further 7 days at which time it was intended to demould the prisms. At this time the lime binder appeared to have undergone carbonation to a degree that might be expected of a standard lime binder. However, it was obvious that the prisms had suffered from severe and catastrophic cracking, especially in areas where large aerogel particles were located (Figure 4.2). Interestingly, it can be seen in that the prisms did not appear to have suffered from significant overall shrinkage.

Due to the apparent carbonation and lack of overall shrinkage, it was decided to continue this work but investigate solutions to the localised shrinkage-cracking problem. From the literature on this subject, it was evident that the inclusion of fibres in the binder would likely be the best solution and that polypropylene would be the best choice of fibre due to their product consistency and because they are treated with a surfactant to reduce agglomeration and aid dispersion. The proprietary lime plaster Fibrelime contains polypropylene monofilament fibres, which it is claimed is flexible and resists shrinkage and cracking (Fibrelime, 2019). As there was very little independent information available on this product, it was decided to carry out some investigation work to assess the effect of polypropylene fibres on lime plaster.

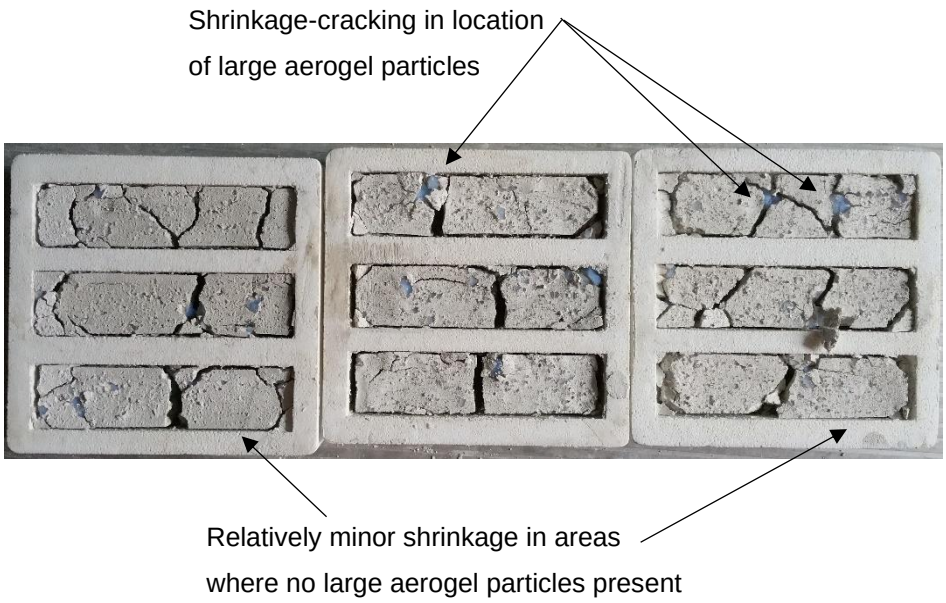

Figure 4.2: Lime putty binder with aerogel granules as aggregate material.

4.3.2 Fibrelime

Fibrelime is the only known ready mixed lime plaster on the market containing polypropylene monofilament fibres. At the time this research was carried out there was no research data available for this material. This material was investigated to establish how the fibres combined with the binder and what effect they had on strength and flexibility. The Fibrelime was prepared for use by mixing with an electric drill with a paddle attachment. The product was mixed thoroughly for approximately twenty minutes, to the point at which it had reached a workable consistency. Prism specimens were then prepared and stored in an environmental chamber at a constant temperature of 20ºC ± 2ºC and relative humidity of 65% ± 5%. At 28 days, the specimens were subjected to compressive and flexural strength testing and the internal structures were examined using X-ray tomography. The X-ray tomography scans (Figure 4.3) were carried out on a 40 x 40 x 160mm prism that had been broken in half after flexural strength testing and show some voids within the mortar.

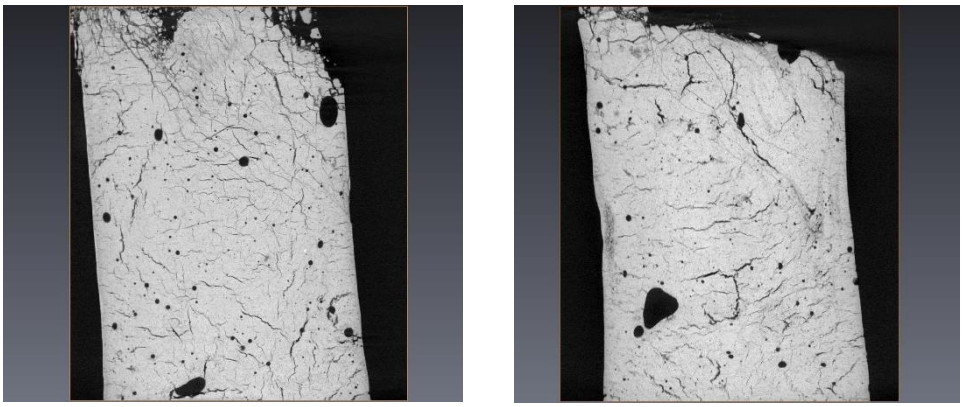

Figure 4.3: Section through X-ray tomography scans of Fibrelime test prisms showing air bubbles within the binder. (Width of prism = 40mm).

The compressive and flexural strength test results show that Fibrelime behaved very differently compared with conventional plaster mixes under load. The test specimens did not have a definite failure point; they failed progressively with increasing load but did not disintegrate. As there was no specific point at which the test specimen can be said to have failed, plots of load against extension are shown here rather than maximum stress. It can be seen in Figures 4.4 and 4.5 that under compressive load the test specimen compressed progressively less whilst resisting the load. The test specimens exhibit similar behaviour during flexural strength testing. The specimens deform progressively under load but did not break in half (Figures 4.6 and 4.7). It can also be seen that the specimens did not deform at an even rate under flexural load.

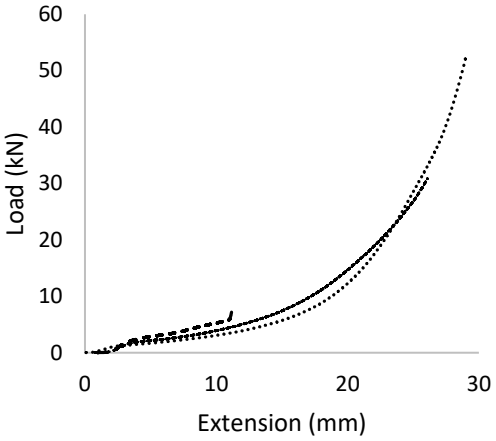

Figure 4.4: Compressive strength test results for Fibrelime.

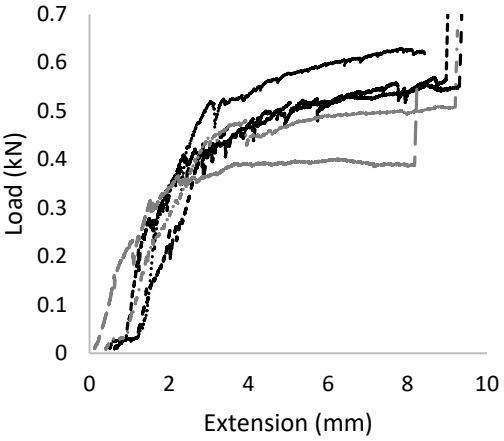

Figure 4.6: Flexural strength test results for Fibrelime.

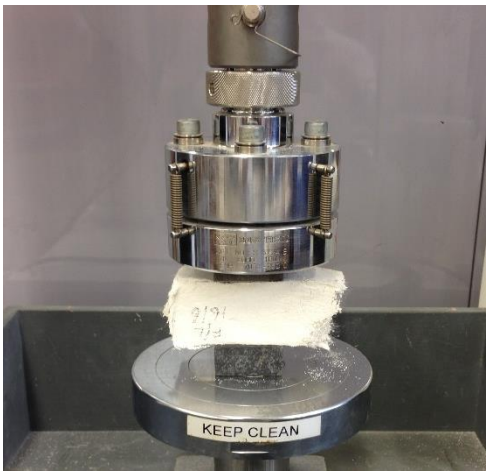

Figure 4.5: Compressive strength test of Fibrelime.

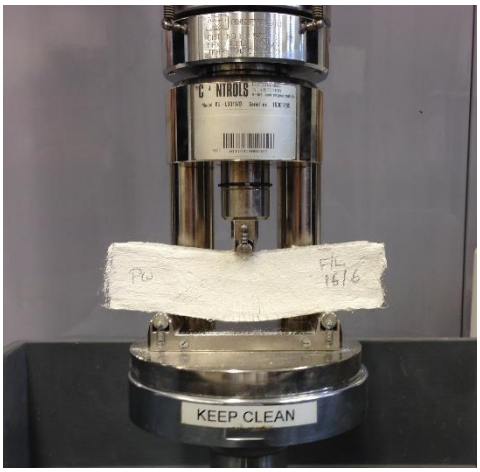

Figure 4.7: Flexural strength test of Fibrelime.

4.3.3 Conclusions on initial investigation

From this initial test work, it was clear that the aerogel could not be used as the only aggregate material without an additive to prevent the localised shrinkage cracking around the aerogel granules. Testing of the Fibrelime confirmed that the polypropylene monofilament fibres bind well with the non-hydraulic binder and help maintain the integrity of the plaster under both compressive and flexural loading. From these results it was decided to continue experimenting with aerogel lime plasters and to introduce the same fibres in an effort to improve the stability of the plaster.

4.4 Experimental methods

4.4.1 Sample preparation

Five different plasters were prepared for testing using a mix ratio of 1:1 aggregate to lime putty by volume, giving a ratio ≈ 2:1 aggregate to lime by volume after allowing for the water to binder ratio of 1:1 of the lime putty. The five specimens all contained fibres and varying ratios of aerogel and sand. The corresponding mix ratios and resulting bulk densities are given in Table 4.2.

Table 4.2: Material composition of experimental aerogel plaster mixes by volume.

Specimen	Lime putty (%)	Standard sand (%)	Aerogel (%)	Polypropylene fibres (%)	Bulk density (kg/m^2)
S0	50	49.5	0	0.5	1,504
S1	50	37.25	12.25	0.5	1,294
S2	50	24.75	24.75	0.5	1,089
S3	50	12.25	37.25	0.5	883
S4	50	0	49.5	0.5	682

The lime and sand were prepared using a paddle mixer for a minimum of twenty minutes to ensure the plaster was suitably workable. Fibres were added to the mixture in small amounts during the mixing process to help ensure an even distribution throughout the matrix. The aerogel was added afterwards and mixed into the plaster by hand using a trowel. This was to avoid subjecting the aerogel to prolonged stress during mixing and possible degradation of the granules. The experimental mixes were then added to the prism moulds in small quantities and tamped down as the material was added, to reduce the occurrence of trapped air bubbles within the specimens. For each experimental mix, three standard 40x40x160 mm prisms were prepared for strength testing, six discs of diameter 100 mm and thickness 25 mm for thermal

conductivity testing and three discs of diameter 175 mm and thickness 15 mm for water vapour permeability testing.

After moulding, the specimens were stored in a climate chamber regulated at a constant temperature of 20ºC ± 2ºC and relative humidity of 65% ± 5% as specified in standard BS EN 1015-11:1999. The specimens were covered with a thin plastic wrap for the first week to maintain a high level of humidity, as exposure to ambient atmospheric conditions during this period can result in significant reduction in strength due to premature drying and subsequent cracking (Livesy, 2010). The specimens were then left in the moulds for a further week to allow them to achieve sufficient rigidity to facilitate demoulding.

4.4.2 Strength testing

Mechanical strength testing was performed using a 50kN Instron 3369 Universal motorised load frame in accordance with BS EN 1015-11:1999 to test both the flexural and compressive strength. Bluehill 3 software monitored and recorded the load on the specimen as a function of extension throughout the test.

4.4.3 Scanning electron microscopy (SEM)

Scanning electron microscopy (SEM) was used to examine the physical condition of the specimens at the lime/aerogel interface to help identify any shrinkage around the aerogel particles or any degradation of the particles themselves. Specimens were analysed using a JEOL 6480 LV scanning electron microscope equipped with an Oxford Instruments INCA X-act X-ray detector (silicon drift detector offering high count rate and reduced operation time). High magnification images of the aerogel internal pore structure were obtained using a JEOL JEM1200EXII transmission electron microscope (TEM) operating at 120 kV.

4.4.4 Thermal conductivity measurement

Thermal conductivity measurements were obtained using the transient hot strip method. To take the measurements, the sensing strip was placed between two of the 100mm diameter disc specimens. The specimens were tested under normal conditions i.e. not dried. Upon commencing the measurement process, the apparatus was allowed to heat up and establish a stable temperature within the test specimens. Temperature data were then recorded at two second intervals for a period of 120 seconds. The power setting for this test was 0.4 W. Measurements were repeated on three different pairs of specimen discs and an average value calculated for each mix.

4.4.5 Water vapour permeability testing

Water vapour permeability testing was carried out in accordance with BS EN 1015-19:1999. Three 175mm diameter specimens were tested for each of the five mixes. The discs were sealed onto the open mouth of a circular test cell, which contained a 10mm deep saturated solution of potassium nitrate, and the discs were sealed around their outside edge with silicon sealant. The air gap between the base of the specimen discs and the top of the saturated potassium nitrate solution was 10 mm (±1 mm). This experimental set up produced a relative humidity within the test cell (in the air gap between the top of the salt solution and the underside of the test specimen) of approximately 95% at 20˚C.

Test samples were placed in a fan-assisted environmental chamber at 20ºC and 50% RH. A precision balance within the chamber logged the sample mass at five minute intervals on a PC. Monitoring was continued until a linear relationship between mass reduction and time could be established.

4.4.6 Fourier Transform Infra-Red Spectroscopy (FTIR)

FTIR was used to help identify any chemical reactions that may have taken place between the lime and the fibres or between the lime and the aerogel particles. FTIR spectra were obtained for the aerogel granules and the polypropylene fibres before and after they were added to the lime mixes.

For this work, a PerkinElmer Frontier FTIR spectrometer was used over a frequency range from 600 – 4000 cm^{-1} and at a resolution of 1 cm^{-1} and 40 accumulations. Before running each sample, a scan was taken with no material on the plate. This served the function of obtaining a reference spectrum, which the software would later subtract from the sample spectrum to give a clean spectrum of the material under test. Before inserting each new sample of material, the plate was cleaned with alcohol to ensure no cross contamination from previous samples.

4.4.7 Stereo microscopy

A Leica M205 C stereo microscope was used to examine the surfaces of a prism sample to assess the relationship between binder, aerogel and polypropylene fibres. A stereo microscope was used because lower magnification and higher depth of field images were required than could be achieved using a scanning electron microscope.

4.5 Results

4.5.1 Compressive and flexural strength

Figures 4.8 and 4.9 show stress as a function of strain during compressive and flexural testing respectively. The data was reported up to a strain value of 0.03 as a consequence of the failure mode behaviour of specimens containing fibres. At higher values of strain the test data indicates that the specimens did not fail in a brittle manner even though their condition was such that they would have been considered to have failed as a building element.

As the flexural test caused test specimen deformation but did not fracture it, the deformed specimen was manually broken in half after the test, and fibres and binder were removed from the fracture faces for further testing.

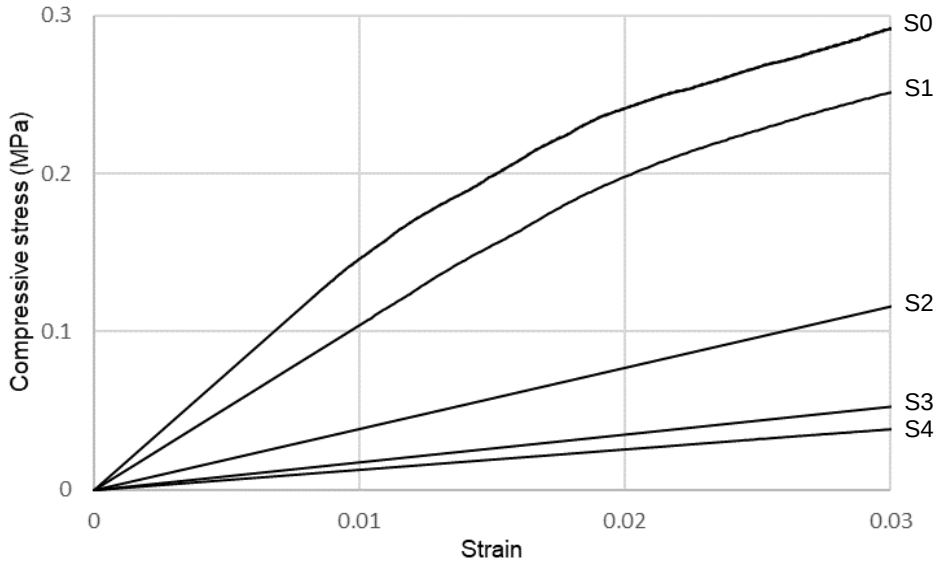

Figure 4.8: Average compressive strength test results for each of the five aerogel plasters.

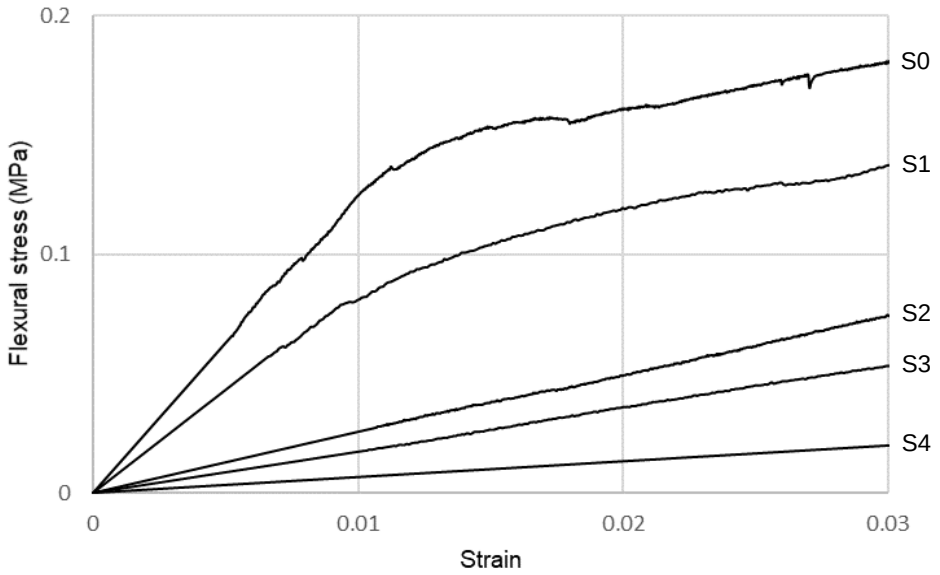

Figure 4.9: Average flexural strength test results for each of the five aerogel plasters.

4.5.2 Effect of fibres on failure mode

Figure 4.10 shows the different behaviours under stress of lime mortars with and without fibres added. Figure 4.10 (A) shows a typical behaviour for a standard lime mortar (without fibres) under compression. At failure, the specimen fractures and fails

at a distinct point in the test. In Figure 4.10 (B) it can be seen from the degree of compression at the base of a specimen containing aerogel (S1) that the addition of 0.5% fibres by mass permits the lime mortar to achieve a high strain capacity, and that the fibres have prevented fracturing and have helped to maintain the integrity of the specimen.

Similarly, during flexural testing a significant difference is observed between the specimens with and without fibres added. It can be seen in Figure 4.11 (A) that the standard mix lime specimen cracked at the point of maximum stress and broke into two halves. Figure 4.11 (B) shows that the specimen containing fibres endured a significantly higher strain without failing and has considerably greater flexibility.

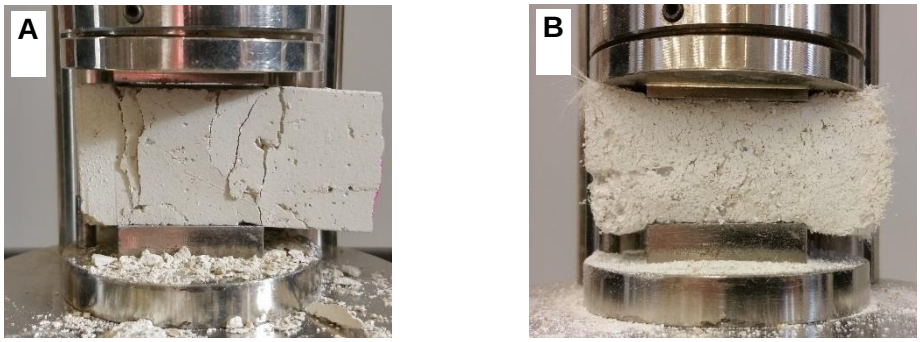

Figure 4.10: Compressive fracture of a reference mortar without fibres (A) and typical deformation of a specimen (S1) containing fibres and aerogel (B).

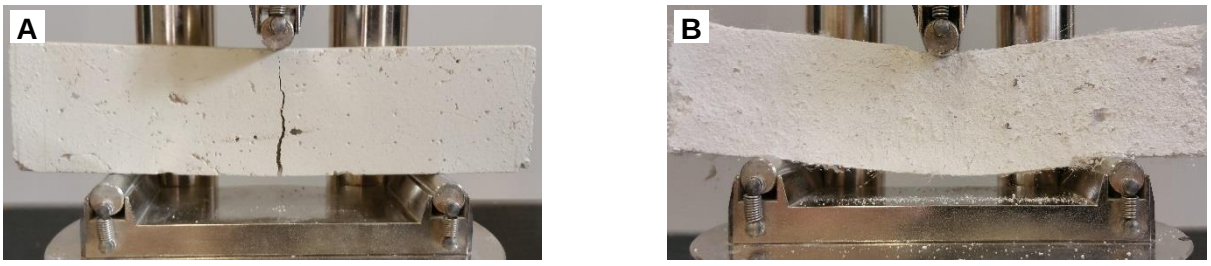

Figure 4.11: Flexural fracture of reference mortar without fibres (A) and deflection of a specimen (S1) containing fibres and aerogel (B).

4.5.3 Scanning electron microscopy (SEM)

It can be seen that the typical morphology of the aerogel granules was an irregular shape and this contained different features including both smooth and rounded surfaces in addition to some sharper edges (Figure 4.12).

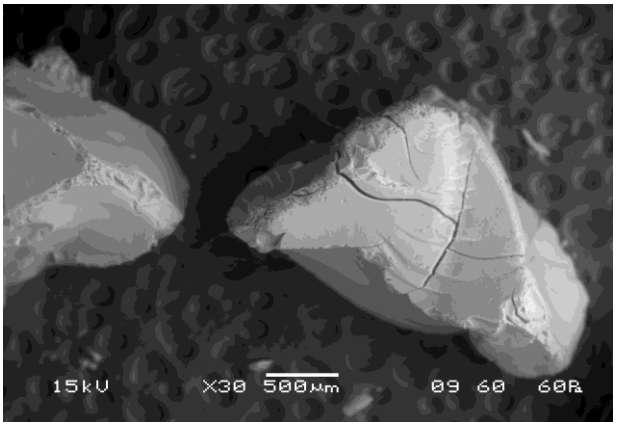

Figure 4.12: Aerogel particles as manufactured.

The images in Figure 4.13 (A) and (B) show aerogel particles in a specimen after 91 days. Figure 4.13 (A) shows a particle embedded in the binder, which has remained intact and not deteriorated in any discernible way. In Figure 4.13 (B) it can be seen that there is no evidence of shrinkage at the aerogel/lime interface. This finding is consistent with a study by Gao, T. et al, which reported that aerogel particles in 'aerogel incorporated concrete' survive the mixing and curing process without suffering degradation. Also, there is no visual evidence of any reaction taking place at the binder aerogel interface.

The images in Figure 4.14 (A) and (B) show the effect of the carbonated lime putty binder on the surface of the fibres. In Figure 4.14 (A), damage to the fibre surface is clearly visible in the form of scratches along the length of the fibre. This fibre was extracted from the fracture face of a test prism after flexural strength testing, and the marking was caused by the abrasion between the fibre surface and the lime matrix during the test. This is consistent with there being a mechanical bond between the binder and fibres as a result of the binder increasing in volume during carbonation and the softer polypropylene fibres accommodating some stress relief in the binder. For

reference, Figure 4.14 (B) shows the smooth and unmarked surface of a fibre in its original unused condition.

Figure 4.15 (A) and (B) shows images of plaster particles removed from the fracture face of a test specimen. In Figure 4.15 (A), it can be seen that these particles have suffered physical stress, as the aerogel particles have fractured and appear as shards. In Figure 4.15 (B), the aerogel particle appears to have remained intact. In both cases, binder remains adhered to the aerogel.

In Figure 4.16 (A) and (B), evidence of the bond between the lime binder and the fibres is visible. These fibres were pulled from the specimen matrix, yet calcite crystals remain firmly attached to the fibres indicating a strong bond.

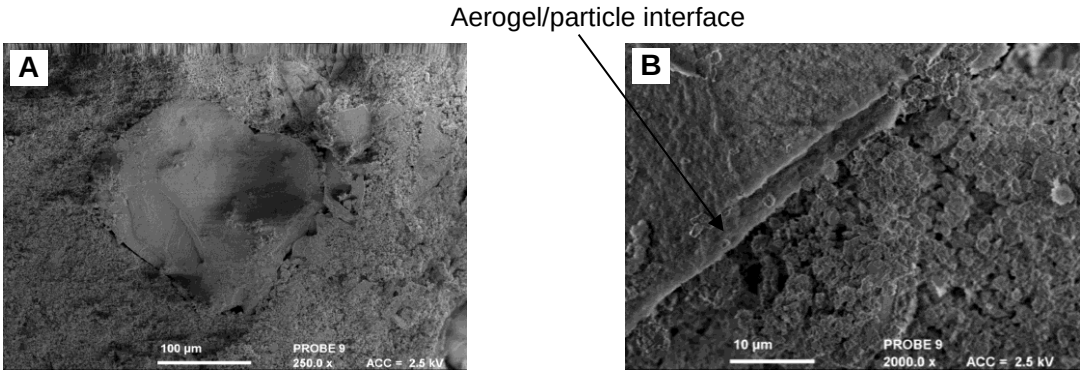

Figure 4.13: Aerogel particle in lime binder after 91 days (image A). Aerogel/lime interface (image B).

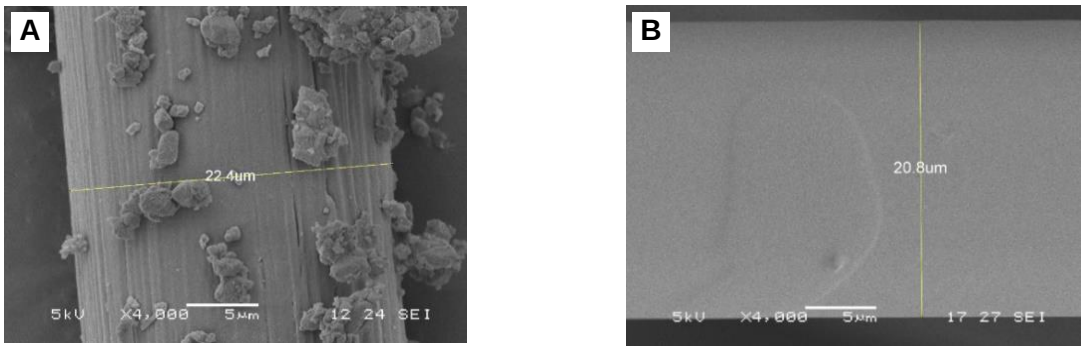

Figure 4.14: Fibre extracted from fracture surface of test specimen (image A). Fibre in as manufactured condition (image B).

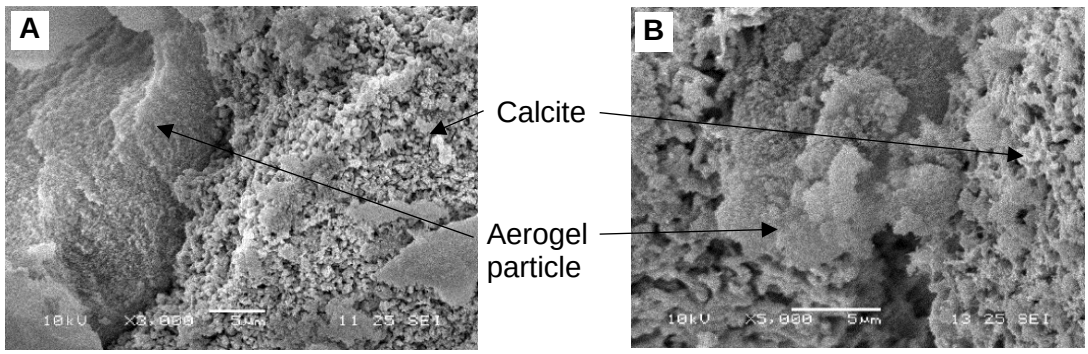

Figure 4.15: Calcite crystals adhering to aerogel particles (image A). Aerogel particle entrapped within calcite (Image B).

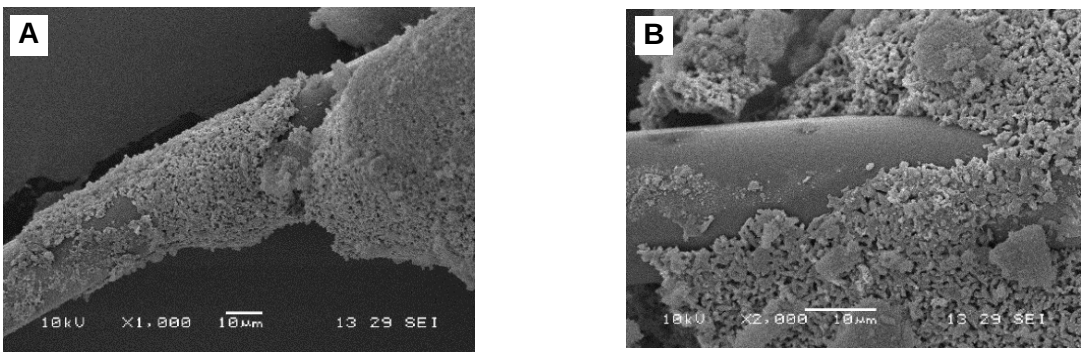

Figure 4.16: Calcite crystals adhering to the surface of a polypropylene fibre (image A). Fibre/binder interface (image B).

4.5.4 Transmission electron microscopy (TEM)

A crushed aerogel particle was examined using TEM in order to analyse the pore structure. The image in Figure 4.17 shows the mesoporous nature of the internal structure, which is the physical property that is responsible for the low conductive and gaseous heat transfer through the material. Accurate measurement of the pore and pore wall dimensions was beyond the capability of the equipment, however.

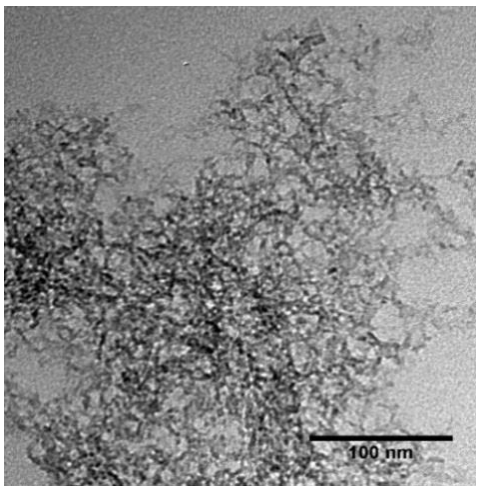

Figure 4.17: TEM image of a crushed aerogel particle showing the highly porous nature of its internal structure. (Magnification = 250,000x).

4.5.5 Thermal conductivity

Figure 4.18 shows the thermal conductivity for each experimental mix. To provide statistically significant results, an average of three separate test runs using a different pair of specimens for each test is reported. The thermal conductivity decreased significantly with increased aerogel content.

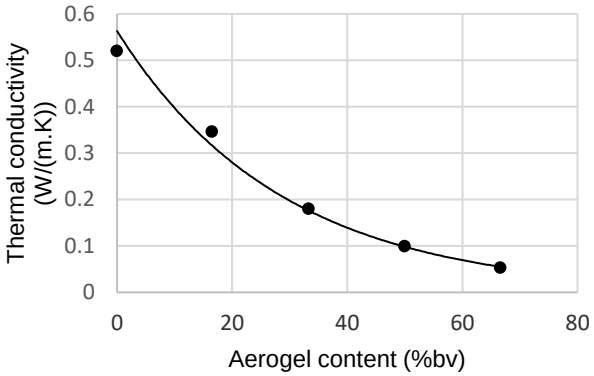

Figure 4.18: Effect of aerogel content on thermal conductivity.

Thermal conductivity values as a function of aerogel content by volume show an exponential relationship as per equation 3 where, λ is thermal conductivity, Ae is aerogel content and k is the rate of change.

$$\lambda_{(Ae)} = \lambda_{(0)} e^{k \cdot Ae} \qquad (4.1)$$

Using a value of 66.6 for Ae gives a value of -0.03428 for k. This exponential relationship can be explained by the fact that as the volume fraction of low density aerogel was increased, the volume fraction of high density quartz sand was decreased proportionally. The thermal insulating performance of the plaster mix comprising only aerogel as aggregate (S4) was only marginally inferior to other experimental insulating plasters being developed using aerogel; however, the plaster mixes investigated here utilised a significantly lower proportion of aerogel compared to those materials developed by Stahl et al (2012) and Burrati et al (2014).

4.5.6 Water vapour permeability

Figure 4.19 shows the mass loss data for each specimen measured over a period of ten hours. The data, when plotted, shows a linear relationship between time elapsed and mass of moisture lost by diffusion through the specimen under test. The permeability clearly increased with higher aerogel content and remained constant throughout the test. This tendency was attributed to the hydrophobicity of the aerogel preventing the blockage of the pores with moisture.

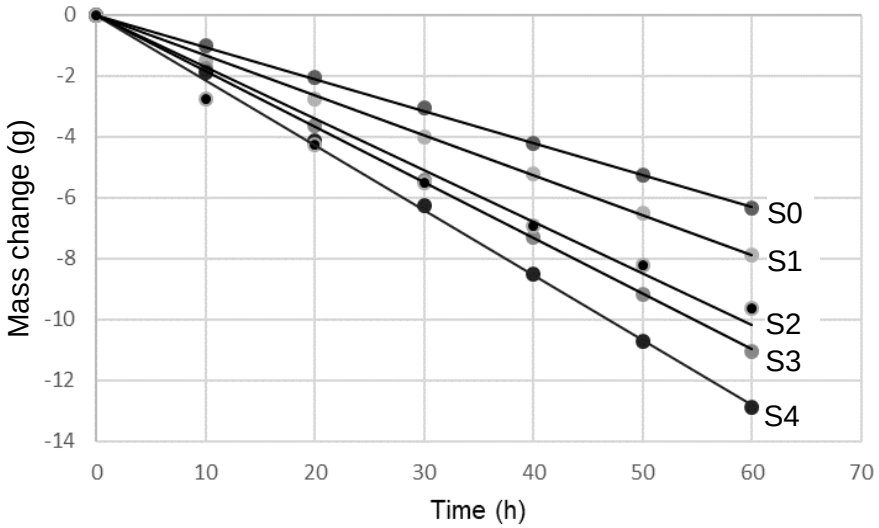

Figure 4.19 Graph of mass loss against time during wet cup permeability test.

The mass loss data from the wet cup test allowed calculation of the water vapour permeance and water vapour permeability values (Figure 4.20) for each mix, using formulae (1) and (2) below.

$$W_{vp} = At \qquad (4.2)$$

$$\Lambda = \frac{1}{A\Delta_P/(\Delta G/\Delta t) - R_A} \qquad (4.3)$$

Where: W_{vp} is water vapour permeability (kg m^{-1} s^{-1} Pa^{-1}), Λ is water vapour permeance (kg m^{-2} s^{-1} Pa^{-1}), A is area of open mouth of test cell (m^2), D_p is the difference in water vapour pressure between ambient air and potassium nitrate KNO_3 solution (Pa), R_A is water vapour resistance of air gap between specimen and KNO_3 solution (0,048 x 10^9 Pa m^2s/kg per 10 mm air gap), DG/Dt is the water vapour flux (kg/s), and t is specimen thickness (m).

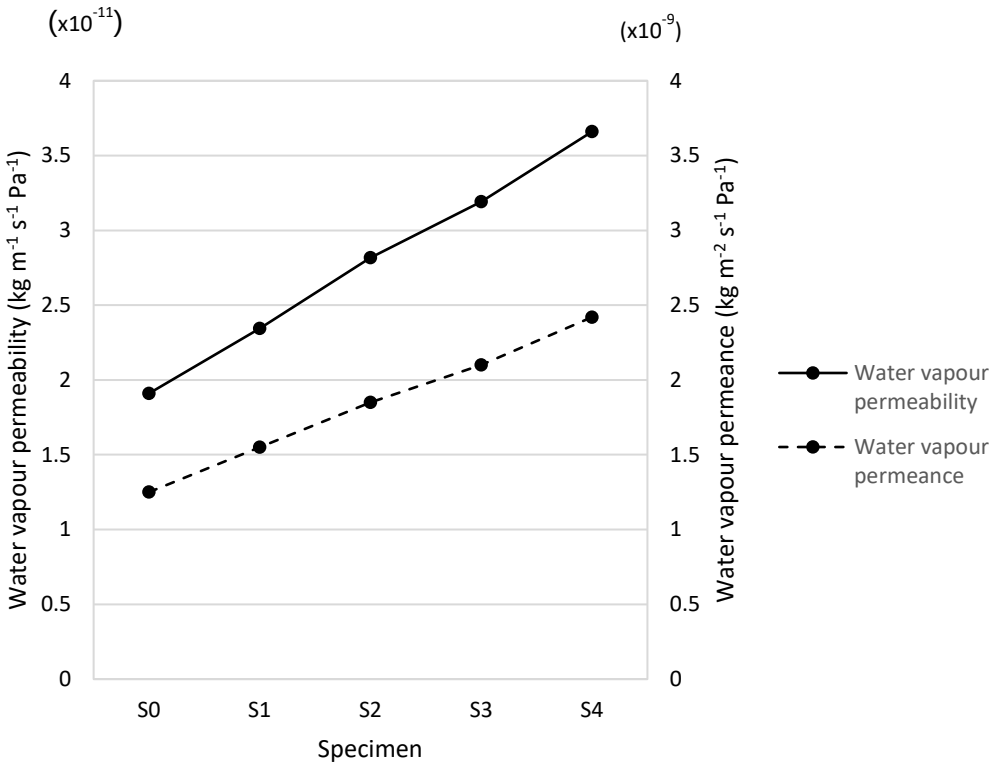

Figure 4.20 Effect of aerogel content on water vapour permeability.

4.5.7 Fourier Transform Infra-Red Spectroscopy (FTIR)

Figures 4.21(A) and (B) show spectra for aerogel obtained from a test specimen and from aerogel as manufactured respectively. The aerogel specimen exhibited a main absorption peak at 1083 cm^{-1}, with a shoulder at around 1200 cm^{-1}, which is characteristic of silica and can be assigned to asymmetric Si-O-Si stretching vibrations [31]. A second peak at 949 cm^{-1} is assigned to silanol (Si-OH) stretching vibrations, indicating that the aerogel is not 100% hydrophobic. An additional characteristic silica Si-O-Si stretching peak was observed at 800 cm^{-1}. (Swann & Patwardham, 2011). The peak at 847 cm^{-1} is assigned to Si-CH_3 rocking vibrations in silanes and is consistent with surface methyl groups produced during hydrophobization (Lambert, 1987).

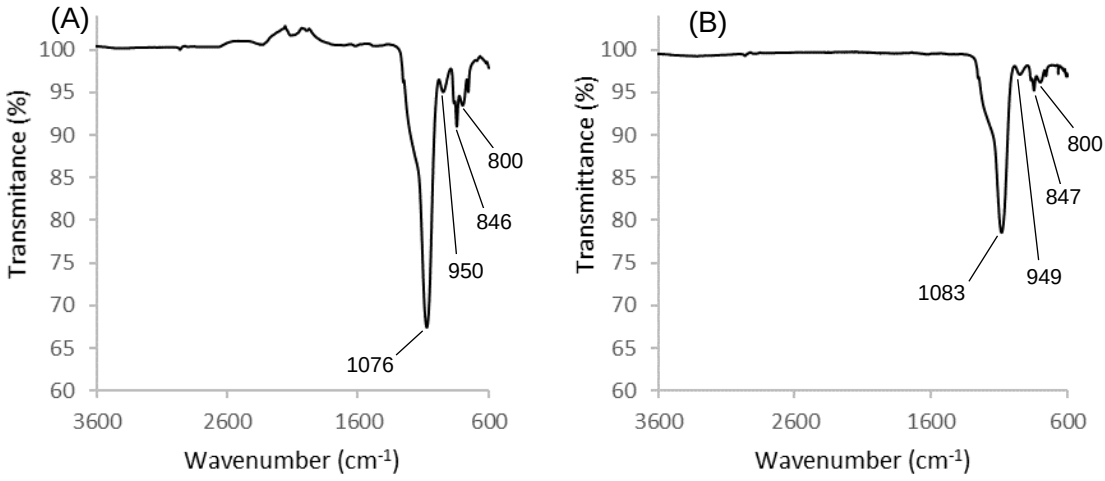

Figure 4.21: FTIR spectra of aerogel taken from test specimen (A) and from aerogel as manufactured (B).

Figures 4.22 (A) and (B) show spectra for a fibre obtained from a test specimen and from a fibre as manufactured respectively. The spectrum obtained from the polypropylene fibre was a match on all the main peaks with the reference polypropylene spectrum (NICODOM, 2012), but there were no significant additional peaks to provide information on the surface treatment. This suggests that the surfactant used on the fibres was an extremely thin surface layer and below the instrument's detection limit.

For both the aerogel and the polypropylene fibres, the absence of any significant difference between the FTIR spectra before and after they had been in contact with the lime binder is consistent with no chemical reaction having taken place between the binder and the additive materials. This supports the evidence from the SEM images indicating that the strength gain from the incorporation of fibres is the result of a physical rather than chemical bond.

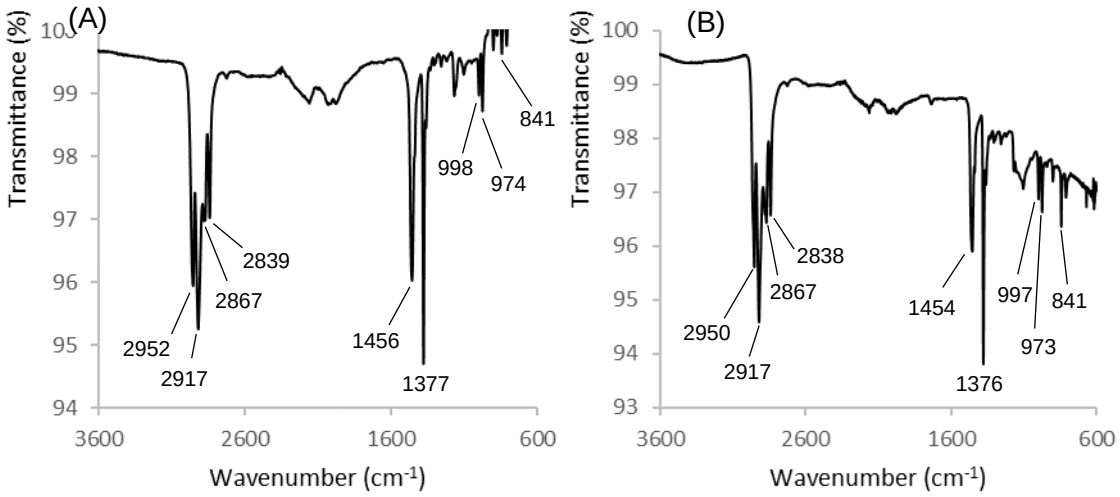

Figure 4.22: FTIR spectrum of polypropylene fibre taken from test specimen (A) and from a polypropylene fibre as manufactured (B).

4.5.8 Stereo microscopy

Figure 4.23 shows stereo microscope images of the surface of a prism specimen. In Figure (A) the aerogel particles can be seen dispersed throughout the lime binder. The higher magnification images in (B) and (C) show large aerogel particles encased in lime binder and covered with polypropylene fibres. There is no evidence of shrinkage around the aerogel particle and the fibres appear to be firmly bound to the binder. In images (C) and (D) it can be seen that the lime binder is adhering to the fibres.

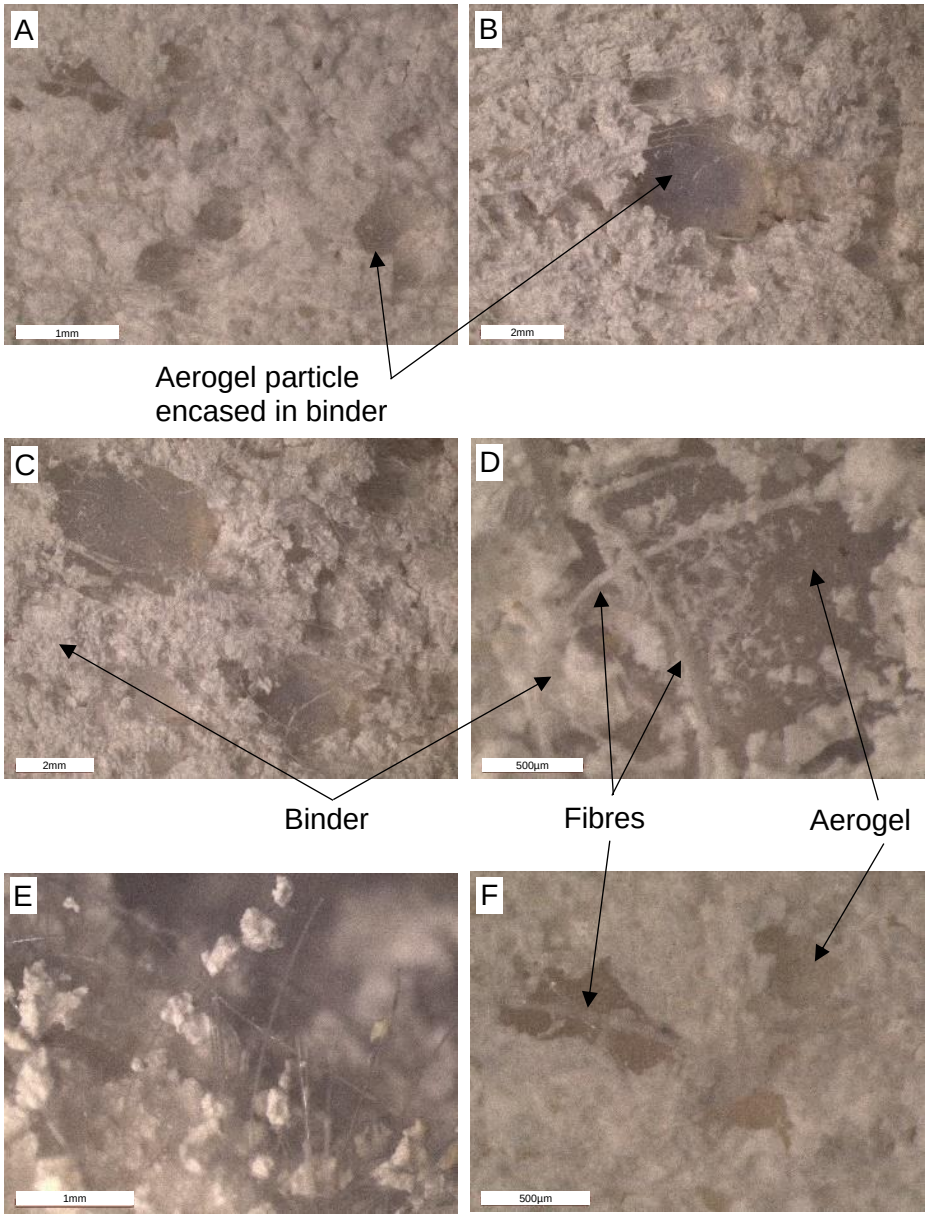

Figure 4.23: Images of the surface of insulating aerogel plaster showing aerogel particles and fibres embedded in the binder.

4.6 Discussion

Whilst the inclusion of aerogel clearly improves the thermal efficiency of the plaster mixes, the only specimen that achieved thermal efficiency comparable to similar aerogel plasters currently reported in the literature was the specimen comprising purely aerogel as the aggregate material (S4). When sand is incorporated into the mix, thermal conductivity rises significantly due to its high density compared to the aerogel. It should be taken into consideration, however, that the proportions of aerogel used in these experimental mixes was lower than those used in the other studies.

Initial attempts at incorporating aerogel into lime binders produced plasters that suffered cracking and very low strength. Significantly, the cracking appears to be most severe in the locations where the large aerogel particles are located. This could possibly be explained by the fact that the functionalisation does not remove all polar groups from the surface of the aerogel. The literature on the subject states that only 30% of the surface needs to be functionalised to achieve hydrophobicity, but it is unknown to what extent this particular aerogel had undergone functionalisation. It is possible that the remaining polar -OH groups present within the aerogel are drawing water away from the binder and this is why there is severe cracking close to the large aerogel particles but not severe overall shrinkage.

It is interesting that other similar investigations have not reported data for compressive and flexural strength. The strength values obtained during this investigation, even with fibres added to the binder, were significantly lower than that which would normally be expected for a lime plaster. However, the high degree of plastic deformation without fracturing demonstrated the superior flexibility and toughness of these experimental mixes in comparison to the more commonly used lime/sand mixes without added fibres. These experimental mixes clearly sacrifice strength for flexibility and toughness, but for a plaster, this can be a distinct advantage because the plaster can accommodate building movement, which helps to avoid cracking.

The specimen comprising only aerogel as the aggregate material exhibited permeability significantly superior to conventional gypsum plasters Wang et al., (2011, p.854) and comparable to a similar developmental aerogel product (Fixit, 2016). This effect can clearly be attributed to the aerogel. The linear relationship between

permeability and aerogel content indicates that changes in the sand proportions had a negligible effect on permeability compared to changes in the aerogel content. This is of particular benefit when using non-hydraulic lime, which sets purely through carbonation and depends on the pore structure of the plaster for diffusion of CO_2. This property of aerogel containing plasters is also beneficial to the 'breathability' of a building, as it can assist the release of moisture absorbed by walls that could otherwise freeze and expand, causing damage to masonry.

The permeability of lime-based construction materials is the physical property that is probably most responsible for the long-term durability of these materials. The fact that aerogel has also proven to be a durable material when compared to more conventional insulation materials suggests that these experimental mixes should possess long-term durability. The experimental work carried out did not reveal any reaction between the lime and aerogel that might cause deterioration in the plaster. Furthermore, being hydrophobic and inorganic, there is no chance of moisture causing decay to the aerogel, as is possible with some natural insulating materials.

The SEM images obtained from the polypropylene fibres support the assumption that they are responsible for imparting flexibility to the plaster. The surface of the new polypropylene fibre is clearly very smooth; however, the surface condition of fibres extracted from the fracture face of test specimens shows score marks along the length of the fibre, which is consistent with there being a physical bond between the binder and the fibres. The nature of the surface damage to the fibres is consistent with the gradual failure mode observed during strength testing, whereby the physical bond between binder and fibres provides resistance to pull-out and hence improved plastic deformation. It is also evident from the measurements taken from these images that the fibres are not stretching or reducing in diameter under tension. The absence of any evidence of chemical bonding between the lime and fibres, and the nature of the linear marking along the axis of fibres extracted from test specimens, is also consistent with resistance to fibre pull-out being responsible for the high levels of flexibility.

The low strength and rough surface texture (Figure 4b) of these experimental mixes would not make this a practical choice for a surface plaster coat. However, they could be utilised as the first coat in a multi-coat plaster. Traditionally, the first coat is the

thickest, which would be the ideal location for incorporation of the aerogel plaster. The subsequent topcoats would then provide the required protection and quality of finish.

4.7 Conclusions

- The results of this investigation confirm that aerogel granules can be successfully incorporated into non-hydraulic lime putty to produce viable lightweight, thermally insulating plasters.

- The thermal performance and permeability of the plaster containing only aerogel aggregate was superior to conventional plasters on the market and comparable to similar aerogel based insulating plasters being developed that contain higher proportions of aerogel.

- Previous investigations into aerogel based plasters have not considered strength or flexibility, which are important factors for in service use. The viability of the plasters developed in this investigation was strongly dependent on the inclusion of fibres, which improved flexibility and toughness and reduced shrinkage and cracking.

- There is considerable scope for further work by investigating different mix proportions and different specification materials.

- Further work is required to investigate the use of these insulating plasters as part of a multi-coat plaster system in order to optimise layer thicknesses to provide the required combination of cost, thermal efficiency, physical strength and quality of finish.

4.8 General observations and further work

The investigation carried out here has confirmed that aerogel can potentially be used to improve the insulation properties of plaster. However, the development of a market ready product is beyond the scope of this work. With a composite material, the number of realistic permutations of material ratios is vast and would require extensive testing to determine optimum ratios. It cannot even be said that there is one best solution, as different physical properties (strength, flexibility, permeability) may take

precedence depending on the application. There exists, therefore, significant scope for further work in this area, specifically the investigation of different binder to aggregate ratios, volume fraction and types of fibres and volumetric proportions of aerogel. As aerogel is a relatively new material (in comparison to other construction materials) and is still being developed, it is likely that new improved and/or functionalised versions of this aerogel will appear on the market in the future and offer new possibilities. Furthermore, this study concentrated on silica aerogel, the most common type, but aerogel produced from other elements exists including carbon and metal oxides. It is possible that in future these or other types of aerogel might be worthy of investigation.

The use of additional additive materials is another potential subject for investigation. The strength of the mixes obtained in this investigation could no doubt be increased by adding cementitious or pozzolanic additives. Again, this presents a vast number of possible material permutations and would depend on the end use of the product. Furthermore, the addition of additives to increase strength would probably be at the cost of water vapour permeability, one of the main advantageous properties of lime-based construction materials.

This work was based on the hypothesis that aerogel granules could be incorporated into lime-based plasters. However, the literature on this subject revealed another potential use for the materials developed here: insulating blankets. These could be used in a variety of applications including loft insulation between joists or rafters, where cold bridging occurs or to wrap around pipes. The low thermal conductivity, low strength and high degree of flexibility of the mixes investigated in this work would seem to be entirely compatible with these applications. Work would be required to determine the optimal thickness of material required to attain a U value competitive with other forms of insulation whilst keeping cost to a minimum. For use as a thermal blanket product, further work would almost certainly be required to investigate incorporating some type of membrane material to ensure the integrity of the part. Also, the membrane would need to be of a suitably permeable nature.

The cost and work involved in using aerogel plaster products would likely mean that at the present time they would be most suited to small scale or specialist retrofit applications. Whilst this might include some period properties, the use of such products would not be entertained on many heritage or conservation buildings.

4.9 References

Adfil, 2016. *Monofilament fibres* [online]. Available from: http://adfil.co.uk/products/micro-synthetic-fibres/monofilament-fibres/ [accessed 12th May 2016].

Buratti, C., Moretti, E., Belloni, E., and Agosti, F., 2014. Development of Innovative Aerogel Based Plasters: Preliminary Thermal and Acoustic Performance Evaluation. *Sustainability*, 6, pp.5839-5852

EN 1015-11:1999. *Methods of test for mortar for masonry - Part 11: Determination of flexural and compressive strength of hardened mortar.* BSI

Fibrelime, 2019. *A Future for Limes* [online]. Available from: http://fibrelime.romanproducts.uk/ [accessed 29 June 2019].

Fixit, 2016. *Aerogel Insulating Plaster System* [online]. Available from: http://www.fixit.ch/aerogel/pdf/Fixit_222_Aerogel_Verarbeitungsrichtlinien_A4_EN.pdf [accessed 7 August 2016].

Ingham, J., 2012. Diagnosing Defects in Lime-Based Construction Materials. In: I. Brocklebank ed. *Building Limes in Conservation*. Shaftsbury: Donhead, pp.175-198

Lambert, J.B., 1987. *Introduction to Organic Spectroscopy.* USA: Macmillan, p.176

Livesey, P., 2010. The Use of Lime Mortars and Renders in Extreme Weather Conditions. *Journal of the Building Limes Forum,* 17, 2010, pp.46-49

NICODOM, 2012. *FTIR Spectra of Polymers* [online]. Nicodom s.r.o.: Czech Republic. Available from: http://www.ftir-polymers.com/soon.htm [accessed: 15th May 2016].

Passivhaus Homes Ltd, 2019. *Spacetherm blanket* [online]. Available from: https://www.phstore.co.uk/aerogel-spacetherm-blanket [accessed 26 June 2019].

Proctor Group Ltd, 2019. *Spacetherm* [online]. Available from: https://www.proctorgroup.com/products/spacetherm?tw [accessed 26 June 2019].

Stahl, S., Brunner, S., Zimmermann, M., Ghazi Wakili, K., 2012. Thermo-hygric

properties of a newly developed aerogel based insulation rendering for both exterior and interior applications, *Energy and Buildings,* 44(2012), pp.114-117

Swann, G.E.A., and Patwardhan, S.V., 2011. Application of Fourier Transform Infrared Spectroscopy (FTIR) for assessing biogenic silica sample purity in geochemical analyses and palaeoenvironmental research*. Climate of the Past,* 7, 65–74, p.67

Wang, Q., Liu, H., 2011. The Experimental Research on the Water Vapour Permeability of Construction Gypsum Plaster Materials. *International Conference on Materials for Renewable Energy & Environment,* May 2011, Vol. 1, pp.854

CHAPTER 5 OLIVINE MORTAR

5.1 Introduction

Olivine that is being mined purely for CO_2 sequestration could potentially be made use of in the construction industry as a building material. A number of studies have previously been undertaken to assess the suitability of olivine as a method of solid stabilisation which exploit its ability to sequester CO_2 (Bemirbas et al., 2006) (Tkavoca, 1989) (Fasihnikoutalab et al., 2017ab).

Here an investigation into the potential for olivine as either an aggregate or, in finely ground form, as a pozzolan in lime-based mortars is presented. An important advantage of olivine additions is increasing the amount of carbonation, and hence CO_2 absorption capacity of the mortar. The widespread use of olivine as an aggregate material has the potential not only to increase the quantity of CO_2 sequestered by lime-based construction materials but also to enhance physical properties. The choice of lime binder for this work is of particular interest because lime mortars have undergone a revival in recent years for conservation work and are now being actively promoted and used in new-build applications (Fasihnikoutalab et al., 2016)((Fasihnikoutalab et al., 2015).

There are two potential reaction mechanisms to be investigated: firstly, the dissociation of olivine incorporated into a lime mortar could release Mg^{2+} cations to facilitate the formation of magnesium carbonates. This could potentially result in an increase in the amount of CO_2 absorbed during the hardening phase compared to quartz aggregate. Also, although much slower to carbonate (Hartshorn, 2012), dolomitic lime mortars have been shown to have higher mechanical strength compared to comparable calcitic lime mortars (Elert, 2002) (Yates, 2008). Secondly, if a pozzolanic reaction occurs, this could help reduce the quantity of lime binder used in a mortar mix.

The choice of binder is an important consideration for the optimal absorption of CO_2. Non-hydraulic lime is the most appropriate material for this type of investigation, as it has lower CO_2 emissions during production compared to hydraulic limes due to lower temperatures used during production. And, as it sets purely by carbonation, there are

no hydraulic phases, resulting in a higher quantity of CO_2 being absorbed during the setting phase.

5.2 Materials

5.2.1 Non-hydraulic lime putty

The binder material used for this work was a calcium hydroxide ($Ca(OH)_2$) lime putty supplied by J.J. Sharpe which had matured for at least twelve months. Weight measurements of a representative sample of the lime putty were taken before and after water removal by drying in a furnace at 100˚C for twenty four hours to determine the solids content. This equated to a solids content of 51%, assumed to be calcium hydroxide. This allowed accurate batching of the mix constituents.

5.2.2 Olivine

The olivine used was supplied by Industrial Minerals & Refractories Olivine India based in Tamil Nadu, India. The olivine sand received had been derived from Dunite ore and had been processed using a Raymond three roller mill to grind raw olivine rocks into a sand at an output of approximately 1.25 tonnes per hour. Two different batches of the mineral were received: a fine sand and a coarse sand (Figure 5.1). The coarse olivine sand was sieved to obtain particles with maximum size of 2mm to match as closely as possible the standard sand. Chemical composition analysis data from the

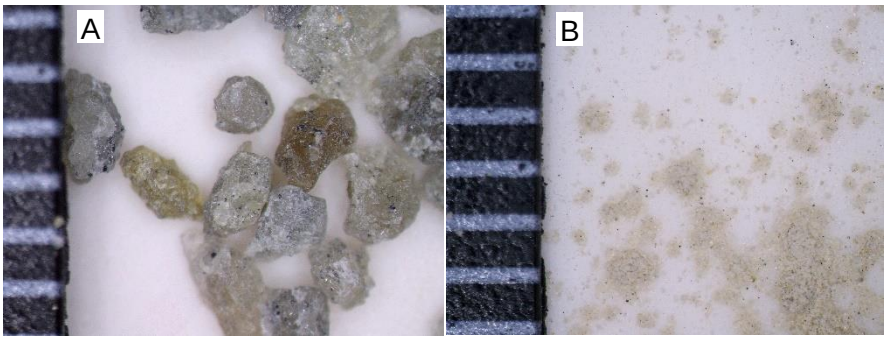

Figure 5.1: Coarse olivine sand (A) and fine olivine sand (B) shown against a 1mm scale.

Material Safety Data Sheets as supplied with the olivine are shown in Table 5.1. The chemical composition confirms the mineral to be high magnesium, forsteritic olivine.

Table 5.1: Chemical composition of olivine supplied from the manufacturer.

Material	MgO	SiO_2	Fe_2O_3	CaO	Al_2O_3
Coarse olivine	49%	21%	8%	1%	-
Fine olivine sand	48.7%	40.2%	8.5%	-	1.2%

The particle size distribution of the fine olivine sand was determined using a Malvern Mastersizer particle size analyser (Figure 5.2). With the 300mm lens fitted to the Mastersizer, the maximum particle size measurable was 600 µm. The data shows that the quantity of particles increases with particle size, up to the limit of 600 µm.

The data sheet supplied with the olivine stated that the particles were of size mesh 200# to 300#, which equates to approximately 50 to 74µm. The majority of the particles do fall within this range; however, the peak at approximately 500 indicates some particle agglomeration.

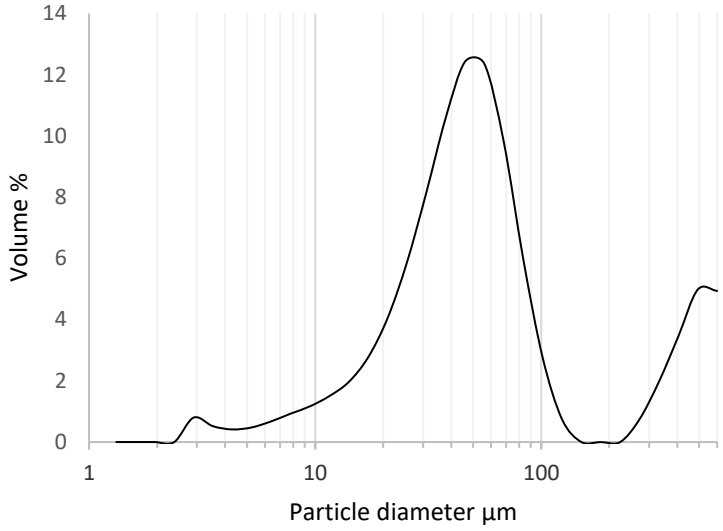

Figure 5.2: Particle size distribution of the fine olivine sand obtained using the Malvern Mastersizer.

5.2.3 Standard sand

The sand used in this investigation was a standard dry siliceous natural sand conforming to BS EN 196-1 and ISO 679: 2009. This grade of sand comprises particles that are generally isometric and rounded in shape with the particle size distribution shown in Figure 5.3. This type of sand was specified for this investigation to facilitate consistency and repeatability of experimental conditions.

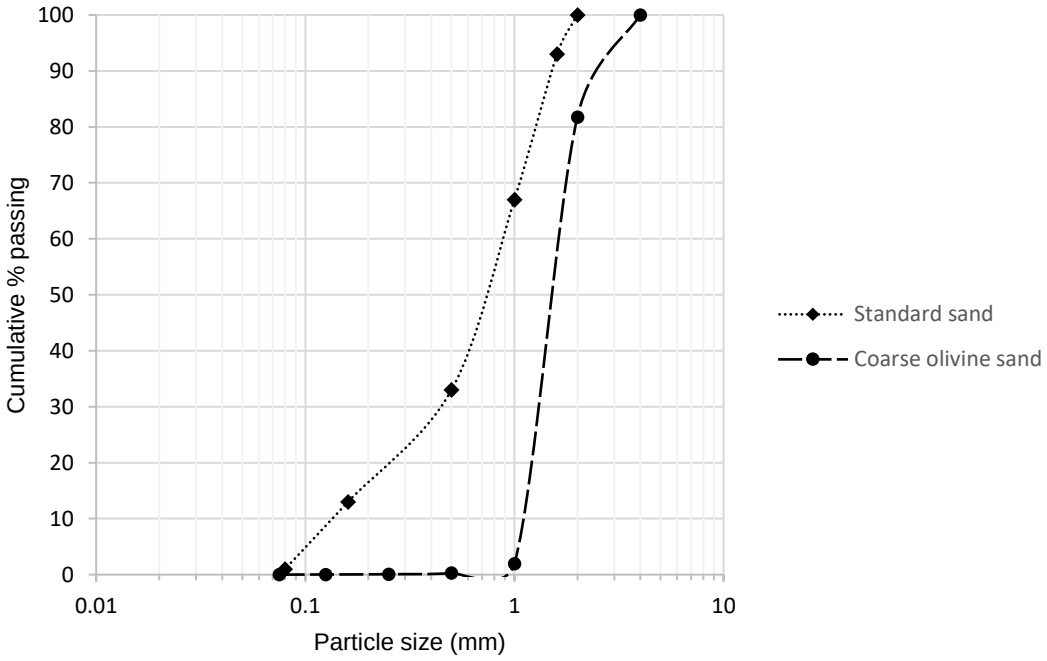

Figure 5.3: Particle size distribution for standard sand and large particle olivine obtained by sieve analysis.

5.3 Methods

5.3.1 Sample preparation

Four different experimental mixes (Table 2) were prepared:

1. S0 – Lime putty binder and standard sand aggregate (2:1)
2. S1 – Lime putty binder and fine olivine sand aggregate (2:1)
3. S2 – Lime putty binder and fine olivine sand aggregate (3:1)
4. S3 – Lime putty binder aggregate and coarse olivine sand (2:1)

The lime and aggregate were prepared using a paddle mixer for a minimum of twenty minutes to ensure the mortar was suitably workable. The experimental mixes were then added to 18 x 38mm cylindrical moulds in small quantities and tamped down as the material was added, to reduce the occurrence of trapped air bubbles within the specimens. After moulding, the specimens were stored in a climate chamber regulated at a constant temperature of 20ºC ± 2ºC and relative humidity of 65% ± 5% as specified in standard EN 1015-11:1999. The specimens were covered with a thin plastic wrap for the first week to maintain a high level of humidity, as exposure to ambient atmospheric conditions during this period can result in significant reduction in strength due to premature drying and subsequent cracking. The specimens were then left in the moulds for a further week to allow them to achieve sufficient rigidity to facilitate demoulding.

Table 5.2: Composition of experimental olivine mortar mixes by volume.

Specimen	Nominal aggregate: binder ratio	Lime putty (cm^3)	Standard sand (cm^3)	Fine olivine sand (cm^3)	Coarse olivine sand (cm^3)	Bulk density kg/m^3
S0	2:1	1,000	1,000	-	-	1.504
S1	2:1	1,000	-	1,000	-	1.309
S2	3:1	1,000	-	2,000	-	1.325
S3	2:1	1,000	-	-	1,000	1.515

5.3.2 Thermodynamic modelling

The thermodynamic modelling software GEM-Selektor v.3 (GEMS3) was used to predict the phase assemblages resulting from lime/olivine mixes. The objective was to predict whether using olivine as an aggregate could theoretically consume more carbon dioxide, through the formation of carbonate phases when compared to a conventional mix of lime and standard sand. Also, the modelling was applied to predict

whether the formation of hydration products such as C-S-H was thermodynamically favourable.

For the purposes of this modelling exercise it was necessary to make certain assumptions:

- The (open) thermodynamic system was considered to comprise of mortar only.
- The small iron content of the olivine, approximately six percent, was not taken into account; the olivine was assumed to be pure fosterite.
- The model assumes that the olivine sand completely dissociates, and equilibrium conditions are achieved.

The GEMS3 geochemical modelling programme uses an advanced convex programming method of Gibbs energy minimisation implemented as an efficient Interior Points Method. The software can be used to model a single reaction, or as a series of reactions in the form of a phase assemblage diagram (Grant, 2016) (Brocklebank, 2012) (GEMS, 2018).

5.3.3 X-ray diffraction

Powder X-ray diffraction was carried out using a BrukeraxsD8 Advance X-ray diffractometer equipped with a super speed PSD Vantec-1 detector and Cu K_α X-ray source of wavelength 1.5418Å. Data was collected over the 2θ range from 5° to 60° at a step size of 0.016° and time per step of 424.8s.

5.3.4 Raman spectroscopy

Raman Spectroscopy was carried out on specimen S2 at 28 days. A Renishaw InVia Raman Spectrometer was used employing a laser of wavelength 532 nm. Streamline image acquisition allowed a 1 x 6 mm scan of the surface to be obtained. 100% laser power of 80mW was used for 10 second exposures with a slit of 65µm and a 5x objective. The wavelength centre was 1000, which gave a data range of 61 to

1835 cm^{-1}. The Raman data obtained from the scan were analysed using Renishaw WiRE 4.4 (Windows Raman Environment) software

5.3.5 Scanning electron microscopy (SEM)

Scanning electron microscopy was used to examine the physical condition of the specimens. Of particular interest was the occurrence of unreacted olivine particles and bonding between any olivine particles and carbonate phases. Specimens were analysed using a JEOL 6480 LV scanning electron microscope equipped with an Oxford Instruments INCA X-act X-ray detector (silicon drift detector offering a high count rate and reduced operation time).

5.3.6 Field emission scanning electron microscopy (FESEM)

Field emission scanning electron microscopy was used to examine the morphology of the binder and aggregate at high magnification. Specimens were coated with a 20nm layer of chromium using a Quorum Q150TS machine. A JEOL JSM-6301F microscope was used with an accelerating voltage of 5kV to obtain images with magnification ranging from 10,000x to 20,000x.

5.3.7 Thermogravimetric analysis (TGA)

TGA analysis was carried out on a sample of each of the two experimental lime/olivine mixes using a Setaram TG-92 with an open alumina crucible and nitrogen as the purge gas. The test was run over a temperature range of 20 - 1000˚C, in 20˚C steps and 2 minutes per step.

5.3.8 Mechanical strength testing

Mechanical strength testing was performed using a 50 kN Instron 3369 Universal motorised load frame based on BS EN 1015-11:1999 to test compressive strength. Bluehill 3 software monitored and recorded the load on the specimen as a function of extension throughout the test.

5.4 Results

5.4.1 Thermodynamic modelling

Figure 5.4 shows the phase assemblage calculated by the thermodynamic modelling program. The program was used to model the mortar mix S1 as used in the physical tests. The x-axis shows the percentage of olivine within the aggregate mass of 1,744 grams.

The results shown are for the reactions at equilibrium when the forsterite will have completely dissociated into magnesium and silica ions; therefore, forsterite does not appear in the diagram. The results show that as the proportion of olivine in the aggregate increases, the amount of dolomite increases, indicating that increasing amounts of magnesium ions become available from the dissociated olivine to undergo carbonation.

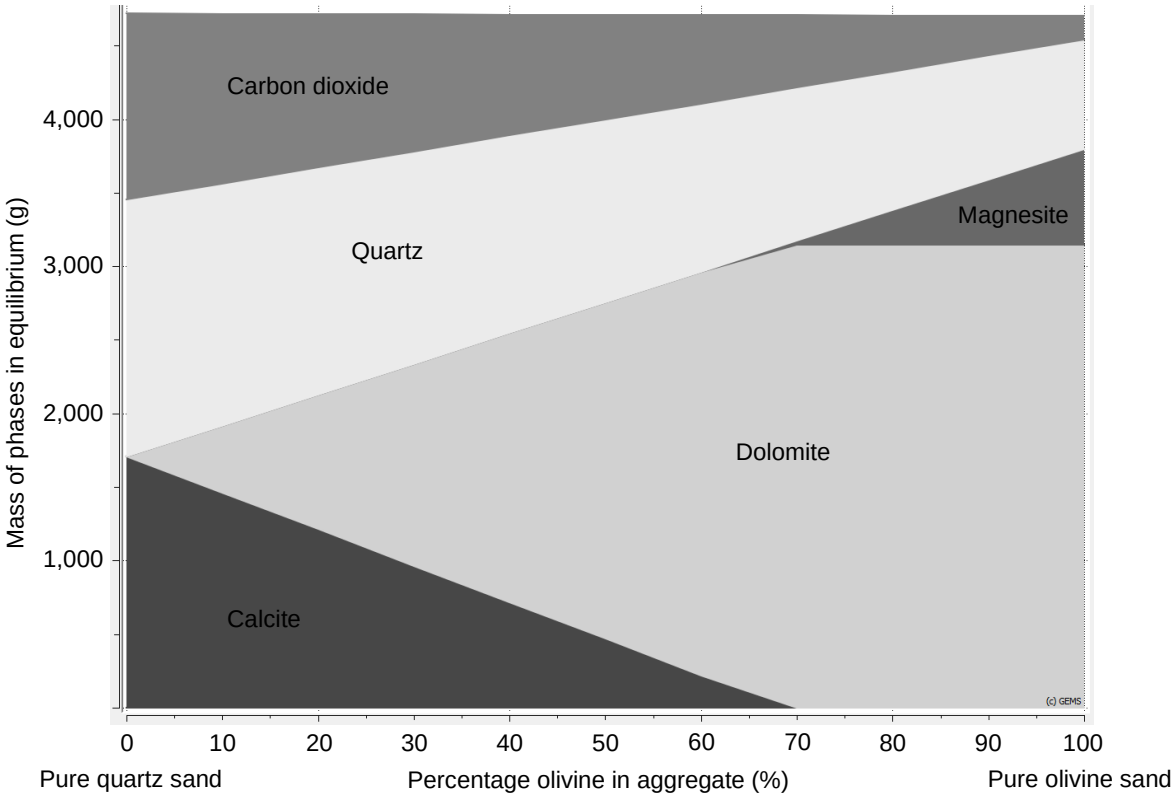

Figure 5.4: Phase assemblage diagram calculated by the GEMS3 Selektor thermodynamic modelling software for the olivine – lime system.

5.4.2 X-ray diffraction

XRD was carried out on the raw olivine as received and on the mortar mixes comprising olivine and lime binder in order to confirm the reactions taken place between the olivine aggregate and lime binder.

Figure 5.5 shows the XRD spectra obtained for the fine olivine sand (A) and the coarse olivine sand (B). They both show high intensity peaks at 2θ values of approximately 23.0, 35.9 and 36.6˚, confirming these to be high magnesium olivine. The absence of a peak at 31.6 indicates the lack of any significant quantity of iron silicate (Mineraldata).

The XRD patterns for the lime/olivine mortar mixes (S2 and S3) show peaks corresponding to the presence of forsterite, calcite and portlandite. The presence of portlandite indicated that the specimen had not completely carbonated, which also accounts for the low intensity peaks for calcite. Dolomite and magnesite could not be positively identified from the data due to having high intensity peaks at approximately 32.5˚ and 31˚ respectively, which overlap with strong forsterite peaks.

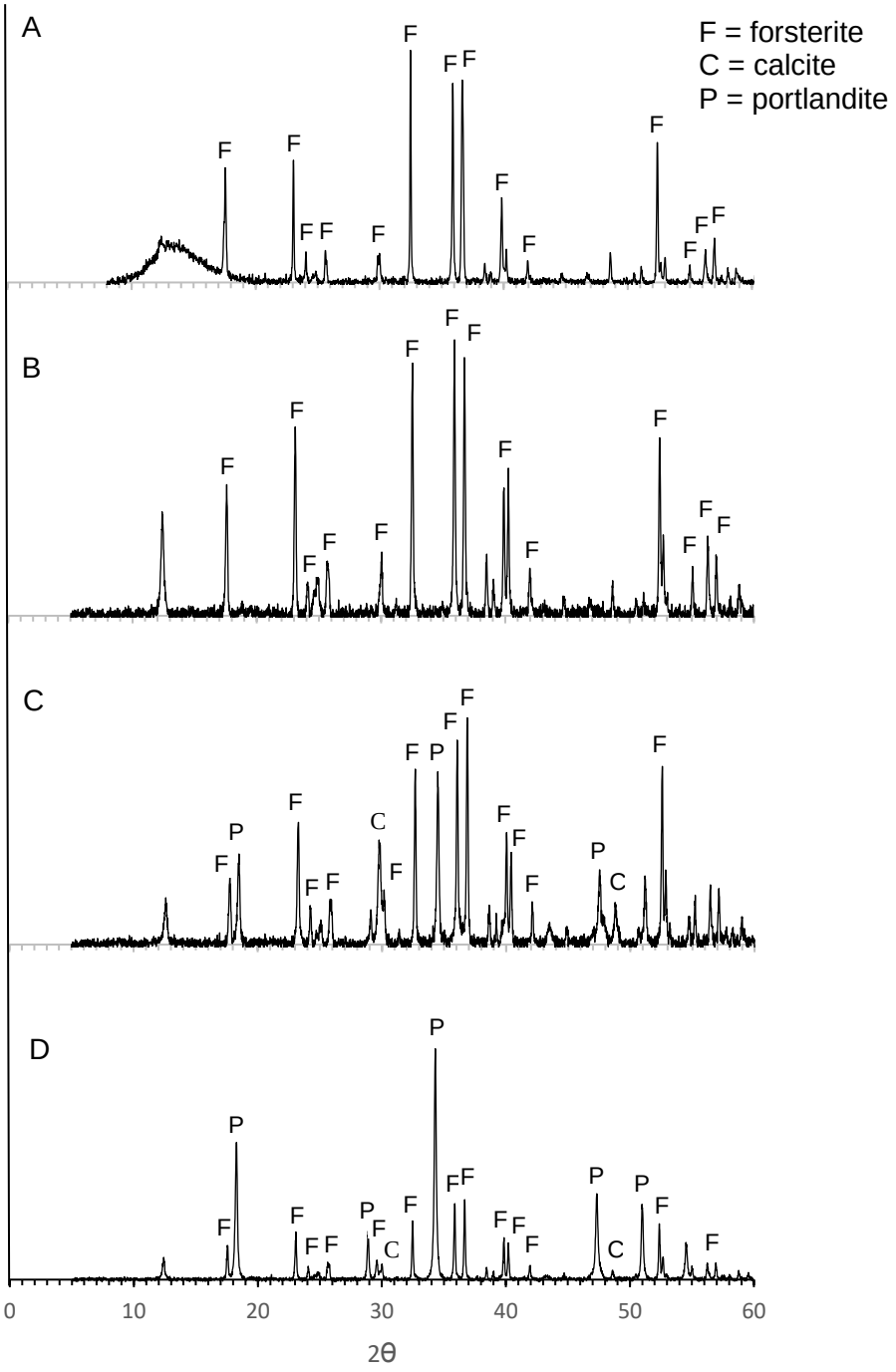

Figure 5.5: X-ray diffraction (XRD) patterns for fine olivine sand (A), coarse olivine sand (B), mortar mix S2 (C) and mortar mix S3 (D).

5.4.3 Raman spectroscopy

The S2 specimen was analysed to determine what reactions had taken place between the olivine and the lime and how closely they were in agreement with the results obtained using the thermodynamic software. The 1 x 6mm Raman scan produced 35,478 spectra. These spectra were interrogated using the Renishaw Wire 4.4 program to search for instances of the phases predicted by the thermodynamic software: calcite ($CaCO_3$), dolomite ($CaMg(CO_3)_2$), magnesite ($MgCO_3$), and quartz (SiO_2). The data were also searched for instances of forsterite (Mg_2SiO_4), which would indicate incomplete dissolution of the olivine. The analysis did identify spectra for calcite, dolomite, magnesite, forsterite and quartz (Figure 5.6). The data were also interrogated to try and identify the presence of any calcium silicate hydrates (C-S-H). Analysis failed to identify the presence of tobermorite or jennite phases, in agreement with the results obtained from the thermodynamic software.

Figure 5.6(A) shows a spectrum that correlates to calcite, with a strong peak at 1085 cm^{-1}, which is attributed to v_1 symmetric stretching of the CO_3 group and medium intensity peaks at 280, 157 cm^{-1}, which are assigned to v_2 lattice vibrations. Two low intensity peaks at 824 and 854 cm^{-1} are assigned to the Si-O symmetric stretching and Si-O antisymmetric stretching respectively and indicate a small quantity of olivine in the specimen. Figure 5.6(B) shows a spectrum from an area of the specimen comprising mainly unreacted olivine. The two high intensity peaks at 822 and 856 cm^{-1} are characteristic of forsteritic olivine and are assigned to the SiO_4 internal stretching vibrational modes. The lower intensity peaks at 1085 and 280 cm^{-1} indicate the presence of calcite in this region. Figure 5.6(C) shows the presence of dolomite and calcite together. The peaks at 1085 and 280 identify the calcite. The high intensity peak at 1098 cm^{-1} is a characteristic symmetrical stretching mode for dolomite, and the lower intensity peaks at 300 and 175 cm^{-1} are assigned to the dolomite lattice vibration mode. The spectrum shown in Figure 5.6 (D) is believed to show the presence of magnesite. The high intensity peak at 1095 cm^{-1} is characteristic of the symmetric stretching mode of the carbonate group in magnesite. The lower intensity peak at 325 cm^{-1} is consistent with the lattice vibration mode peak for magnesite, which is somewhat shifted from its expected position of approximately 330 cm^{-1}. There were not found to be any alternative phases to which this peak could be assigned, given the chemical composition of the specimen under test. The peaks at 202 and 459 cm^{-1} in Figure

5.6(E) indicate the presence of quartz. This is consistent with the thermodynamic software prediction that quartz should be produced from the dissociation of olivine.

The distribution of each of these minerals within the binder is shown in Figure 5.7. The lighter areas of the image represent the highest concentration of the mineral being detected.

.

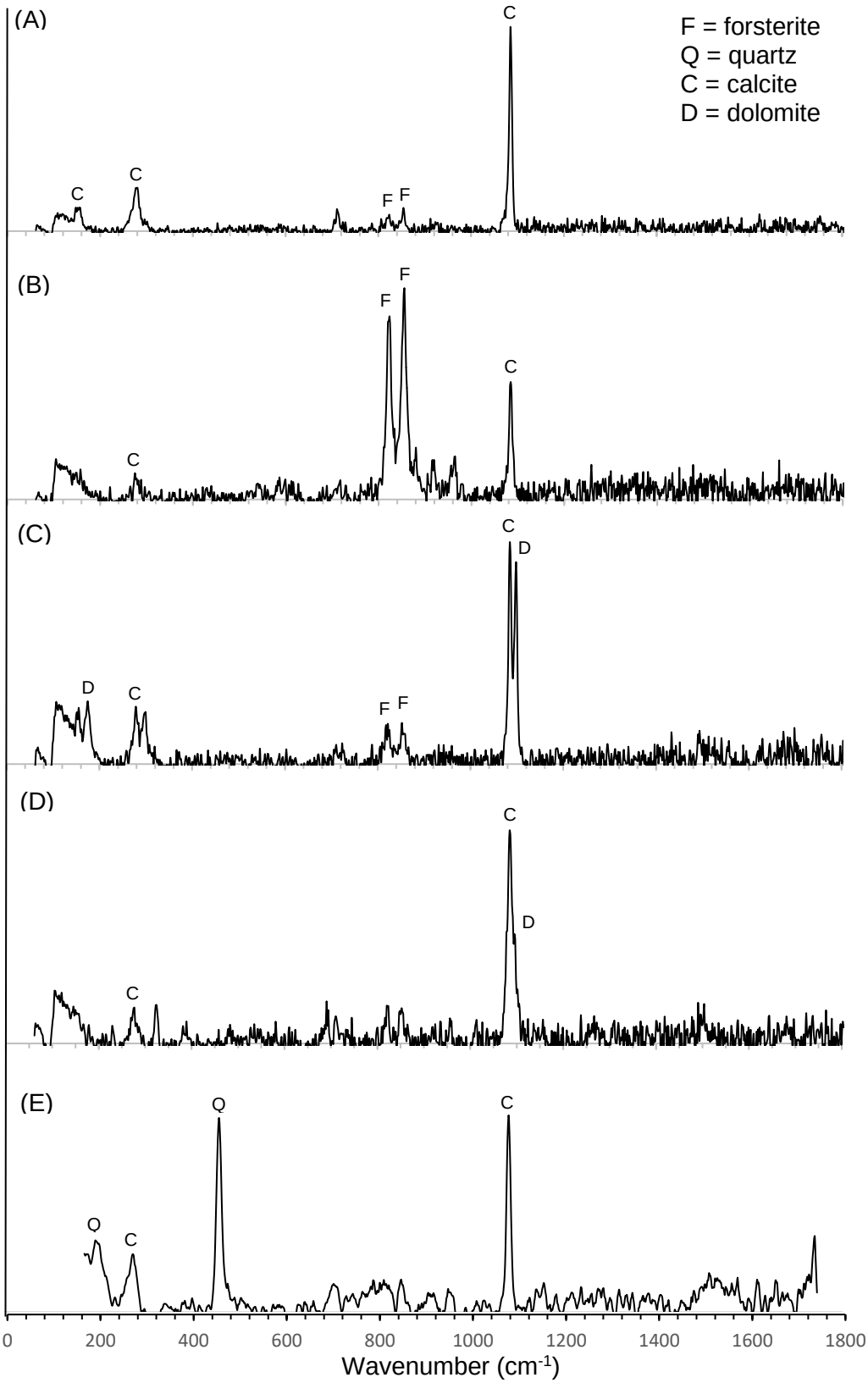

Figure 5.6: Raman spectra obtained from surface scan of mortar specimen S2 confirming presence of calcite (A), forsterite (B), dolomite (C) magnesite (D) and Quartz (E).

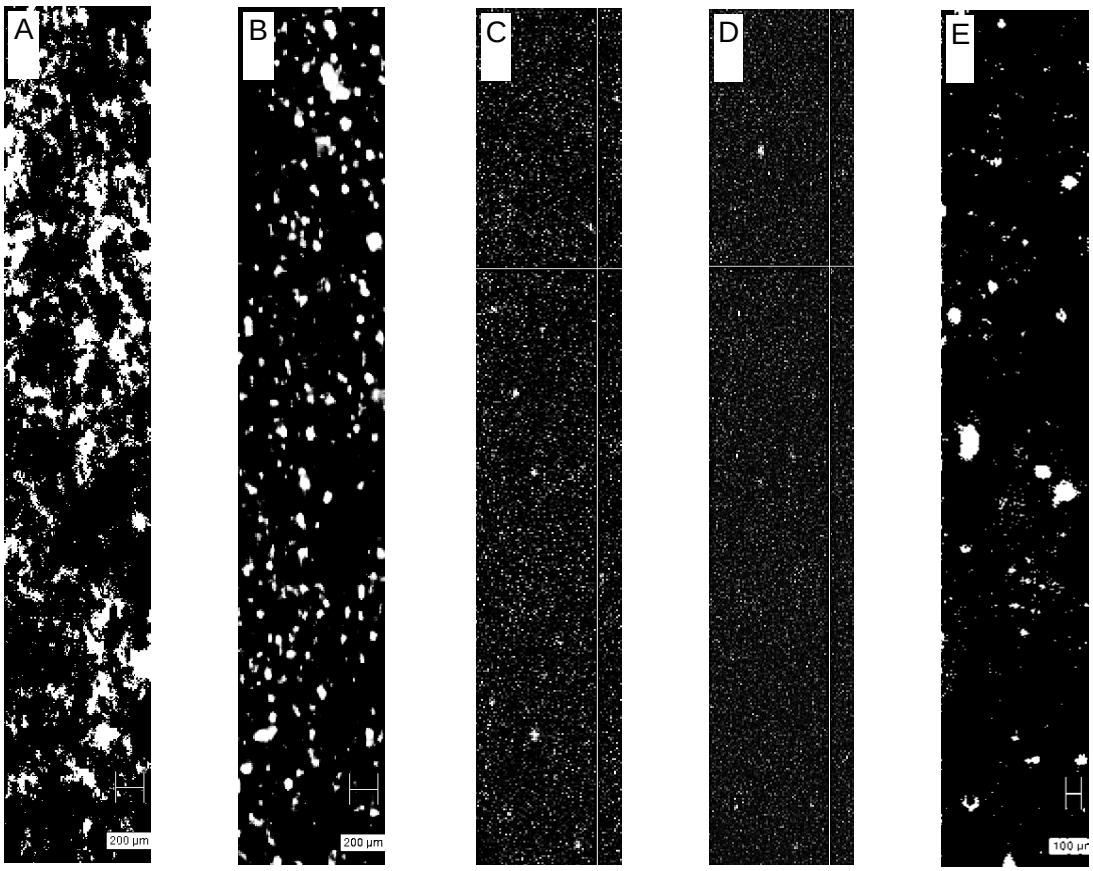

Figure 5.7: 1 x 6mm Raman scan of S2 specimen surface showing the phase distribution of calcite (A), forsterite (B), dolomite (C), magnesite (D) and quartz (E).

5.4.4 Scanning electron microscopy and field emission scanning electron microscopy

Images of magnification up to 5,000X were obtained using SEM, and FESEM was used to obtain higher resolution images. The images in Figure 5.8 show the three different types of aggregate used. Images (A) and (B) are of standard sand and show the typical rounded shape of the particles. The fine olivine sand seen in images (C) and (D) shows a much more angular shape and rough surface condition, which is typical of the conchoidal fracture associated with olivine. Images (E) and (F) show the coarse olivine sand particles, which are also rounded in shape but show the typical conchoidal fracture faces.

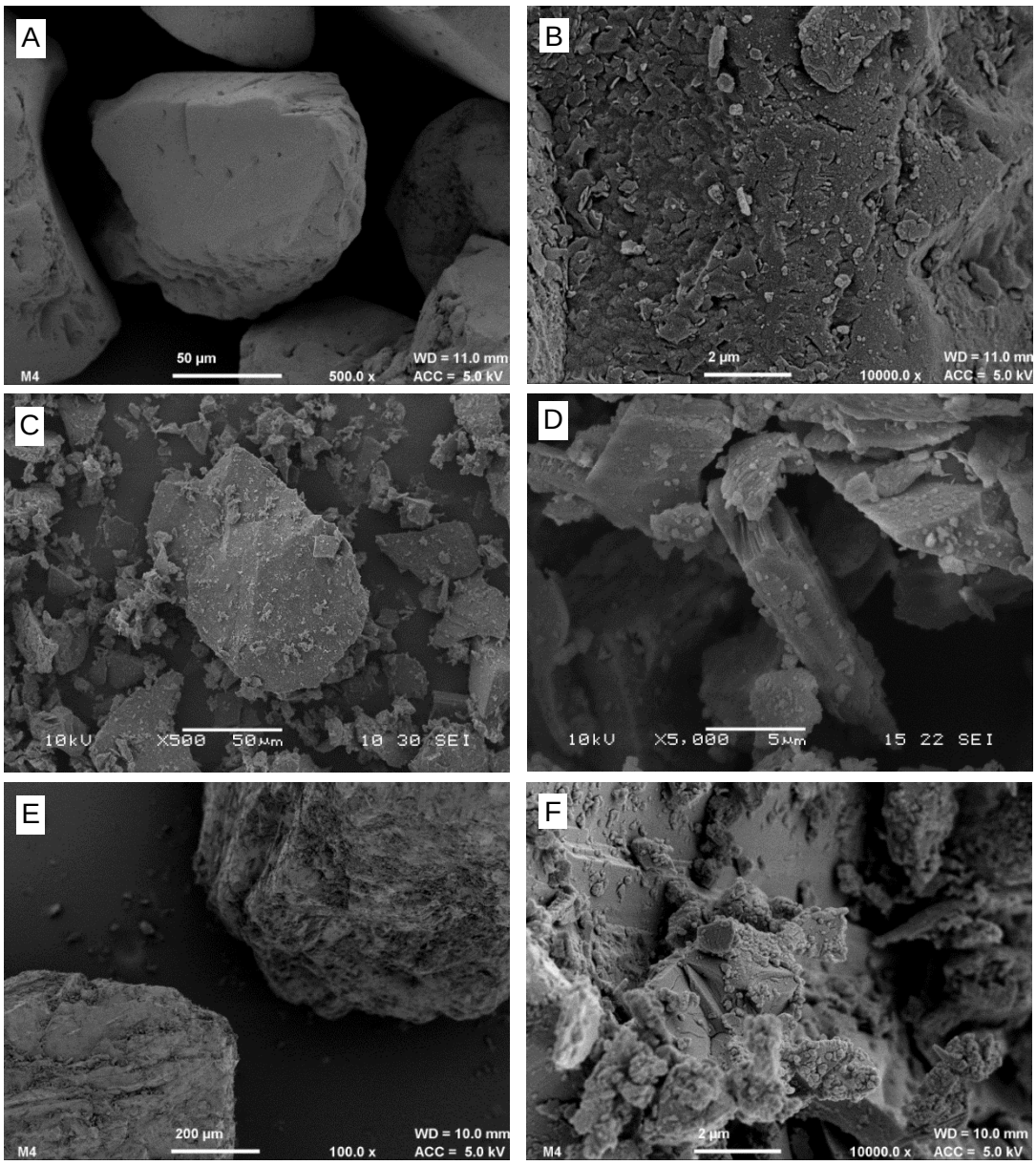

Figure 5.8: Morphology of aggregate particles – standard sand (A) (B), fine olivine sand (C) (D) and coarse olivine sand (E) (F).

The images in Figure 5.9 show mortar mixes after 91 days. There is widespread occurrence of well-formed scalenohedral calcite crystals throughout the mortars containing the fine olivine sand aggregate (C)(D)(E)(F). Images of the two mortars containing standard sand and large particle sand aggregates (A)(B)(G)(H) show more granular or massive calcite formations. In the images showing both fine and coarse olivine sand (E)(F)(G)(H), unreacted olivine particles can be seen.

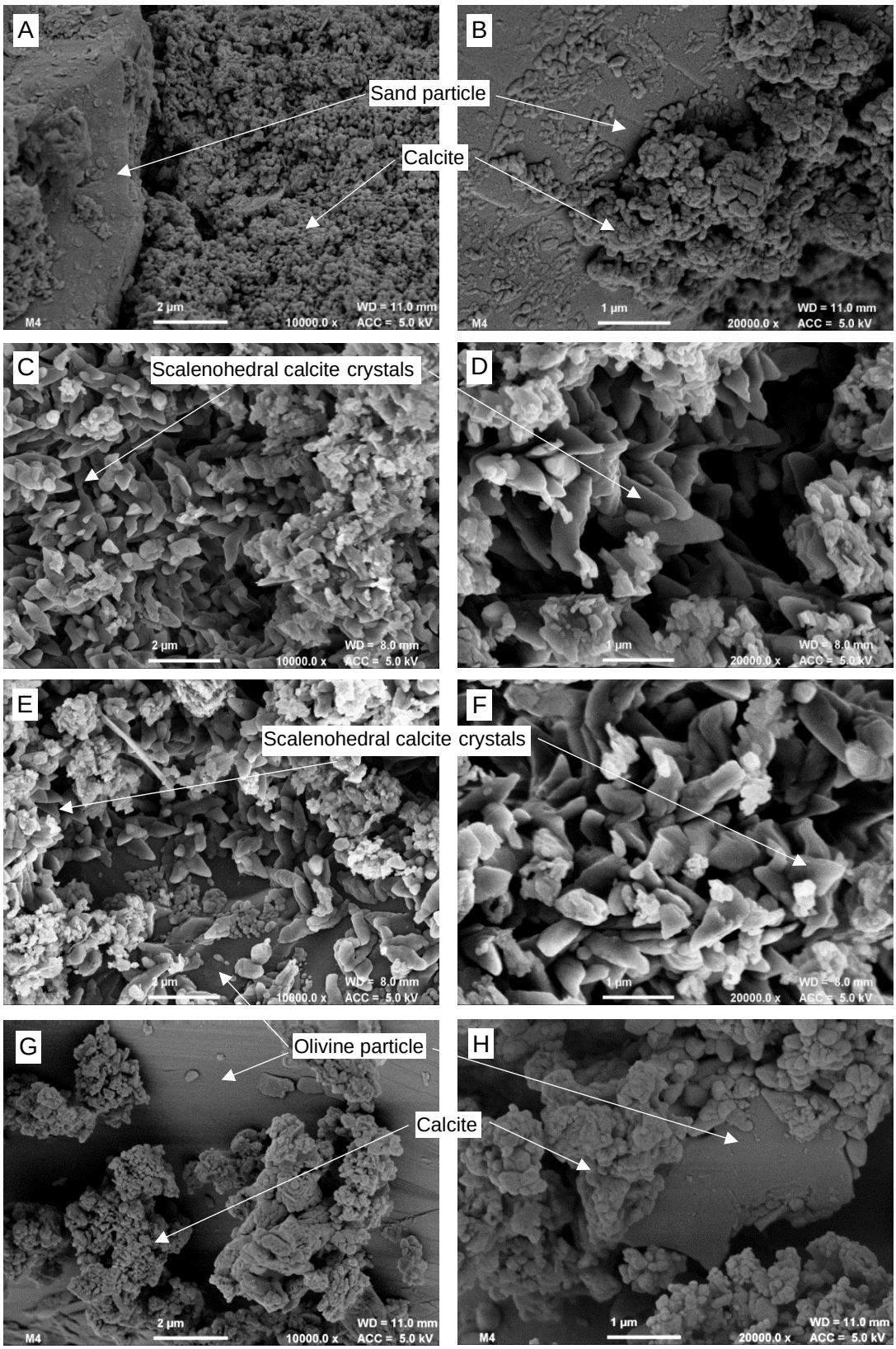

Figure 5.9: Images of experimental mortar mixes S0 (A)(B), S1 (C)(D), S2 (E)(F) and S3 (G)(H) at 91 days.

5.4.5 Thermogravimetric analysis (TGA)

TGA analysis was carried out after 28 days on all four of the experimental mixes. Two distinct instances of mass loss (Figure 5.10) were observed in each case. The smaller mass loss curve occurred between 420 and 460°C, and this was attributed to dehydration of portlandite. The largest mass loss occurred between 700 and 800°C, which is a result of the decomposition of carbonate material (Kulik et al., 2013) (Wagner et al., 2012).

The equipment did not have high enough resolution to distinguish between the different carbonate phases; however, it can be seen that the mortars containing olivine sand aggregate were shown to contain the highest proportion of carbonate material. In specimen S0 the percentage carbonate of the material that decomposed was 69.1%. In specimens S1, S2 and S3 it was 79.5%, 83.1% and 86% respectively.

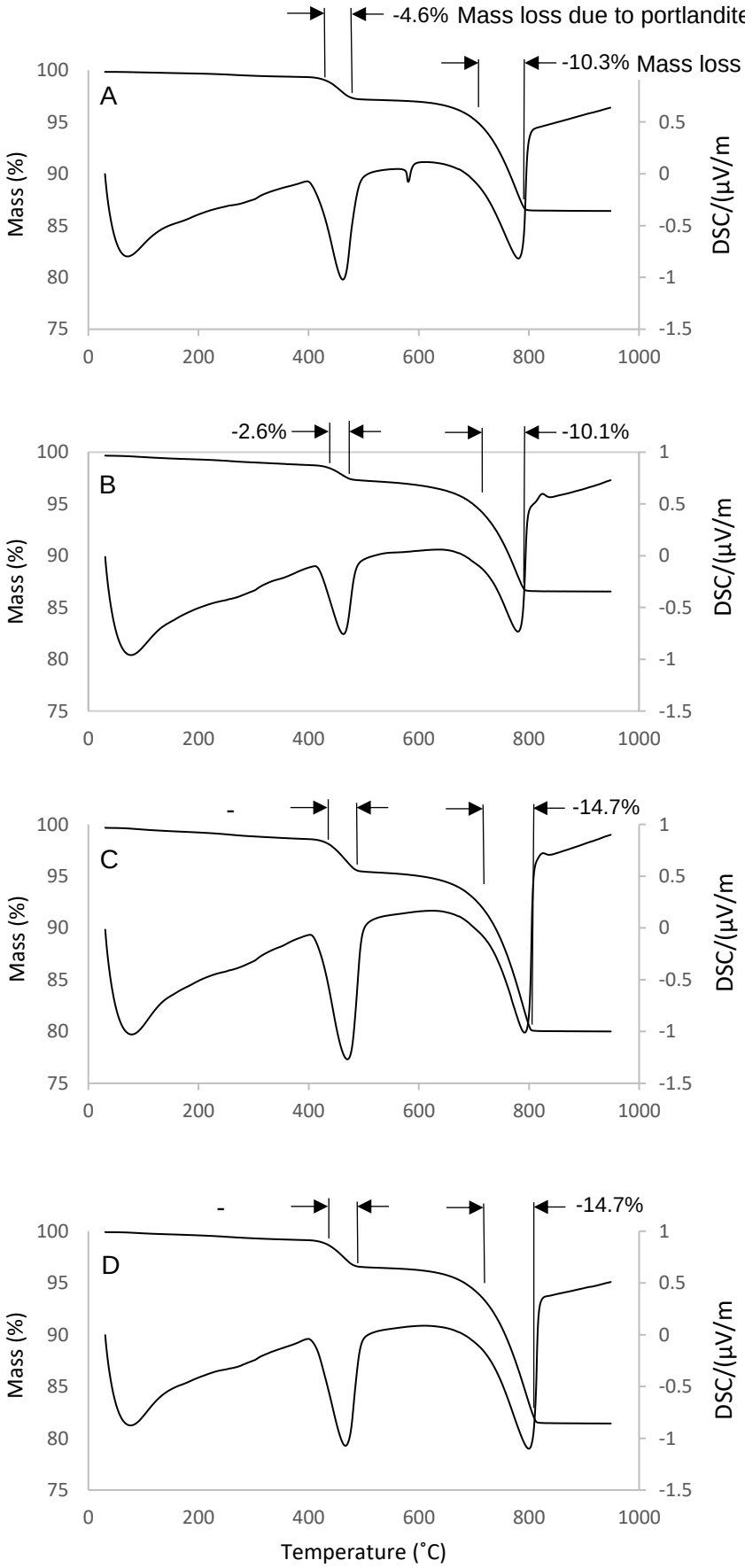

Figure 5.10: TGA curves for mass and DSC for each mortar mix. S0 (A), S1 (B), S2 (C) and S3 (D).

5.4.6 Mechanical strength testing

Figure 5.11 shows the compressive strength at twenty eight days for each of the four mortar mixes. The reference mortar comprising lime and sand (S0) achieved a level of strength that would be considered typical for a non-hydraulic mortar at twenty-eight days (Valverde, 2015). However, the specimens incorporating fine olivine sand as aggregate (S1 and S2) obtained compressive strength values that were 278% and 370% higher than with conventional sand. Significantly, the specimen with the highest olivine content (S2) obtained the greatest strength. The specimen comprising lime and coarse olivine sand was the weakest of the mixes.

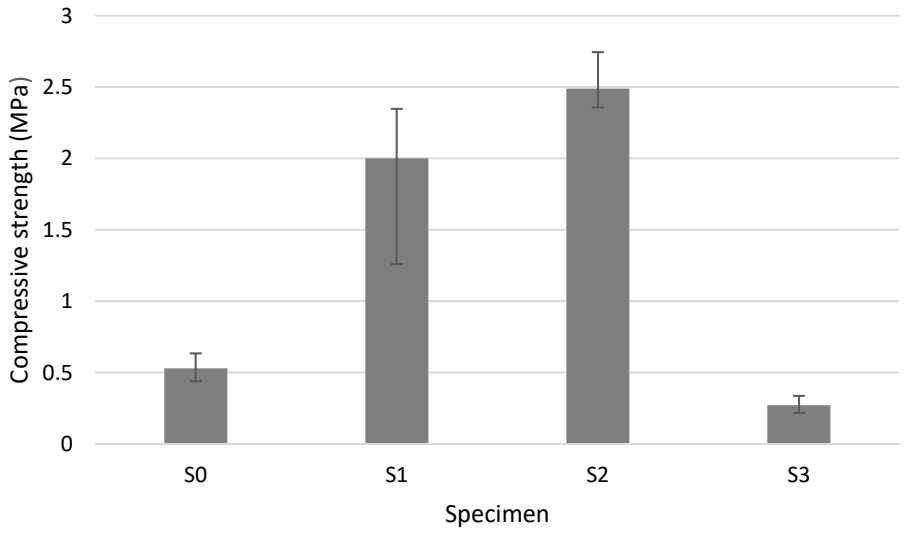

Figure 5.11: 28 day compressive strength test results for the four experimental mixes; S0=lime and standard sand, S1=lime and fine olivine sand 2:1, S2=lime and fine olivine sand 3:1, S3=lime and coarse olivine sand. Error bars show maximum and minimum values.

5.5 Discussion

The research described here has shown conclusively that olivine aggregate, in finely divided form, will react in the presence of lime and water to produce magnesium carbonates, which not only increase the amount of CO_2 absorbed by the mortar during setting, but also provide a strength enhancing ability.

The thermodynamic model shows that, at equilibrium, when olivine is the sole aggregate, there should theoretically still be a significant amount of quartz within the system. This can be attributed to new quartz forming from the silica anions released by the dissolution of the olivine. In the experimental mixes, there is significantly less quartz present due to the fact that the system has not reached equilibrium and the olivine has not completely dissociated.

The diagram also shows that as the proportion of olivine aggregate is increased, the total mass of the carbonate phases (calcite, dolomite and magnesite) at equilibrium increases as the olivine dissociates to leave magnesium cations free to form increasing amounts of magnesium carbonates (dolomite and magnesite). This in turn results in a corresponding increase in CO_2 consumption, as seen by the decreasing amount of CO_2 within the system as the proportion of olivine is increased. Magnesite is only shown to be formed when the aggregate comprises 75% or higher of olivine. The increase in carbonate products when olivine is present can be accounted for by the fact that olivine is a nesosilicate and the most reactive mineral on the Goldich dissolution series, whereas quartz is the least reactive and can be considered inert (Wulandari et al., 2017). The model did not predict the production of any hydration products.

The physical tests carried out during this investigation exhibited varying degrees of agreement with the thermodynamic modelling. Although the phases present agree with the thermodynamic software predictions, the quantities present were somewhat different. This is explained by the fact that the software calculated the minerals present at equilibrium, as if the olivine had completely dissociated and reacted with the lime. However, it can be seen from both the XRD and Raman data that there remains a significant quantity of unreacted olivine still present in the mortar. As the quantity of olivine that dissociated was small, the amount of magnesium carbonates (dolomite, magnesite) produced was correspondingly small, which left much of the portlandite free to carbonate and accounts for the large proportion of calcite detected.

The phases identified by Raman spectroscopy aligned more closely with those predicted by the thermodynamic software compared to phases identified from XRD studies. This may be due to the nature of the sample material under test. The XRD samples comprised small amounts of material (20 – 80mg) which was ground into a

powder. This sample, therefore, contained material both from the surface and from the bulk, which would account for the presence of unreacted lime (portlandite) from deeper within the specimen. In contrast, Raman spectra were obtained from the surface of the material only where the reactions initiated, which is consistent with the absence of portlandite. The dissociation of the olivine and the carbonation of the lime binder may continue as more water is added to the system over time.

In the absence of any hydration products such as C-S-H, the increased strength of the mixes incorporating olivine can be attributed to the creation of increased amounts of carbonates as shown by the model and by the XRD and Raman spectroscopy analysis. The specimen comprising lime binder to fine olivine aggregate at a ratio of 1:3 (S2) was significantly greater than the specimen comprising the same materials at 1:2 ratio (S1). As specimen S2 contained a higher proportion of carbonate material, this provides further support to the inference that higher compressive strength is correlated with higher carbonate content.

The higher carbonate content of the mortars containing fine olivine sand is consistent with the crystal structures identified with the electron microscopy images. The well-formed scalenohedral crystal structures in specimens S1 and S2 indicate that during carbonation there was room for these crystals to grow unconstrained, which would also have provided generous pathways for CO_2 and water vapour diffusion. Specimens S0 and S3, in contrast, consist of tightly packed granular carbonate crystals, which would be less conducive to carbonation.

Whether all of the strength increases obtained with olivine aggregate can be attributed to increased carbonation is uncertain. It is possible that there are physical effects too. For example, the shape and surface morphology of small particle olivine is substantially different from that of the large particle olivine and the normal silica sand. The small olivine particles are very angular in shape and have rough surfaces, both of which are conducive to higher strength due to bonding between the aggregate and the lime paste. The lower strength of the mix containing coarse olivine sand must be attributed to the larger particles of olivine possessing lower strength than the fine olivine sand, which could be due to the more intense milling that must be carried out to obtain the smaller particles.

5.6 Conclusions

This research has, for the first time, investigated the effect of using olivine as an aggregate in lime mortars. The following conclusions may be drawn:

- Olivine sand will dissociate in a lime mortar mix to facilitate the formation of magnesium carbonates, increasing CO_2 absorption.
- The total carbonate content of aged mortars containing fine olivine sand aggregate is greater than that found in a conventional silica sand lime mortar of similar mix proportions that contains a purely silica sand aggregate.
- The increased formation of carbonates when olivine aggregates are used promotes a greater compressive strength of 2.5 MPa compared to conventional mortar mixes 0.5 MPa incorporating quartz sand aggregate.
- The particle size of the olivine sand and corresponding surface area is of significance in promoting the necessary dissociation and carbonation reactions.

5.7 General observations and further work

Although it was found that olivine can be utilised to sequester carbon dioxide and increase strength in lime mortars (through increased carbonation), the limited research done for this work clearly showed that particle size is a critical factor. Therefore, in order for olivine aggregate to be accepted as a viable option, further work would need to be carried out relating to optimum particle size.

There is also another reason why optimum particle size is so relevant. Processing olivine, by crushing and milling to produce sand, consumes energy, and this should be compared with the carbon dioxide sequestration capacity of the olivine. The environmental case for using olivine to sequester carbon dioxide could be put into question if the energy cost were excessive. If processing produces ever diminishing returns in terms of reactivity, there could be found an optimum particle size that delivers the most carbon dioxide sequestration for the least amount of processing.

Another important issue to keep under consideration is the chemical composition of Olivine. This work focussed on fayalitic olivine, which is high in magnesium, but the

proportions of iron to magnesium can vary in any ratio, depending on the geological source, and this could have an influence on the properties of the sand. It would be of value to carry out work to investigate the viability of olivine from different sources.

5.8 References

Brocklebank, I., ed., 2012. *Building Limes in Conservation.* Shaftsbury: Donhead Publishing Ltd. p.10

Demirbas, A., 2006. Carbon Dioxide Disposable via Carbonation. *Energy Sources, Part A: Recovery, Utilisation and Environmental Effects,* 29(1) pp59-65

Elert, K., Rodriguez-Navarro, C., Pardo, E. S., Hansen, E., and Cazalla, O., 2002. Lime Mortars for the Conservation of Historic Buildings. *Studies in Conservation,* Vol. 47, No. 1, pp. 62-75

Fasihnikoutlab, M. H., Asadi, A., Huat, B. B. K., Westgate, P., Ball, R. J., and Pourakbar, S., 2016. Laboratory-scale model of carbon dioxide deposition for soil stabilisation. *Journal of Rock Mechanics and Geotechnical Engineering,* 8[2016], pp.178-186

Fasihnikoutalab, M. H., Asadi, A., Unuler, C., Huat, B. K., Ball, R. J. and Pourakbar, S., 2017a. Utilization of Alkali-Activated Olivine in Soil Stabilization and the Effect of Carbonation on Unconfined Compressive Strength and Microstructure. *ASCE Journal of Materials in Civil Engineering*, 29 (6), 06017002.

Fasihnikoutalab, M., Pourakbar, S., Ball, R. and Huat, B., 2017b. The Effect of Olivine Content and Curing Time on the Strength of Treated Soil in Presence of Potassium Hydroxide. *International Journal of Geosynthetics and Ground Engineering*, 3 (12).

Fasihnikoutlab, M. H., Westgate, P., Huat, B. B. k., Asadi, A., Ball, R. J., Nahazanan, H. and Singh, P, 2015. New Insights into Potential Capacity of Olivine in Ground Improvement. *Electronic Journal of Geotechnical Engineering,* 20[2015], pp.2137-2148

GEMS, 2018. *Gibbs Energy Minimization Software for Geochemical Modelling* [online]. Villingen: Paul Scherer Institut. Available from: http://gems.web.psi.ch [Accessed 7 February 2018].

Grant, J., Pesce, G. L., Ball, R. J., Molinari, M. & Parker, S. C. 2016. An experimental and computational study to resolve the composition of dolomitic lime In: RSC Advances, 2016, Vol.6(19), pp.16066-16072.

Kulik D.A., Wagner T., Dmytrieva S.V., Kosakowski G., Hingerl F.F., Chudnenko K.V., Berner U. (2013): GEM-Selektor geochemical modelling package: revised algorithm and GEMS3K numerical kernel for coupled simulation codes. *Computational Geosciences* 17, 1-24. doi.

Mineraldata, 2019. *Mineral Arranged by X-ray Powder Diffraction* [online]. Available from: http://www.webmineral.com/MySQL/xray.php?st=201&minmax=2&lambda=1.54056%20-%20CuKa1&ed1=2.831&#.XR3eA-hKhaQ [accessed 4 July 2019].

Tkacova, K., 1989. *Mechanical activation of minerals.* Amsterdam: Elsever Science Publishers

Yates, T., Ferguson, A., 2008. The use of lime-based mortars in new build. Amersham: NHBC Foundation

Valverde, J. M., Perejon, A., Medina, S. and Perez-Maquedad, L. A., 2015. Thermal decomposition of dolomite under CO2: insights from TGA and in situ XRD analysis. *Phys. Chem. Chem. Phys*., 2015, 17, p.30166

Wagner T., Kulik D.A., Hingerl F.F., Dmytrieva S.V. (2012): GEM-Selektor geochemical modelling package: TSolMod library and data interface for multicomponent phase models. *Canadian Mineralogist* **50**, 1173-1195. doi.

CHAPTER 6 HOT LIME MORTARS

6.1 Introduction

Global concern regarding CO_2 emissions in recent years has resulted in a resurgence in the use of lime mortars and plasters. Lime is considered more environmentally friendly than cementitious construction materials because it consumes less energy during production, absorbs CO_2 during the setting phase and allows recycling of masonry materials (Greenspec, 2017). Hot lime mortars have also proven to be a very durable construction material. There exist many examples of hot lime mortars that have lasted hundreds of years, as well as a wealth of anecdotal evidence to support their reputation for durability (Ingham, 2012).

Lime binders used for construction are manufactured from quarried limestone, which is mainly comprised of calcium carbonate. The limestone is then heated at around 900˚C, which liberates carbon dioxide, leaving calcium oxide. The calcium oxide, commonly referred to as quicklime, is then slaked with water to produce calcium hydroxide. If a controlled amount of water is added to the quicklime to produce a powder, this is known as 'hydrated lime'. When an excess of water is added, the result is a lime putty. Prior to the second world war, lime was often delivered to site unslaked, as quicklime. The bricklayer or plasterer would then add water to the quicklime and aggregate. Combining water with quicklime results in a highly exothermic reaction, and it is because of the large amount of heat generated that this type of mix is known as 'hot lime'. The temperature during slaking can potentially exceed 250°C very quickly, but in hotspots only, and the overall temperature of the mortar should not normally exceed 100°C Cornish Lime, 2019).

The form of quicklime used in a hot lime mix will have an effect on the mortar produced. There are two, chemically identical (CaO), forms of quicklime available: kibbled quicklime, which is granular and has particles of 1mm and larger and powdered quicklime. Kibbled quicklime reacts more slowly than the powdered form, but the larger particles can reach higher temperatures and cause hotspots. Powdered quicklime reacts faster and does not suffer from hotspots but the reaction can be harder to control. The physical properties are also different: kibbled quicklime is denser and

expands to approximately 2.7 times its original volume, whereas powdered quicklime expands to approximately 2.1 times (Brown, 2017).

Hot lime mortars are believed by many conservationists to perform better than other lime mortars in terms of mechanical and bond strength, one theory is that the heat generated during slaking may have a beneficial effect on the bond characteristics between binder and aggregate (Forster, 2004). It has also been hypothesised that the high calcite content of these mixes imparts a salt and frost resistant pore structure, making them more durable. (Henry, 2018). A further benefit claimed for hot lime mixes is their ability to eliminate voids within the mortar. Quicklime expands when it is slaked and can continue to increase in volume after it has been laid. It is claimed that this expansion fills voids and reduces shrinkage (Historic Environment Scotland, 2019). This last claimed benefit is somewhat inconsistent with another claim that testing has proven that hot-mix mortars offer ‘extremely high vapour permeability’ (Cornish Lime, 2019).

Despite its favourable reputation, there is little published scientific information to support the hypothesis that hot lime mortars are superior to other forms of lime mortar. This paper investigates the physical properties of hot-lime mortars incorporating three different aggregate materials and compares them with lime putty mortars incorporating the same aggregate materials.

The two novel aggregate materials, slate and granite, were selected for this investigation for two reasons. Firstly, when comparing hot lime mortars with lime putty mortars, a more comprehensive understanding of the differences between the two mortars can be obtained by comparisons of mixes containing different aggregates. Of secondary interest was whether slate or granite could be successfully used as aggregate materials. There is much interest in the recycling of these materials for construction materials, and whilst there is a wealth of research relating to their use with cementitious materials, little research has been carried out relating to lime-based construction materials (Barluenga, 2010) (Shankar, 2015).

6.2 Materials

The three aggregate materials were sieved to achieve similar particle size distributions (Figure 6.1). The objective of this was to eliminate as far as possible any differences in performance of the aggregates due to differences in size.

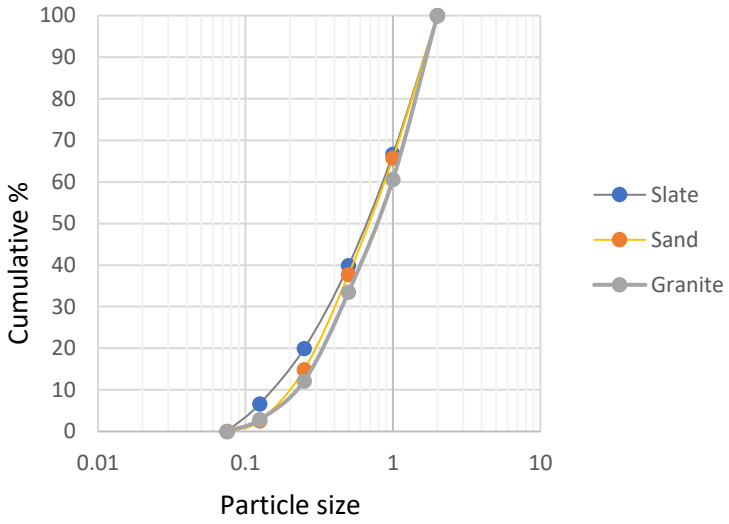

Figure 6.1: Particle size distribution comparison for the three aggregate materials.

6.2.1 Quicklime (Calcium oxide)

The binder material used for this work was a knibbled quicklime . The XRD pattern obtained for the quicklime (Figure 6.2) confirm it to be a high purity calcium oxide with small amounts of calcium hydroxide and calcium carbonate, which are presumed to be as a result of contact with atmospheric water vapour.

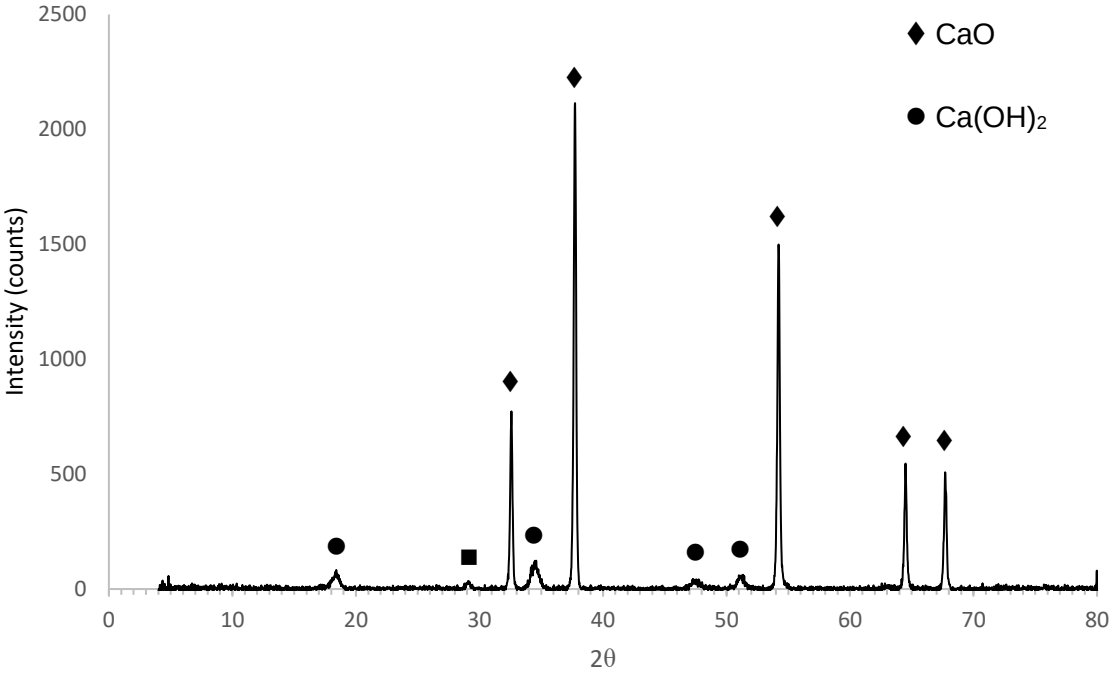

Figure 6.2: XRD pattern for calcium oxide.

6.2.2 Standard sand

The sand used in this investigation was a dry siliceous natural sand conforming to BS EN 196-1 and ISO 679: 2009. This grade of sand comprises particles that are generally isometric and rounded in shape and having a particle size distribution as shown in Figure 1.

6.2.3 Slate

Slate is a fine-grained, foliated metamorphic rock that has been formed through the metamorphosis of shale. It is mainly composed of silica and clay minerals and can also contain smaller amounts of calcite, pyrite, hematite and feldspar. The possible presence of pyrite in an aggregate material is of concern, as it has been proven that pyrite will oxidise when exposed to moisture and air, which is expansive and can result in the production of sulphuric acid.

The slate in this study was Welsh blue chippings obtained from crushing the slate waste stockpiles in Wales. It was supplied as 40mm chippings, which were reduced in size using a crusher and then sieved to obtain the required particle size distribution.

6.2.4 Granite

Granite is an intrusive igneous rock comprised mainly of quartz and feldspar plus smaller amounts of mica, amphiboles and other minerals. It is formed below ground from very hot liquid magma, which is forced upwards until it comes into contact with cooler rock. This causes the magma to cool slowly and form rocks that have large crystals.

The granite for this work was received as 6mm to dust chippings, which were put through a crusher and then sieved to obtain the desired particle size distribution.

6.3 Methods

6.3.1 Sample preparation

Three different experimental hot lime mortars were prepared for this investigation each having a volumetric binder to aggregate ratio of 1:3 (Table 6.1). 24 cylinders of each mix were prepared. The aggregate was placed in a heap on a concrete floor and a depression was made in the centre of the aggregate, into which the quicklime was added. Water was then added to the quicklime gradually and the sand was mixed thoroughly with the aggregate by hand using a trowel. The water was added until the mortar was a workable consistency but thick enough to adhere to an upturned trowel.

Table 6.1: Material composition by volume of experimental mixes.

Specimen	Calcium oxide (%)	Sand (%)	Slate (%)	Granite (%)
S0	25	75	0	0
S1	25	0	75	0
S2	25	0	0	75

Three different lime putty mixes were also prepared with a volumetric binder to aggregate ratio of 1:3 and using the same aggregate materials. The materials were mixed using a paddle mixer for a minimum of twenty minutes to ensure the mortar was suitably workable. The lime putty was placed in the mixer at the start of the process and the aggregate was added in small amounts. No extra water was added.

The experimental mixes were then added to 18 x 38mm cylindrical moulds in small quantities and tamped down as the material was added, to reduce the occurrence of trapped air bubbles within the specimens. After moulding, the specimens were stored in a climate chamber regulated at a constant temperature of 20ºC ± 2ºC and relative humidity of 65% ± 5% as specified in standard EN 1015-11:1999. The specimens were covered with a thin plastic wrap for the first week to maintain a high level of humidity, as exposure to ambient atmospheric conditions during this period can result in significant reduction in strength due to premature drying and subsequent cracking [8]. The specimens were then left in the moulds for a further week to allow them to achieve sufficient rigidity to facilitate demoulding.

6.3.2 Compressive strength testing

Mechanical strength testing was performed using a 50kN Instron 3369 Universal motorised load frame in accordance with BS EN 1015-11:1999 to test compressive strength. Bluehill 3 software monitored and recorded the load on the specimen as a function of extension throughout the test.

6.3.3 Optical microscopy

Optical microscopy was carried out on 30µm thin polished section slides of the three mortar mixes to analyse the aggregate particle morphology and the pore structure within the binder. Images were captured using a Brunel SP100 microscope with a polariser/analyser attachment. A camera adapter attachment was used to connect a Canon EOS1300D camera.

6.3.4 Field emission scanning electron microscopy

Field emission scanning electron microscopy was used to examine the morphology of the binder and aggregate at high magnification. Specimens were coated with a 20nm layer of chromium using a Quorum Q150TS machine. A JEOL JSM-6301F microscope was used with an accelerating voltage of 5kV to obtain images with magnification ranging from 2,000x to 100,000x.

6.3.5 Mercury intrusion porosimetry (MIP)

Porosimetry of the mortar mixes was determined using a Pascal 140/440 Porosimeter. The Porosimeter forces mercury under pressure into the pores of the specimen material to provide information about pore size, pore volume distribution, particle size distribution, bulk density and specific surface. The Pascal 140 performs low pressure porosimetry from vacuum up to 400 KPa and was used to analyse the pores in the 116 – 3.8 μm diameter size range. The Pascal 440 operates at pressures up to 400 MPa and was used to analyse the pores in the 15 – 0.0036 μm diameter size range.

6.3.6 X-ray diffraction (XRD)

The crystallinity of the samples was examined by powder X-ray diffraction using a BrukeraxsD8 Advance X-ray diffractometer equipped with a super speed PSD Vantec-1 detector and Cu K_α X-ray source of wavelength 1.5418Å. Data was collected over the 2θ range from 5° to 60° at a step size of 0.016° and time per step of 424.8s.

6.4 Results

6.4.1 Compressive strength testing

The graphs in Figure 6.3 shows the compressive strength of mortar mixes comprising the three different aggregates with the hot lime binder (A) and lime putty binder (B). The mortars containing sand aggregate were significantly weaker than the mortars containing slate or granite aggregate. The results for the mixes containing sand indicate a steady development of strength throughout the 91 days; however, the results for the mixes containing slate and granite are more erratic. These mixes obtained a high level of initial strength but the error bars indicate a wide range of values and similar strength levels at 56 and 91 days.

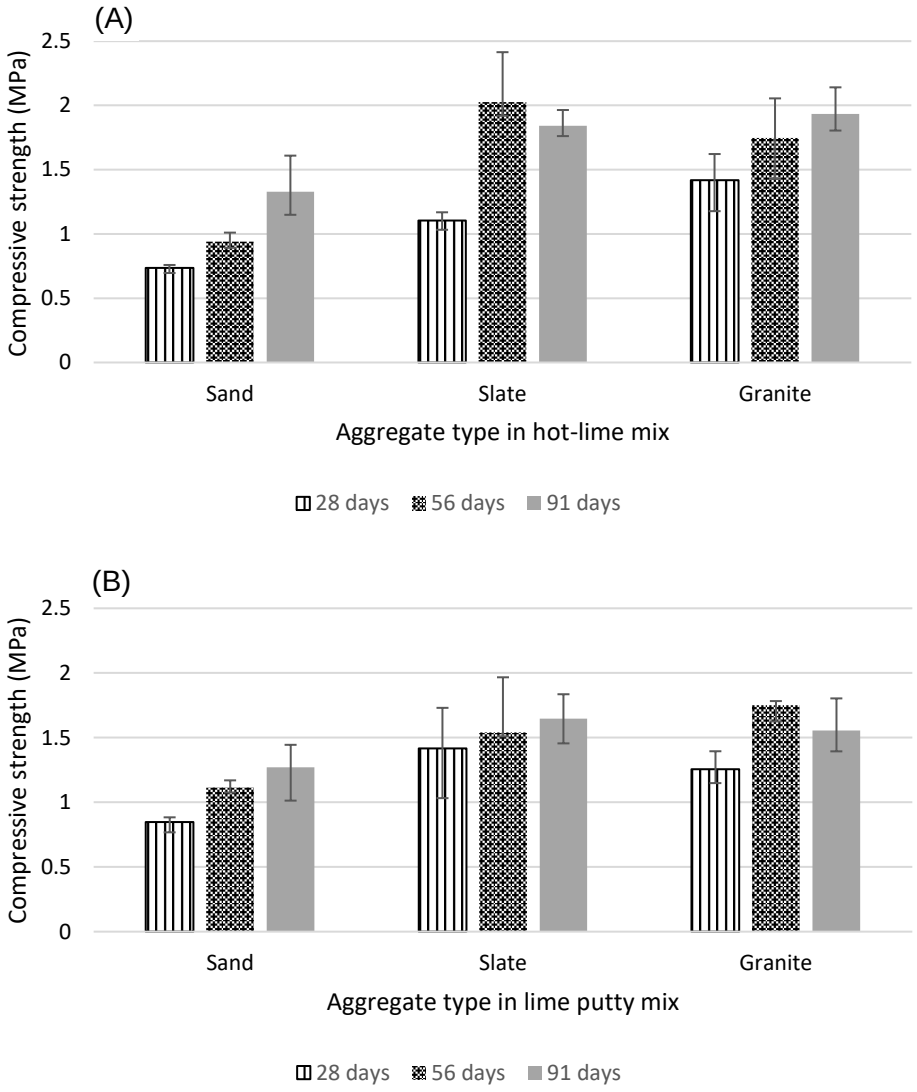

Figure 6.3: Compressive strength of hot-lime mortars (A) and lime putty mortars (B) at 28, 56 and 91 days with error bars showing maximum and minimum values.

A paired student's t-test analysis was carried out to compare the compressive strength levels of the lime putty mortar mixes and the hot lime mortar mixes with the same aggregate material and at the same periods of curing (Table 6.2). The null hypothesis for the test is that there is no difference between the results for hot lime mortars and lime putty mortars when prepared using the same aggregate material. The results show that at 5% level of significance the null hypothesis is rejected for five of the nine tests, and at 1% significance level the null hypothesis is rejected for only two of the tests.

Table 6.2: Student's t-test results.

	Test	t-value	critical t-value at p < 0.05	critical t-value at p < 0.01	significant difference at p < 0.05	significant difference at p < 0.01
Sand	28 day	3.4538	2.447	3.707	yes	no
	56 day	6.6527	2.571	4.032	yes	yes
	91 day	0.2914	2.447	3.707	no	no
Slate	28 day	2.4988	2.571	4.032	no	no
	56 day	3.196	2.447	3.707	yes	no
	91 day	2.5246	2.365	3.499	yes	no
Granite	28 day	1.4021	2.776	4.604	no	no
	56 day	0.0248	2.776	4.604	no	no
	91 day	4.022	2.365	3.499	yes	yes

6.4.2 Optical microscopy

It can be seen from the images in Figures 6.4, 6.5 and 6.6 that there are fundamental differences between the pore structures of the mortars prepared with silica sand aggregate and those prepared with slate or granite aggregate. The pores within the mortar containing sand (Figure 6.4) are noticeably shorter and less extensive than in the other two mortars (Figure 6.5 and 6.6). Also, in the slate and granite aggregates the pores occur frequently in the binder/aggregate interface, which is not the case with the sand mortar.

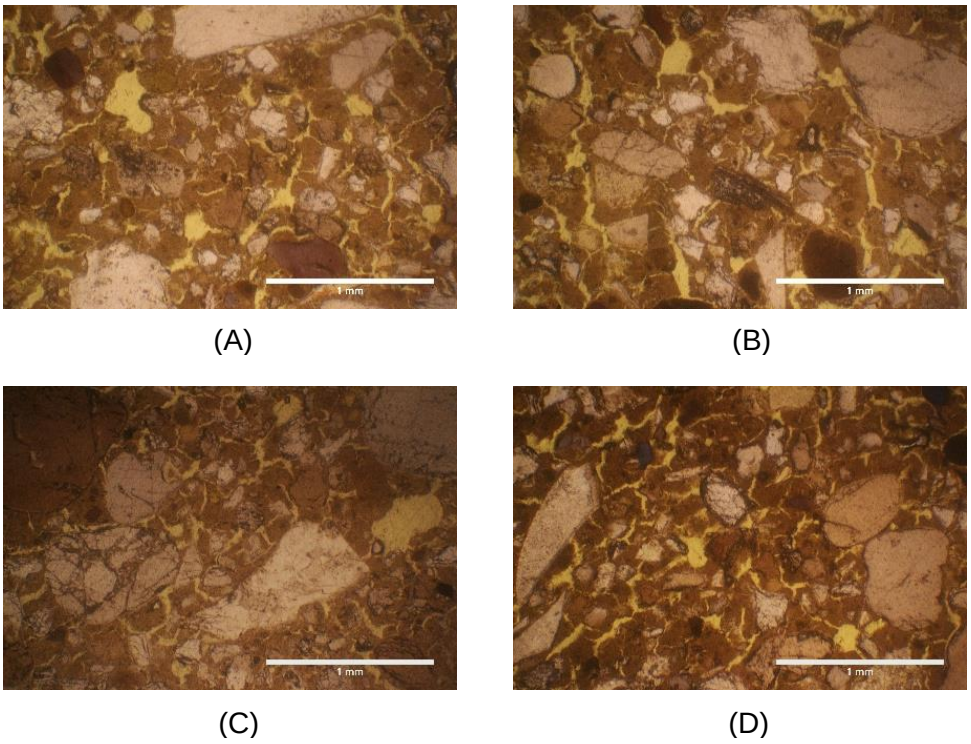

(A) (B)

(C) (D)

Figure 6.4: Images of thin section slides of mortar mixes after 91 days. Hot lime binder and silica sand (A)(B) and lime putty binder and silica sand (C)(D).

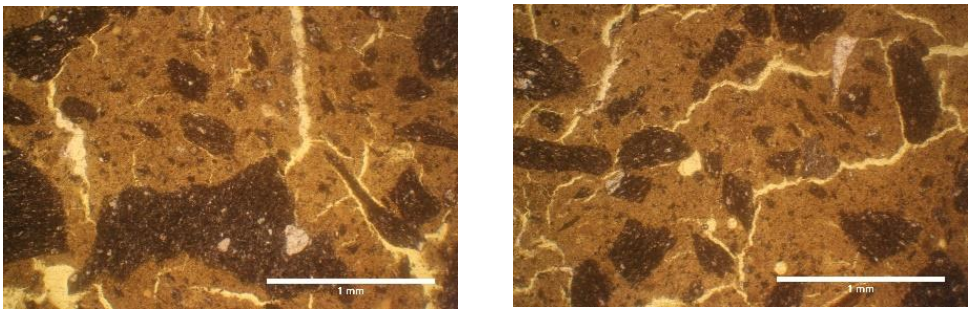

(A) (B)

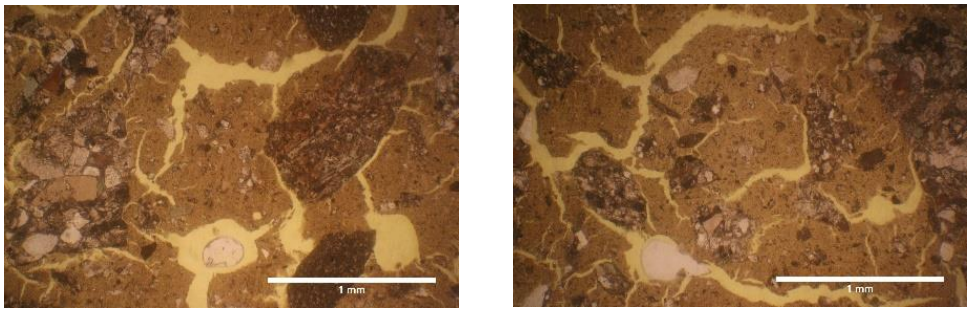

(C) (D)

Figure 6.5: Images of thin section slides of mortar mixes after 91 days. Hot lime binder and slate (A)(B) and lime putty binder and slate (C)(D).

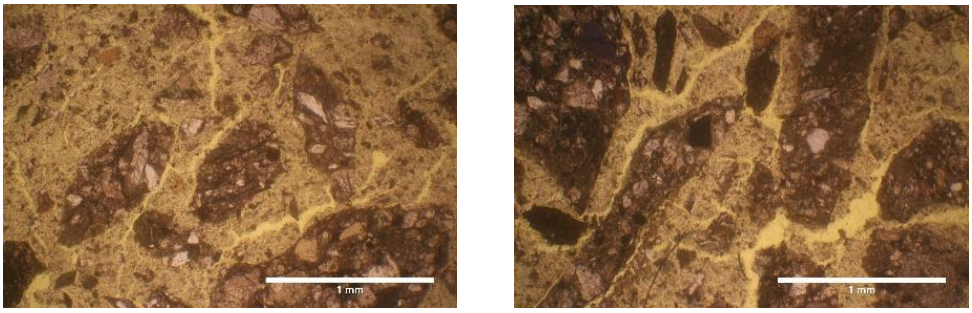

(A) (B)

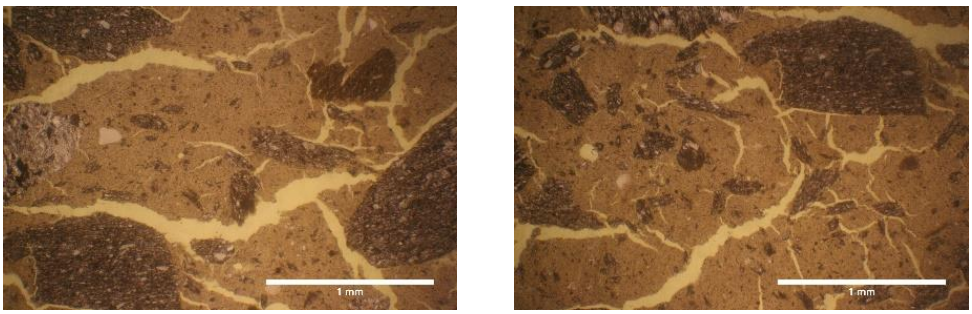

(C) (D)

Figure 6.6: Images of thin section slides of mortar mixes after 91 days. Hot lime binder and granite (A)(B) and lime putty binder and slate (C)(D).

6.4.3 Field emission scanning electron microscopy (FESEM)

The images in Figures 6.7, 6.8 and 6.9 show the surfaces of the sand, slate and granite aggregate particles respectively. It is evident that the sand particles are comparatively compact, whilst both the slate and granite particles are very flaky in nature.

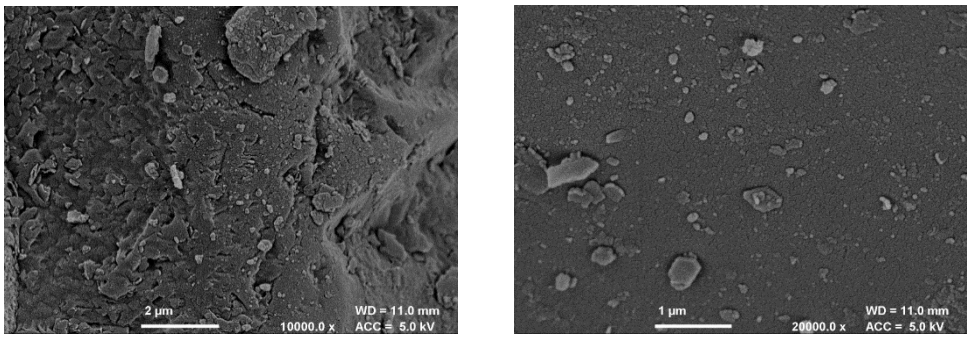

Figure 6.7: FESEM images of the surface of standard sand aggregate.

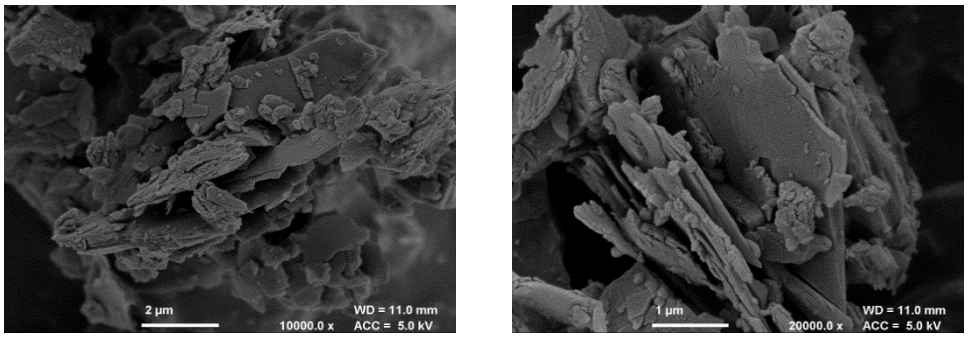

Figure 6.8: FESEM images of the surface of slate aggregate.

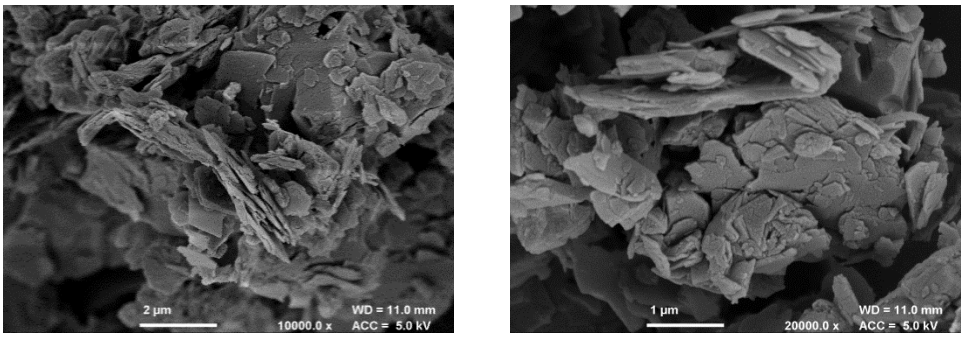

Figure 6.9: FESEM images of the surface of granite aggregate.

The images in Figure 6.10 show the hot lime mortar with the three different aggregate materials. The lime has carbonated to form calcium carbonate (calcite), which in all three mortars appears to adhere well to the aggregate.

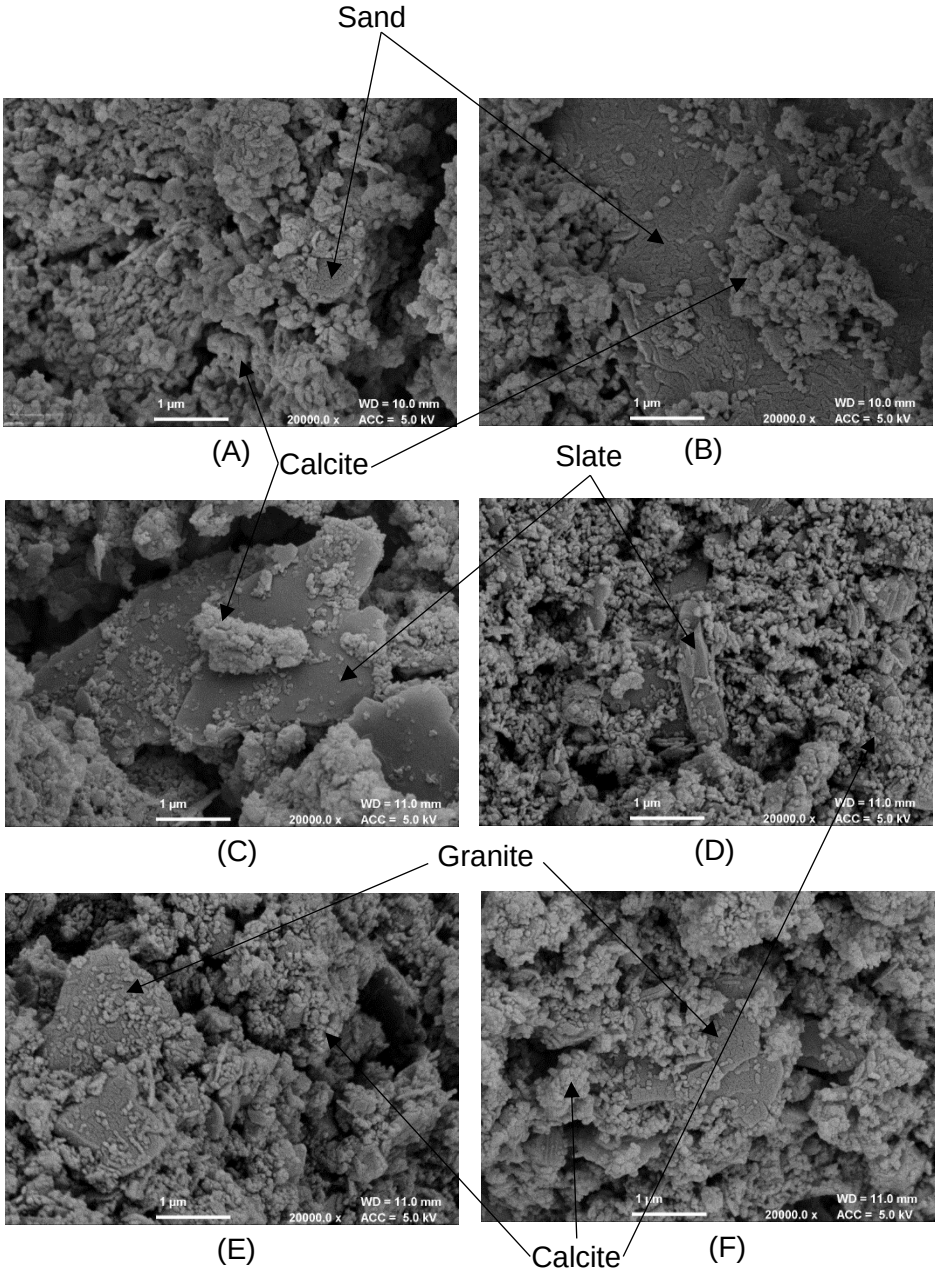

Figure 6.10: FESEM images of lime/sand mortar (A) (B) lime/slate mortar (C) (D) lime/granite mortar (E) (F).

6.4.4 Mercury intrusion porosimetry

The images in Figure 6.11 show the differential pore size distribution for the mortars comprising the hot lime mortars (A) and the lime putty mortars (B). The mortars prepared with silica sand possessed a higher proportion of large sized pores than both the slate mortar and the granite mortar independent of whether the binder was a hot lime or a lime putty.

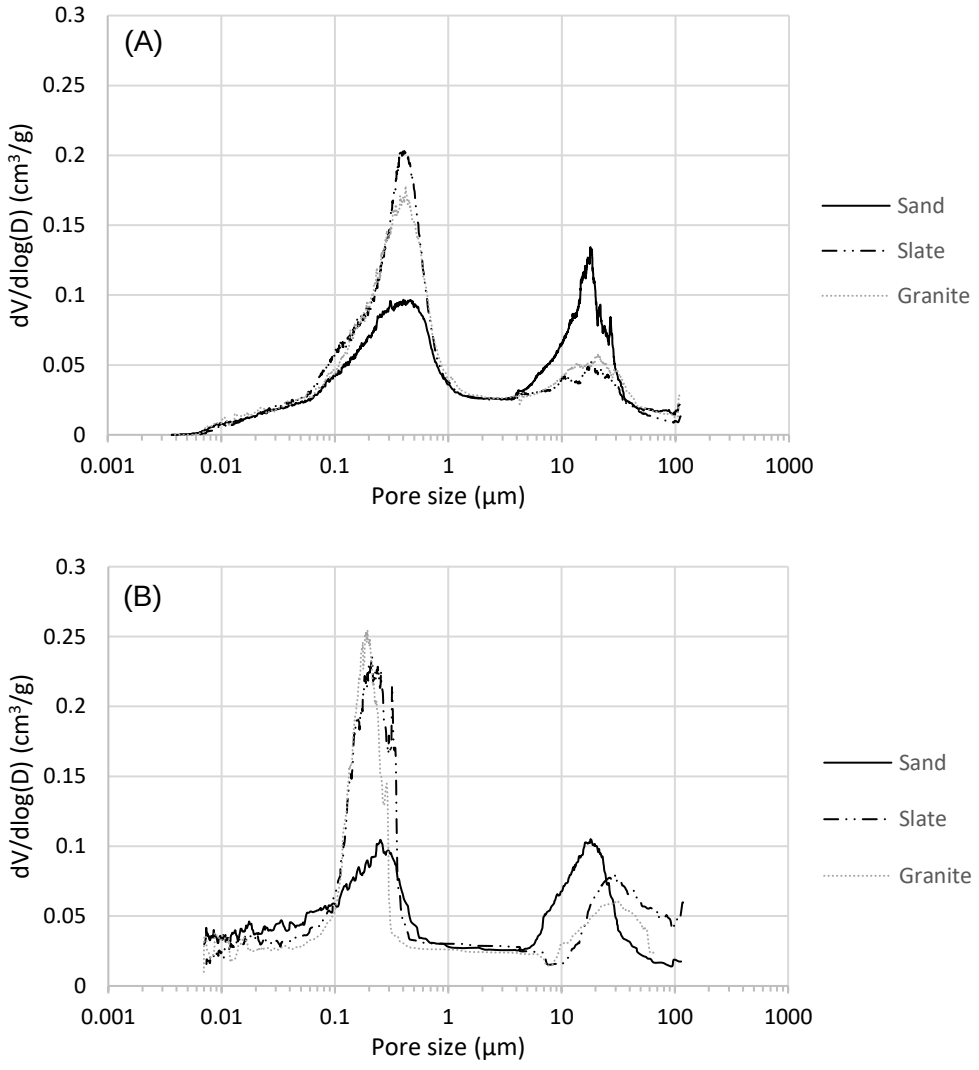

Figure 6.11: Pore size distribution for hot lime mortars (A) and lime putty mortars (B).

6.4.5 X-ray diffraction (XRD)

X-ray diffraction was carried out on the three aggregate materials as received and on the mortar mixes comprising hot lime binder and lime putty binder with each of the three aggregate materials. The XRD pattern for the standard sand aggregate shown in Figure 6.12 (A) confirms that the sand is pure and free from any clay impurities. Quartz is the most abundant phase identified in the slate, with lower amounts of hematite, muscovite and the chamosite form of chlorite. Quartz is also the most abundant phase identified in the granite, with lower amounts of muscovite, chamosite and plagioclase. The X-ray diffraction patterns of the mortar mixes (Figure 6.13) all show similar ratios of calcite and portlandite, indicating that carbonation had progressed at a comparable rate in all samples. The absence of peaks at 33.04˚ and 56.29˚ in the aggregate samples indicate that there is no discernible amount of crystalline pyrite present.

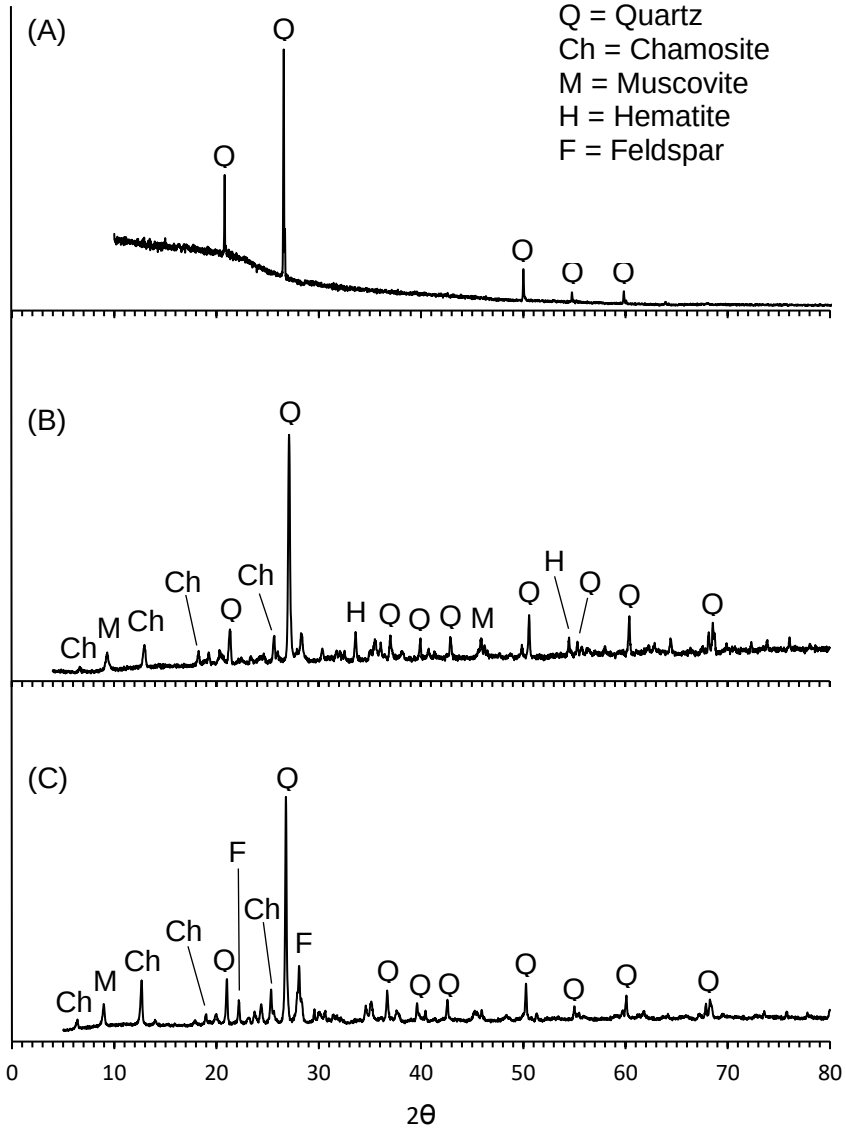

Figure 6.12: XRD diffraction patterns for the three different aggregate materials as received: silica sand (A) slate (B) and granite (C).

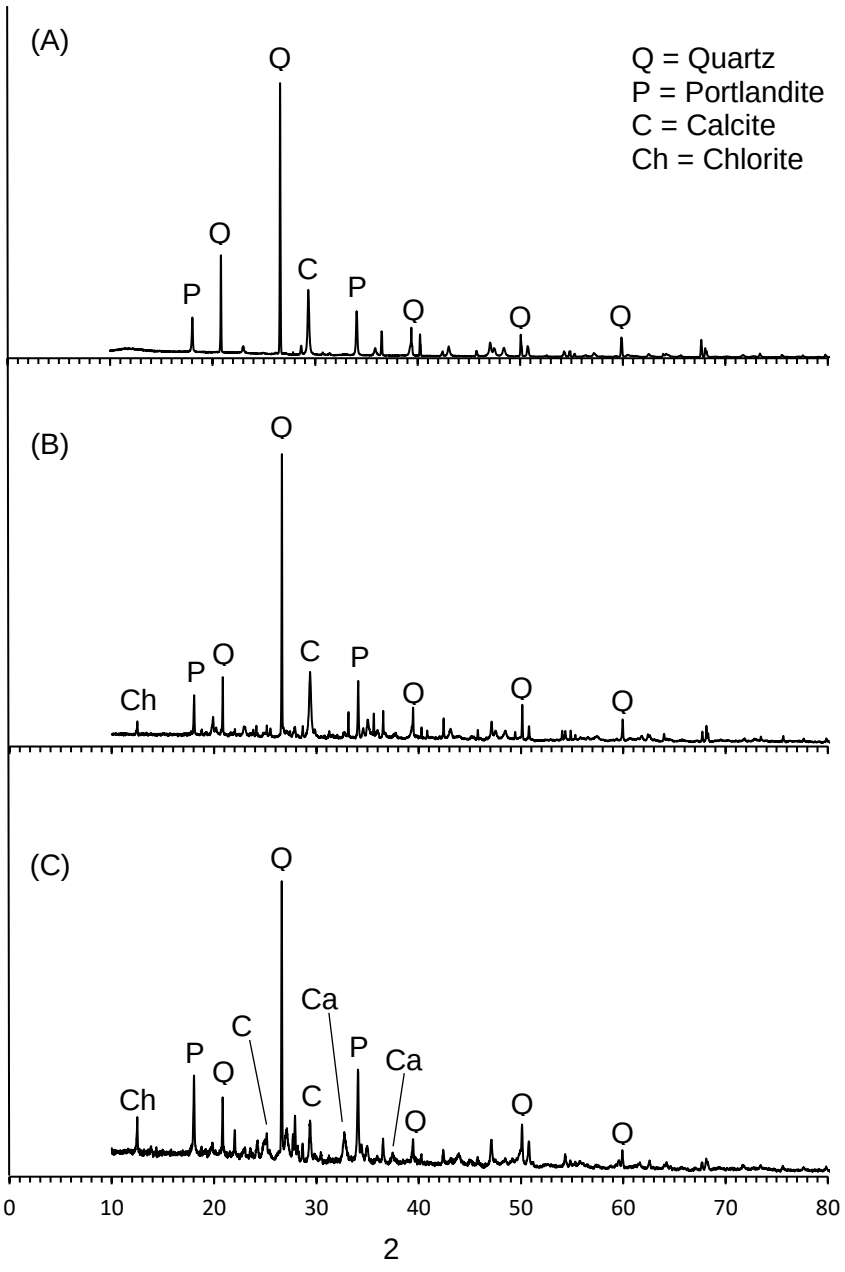

Figure 6.13: XRD diffraction patterns for the three hot lime mortar mixes after 91 days: Hot lime binder and silica sand (A) Hot lime binder and slate (B) hot lime binder and granite (C).

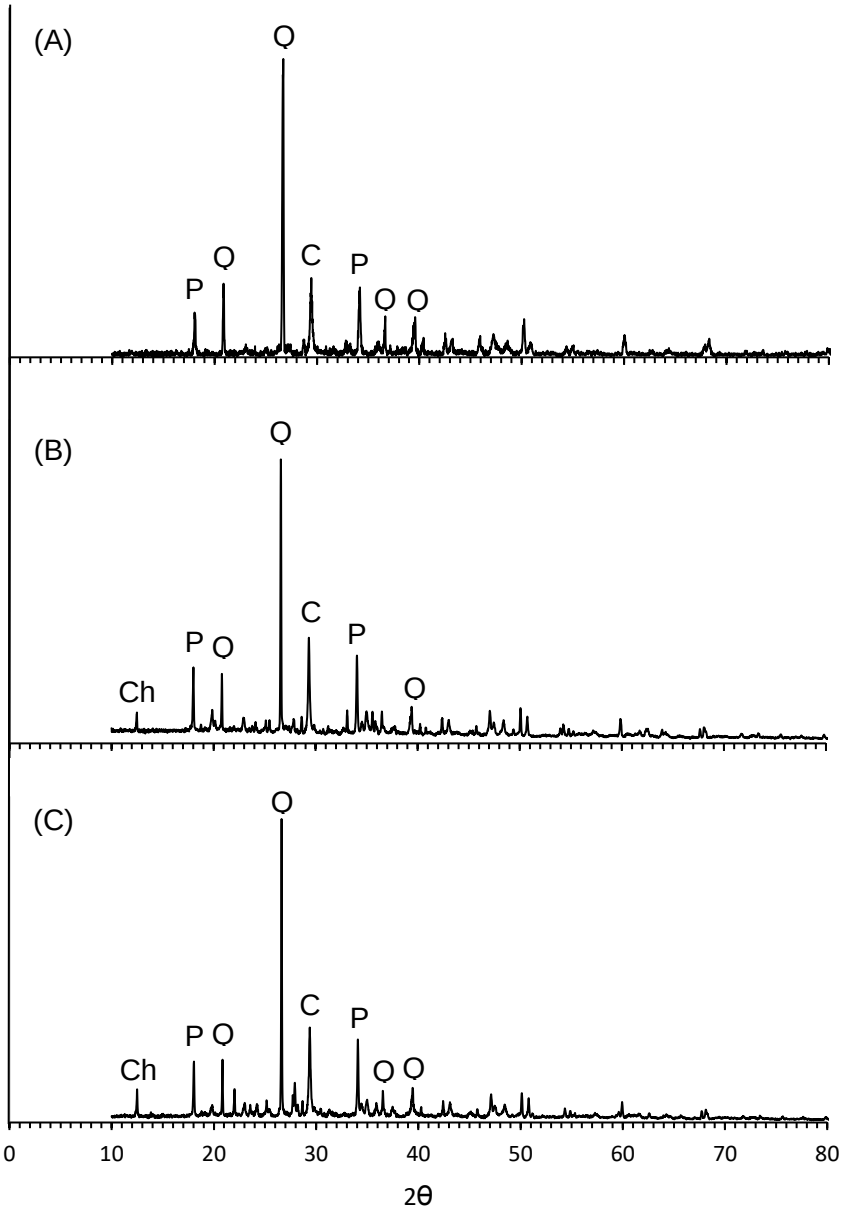

Figure 6.14: XRD diffraction patterns for the three lime putty mortar mixes after 91 days. Lime putty binder and silica sand (A) lime putty binder and slate (B) and lime putty binder and granite (C).

6.5 Discussion

The most significant finding from this investigation was the compressive strength levels that were achieved. The mortar containing standard silica sand aggregate achieved values that would be considered in the normal range for a lime mortar (Lawrence, 2006); however, the mixes containing slate and granite achieved considerably higher values. Mortars prepared with standard sand aggregate show progressive strength increase over 91 days regardless of binder type, which is consistent with continuing carbonation. The mortars prepared with slate and granite aggregate, however, showed inconsistent results. These mortar mixes gained a high level of strength by 28 days, but the progress of strength development after this point is difficult to analyse, as there is no significant difference between the values 56 and 91 days.

Statistical analysis of the compressive strength data provided inconclusive evidence of a statistically significant correlation between mortars prepared with the two types of lime binder. The fact that some of the differences between the two types of mortar were statistically significant can be attributed to the wide range of values obtained. The error bars show an uneven spread of values, suggesting that there were some anomalous results.

The results obtained during this investigation did not reveal any evidence that hot lime mortars have significantly different or superior properties. Comparison of the pore size distribution of hot lime mixes with lime putty mixes show approximately similar results when prepared using the same aggregate material. The type of aggregate was the determiner of pore structure rather than binder type. As with strength, pore size distribution for the binders containing slate and granite were similar The superior strength in the mortars containing slate or granite aggregate is consistent with the lower porosity found in these mortars. The pore structure of the mortar containing sand, as seen in the thin section slides, was significantly different in nature from the mortars containing slate or granite. The sand mortar appeared to contain pores that were not as extensive or as well interconnected as the other two mortars.

The difference in size distribution of the pores was also significant. Mortars containing slate or granite exhibited a greater distribution of sub-micron sized pores, whilst the mortars containing sand had a greater distribution of pores of size greater

than ten microns in size. The greater number of larger but not as interconnected pores in the sand mortar is a possible reason for the comparative weakness of this mortar

Comparison of the two binders does not indicate a significant difference in strength or porosity when prepared using the same aggregate material. Greater strength was achieved with the slate and granite mixes, regardless of binder type. This is consistent with similar results obtained by Lawrence et al. (2007, pp.7-33). There are two possible reasons for this. Firstly, the morphology of the slate and aggregate are significantly different from the silica sand. The higher surface roughness nature of the slake and granite are likely to provide a better mechanical adhesion with the binder compared with the relatively smooth surface of the silica sand. Secondly, the more extensive and interconnected nature of pore structure in the mortars containing slate and granite mortars might be responsible for facilitating more widespread CO_2 diffusion, and therefore carbonation, throughout the sample because the diffusivity of mortar is dependent on the openness of the pore structure (Van Balen, 2005, pp.647-657). This is also consistent with the assertion by Thomson et al. (2007, pp.75-103) that moisture transport within the pores of mortar only occurs within interconnected pores. This theory could also explain why the compressive strength at 56 and 91 days is not progressive, as seen with the silica sand mortars. The initial fast carbonation of the slate and granite mortars would have decreased porosity, as supported by the MIP data, which would have slowed down later CO_2 diffusion and carbonation.

Whilst this work did not find conclusive evidence that hot-lime mixes are superior to other forms of lime binder, the investigation was not exhaustive; there remains a considerable amount of research that could be undertaken. The quicklime used for this work was in knibbled form, but the more reactive powdered form may produce different results. Alternative aggregate materials and varying the particle sizes may also produce different results, and these areas should be researched further. Furthermore, as identified by Margalha et al., the physical properties of hot limes improve with increasing maturation time. Whilst increasing maturation duration might produce different and possibly superior results, this would likely not be practical in most construction applications due to time constraints.

6.6 Conclusions

- The compressive strength of mortars containing slate or granite were significantly stronger than mortars containing silica sand as the aggregate.
- The compressive strength of hot-lime mortars and lime putty mortars was not significantly different when prepared with the same aggregate material.
- The morphology of slate and granite facilitates a superior binder to aggregate interfacial bonding compared with silica sand.
- The pore structure of the mortar containing sand was less extensive and continuous than that of the mortars containing slate or granite.
- This work does not support the hypothesis that hot lime mortars are superior to mortars made with lime putty.

6.7 References

Barluenga, G & Hernandez-Olivaries, F., 2010. Self-levelling cement mortar containing grounded slate from quarrying waste. *Construction and Building Materials,* 24(9), pp.1601-1607.

Brown, A., 2017. *Hot-mixed Mortars Advantages and Limitations.* The Building Conservation Directory.

Cornish Lime, 2019. *Hot Mixed Mortars* [online]. Available from: http://cornishlime.co.uk/information/hot-mixed-mortars/ [accessed 24 July 2019].

Forster, A., 2004. Hot-Lime Mortars A Current Perspective. *Journal of Architectural Conservation,* 10(3), pp.7-27

Greenspec, 2017, *Lime mortar, render and plaster* [online]. Available from: http://www.greenspec.co.uk/building-design/lime-mortar-render/ [acessed 18th January 2017].

Henry, A, 2018. Hot mixed mortars: the new lime revival. *Context,* 154, pp.30-33

Historic Environment Scotland, 2019. *Using hot-mixed lime mortars* [online]. Available from: https://www.engineshed.scot/building-advice/building-

materials/lime/#using-hot-mixed-lime-mortars [accessed 23 July 2019].

Ingham, J., 2012. Laboratory Investigation of Lime Mortars, Plasters and Renders. In: I. Brocklebank, ed. *Building Limes in Conservation*. Shaftsbury: Donhead Publishing, p.155

Lawrence, R. M. H., 2006. *A Study of Carbonation in Non-Hydraulic Lime Mortars.* Thesis (PhD). University of Bath

Lawrence, M., Walker, P., & D'Ayala,D., (2006) Non-Hydraulic Lime Mortars. *Journal of Architectural Conservation*, 12(1), pp.7-33

Thomson, Margaret & Lindqvist, Jan & Elsen, Jan & Groot, Caspar. (2007). *Characterisation of Old Mortars with Respect to their Repair*. RILEM publications SARL

Van Balen, K., 2005. Carbonation reaction of lime, kinetics at ambient temperature, *Cement and Concrete Research,* 35(2005, pp.647-657.

Vishnu Shankar, S., Saravana Raja Mohan, K., 2015. Durability studies on cement mortar with granite powder as a partial replacement of cement, *International Journal of ChemTech Research,* 8(3), pp.1417-1422

CHAPTER 7 LIME AND GRAPHENE OXIDE

7.1 Introduction

The information that is available relating to the use of graphene oxide as an additive in mortars mainly concentrates on the mechanical and physical characteristics of these materials (Faria et al., 2017) (Shenghua et al., 2013). This work investigates the chemical reactions that take place between a non-hydraulic lime (calcium hydroxide) and graphene oxide flakes. Understanding these interactions between matrix and additive material will better inform the use of this promising additive material.

7.2 Experimental details

7.2.1 Materials

The Graphene Oxide used for this investigation was in powdered form supplied by the firm 2_DTech. Calosil E25 was used as the source of lime, supplied by the company Hirst Conservation. It comprises nano particles of calcium hydroxide in suspension with ethanol and having an average particle size of 150nm.

7.2.2 Sample preparation

Due to the nature of the materials, precise measurement by mass was impractical. A level laboratory micro spoon spatula of graphene oxide (0.2ml) was added to half a pipette (0.5ml) of Calosil nanolime and mixed together. Samples for optical microscopy were prepared on mica slides. A small amount of graphene oxide/nanolime mix was spread over the centre area of the slide. The volatile ethanol within the nanolime evaporated from the outer region of the specimen to leave pure portlandite (Figure 7.1)

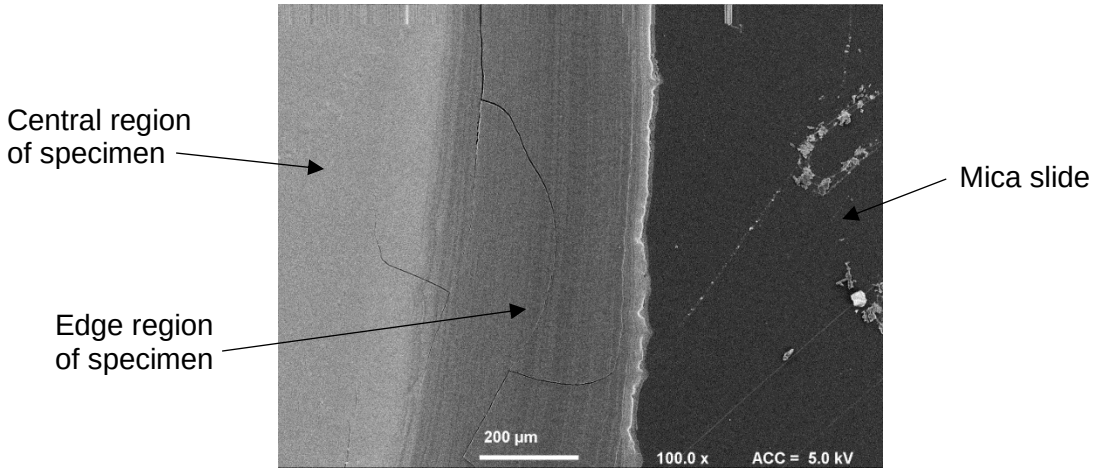

Figure 7.1: E25 nanolime specimen prepared on mica slide.

7.2.3 Characterisation

FTIR was used to confirm the identity and purity of the research materials, to identify the functional groups attached to the graphene and to help identify any chemical changes that might have taken place after mixing the two materials together. A PerkinElmer Frontier FTIR spectrometer was used over a frequency range from 600 – 4000 cm^{-1} and at a resolution of 1 cm^{-1} and 40 accumulations.

Raman spectra were obtained using a Renishaw InVia Raman Spectrometer employing a laser of wavelength 532nm.

Imaging was carried out using a Visicam optical microscope for low magnification images and a JEOL JSM-6301F microscope was used with an accelerating voltage of 5kV to obtain images with magnification ranging from 50,000x to 100,000x.

7.3 Results

7.3.1 Fourier transform infrared microscopy

FTIR spectra were obtained for the graphene oxide, the nanolime and the two materials mixed. The data were collected immediately upon removing the materials from their containers and again after four hours exposure to the atmosphere. The FTIR spectra shown in Figure 7.2 are for the material as received (A) and after four hours exposure to the atmosphere (B). The broad peak around 3239 cm^{-1} is assigned to O-H bonds stretching and the peak at 1715 cm^{-1} is assigned to C=O stretching in

carboxylic groups that are located mostly at the edges of the graphene oxide sheet (Kudzma et al., 2019). The peak at 1625 cm^{-1} is assigned to the C=C aromatic ring stretching (Gographene, 2019), and the peak at 1052 cm^{-1} is assigned to the C-O stretch in alkoxy groups (Frogley et al., 2014). The peak at 848 cm^{-1} is attributed to the C–O–C stretching vibration of the epoxy ring (Khalili, 2016). The spectrum in Figure 7.2 (B) is for graphene oxide after four hours exposure to the atmosphere and shows no significant difference.

The spectra in Figure 7.2 (C) is for the E25 nanolime as received. The spectrum is dominated by the very strong ethanol signal (Institute of Chemistry, 2019). All the peaks are a close match for ethanol except the very small peak at 3645 cm^{-1}, which indicates the presence of portlandite. At this stage it was not expected that any calcium carbonate ($CaCO_3$) would be present, as calcium hydroxide ($Ca(OH)_2$) does not exhibit carbonation inside the nanolime suspension (Taglieri et al., 2013). The spectrum in Figure 7.2 (D) is for the nanolime after it has been exposed to the atmosphere for four hours. The volatile ethanol within the nanolime has evaporated to leave just the lime remaining. The prominent sharp peak at 3645 cm^{-1} is due to the OH stretching vibration typical in $Ca(OH)_2$. The peak at 861 cm^{-1} and the split peak at 1420 cm^{-1} and 1481 cm^{-1} are typical for amporphous calcium carbonate (Cai et al., 2010). This is further confirmed by a lack of a calcite peak at 713 cm^{-1} (Cai et al., 2010)). The peak at 1077 cm^{-1} is assigned to the C-O vibrational mode in carbonates (Rodriguez-Navarro et al., 2016).

The spectra for the graphene oxide/nanolime mix immediately after mixing and after having been left exposed to the atmosphere for four hours are shown in shown in Figures 7.2 (E) and (F). It can be seen that the broad OH peak at 3316 cm^{-1} is weak after mixing the graphene oxide and nanolime together and almost completely absent after four hours. This is consistent with evaporation of the volatile ethanol in the nanolime. The presence of the peak at 1625 cm^{-1} in the specimen after four hours is consistent with the main aromatic ring structure remaining intact after some of the polar functional groups have been removed by interaction with the polar -OH functional group in the ethanol. The increase in the peaks around 1400 cm^{-1} are indicative of carbonation having occurred, but the increase is modest compared to the increase in the peaks around 1100 cm^{-1}, which can be attributed to C-O-C asymmetric stretching in the aromatic ring (Horiba, 2019).

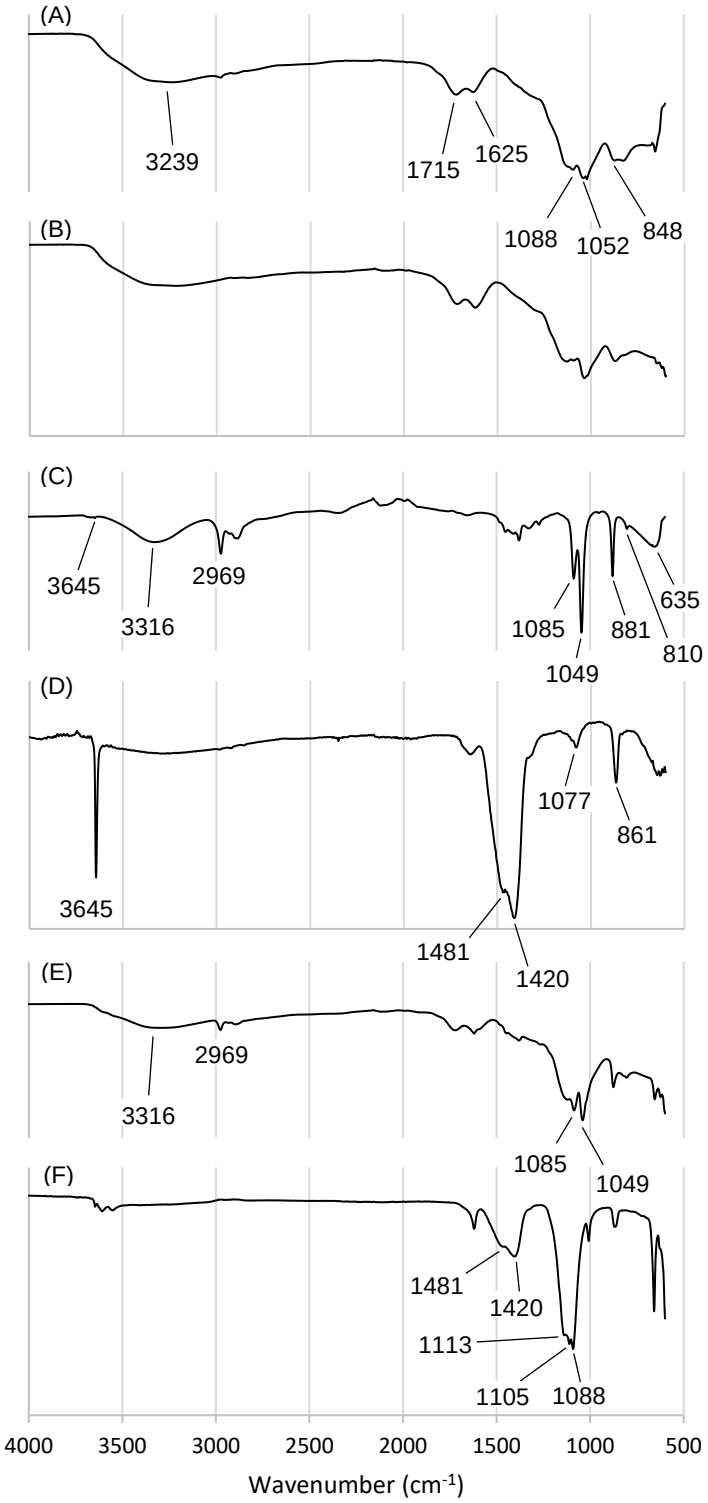

Figure 7.2: FTIR spectra of Graphene oxide (A), Graphene oxide after 4hrs exposure to atmosphere (B), Nanolime (C), Nanolime after 4hrs exposure to atmosphere (D), Graphene oxide/Nanolime mix (E) and Graphene oxide/Nanolime mix after 4hrs exposure to the atmosphere (F).

7.3.2 Raman spectroscopy

Raman spectroscopy was carried out on the graphene oxide and nanolime as received and then after mixing the two materials together.

The spectrum of graphene oxide in Figure 7.3 (A) shows the two main peaks that dominate carbon-based materials: the G peak at 1620 cm^{-1} and the D peak at 1367 cm^{-1}. The G peak is caused by the in-plane stretching of the sp2 hybridised C-C bonds in the lattice and the D peak indicates disorder from structural defects, edge effects and dangling sp2 carbon bonds that break the symmetry (Dubale et al., 2014). The ID/IG ratio of approximately one is typical for graphene oxide and indicates that it is fully oxidised (Gographene, 2019).

The spectra in Figures 7.3 (B) and (C) are for nanolime as received and after it had been left exposed to the atmosphere for four hours respectively. The spectrum in (B) is an exact match for silicon (RUFF, 2019), and it is believed that this may be because of contamination, as there is no silicon in nanolime. The spectrum in (C) and is an exact match for portlandite (RUFF, 2019), indicating that the ethanol had completely evaporated.

Figure 7.2 (D) shows the spectrum for the nanolime and graphene oxide mix after it had been left exposed to the atmosphere for four hours. The strongest signals are from the graphene oxide. The peak at 1020 cm^{-1} is assigned to the aromatic ring and the peak at 630 cm^{-1} to C-C aliphatic bond stretching (Horiba, 2019). The peaks at 1078 cm^{-1} and 1088 cm^{-1} are attributed to calcium carbonate polymorphs aragonite and calcite respectively. Calcite normally displays an intense peak at approximately 1087 cm^{-1} and aragonite 1084 cm-1 (Gillet, 1993). The peak at 630 cm^{-1} is assigned to C-C aliphatic chain vibrations and the peak at 488 cm^{-1} is attributed to Si-O-Si vibrations, further confirming the presence of silicon (Horiba, 2019).

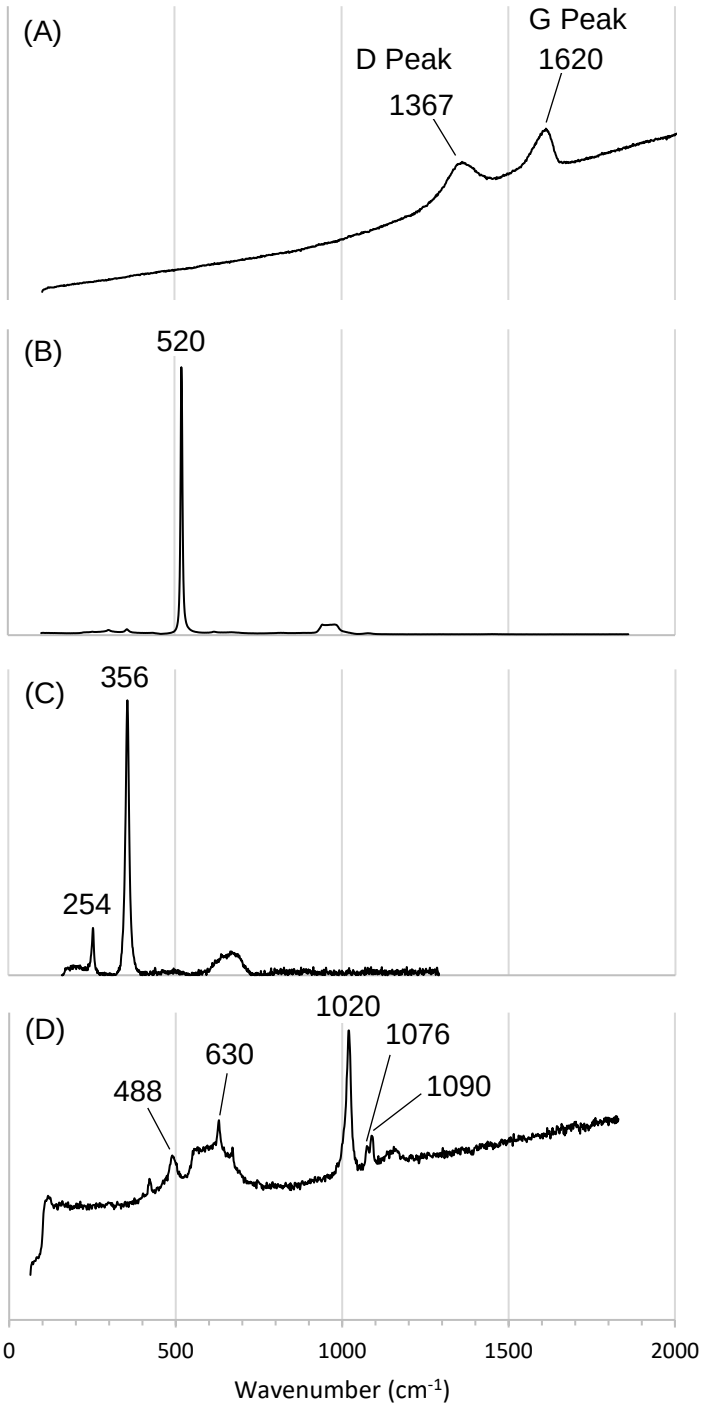

Figure 7.3: Raman spectra of graphene oxide (A) nanolime as received (B) nanolime after four hours exposure to the atmosphere (C) nanolime/graphene oxide mix after four hours exposure to the atmosphere.

7.3.3 Visicam optical microscopy

The images in Figure 7.4 (A) and (B) show the graphene oxide sheets as received from the supplier. It can be seen that the thickness of the material varies where the sheets have agglomerated through crosslinking. In images (C) and (D) the effect of mixing graphene oxide with nanolime can be seen. Sections around the edge of the graphene oxide sheets appear to have been separated from the main structure, which may be due to the fact that the highly polar carboxyl functional groups are mostly located at the edges of the graphene oxide sheet (Dreyer et al., 2009).

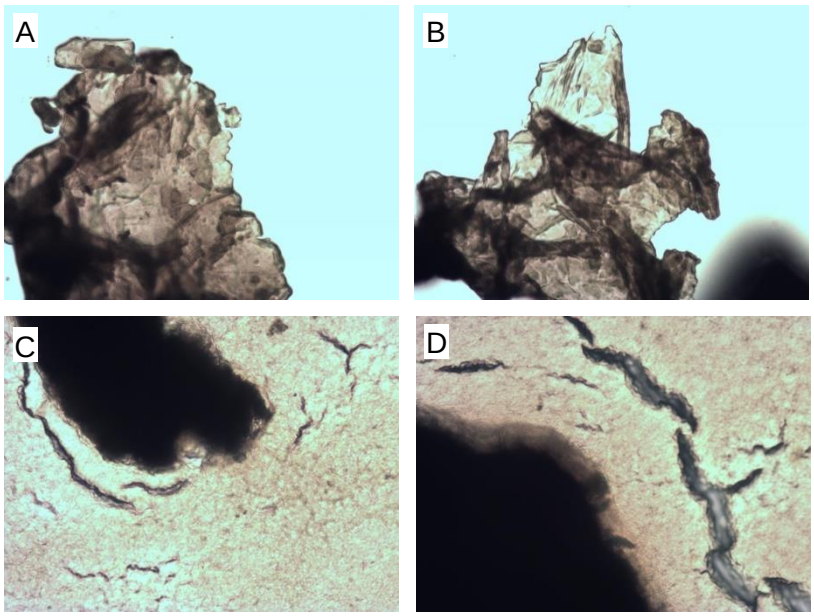

Figure 7.4: Graphene oxide sheets (A) (B) and graphene oxide mixed with nanolime (C) (D).

7.3.4 Field emission scanning electron microscopy

The images in Figure 7.5 show the graphene oxide as received from the supplier (A) and after 4 hours exposure to the atmosphere (B). It can be seen that the thickness of the graphene oxide varies, which is due to the tendency of layers to stack on top of each other (Bazrafshan, 2018). It can also be seen that fragmentation damage.

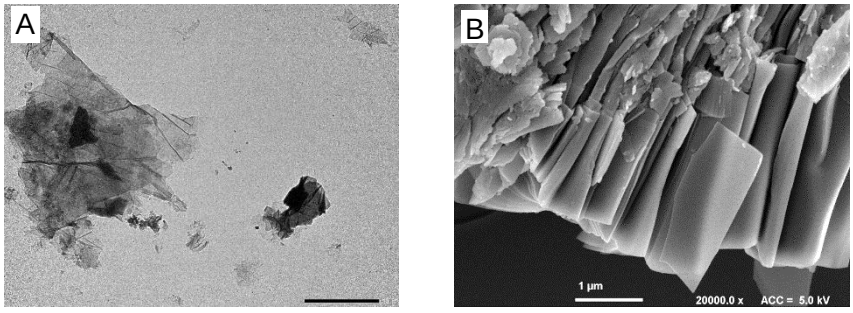

Figure 7.5: Graphene oxide sheets as received (A) and after four hours exposure to the atmosphere (B) and nanolime as received (C)(D).

The images in Figure 7.6 (A) and (B) are of the nanolime as received. Image A was obtained from the centre region of the specimen and image (B) from the outer region. Images (C) and (D) were obtained after the nanolime had been left exposed to the atmosphere for four hours. Image (C) was obtained from the centre region of the specimen and Image (D) from the outer region. It can be seen that there is an abundance of well-formed hexagonal portlandite crystals and no visible signs of carbonation after four hours.

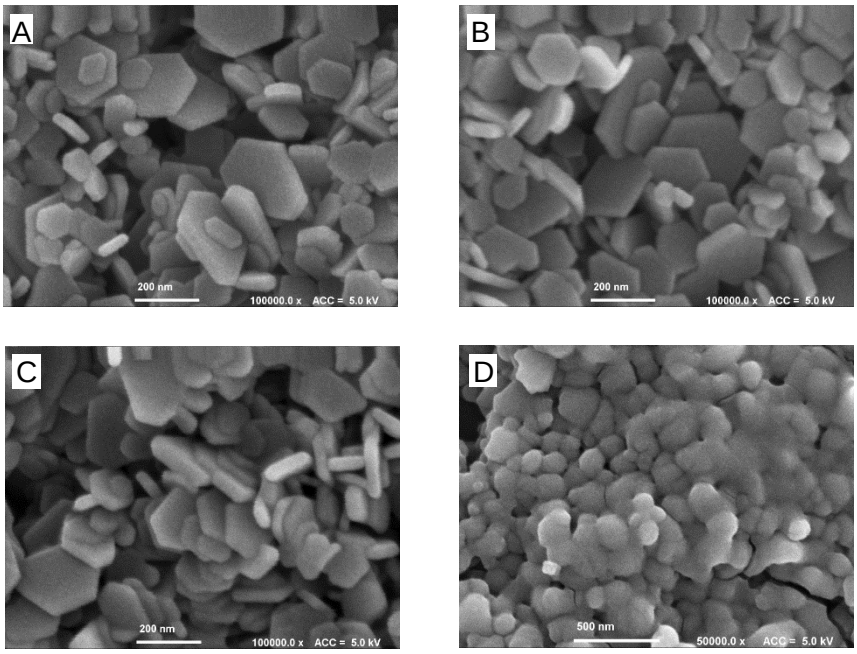

Figure 7.6: Hexagonal portlandite crystals in nanolime as received (A) (B) and after four hours exposure to the atmosphere (C) (D).

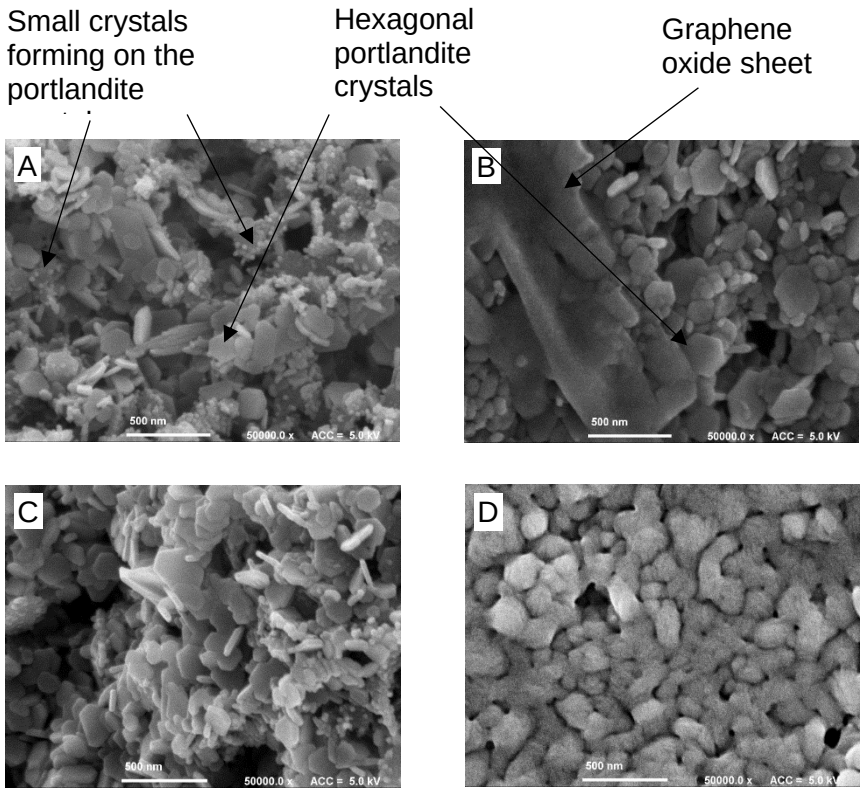

Figure 7.7: Nanolime/graphene oxide mix after four hours exposure to the atmosphere (A)(B) and after four days (C)(D).

7.3.5 X-ray diffraction

Figure 7.8 shows the diffraction patterns for graphene oxide as received (A) and a mix of nanolime and graphene oxide after four hours (B).

The diffraction pattern for the graphene oxide indicates that this material is not pure graphene oxide. The peaks identified as graphene oxide (Stobinski, 2014) are of lower intensity than other peaks in the diffraction pattern. The sharp peak at $2\theta = 26.5°$ is characteristic of graphite, the peaks at $2\theta = 27.8°$, $47.3°$ and $56°$ appear to be consistent with contamination from silicon and the peak at $2\theta = 29.6°$ confirms the presence of calcite, confirming that carbonation has been initiated.

The double peak at $2\theta = 18°$ is difficult to identify conclusively. In the literature, the only graphene oxide with a peak at this value is a hybrid C60/rGO (Zhang et al., 2013). This peak is in the same position as the most intense peak for portlandite, so the presence of portlandite cannot be verified.

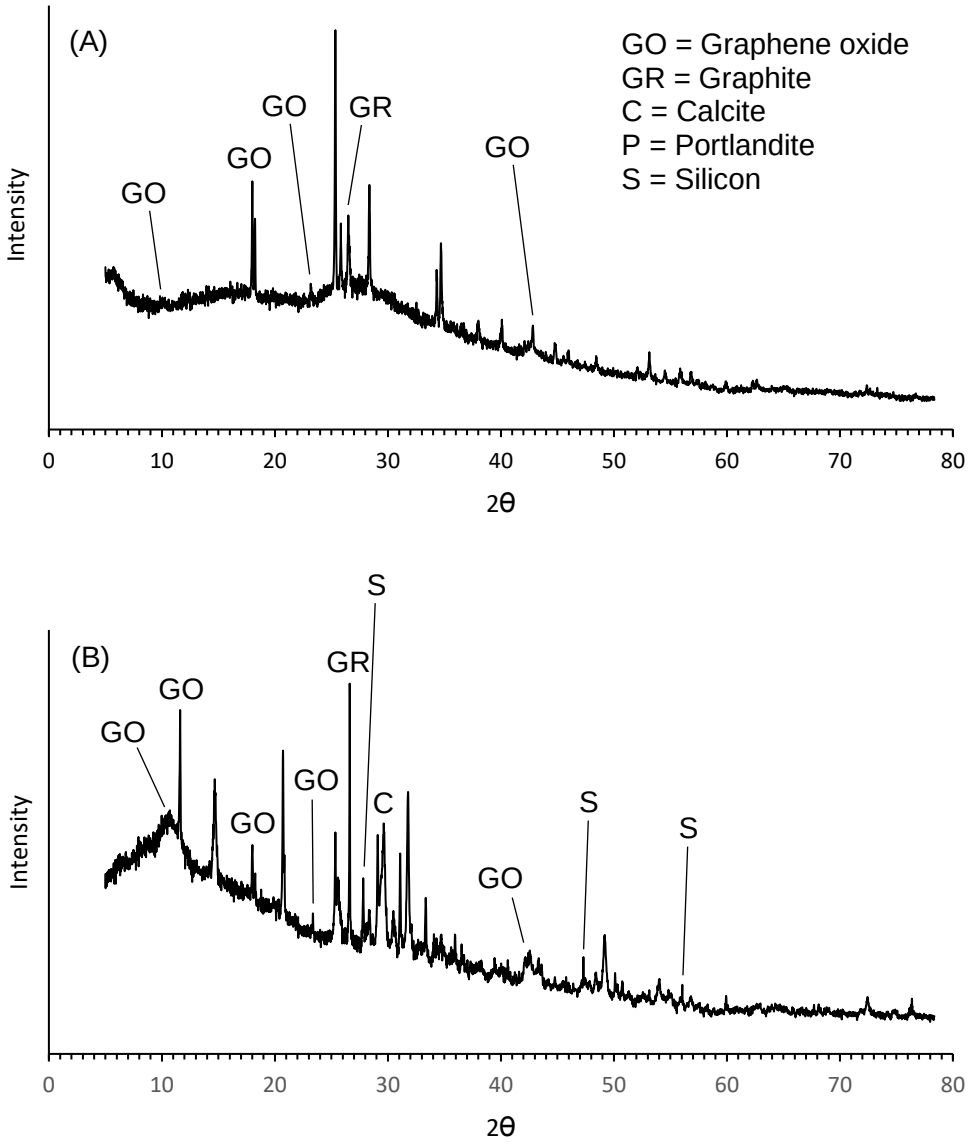

Figure 7.8: XRD diffraction patterns for graphene oxide (A) and nanolime/graphene oxide mix after four hours (B).

7.4 Discussion

The SEM images of the portlandite crystals mixed with graphene oxide show distinct small crystals forming on them after four hours exposure to the atmosphere (Figures 7.7 (A) and (C)). This same reaction is not seen when the nanolime in isolation is left exposed to the atmosphere for four hours. Taking into account the elements present in the system, it is most probable that these are an indication of carbonation initialising. This is supported by the presence of carbonate peaks in the spectrum from the nanolime and graphene oxide mix at four hours (Figure 7.3 (D)).

The identification of carbonation was complicated by the proportion of the hydrocarbon functional groups present in the system. The nature of the materials, and absence of any literature on this subject made it difficult to judge the appropriate proportions of each material to use. A lower proportion of graphene oxide would have been optimal.

Another issue encountered was accurately characterising the graphene oxide. XRD analysis showed the graphene oxide used in this study to be significantly different from pristine graphene oxide. A strong graphite signal was observed, which could be from agglomeration of the graphene layers. Image analysis by SEM confirmed that there is stacking of the layers.

7.5 Conclusions

The following conclusions have been drawn:

- The presence of graphene oxide promotes crystal growth on portlandite – believed to be carbonation.
- Polar functional groups from the graphene oxide help promote dissociation of calcium hydroxide to liberate calcium ions for carbonation.
- At four hours reaction time, the principle carbonate phase being formed was amorphous calcium carbonate.

7.6 General observations and further work

This work presented challenges in judging the proportions of materials to use. This work could be improved upon by establishing the effect of different graphene oxide to lime ratios. The timing of test work was also based on judgement due to the lack of any empirical evidence relating to this area of research. It was judged that the reactions would occur rapidly using nanomaterials, but based on the results obtained here it would be beneficial to carry out tests at different time intervals to investigate the progression of the carbonation process from amorphous calcium carbonate to metastable aragonite to thermodynamically stable calcite.

7.7 References

Bazrafshan, Z., Stylios, G. K., 2018. High Performance of Covalently Grafting onto Collagen in the Presence of Graphene Oxide. *Nanomaterials,* 8(9), p.703

Cai, G., Chen, S., Liu, L., Jiang, J., Yao, H., Xu, A., Yu, S., 2010. 1,3-Diamino-2-hydroxypropane-***N***,***N***,***N′***,***N′***-tetraacetic acid stabilized amorphous calcium carbonate: nucleation, transformation and crystal growth. CrystEngComm, 1(2010)

Dreyer D. R., Park, S., Bielawski, C. W., Ruoff, R. S., 2009. The chemistry of graphene oxide. *Chemical Society Reviews,* DOI: 10.1039/b917103g, pp.228-240

Dubale, A. A., Su, W., Tamirat, A. G., Pan, C., Aragaw, A., Chen, H., Chen, C. H., Hwang, B., 2014. Synergetic effect of Graphene on Cu2O Nanowire arrays as highly efficient hydrogen evolution photocathode in water splitting. *Electronic Supplementary Material for Journal of Materials Chemistry,* pp.1-12.

Faria, P., Duarte, P., Barbosa, D., Ferreia, I., 2017. New composite of natural hydraulic lime mortar with graphene oxide. *Construction and Building Materials,* 156, pp.1150-1157.

Frogley, M. D., Wang, C., Cinquea, C., Barber, A. H., 2014. Polarised infrared microspectroscopy of edge-oriented graphene oxide papers. *Vibrational Spectroscopy,* 75(2014), pp.178-183.

P. Gillet, C. Biellmann, B. Reynard, and P. F. McMillan, Phys. Chem. Minerals, 20, 1-18 (1993)

Gographene, 2019. *Graphene oxide analysis* [online]. Available from: https://www.go-graphene.com/pages/graphene-oxide-analysis [accessed 31 June 2019].

Horiba, 2019. *Raman Spectroscopy for Analysis and Monitoring.* Application Note

Institute of Chemistry, 2019. *ATR-FT-IR spectrum of Ethanol (4000 – 225 cm–1).* [online]. Available from: http://lisa.chem.ut.ee/IR_spectra/conservation_materials/ethanol/ [accessed 1 July 2019].

Khalili, D., 2016. Graphene oxide: a promising carbocatalyst for the regioselective thiocyanation of aromatic amines, phenols, anisols and enolizable ketones by hydrogen peroxide/KSCN in water. *New Journal of Chemistry,* pp.1-11

Kudžma, A., Škamat, J., Stonys, R., Krasnikovs, A., Kuznetsov, D., Girskas, G., Antonovic, V., 2019. Study on the Effect of Graphene Oxide with Low Oxygen Content on Portland Cement Based Composites. *Materials,* 12(802), pp.1-17

Rodriguez, C., Elert, K., Sevcik, R., 2016. Amorphous and crystalline calcium carbonate phases during carbonation of nanolimes: Implications in heritage conservation. *CrystEngComm,* The Royal Society of Chemistry

RUFF, 2019. *Portlandite R070210* [online]. Available from: http://rruff.info/portlandite/display=default/ [accessed 3 July 2019]

RUFF, 2019. *Silicon R050145* [online]. Available from: http://rruff.info/silicon/display=default/ [accessed 3 July 2019]

Shenghua Lv, S., Ma, Y., Qiu, C., Sun, T., Liu, J., and Zhou, Q., 2013. Effect of graphene oxide nanosheets of microstructure and mechanical properties of cement composites. *Construction and Building Materials,* 49(2013), pp.121-127

Stobinski, L., Lesiaka, B., Malolepszyc, A., Mazurkiewiczc, M., Mierzwaa, B., Zemek, J., Jiricek, P., Bieloshapka, I., 2014. Graphene oxide and reduced graphene oxide studied by the XRD, TEM and electron spectroscopy methods. *Journal of Electron Spectroscopy and Related Phenomena,* 195(2014), pp.145-154

Taglieri, G., Mondelli, C., Daniele, V., Pusceddu, E., Trapananti, A., 2013. Synthesis and X-ray Diffraction Analyses of Calcium Hydroxide Nanoparticles in Aqueous Suspension. *Advances in Materials Physics and Chemistry,* 2013(3), pp.108-112

Zhang, K., Zhang, Y., Wang, S., 2013. Enhancing thermoelectric properties of organic composites through hierarchical nanostructures. *Scientific Reports,* DOI: 10.1038/srep03448

CHAPTER 8 LIME AND NANOSILICA

8.1 Introduction

The use of Nanosilica in construction materials has been widely researched. The findings are generally in agreement that the addition of small proportions of nanosilica improves early setting and compressive strength in hydraulic lime and cementitious mortars (Singh et al., 2013). However, there does not currently appear to be any research specifically relating to the effect of colloidal nanosilica on non-hydraulic lime putty. This work aims to investigate whether nanosilica can be successfully incorporated into lime putty binders and plasters to increase strength. This could have a twofold benefit. Increased strength could allow less material to used. A stronger lime putty could also be used in a wider range of applications.

8.2 Materials

8.2.1 Non-hydraulic lime putty

The non-hydraulic lime used in the test work for this research was a well matured lime putty supplied by Singleton Birch in 23kg tubs. The putty was stored completely immersed in water within a plastic tub having an airtight seal around the rim. This ensured no premature carbonation occurred.

8.2.2 Natural hydraulic lime (NHL2)

The natural hydraulic lime used in this research was NHL 2 grade, supplied by Singleton Birch in dry powdered form in 25kg bags.

8.2.3 Nanosilica

The nanosilica used in this investigation was Ludox SM colloidal nanosilica supplied by Sigma Aldrich. It comprises a 30% by weight suspension in water of silica nanoparticles having a surface area of ~320-400 m^2/g, density of 1.22 g/mL at 25˚C and a pH of 9.7 – 10.3. Nanosilica is available as a powder or in colloidal form. The health and safety risks associated with the use of nano powders is not yet fully understood, and for this reason colloidal nanosilica was selected for this work.

8.2.4 Standard sand

The sand used in this investigation was a standard dry siliceous natural sand conforming to BS EN 196-1 and ISO 679: 2009. This grade of sand comprises particles that are generally isometric and rounded in shape with the particle size distribution shown in Figure 3. This type of sand was specified for this investigation to facilitate consistency and repeatability of experimental conditions.

8.3 Methods

8.3.1 Sample preparation

The lime putty and sand mix was prepared using a paddle mixer for a minimum of twenty minutes to ensure the plaster was suitably workable. The colloidal nanosilica was added to the mixture in small amounts during the mixing process to help ensure an even distribution throughout the matrix. No additional water was added to this mix.

The NHL lime specimens were prepared using a of 2:1 ratio of aggregate to binder by volume. The samples were prepared using a using a Test International 2-speed planetary mixer. A small quantity of water was put into the mixer first and then the lime was added. The sand and water were then added to produce what was at first a rather dry looking mix. The mixer was then left to run for a further twenty minutes, at which time the mix was an appropriate workable consistency.

The experimental mixes were then added to 40x40x160mm prism moulds in small quantities and tamped down as the material was added, to reduce the occurrence of trapped air bubbles within the specimens. After moulding, the specimens were stored in a climate chamber regulated at a constant temperature of 20ºC ± 2ºC and relative humidity of 65% ± 5% as specified in standard BS EN 1015-11:1999. The specimens were covered with a thin plastic wrap for the first week to maintain a high level of humidity, as exposure to ambient atmospheric conditions during this period can result in significant reduction in strength due to premature drying and subsequent cracking (Livesey, P., 2010, pp.46-49). The specimens were then left in the moulds for a further week to allow them to achieve sufficient rigidity to facilitate demoulding.

8.3.2 Mechanical strength testing

Mechanical strength testing was performed using a 50kN Instron 3369 Universal motorised load frame based on BS EN 1015-11:1999 to test compressive strength. Bluehill 3 software monitored and recorded the load on the specimen as a function of extension throughout the test.

8.3.3 Mercury intrusion porosimetry

Porosimetry of the mortar mixes was determined using a Pascal 140/440 Porosimeter. The Porosimeter forces mercury under pressure into the pores of the specimen material to provide information about pore size, pore volume distribution, particle size distribution, bulk density and specific surface. The Pascal 140 performs low pressure porosimetry from vacuum up to 400 KPa and was used to analyse the pores in the 116 – 3.8 µm diameter size range. The Pascal 440 operates at pressures up to 400 MPa and was used to analyse the pores in the 15 – 0.0036 µm diameter size range.

8.3.4 X-ray diffraction

The crystallinity of the samples was examined by powder X-ray diffraction using a BrukeraxsD8 Advance X-ray diffractometer equipped with a super speed PSD Vantec-1 detector and Cu K_α X-ray source of wavelength 1.5418Å. Data was collected over the 2θ range from 5° to 60° at a step size of 0.016° and time per step of 424.8s.

8.4 Results

The samples appeared to set rapidly. After the first week, the samples felt solid to the touch, in comparison to other experimental non-hydraulic lime specimens that were still relatively soft at this stage of curing. However, upon demoulding it became apparent that some of the specimens were somewhat friable and possessed low levels of strength. It can be seen in Figure 8.1 that one of the samples has already cracked before demoulding, although shrinkage does not appear to be excessive.

The fractured ends of the samples after flexural testing were sprayed with Phenolphthalein solution to determine the extent of carbonation in each sample. It can be seen in Figure 8.2 and 8.3 that the lime putty specimens containing nanosilica have carbonated to a lesser degree than the samples comprising only lime putty and standard sand at the same duration of curing. Interestingly, the mix without nanosilica is displaying Liesegang pattern development in the 91 day old specimen.

Figure 8.1: Lime putty, standard sand and nanosilica prism samples before demoulding.

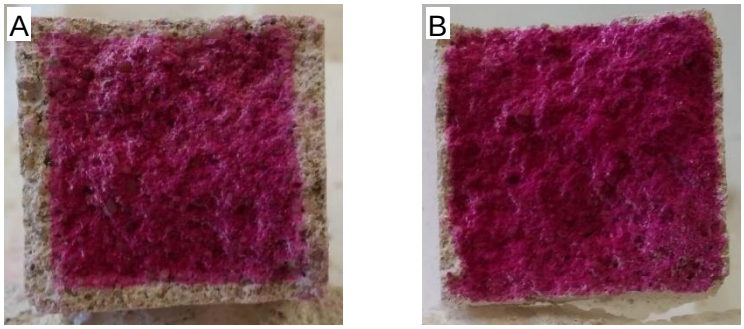

Figure 8.2: Carbonation progress at 28 days for lime putty and standard sand mix (A) and lime putty and sand with added nanosilica (B).

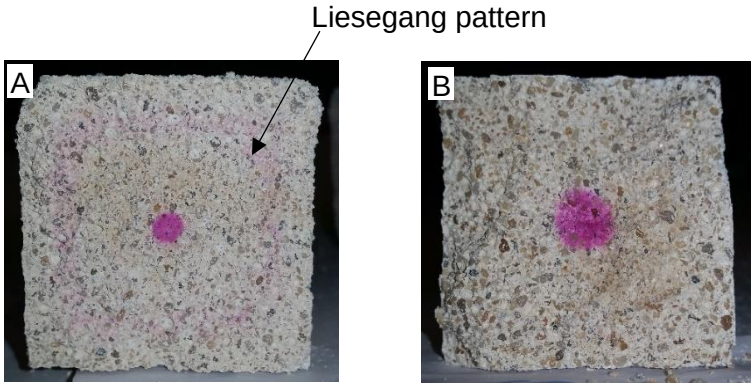

Figure 8.3: Carbonation progress at 91 days for lime putty and standard sand mix (A) and lime putty and standard sand with added nanosilica (B).

Figures 8.4 and 8.5 show the specimens prepared with NHL2 lime after 28 and 56 days of curing respectively. The extent of the carbonation does not appear to differ significantly with added nanosilica, although some of the specimens containing nanosilica did appear to have carbonated unevenly compared to the specimens without. Also, the specimens without nanosilica displayed clear Liesegang pattern markings, but these were not present in the specimens containing nanosilica.

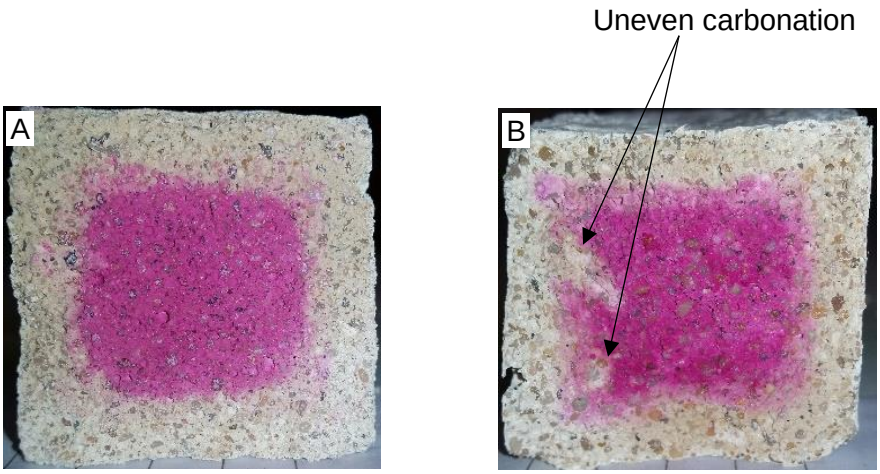

Figure 8.4: Carbonation at 28 days for NHL2 lime and standard sand (A) and NHL2 lime and sand with added nanosilica (B).

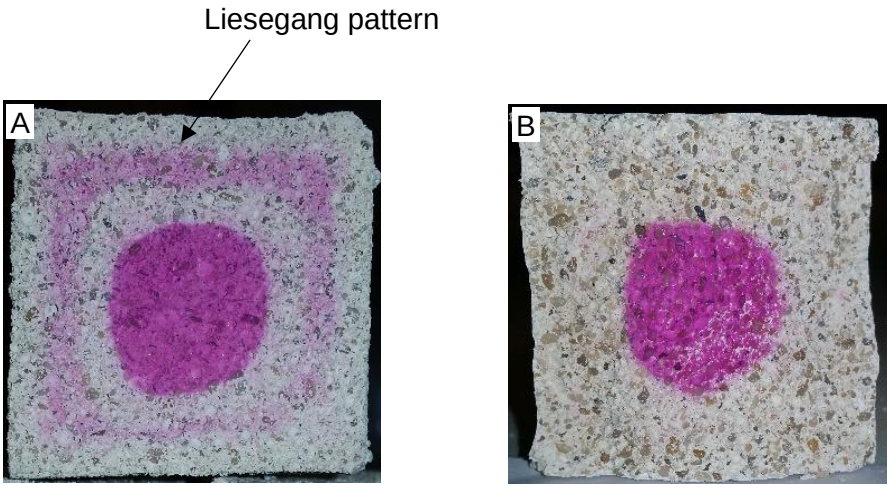

Figure 8.5: Carbonation at 56 days for NHL2 lime and standard sand (A) and NHL2 lime and sand with added nanosilica (B).

8.4.1 Mechanical strength testing

Compressive and flexural strength tests were carried out on 40x40x160mm specimen prisms of lime putty and standard sand only and a mix of lime putty with standard sand and a 1% by weight of nanosilica (Figure 8.6 and Figure 8.7). The flexural strength tests were completed first, and then the two resultant halves of the sample were used for the compressive strength testing.

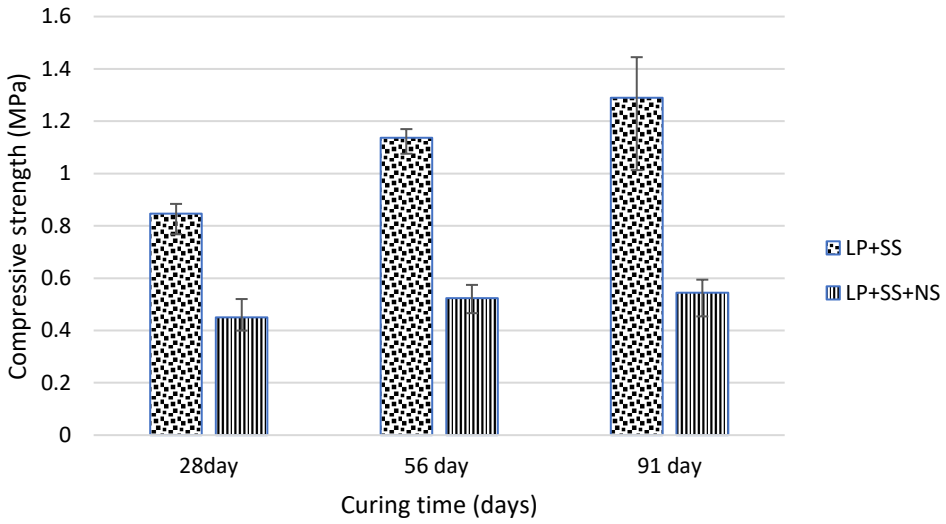

Figure 8.6: Plot of compressive strength at 28, 56 and 91 days. Error bars show maximum and minimum values.

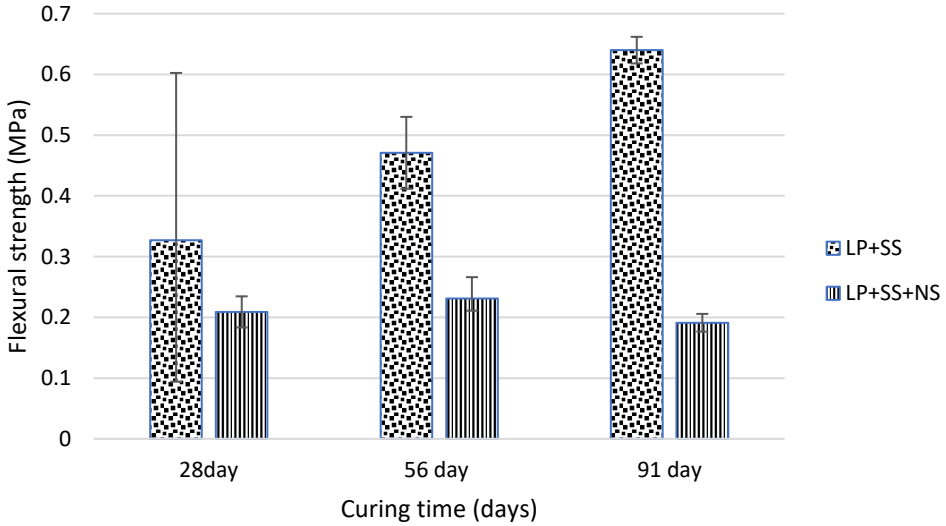

Figure 8.7: Plot of flexural strength at 28, 56 and 91 days. Error bars show maximum and minimum values.

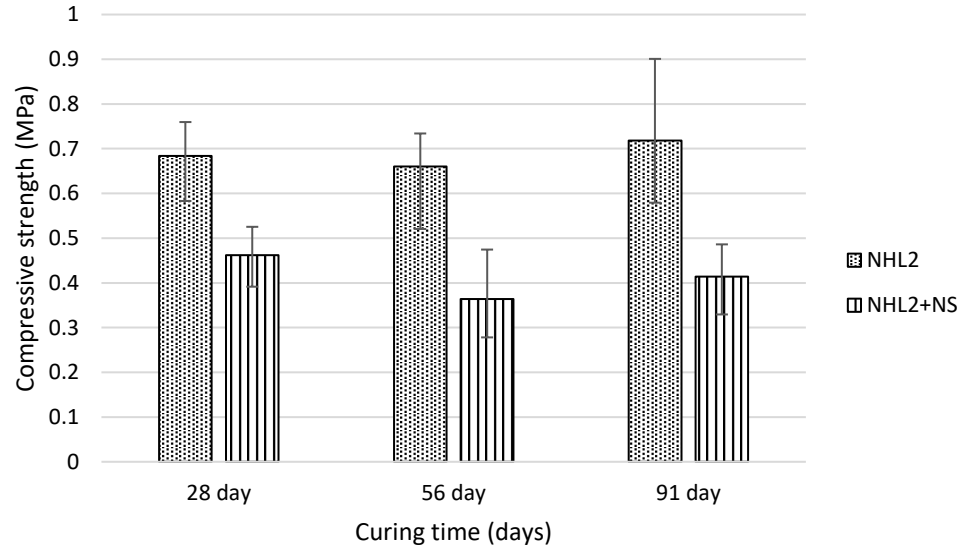

Figure 8.8: Plot of compressive strength at 28, 56 and 91 days. Error bars show maximum and minimum values.

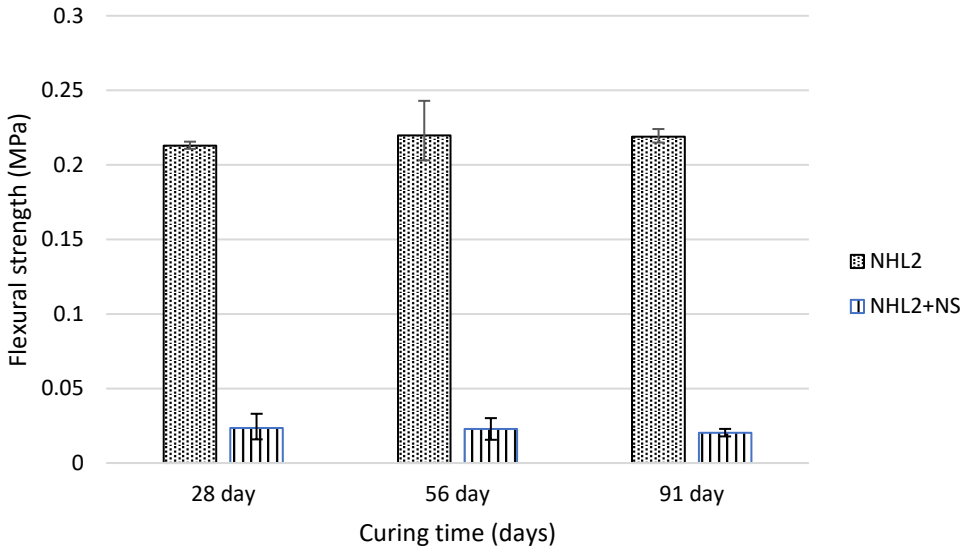

Figure 8.9: Plot of flexural strength at 28, 56 and 91 days. Error bars show maximum and minimum values.

8.4.2 Mercury intrusion porosimetry (MIP)

The graphs in Figure 8.10 show the pore size distribution for the lime putty mortar prepared with nanosilica in comparison with the same mortar mix but without added nanosilica.

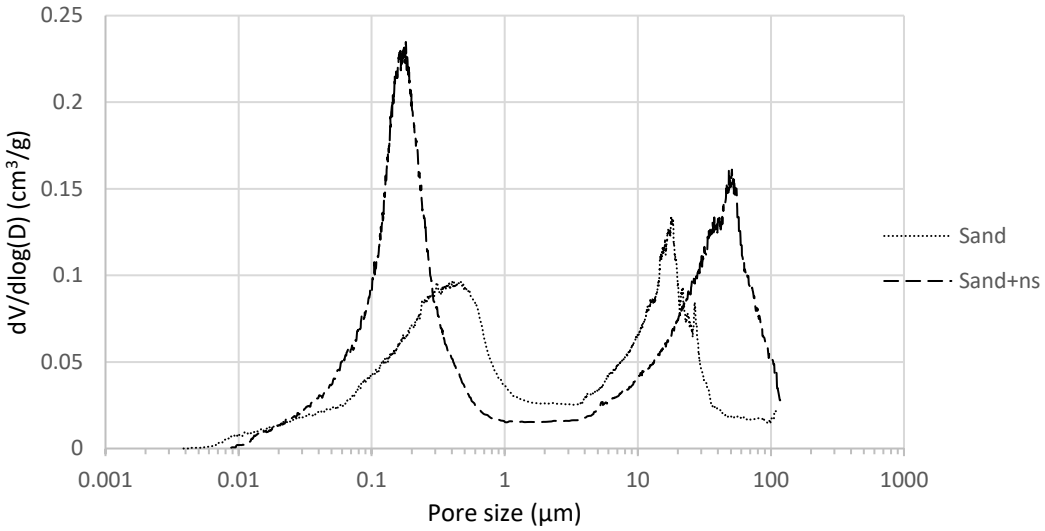

Figure 8.10: Pore distribution of lime putty and sand mix with and without added nanosilica.

8.4.3 X-ray diffraction (XRD)

X-ray diffraction patterns for lime putty and sand mortar (Figure 8.11) and with 1% by weight nanosilica (Figure 8.12). There is no indication of any hydration products such as C-S-H having formed from the addition of the nanosilica.

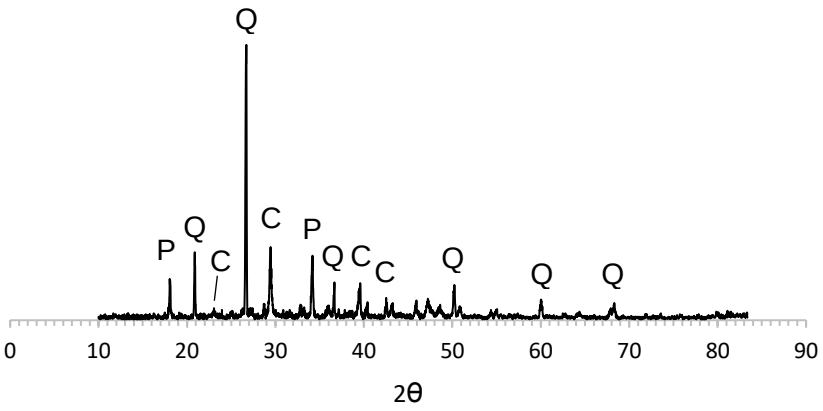

Figure 8.11: XRD pattern for lime putty with standard sand.

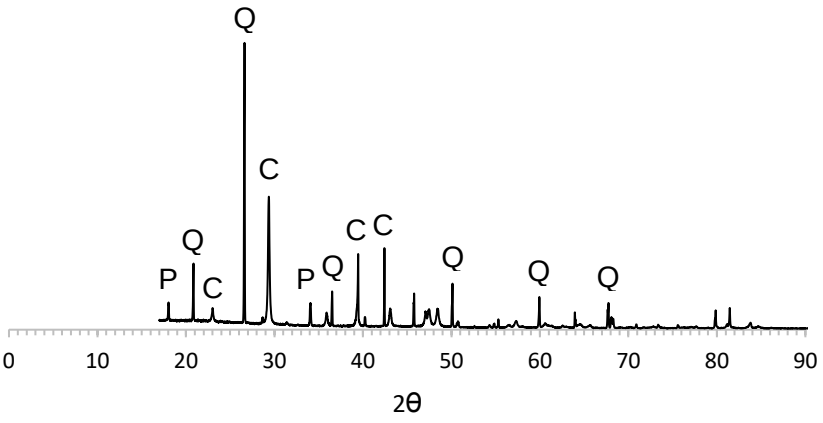

Figure 8.12: XRD pattern for lime putty with standard sand and nanosilica added at 1% bwt.

8.5 Discussion

The results obtained during this investigation are in contradiction with the literature on the subject that reports an increase in strength with the addition of nanosilica (Alvarez, 2013). The strength levels obtained with the addition of nanosilica were below the level that would be acceptable for a mortar. This was a surprising result considering that the extent of carbonation in the samples with and without nanosilica are similar.

The difference in strength maybe explained by comparing the pore structure of the two mixes. Analysis shows a significant difference in the quantity of both small and larger sized pores. The most obvious difference was that the sample containing nanosilica contained a much larger quantity of small, sub-micron pores and the majority of these were approximately 0.2 µ in size. The small pores in the sample without nanosilica were far fewer and were and mostly between 0.3 and 0.6 µ. The overall greater porosity of the nanosilica mix may at least partially account for its comparative weakness.

The effect of the nanosilica on carbonation does not appear to be significant. Although carbonation in the lime putty specimens was slightly retarded with nanosilica added, this alone cannot account for the friable nature of the specimens.

The weakness of the mortar containing nanosilica can be attributed to the increased water demand from the nanosilica. Achieving the optimum mix proportions is difficult to achieve when working with very small particle sizes (Vandenberg, 2015), and further work should be carried out to better understand this issue..

8.6 Conclusions

- This investigation found no benefit to using nanosilica in lime mortar with the methods, materials and proportions specified for this investigation.
- The strength levels achieved for the experimental mixes were below the level reasonably expected for a lime mortar
- The pore structure was altered significantly with the addition of nanosilica: it had the effect of increasing the volume of smaller pores whilst also adding larger pore sizes.

8.7 General observations and further work

The water content of the experimental mixes comprising lime putty as the binder produced for this work was dictated by the form of nanosilica used. The only option available to vary this parameter of the mix would have been to increase the water content. Carrying out tests using powdered nanosilica would permit a more flexible approach to mix design and the ability to better understand the effect of varying water content; however, the use of powdered nano particles is considered a health hazard and the potential harmful effects are not completely understood at this time.

8.8 References

Alvarez, J. I., Fernandez, J. M., Navarro-Blasco, I., Duran, A., Sirera, R., 2013. Microstructural consequences of nanosilica addition on aerial lime binding materials: Influence of different drying conditions. *Materials Characterisation,* 80, pp.36-49.

BS EN 1015-11:1999. *Methods of test for mortar for masonry - Part 11: Determination of flexural and compressive strength of hardened mortar.* BSI

Livesey, P., 2010. The Use of Lime Mortars and Renders in Extreme Weather Conditions. *Journal of the Building Limes Forum,* 17, 2010, pp.46-49

Singh L.P., Karade S.R., Bhattacharyya S.K., Yousuf M.M. and S. Ahalawat S., 2013. Beneficial role of nanosilica in cement based materials. *Construction and Building Materials,* 47, p.1071

Vandenberg, A., Willie, K., 2015. Understanding the Dispersion Mechanisms of Nanosilica in Ultra High Performance Concrete. *Nanotechnology in Construction: Proceedings of NICOM5.* 24-26 May 2015 Chicago. Springer. Pp.311-316

CHAPTER 9 DISCUSSION

This research investigated the potential of seven different additive materials to enhance the physical properties of lime-based construction materials and consequently reduce their environmental impact in some way. Four of these materials – aerogel granules, olivine, slate and granite - were used as aggregate materials as a direct replacement for the silica sand that is traditionally used. The other three materials – graphene oxide, nanosilica and polypropylene monofilament fibres – were used as supplementary additive materials.

The first area of research was the development of an experimental insulating plaster containing aerogel granules as a lightweight aggregate. Thermal conductivity testing carried out using the 'hot strip method' confirmed the plaster achieved thermal conductivity of approximately 0.05 W/m.K at 50% aerogel content by volume. This is significantly lower than traditional gypsum and sand plasters, which can have values as high as 0.72 W/m.K. This type of insulation has potential to be used as a plaster on internal walls or as roof insulation between joists or rafters and could be used on surfaces that are uneven, curved or irregular in shape. An additional benefit of this type of material is waste reduction. Insulation products produced in the form of boards or batts require cutting to size, and this generates waste. These findings have significance for the effort to improve the thermal efficiency of buildings and reduce waste, particularly in relation to retrofitting of buildings.

Initial experiments mixing aerogel granules with lime putty binder produced plasters that were very friable and would not be viable. Interestingly, the literature on this subject provides data on thermal conductivity achieved in other studies, but no data on strength. The one aerogel insulating plaster currently on the market uses a lime binder but also contains cement as an additive to add strength. For this work, the use of cementitious materials was avoided to maintain vapour permeability and flexibility and avoid the introduction of sulfates into the plaster. Because of this, it was decided to investigate the use of polypropylene monofilament fibres to improve the integrity of the plaster, as there is a large amount of information in the literature, attesting to their ability to reduce shrinkage cracking and increase strength. The addition of the fibres eliminated shrinkage cracking and greatly improved flexibility and flexural strength.

There are challenges that would need to be overcome with the use of this material, however. The main issue at the present time is cost. Being a niche product, aerogel does not currently benefit from the economies of scale that bring about downward pressure on prices. Another issue could be the low level of strength that aerogel possess in comparison with other insulating materials. This would be an important consideration where the material could be subject to impact damage. This area of research has particular importance and value, though, because, as identified in the literature, energy consumed by a building over its lifetime greatly exceeds that of the materials used in construction (Iddon and Firth, 2013, p.479).

The literature also highlighted the changing nature of the construction industry. Modern methods of working are introducing new skills and processes to the industry, which will present both challenges and opportunities. As it is intended that more work should take place off site, the use of premixed composite materials would potentially be a benefit, and this would be compatible with a lime, fibre and aerogel composite manufactured under factory conditions.

The second area of research investigated the use of olivine as an aggregate material with the potential to sequester CO_2. Mortars were prepared with three different aggregate materials: fine olivine sand, coarse olivine sand and standard silica sand. The coarse olivine sand proved to be unsuitable as an aggregate material. The mortar prepared with the coarse olivine was friable and completely unsuitable for use. The mortar prepared with fine olivine sand produced a mortar that possessed approximately 278% greater strength than the mortar containing silica sand. The superior strength was attributed to the higher carbonate content, as confirmed by thermogravimetric analysis, which was a result of Mg^{+2} cations from the dissociation of olivine becoming available to form $MgCO_3$ and $MgCa(CO_3)_2$. The higher carbonate content of the mortar containing olivine was confirmed using X-ray diffraction and Raman spectroscopy.

Work is being carried out to investigate the potential to store CO_2 in olivine that has been ‘activated’ by milling to reduce particle size and increase reactivity. The olivine is then spread on beaches to weather and sequester CO_2. As an alternative, this work indicates that olivine could put to profitable use as a construction material. The strength enhancing properties of olivine are an additional advantage. Olivine could be used as

a strength enhancing additive in mortars by replacing a proportion of ‘normal’ sand aggregate with olivine sand. The findings of this area of research have particular significance considering the recent government announcement that the UK will commit to reaching a legally binding net zero target by 2050.

The third area of research investigated the properties of ‘hot lime’ mortars to assess a hypothesis that they have superior properties compared with other forms of lime binder. Hot lime mortars were compared with mortars prepared with lime putty. Both types of lime binder were used to prepare mortars with three different types of aggregate: standard silica sand, slate and granite. Slate and granite were chosen as experimental aggregate materials because they are both potential sources of waste or recycled material. Compressive strength test results for the hot lime mortars and lime putty mortars were not significantly different when prepared using the same aggregate material. The mortars prepared with slate or granite aggregate, however, possessed significantly higher strength than mortars prepared using silica sand aggregate, regardless of binder type. For the mortars tested, aggregate type had a significant impact on compressive strength, whilst binder type displayed no significance. Pore size distribution was also similar for the hot lime and lime putty binders when prepared using the same aggregate, but the pores in the slate and granite mortars were significantly more extensive and interconnected for both types of lime binder. The superior pore structure of the slate and granite mortars was believed to have facilitated better CO_2 diffusion throughout the binder and hence greater strength development.

These findings have significance for the reduction of waste within the construction industry. As highlighted by Network Waste (2019), construction is one of the highest waste producing industries in the UK, generating 72 million tonnes of waste per year (Bradley, 2019). The cutting of slate and granite generates a large amount of waste, much of which is left in waste tips, where it can sterilise the resources under tips and create safety issues. This work demonstrates that there is potential to mitigate this problem by utilising these waste products as aggregate materials.

As demonstrated by strength testing, slate and granite also have potential to be used as strength enhancing additive materials to lime mortars where greater strength is required such as on taller buildings.

The fourth area of research was the addition of graphene oxide as an additive to lime. Unlike the other research objectives, this investigation concentrated on the chemical aspect of the experimental mix. In particular, the effect on carbonation was of interest. The addition of graphene oxide to nanolime had promoted the growth of carbonate crystals on the face of portlandite crystals after four hours, whilst the same reaction was not seen on the portlandite crystals of nanolime to which no graphene had been added.

This area of research is of importance in adding knowledge to the understanding of the carbonation process and how it may be controlled or optimised. Analysis of this work was difficult, though, due to the number of similar chemical bonds in the reactants and products.

The fifth area of research investigated the effects of using nanosilica as an additive. Compared with a reference mortar prepared without nanosilica, the mortar possessed considerably lower strength. Also, nanosilica significantly altered the pore structure, increasing the number of sub-micron pores. The mortar produced was not a viable product.

CHAPTER 10 CONCLUSIONS

In this thesis, the ability of novel additive materials to enhance the physical properties of lime-based construction materials was investigated. The overarching aim of the research was to identify ways in which enhancing lime mortars, renders and plasters can reduce the environmental impact of these materials.

10.1 Insulating aerogel plaster incorporating polypropylene monofilament fibres

An insulating plaster was developed that incorporated aerogel granules to significantly reduce thermal conductivity. The effect of replacing different proportions of sand aggregate with aerogel granules was investigated and an exponential equation developed that mathematically describes the relationship between aerogel content and thermal conductivity. Polypropylene monofilament fibres were added to the plaster at 0.5% by weight to reduce shrinkage and cracking. The result was a highly flexible plaster that has thermal conductivity significantly lower than traditional plasters.

10.2 Olivine mortar

A lime mortar was developed that incorporated fine olivine sand as the aggregate material to assess its potential for use in CO_2 sequestration. It was determined that the dissociation of olivine makes Mg^{+2} cations available for carbonation to form $MgCO_3$ and $CaMg(CO_3)_2$. The $MgCO_3$ and $CaMg(CO_3)_2$ formed is additional to the $CaCO_3$ formed as a normal part of lime binder carbonation and so the total carbonate formed, and hence CO_2 absorbed, is greater compared with mortars prepared using inert silica sand aggregate. The higher carbonate content of mortars containing olivine was found to increase compressive strength significantly.

10.3 Hot lime mortars

The use of slate and granite as aggregate materials in lime putty and hot lime mortars was investigated. The findings did not support a hypothesis that hot lime mortars are superior to other types of lime mortar. However, it was found that slate and

granite can impart greater compressive strength than standard sand aggregate, which was attributed to their angular morphology. The results confirmed the potential viability of using waste and recycled slate and granite for use in construction materials.

10.4 Lime and graphene oxide

The chemical interaction between graphene oxide and nanolime was investigated in order to gain insight into its impact on carbonation. Small crystals formed on the face of the nanolime (portlandite) crystals after four hours, which did not occur on the nanolime without graphene oxide present. The graphene oxide was believed to accelerate carbonation, but the results obtained were not conclusive.

10.5 Lime and nanosilica

The addition of nanosilica was added to lime putty mortar to assess its effect on strength. Contrary to what was expected, strength was significantly reduced. There was a significant increase of sub-micron size pores compared with the mortar without added nanosilica. The decrease in strength was thought to be as a result of the increased water demand from the nanosilica. The smaller pore size distribution was attributed to pore blocking from the nanosilica.

From the above conclusions, it is evident that the use of additive materials in lime-based construction materials has significant potential to fulfil the research aim of improving the physical and chemical properties of lime-based construction materials. The incorporation of aerogel and polypropylene fibres in lime plaster has potential to reduce thermal conductivity and increase the thermal efficiency of buildings. Using olivine as an aggregate material in mortar can be utilised to increase CO_2 absorption compared to conventional mortar mixes and the use of slate and granite as aggregate in lime mortar has the duel advantages of increasing strength and consuming a waste product.

CHAPTER 11 FUTURE WORK

The work carried out for this thesis has achieved the aim of providing evidence that certain novel additives have the ability to improve the physical properties of lime-based construction materials and reduce their environmental impact. However, there is much work that should be carried out to develop these areas of research. Specific recommendations for further work have been provided already, but there are certain general recommendations that apply across all of this research

A challenging aspect of this research was the number of variable parameters for each experimental material mix. The type of lime, aggregate particle size, binder/aggregate ratio and proportion of additive can all be varied, and the number of possible permutations for each mix is vast. Future work should investigate in more detail the effects of varying the parameters for each experimental mix in order to optimise the results.

The results presented in this thesis confirm that these materials have the potential to help reduce the environmental impact of construction materials by helping to reduce atmospheric CO_2, Improving thermal efficiency of buildings and using recycled materials. However, these benefits are only one aspect of the overall environmental impact of these materials. Further research should be carried out into the full lifecycle of these materials taking into account production, transport, lifespan and recyclability. Unfortunately, a full life cycle assessment was beyond the scope of this work.

APPENDIX 1 – PHYSICAL AND MECHANICAL PROPERTIES OF PLASTERS INCORPORATING AEROGEL GEANULES AND POLYPROPYLENE MONOFILAMENT FIBRES

Construction and Building Materials 158 (2018) 472–480

Contents lists available at ScienceDirect

Construction and Building Materials

journal homepage: www.elsevier.com/locate/conbuildmat

Physical and mechanical properties of plasters incorporating aerogel granules and polypropylene monofilament fibres

Paul Westgate *, Kevin Paine, Richard J. Ball

BRE Centre for Innovative Construction Materials, Department of Architecture and Civil Engineering, University of Bath, Bath BA2 7AY, UK

HIGHLIGHTS

- Experimental insulating plasters comprising lime, aerogel particles and polypropylene monofilament fibres are investigated.
- Replacing sand aggregate with aerogel significantly reduces both thermal conductivity and strength.
- Incorporating polypropylene fibres greatly improves flexibility and toughness.
- Incorporating aerogel granules in a plaster mix significantly improves vapour permeability.

ARTICLE INFO

Article history:
Received 20 March 2017
Received in revised form 15 September 2017
Accepted 26 September 2017
Available online 15 October 2017

Keywords:
Aerogel
Thermal insulation
Nanomaterials
Polypropylene fibres
Insulating plaster

ABSTRACT

Growing concern over global warming in recent years has required buildings to become significantly more energy efficient. One of the main ways of achieving this aim has been through the use of innovative materials to facilitate improvements in levels of building insulation. This paper describes the use of aerogel granules as an additive material for lime-based plasters, with the objective of improving the thermal efficiency of buildings whilst maintaining or improving vapour permeability.

Five experimental lime composite mixes were prepared, with lime putty as the binder material and aggregate comprising differing proportions of standard sand and aerogel granules. Previous work had already confirmed very low strengths for plaster mixes containing aerogel granules alone as the aggregate material; therefore, polypropylene fibres were incorporated as a secondary additive material to improve the mechanical properties and reduce strength loss attributed to shrinkage and cracking.

The flexural strength, compressive strength, thermal conductivity and water vapour permeability of lime composite mortars containing different volume fractions of aerogel were determined. Microstructures were examined using scanning electron microscopy and transmission electron microscopy. The results showed that aerogel granules can be successfully incorporated into lime plasters to improve thermal efficiency. The addition of aerogel was also found to improve moisture vapour permeability. The inclusion of polypropylene fibres in aerogel plasters was effective in reducing shrinkage and cracking to acceptable levels. Experimental mixes exhibited a slight reduction in strength compared to standard plaster mixes, although this was compensated for by a high level of flexibility and toughness.

This work provides innovative information on utilising aerogel granules as an insulating plaster additive by addressing the issues of strength and flexibility, properties that are not normally associated with aerogel but which are of importance in a functional plaster material.

1. Introduction

Global warming continues to be one of the most challenging environmental problems we face today. Despite a growing number of climate change mitigation policies, total anthropogenic greenhouse gas emissions were the highest in history from 2000 to 2010 [1]. In the UK, the government is putting special emphasis on retrofitting and refurbishment of the existing housing stock in an effort to tackle this problem, as this offers the greatest potential for CO_2 reduction in the short to medium term. This will be an enormous challenge, with approximately 25 million homes requiring upgrading by the end of 2050 if carbon reduction targets are to be met [2]. One of the most promising ways in which buildings can be adapted to help meet these goals is through the use of state of the art insulation materials, and a highly insulating material in this respect is silica aerogel.

* Corresponding author.
E-mail address: pw415@bath.ac.uk (P. Westgate).

https://doi.org/10.1016/j.conbuildmat.2017.09.177
0950-0618/

Aerogel is most often incorporated into buildings in the form of blankets for loft insulation or boards for wall and ceiling insulation. However, insulating boards can be wasteful of material due to the requirement to be cut to size. Also, insulating boards have the disadvantage of requiring a flat surface for fixing onto. As a solution to these limitations, several organisations are developing plaster mixes that incorporate aerogel in granular form. One experimental product developed by Stahl et al. [3], comprised of a mineral and cement free binder and hydrophobised granular aerogel at up to 90% by volume, has achieved a thermal conductivity value of 0.025 W/mK. A similar composite material developed by Burrati et al. [4] reportedly achieved a thermal conductivity value of 0.05 W/mK with 90% aerogel by volume; the equivalent material without aerogel had a value of 0.5 W/mK. To date, however, there is only one known commercially available plaster that incorporates aerogel granules as the insulating element: the Fixit 222 Aerogel Insulating Plaster System. Fixit 222 is a highly developed product, comprising aerogel granules, light weight mineral aggregate, natural hydraulic lime, white cement and calcium hydroxide. Despite the use of cement and mineral aggregate, it still claims to achieve a thermal conductivity value of 0.028 W/mK [5]. These new plasters have significantly better thermal insulation performance than traditional cement or gypsum plasters with sand aggregate, which typically have thermal conductivity values of between 0.22 and 0.72 W/mK [6]. Interestingly, though, there appears to be no published information relating to strength or flexibility for any of these new insulating lime plaster materials. Two studies, involving cementitious mortars incorporating aerogel, which did investigate strength, reported compressive strength, flexural strength and thermal conductivity all reducing with increased aerogel content [7,8].

Aerogels are a special class of extremely low density, amorphous, mesoporous materials with a nanostructure. In the case of aerogels, the 'nano' designation refers to the size of the pores within the material rather than the actual particle size. Pore sizes in aerogels are generally between 5 and 70 nm and have a pore density of between 85 and 99.8% by volume [9], resulting in a very low thermal conductivity, a low gaseous conductivity and a low radiative infrared transmission, making them an extremely efficient insulating material.

An important property of aerogel for use in construction materials is its behaviour in the presence of water. There are several methods of manufacturing an aerogel, and the method used determines whether the finished product is hydrophilic or hydrophobic. Hydrophilic aerogels possess a large number of surface hydroxyl groups, making them extremely hygroscopic. When liquid water enters the pore structure, the surface tension of the water exerts strong capillary forces on the pore walls, causing collapse. This problem can be easily solved, however, by converting the surface hydroxyl groups (-OH) to non-polar (-OR) groups, where R is typically a methyl group [10].

Aerogel possesses a very high strength to mass ratio and can support up to 1600 times its own mass [11]; however, as manufactured, it is a brittle material, having a fracture toughness of only ~0.8 kPa $m^{1/2}$. Although easily crushed, this does not destroy its porous structure; aerogel that has been ground into a powder occupies approximately the same space as the original sample, demonstrating that the pore structure of the material does not change significantly [12].

In addition to its low weight and lower space requirements, aerogel's higher durability makes it an attractive alternative to fibre and foam insulation materials [13].

Initial attempts during this investigation to incorporate aerogel granules with lime plasters resulted in high shrinkage and extensive cracking of the lime matrix. This work seeks to mitigate these problems through the incorporation of monofilament polypropylene fibres. These fibres have been used extensively in cementitious building materials, and are considered one of the most effective methods to reduce plastic shrinkage and cracking in mortars [14]. The effects of the volume fraction of polypropylene fibre on the mechanical properties of concrete was investigated by Rajguru R.S. et al. [15]. It was found that the flexural strength of test beams increased significantly with increased fibre content from 0.25% to 0.5%, but the rate of strength increase achieved by increasing fibre content from 0.5% to 1% was marginal. Work has also been carried out to investigate ways of improving the mechanical properties of aerogel by incorporating fibres into the actual aerogel structure itself to produce fibre-reinforced aerogel composites. It was found that composites could be produced that had a higher strength compared to non-reinforced aerogel, but sacrificed little thermal performance [16].

Whilst aerogel may have the potential to help reduce energy usage in buildings, it is also important to consider the properties of the binder material. Prior to the introduction of hydraulic cements, non-hydraulic lime putty was routinely used as a binder material for mortars, plasters and renders in building construction and has proved to be durable over many centuries [17]. It has a significantly lower environmental impact than that of the more commonly used Portland cement, which requires higher temperatures during production, and hence results in higher CO_2 output, than lime. But the case for lime as a low carbon material is strengthened further by the fact that it actually reabsorbs CO_2 whilst setting; a non-hydraulic lime putty can absorb nearly its own weight in CO_2 [18].

A further advantage of non-hydraulic lime is its long shelf life. It is common for manufacturers to recommend that, once opened, bags of lime are used within a specified time or discarded. In practice, practitioners may keep lime from a few days to one year depending on the storage conditions and risk of excessive hydration and carbonation within the bag. Non-hydraulic lime putty, however, can be stored for significantly longer due to the effectiveness of the milk-of-lime layer on the surface of the putty at preventing carbonation. The carbonation rate and plasticity of lime putty have been found to be still improving after periods in excess of five years [19].

The use of a lime putty as a binder is also advantageous for the recycling of materials. Hardened lime binder can be removed from masonry relatively easily, whereas the high strength bonding of cement mortars and renders can prevent recycling of materials, as it cannot be removed easily from brick and stone without causing damage.

An additional benefit to using lime is its superior water vapour permeability compared to modern commercial plasters [20]. When used as a render, the higher permeability of lime plaster helps moisture to escape from within the walls, preventing freeze thaw damage [21]. When used as a plastering material, its ability to release moisture helps to prevent mould formation and reduction in thermal resistance. Although there is little published data on the permeability of aerogel plasters, one study by Ibrahim et al. reported a figure of 5.1×10^{-11} kg/s m Pa for an experimental aerogel based external render [22]. This figure is significantly higher than was found in a study by Wang et al., where five commercially available gypsum plasters were found to achieve figures of between 1.62 and 2.53 kg/s m Pa [23].

Compared to other insulation materials such as glass and natural fibre, aerogel is still of higher cost. However, it should be noted that it is still a relatively new material for construction applications. As its use becomes more widespread, higher production quantities and economies of scale will help lower the cost [24]. Aerogel is the insulation material of choice for applications where the space available for insulation is limited but performance cannot be compromised. It is also noteworthy that over the service life

of a building a reduction in operational costs associated with better insulation can be realised. Iddon and Firth (2013) report that for a typical building between 74 and 80% of the total energy in the first 60 years of service is consumed during operation and use. The remainder is the embodied energy and energy used during the construction process [25].

This paper investigates the use of granular aerogel incorporated into non-hydraulic lime-based plasters with the aim of developing a product that is highly insulating and has good vapour permeability, with the capability of reducing the operational energy consumption of buildings.

2. Experimental materials

2.1. Lime putty

The binder material used for this work was a lime putty supplied by J J Sharpe, which was matured for at least 6 months. The lime putty was weighed before and after drying in an oven to remove the water content and was found to have a solids content, assumed to be calcium hydroxide of 51%. This allowed accurate batching of the mix constituents.

2.2. Aerogel granules

The silica aerogel was supplied by Aerogel UK. The material comprised open cell, hydrophobic aerogel granules ranging in size from 125 μm to 5 mm.

2.3. Standard sand

The sand used in this investigation was a dry siliceous natural sand conforming to BS EN 196-1 and ISO 679: 2009. This grade of sand comprises particles that are generally isometric and rounded in shape and having a particle size distribution as shown in Fig. 1. This type of sand was specified for this investigation to facilitate consistency and repeatability of experimental conditions.

2.4. Polypropylene fibres

Polypropylene monofilament fibres from Adfil [26] having lengths 12 and 18 mm and a diameter of 20 μm were added to the experimental plaster mixes at 0.5% by volume, to help reduce shrinkage and cracking. The fibres had been treated with a surfactant for optimum dispersion and bonding. No details of the surface treatment were provided by the manufacturer.

The volume fraction was kept at 0.5%, as it was considered that higher proportions of fibres might negatively affect the rheology of the plaster and that strength per se was not the most important physical property for a plaster.

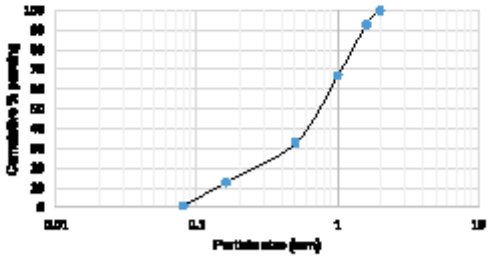

Fig. 1. Particle size distribution for standard sand.

2.5. Sample preparation

Five different plasters were prepared for testing using a mix ratio of 1:1 aggregate to lime putty by volume, giving a ratio ≈2:1 aggregate to lime by volume after allowing for the water content of the putty. The five specimens all contained fibres and varying ratios of aerogel and sand. The corresponding mix ratios and resulting bulk densities are presented in Table 1.

The lime and sand were prepared using a paddle mixer for a minimum of twenty minutes to ensure the plaster was suitably workable. Fibres were added to the mixture in small amounts during the mixing process to help ensure an even distribution throughout the matrix. The aerogel was added afterwards and mixed into the plaster by hand using a trowel. This was to avoid subjecting the aerogel to prolonged stress during mixing and possible degradation of the granules. The experimental mixes were then added to the prism moulds in small quantities and tamped down as the material was added, to reduce the occurrence of trapped air bubbles within the specimens. For each experimental mix, three standard 40 × 40 × 160 mm prisms were prepared for strength testing, six discs of diameter 100 mm and thickness 25 mm for thermal conductivity testing and three discs of diameter 175 mm and thickness 15 mm for water vapour permeability testing.

After moulding, the specimens were stored in a climate chamber regulated at a constant temperature of 20 °C ± 2 °C and relative humidity of 65% ± 5% as specified in standard EN 1015-11:1999 [27]. The specimens were covered with a thin plastic wrap for the first week to maintain a high level of humidity, as exposure to ambient atmospheric conditions during this period can result in significant reduction in strength due to premature drying and subsequent cracking [28]. The specimens were then left in the moulds for a further week to allow them to achieve sufficient rigidity to facilitate demoulding.

3. Experimental methods

3.1. Strength testing

Mechanical strength testing was performed using a 50 kN Instron 3369 Universal motorised load frame in accordance with BS EN 1015-11:1999 to test both the flexural and compressive strength. Bluehill 3 software monitored and recorded the load on the specimen as a function of extension throughout the test.

3.2. Electron microscopy

Scanning electron microscopy (SEM) was used to examine the physical condition of the specimens at the lime/aerogel interface to help identify any shrinkage around the aerogel particles or any degradation of the particles themselves. Specimens were analysed using a JEOL 6480 LV scanning electron microscope equipped with an Oxford Instruments INCA X-act X-ray detector (silicon drift detector offering high count rate and reduced operation time). High magnification images of the aerogel internal pore structure were obtained using a JEOL JEM1200EXII transmission electron microscope (TEM) operating at 120 kV.

3.3. Thermal conductivity measurement

Thermal conductivity measurements were obtained using the transient hot strip method. This method is suitable for thermal conductivity measurement of porous substances and has previously been used on plasters [29]. This method works by measuring the temperature rise at a known distance from a linear heat source. The linear heat source and the temperature sensor (thermocouple) are incorporated, at a known distance, within the sensing strip.

Table 1
Material composition by volume of experimental mixes.

Specimen	Lime putty (%)	Standard sand (%)	Aerogel (%)	Polypropylene fibres (%)	Bulk density (kg/m^3)
S0	50	49.5	0	0.5	1504
S1	50	37.25	12.25	0.5	1294
S2	50	24.75	24.75	0.5	1089
S3	50	12.25	37.25	0.5	883
S4	50	0	49.5	0.5	682

To take the measurements, the sensing strip was placed between two of the 100 mm diameter disc specimens. The specimens were tested under normal conditions i.e. not dried. Upon commencing the measurement process, the apparatus heats up and establishes a stable temperature within the test specimens. Temperature data were recorded at two second intervals for a period of 120 s. The power setting for this test was 0.4 W. Measurements were repeated on three different pairs of specimen discs and an average value calculated for each mix.

3.4. Water vapour permeability testing

Water vapour permeability testing was carried out in accordance with BS EN 1015-19:1999. Three 175 mm diameter specimens were tested for each of the five mixes. The discs were sealed onto the open mouth of a circular test cell, which contained a 10 mm deep saturated solution of potassium nitrate, and the discs were sealed around their outside edge with silicon sealant. The air gap between the base of the specimen discs and the top of the saturated potassium nitrate solution was 10 mm (±1 mm). This experimental set up produced a relative humidity within the test cell (in the air gap between the top of the salt solution and the underside of the test specimen) of approximately 95% at 20 °C.

Test samples were placed in a fan-assisted environmental chamber at 20 °C and 50% RH. A precision balance within the chamber logged the sample mass at five minute intervals on a PC. Monitoring was continued until a linear relationship between mass reduction and time could be established.

3.5. Fourier Transform Infra-Red Spectroscopy (FTIR)

FTIR was used to help identify any chemical reactions that may have taken place between the lime and the fibres or between the lime and the aerogel particles. FTIR spectra were obtained for the aerogel granules and the polypropylene fibres before and after they were added to the lime mixes. A PerkinElmer Frontier FTIR spectrometer was used over a frequency range from 600 to 4000 cm^{-1} and at a resolution of 1 cm^{-1} and 40 accumulations.

4. Results

4.1. Compressive and flexural strength

Figs. 2 and 3 show stress as a function of strain during compressive and flexural testing respectively. The data was reported up to a strain value of 0.03 as a consequence of the failure mode behaviour of specimens containing fibres. At higher values of strain the test data indicates that the specimens did not fail in a brittle manner

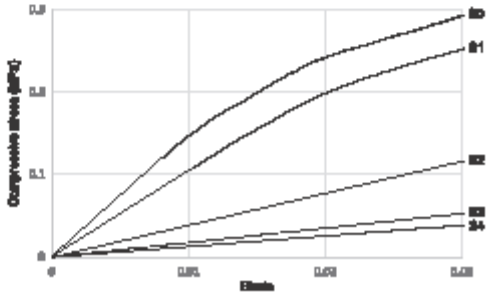

Fig. 2. Average compressive strength test results for each of the five plasters.

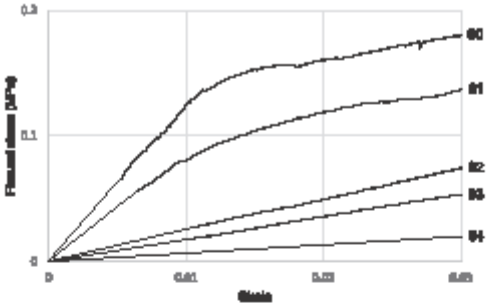

Fig. 3. Average flexural strength test results for each of the five plasters.

even though their condition was such that they would have been considered to have failed as a building element.

As the flexural test caused test specimen deformation but did not fracture it, the deformed specimen was manually broken in half after the test, and fibres and binder were removed from the fracture faces for further testing.

4.2. Effect of fibres on failure mode

Fig. 4 shows the different behaviours under stress of lime mortars with and without fibres added. Fig. 4(A) shows a typical behaviour for a standard lime mortar (without fibres) under compression. At failure, the specimen fractures and fails at a distinct point in the test. In Fig. 4(B) it can be seen from the degree of compression at the base of a specimen containing aerogel (S1) that the addition of 0.5% fibres by mass permits the lime mortar to achieve a high strain capacity, and that the fibres have prevented fracturing and have helped to maintain the integrity of the specimen.

Similarly, during flexural testing a significant difference is observed between the specimens with and without fibres added. The standard mix lime specimen cracked at the point of maximum stress (Fig. 5(A) and broke into two halves. Fig. 5(B) shows that the specimen containing fibres endured a significantly higher strain without failing and has considerably greater flexibility.

4.3. Scanning electron microscopy (SEM)

It can be seen that the typical morphology of the aerogel granules was an irregular shape and this contained different features including both smooth and rounded surfaces in addition to some sharper edges (Fig. 6).

The images in Fig. 7(A) and (B) show aerogel particles in a specimen after 91 days. Fig. 7(A) shows a particle embedded in the binder, which has remained intact and not deteriorated in any discernible way. In Fig. 7(B) it can be seen that there is no evidence of shrinkage at the aerogel/lime interface. This finding is consistent with a study by Gao, T. et al, which reported that aerogel particles in 'aerogel incorporated concrete' survive the mixing and curing process without suffering degradation [30]. The images in Fig. 8 (A) and (B) show the effect of the binder on the surface of the fibres. In Fig. 8(A), damage to the fibre surface is clearly visible in the form of scratches along the length of the fibre. This fibre was extracted from the fracture face of a test prism after flexural strength testing, and the marking was caused by the fibres being pulled with force from the binder matrix during the test. For reference, Fig. 8(B) shows the smooth and unmarked surface of a fibre in its original unused condition. Fig. 9(A) and (B) shows images of plaster particles removed from the fracture face of a test specimen.

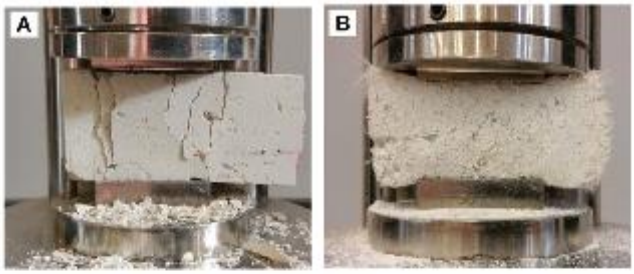

Fig. 4. Compressive fracture of a reference mortar without fibres (A) and typical deformation of a specimen (S1) containing fibres and aerogel (B).

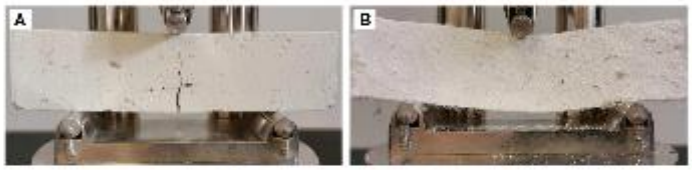

Fig. 5. Flexural fracture of reference mortar without fibres (A) and deflection of a specimen (S1) containing fibres and aerogel (B).

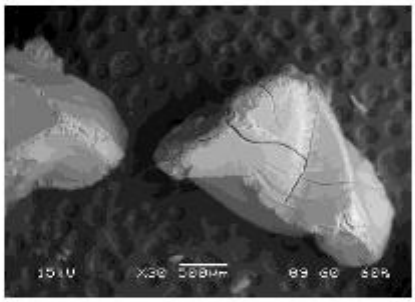

Fig. 6. Aerogel particles as manufactured.

In Fig. 9(A), it can be seen that these particles have suffered physical stress, as the aerogel particles have fractured and appear as shards. In Fig. 9(B), the aerogel particle appears to have remained intact. In both cases, binder remains adhered to the aerogel. In Fig. 10(A) and (B), evidence of the bond between the lime binder and the fibres is visible. These fibres were pulled from the specimen matrix, yet calcite crystals remain firmly attached to the fibres indicating a strong bond.

4.4. Transmission electron microscopy (TEM)

A crushed aerogel particle was examined using TEM. The image in Fig. 11 shows the mesoporous nature of the internal structure, which is the physical property that is responsible for the low conductive and gaseous heat transfer through the material. Accurate measurement of the pore and pore wall dimensions was beyond the scope of this study.

4.5. Thermal conductivity

Fig. 12 shows the thermal conductivity for each experimental mix. To provide statistically significant results, an average of three separate test runs using a different pair of specimens for each test is reported. The thermal conductivity decreased significantly with increased aerogel content. Thermal conductivity values as a function of aerogel content by volume show an exponential relationship as per Eq. (3) where, λ is thermal conductivity, Ae is aerogel content and k is the rate of change.

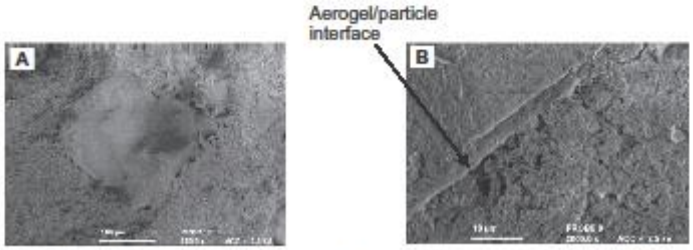

Fig. 7. Aerogel particle in lime binder after 91 days (image A). Aerogel/lime interface (image B).

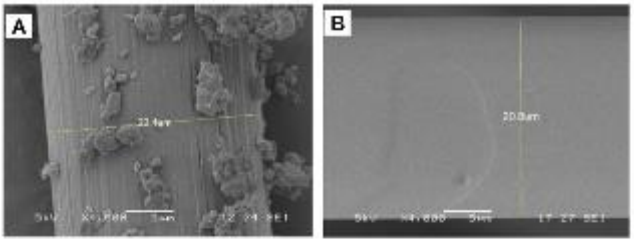

Fig. 8. Fibre extracted from fracture surface of test specimen (image A). Fibre in as-manufactured condition (image B).

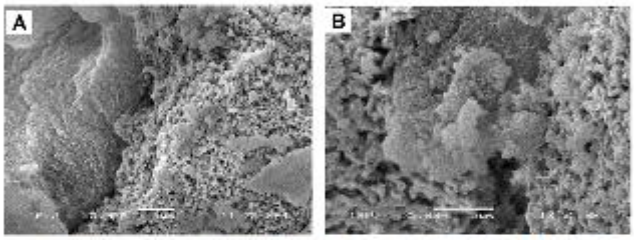

Fig. 9. Calcite crystals adhering to aerogel particles (image A). Aerogel particle entrapped within calcite (image B).

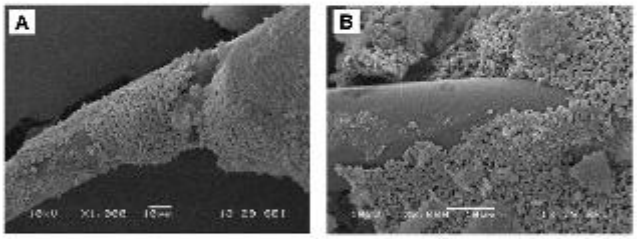

Fig. 10. Calcite crystals adhering to the surface of a polypropylene fibre (image A). Fibre/binder interface (image B).

$$\lambda_{(Ae)} = \lambda_{(0)}e^{kAe} \quad (3)$$

Using a value of 66.6 for Ae gives a value of −0.034 for k. This exponential relationship can be explained by the fact that as the volume fraction of low density aerogel was increased, the volume fraction of high density quartz sand was decreased proportionally. The thermal insulating performance of the plaster mix comprising only aerogel as aggregate (S4) was only marginally inferior to other experimental insulating plasters being developed using aerogel; however, the plaster mixes investigated here utilised a significantly lower proportion of aerogel compared to those materials developed by Stahl et al. [3] and Burrati et al. [4].

4.6. Water vapour permeability

Fig. 13 shows the weight loss data for each specimen measured over a period of ten hours. The data, when plotted, shows a linear relationship between time elapsed and weight of moisture lost by diffusion through the specimen under test. The permeability clearly increased with higher aerogel content and remained constant throughout the test. This tendency was attributed to the hydrophobicity of the aerogel preventing the blockage of the pores with moisture.

The weight loss data from the wet cup test allowed calculation of the water vapour permeance and water vapour permeability values (Fig. 14) for each mix, using formulae (1) and (2) below.

$$W_{vp} = \Lambda t \quad (1)$$

$$\Lambda = \frac{1}{A\Delta_p/(\Delta G\Delta t) - R_A} \quad (2)$$

where: W_{vp} is water vapour permeability (kg m^{-1} s^{-1} Pa^{-1}), Λ is water vapour permeance (kg m^{-2} s^{-1} Pa^{-1}), A is area of open mouth of test cell (m^2), D_p is the difference in water vapour pressure between ambient air and potassium KNO_3 solution (Pa), R_A is water vapour resistance of the air gap between the specimen and KNO_3 solution (0,048 x 10^9 Pa m^{2}s/kg per 10 mm air gap), DG/Dt is the water vapour flux (kg/s), and t is specimen thickness (m).

4.7. FTIR

Fig. 15(A) and (B) show spectra for aerogel obtained from a test specimen and from aerogel as manufactured respectively. The aerogel specimen exhibited a main absorption peak at 1083 cm^{-1}, with a shoulder at around 1200 cm^{-1}, which is characteristic

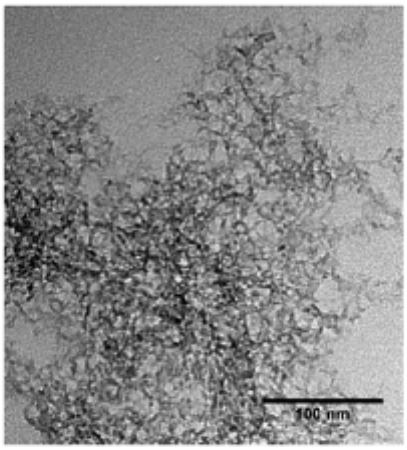

Fig. 11. TEM image of a crushed aerogel particle showing the highly porous nature of its internal structure. (Magnification = 250,000×).

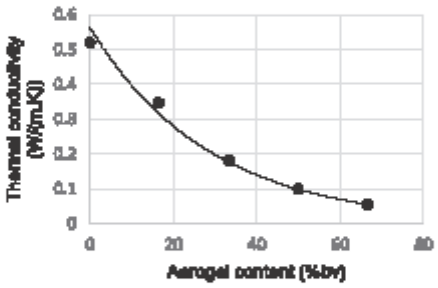

Fig. 12. Effect of aerogel content on thermal conductivity.

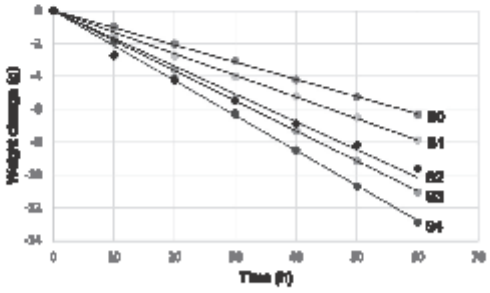

Fig. 13. Graph of weight loss against time during wet cup permeability test.

of silica and can be assigned to asymmetric Si-O-Si stretching vibrations [31]. A second peak at 949 cm^{-1} is assigned to silanol (Si-OH) stretching vibrations, indicating that the aerogel is not 100% hydrophobic. An additional characteristic silica Si-O-Si stretching peak was observed at 800 cm^{-1}. [32]. The peak at 847 cm^{-1} is assigned to Si-CH_3 rocking vibrations in silanes and is consistent with surface methyl groups produced during hydrophobization [33].

Fig. 16(A) and (B) show spectra for a fibre obtained from a test specimen and from a fibre as manufactured respectively. The spectrum obtained from the polypropylene fibre was a match on all the main peaks with the reference polypropylene spectrum [34], but there were no significant additional peaks to provide information on the surface treatment. This suggests that the surfactant used on the fibres was an extremely thin surface layer and below the instrument's detection limit.

For both the aerogel and the polypropylene fibres, the absence of any significant difference between the FTIR spectra before and after they had been in contact with the lime binder is consistent with no chemical reaction having taken place between the binder and the additive materials. This supports the evidence from the SEM images indicating that the strength gain from the incorporation of fibres is the result of a physical rather than chemical bond.

5. Discussion

Whilst the inclusion of aerogel clearly improves the thermal efficiency of the plaster mixes, the only specimen that achieved thermal efficiency comparable to similar aerogel plasters currently reported in the literature was the specimen comprising purely aerogel as the aggregate material (S4). When sand is incorporated into the mix, thermal conductivity rises significantly due to its high density compared to the aerogel. It should be taken into consideration, however, that the proportions of aerogel used in these experimental mixes was lower than those used in the other studies.

As initial attempts at incorporating aerogel into lime binders produced plasters that suffered shrinkage, cracking and very low strength, it is interesting that other similar investigations have not reported data for compressive and flexural strength. The strength values obtained during this investigation, even with fibres added to the binder, were significantly lower than that which would normally be expected for a lime plaster. However, the high degree of plastic deformation without fracturing demonstrated the superior flexibility and toughness of these experimental mixes in comparison to the more commonly used lime/sand mixes without added fibres. These experimental mixes clearly sacrifice strength for flexibility and toughness, but for a plaster, this can be a distinct advantage because the plaster can accommodate building movement, which helps to avoid cracking.

The specimen comprising only aerogel as the aggregate material exhibited permeability significantly superior to conventional gypsum plasters and comparable to a similar developmental aerogel product. This effect can clearly be attributed to the aerogel. The linear relationship between permeability and aerogel content indicates that changes in the sand proportions had a negligible effect on permeability compared to changes in the aerogel content. This is of particular benefit when using non-hydraulic lime, which sets purely through carbonation and depends on the pore structure of the plaster for diffusion of CO_2. This property of aerogel containing plasters is also beneficial to the 'breathability' of a building, as it can assist the release of moisture absorbed by walls that could otherwise freeze and expand, causing damage to masonry.

The permeability of lime-based construction materials is the physical property that is probably most responsible for the long-term durability of these materials. The fact that aerogel has also proven to be a durable material when compared to more conventional insulation materials suggests that these experimental mixes should possess long-term durability. The experimental work carried out did not reveal any reaction between the lime and aerogel that might cause deterioration in the plaster. Furthermore, being hydrophobic and inorganic, there is no chance of moisture causing decay to the aerogel, as is possible with some natural insulating materials.

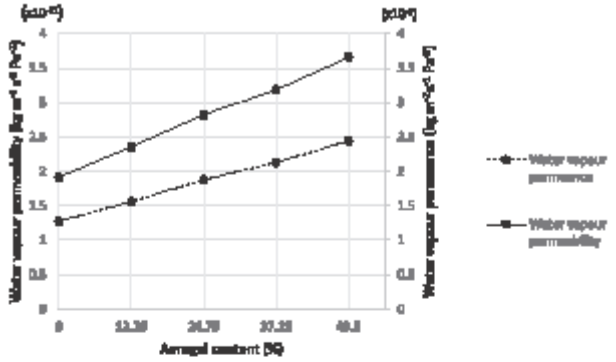

Fig. 14. Aerogel effect on water vapour permeability.

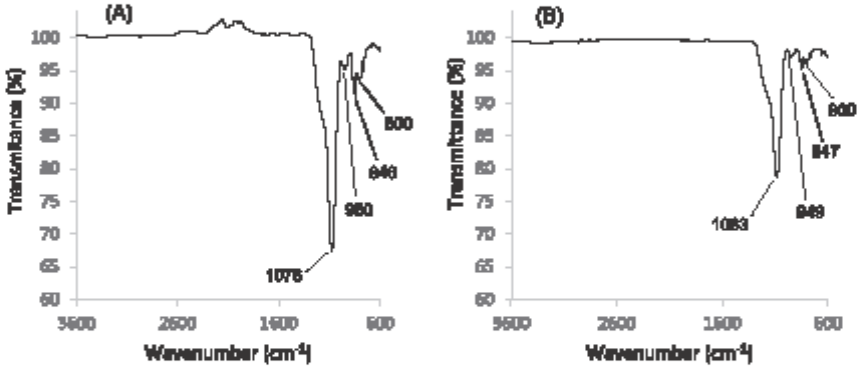

Fig. 15. FTIR spectra of aerogel taken from test specimen (A) and from aerogel as manufactured (B).

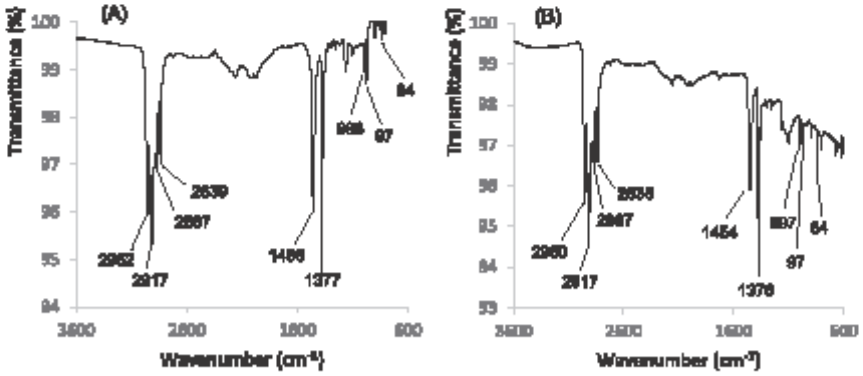

Fig. 16. FTIR spectrum of polypropylene fibre taken from test specimen (A) and from a polypropylene fibre as manufactured (B).

The SEM images obtained from the polypropylene fibres support the assumption that they are responsible for imparting flexibility to the plaster. The surface of the new polypropylene fibre is clearly very smooth; however, the surface condition of fibres extracted from the fracture face of test specimens shows score marks along the length of the fibre, which is consistent with there being a physical bond between the binder and the fibres. The nature of the surface damage to the fibres is consistent with the grad-

ual failure mode observed during strength testing, whereby the physical bond between binder and fibres provides resistance to pull-out and hence improved plastic deformation. It is also evident from the measurements taken from these images that the fibres are not stretching and thinning under tension. The absence of any evidence of chemical bonding between the lime and fibres, and the nature of the linear marking along the axis of fibres extracted from test specimens, is also consistent with resistance to fibre pull-out being responsible for the high levels of flexibility.

The low strength and rough surface texture (Fig. 4b) of these experimental mixes would not make this a practical choice for a surface plaster coat. However, they could be utilised as the first coat in a multi-coat plaster. Traditionally, the first coat is the thickest, which would be the ideal location for incorporation of the aerogel plaster. The subsequent top coats would then provide the required protection and quality of finish.

The number of permutations of different mixes using the materials considered here is vast and beyond the scope of one study. There exists, therefore, significant scope for further work in this area, specifically the investigation of different binder to aggregate ratios, volume fraction and types of fibres and volumetric proportions of aerogel.

6. Conclusions

- The results of this investigation confirm that aerogel granules can be successfully incorporated into non-hydraulic lime putty to produce viable lightweight, thermally insulating plasters.
- The thermal performance and permeability of the plaster containing only aerogel aggregate was superior to conventional plasters on the market and comparable to similar aerogel based insulating plasters being developed that contain higher proportions of aerogel.
- Previous investigations into aerogel based plasters have not considered strength or flexibility, which are important factors for in service use. The viability of the plasters developed in this investigation was strongly dependent on the inclusion of fibres, which improved flexibility and toughness and reduced shrinkage and cracking.
- There is considerable scope for further work by investigating different mix proportions and different specification materials.
- Further work is required to investigate the use of these insulating plasters as part of a multi-coat plaster system in order to optimise layer thicknesses to provide the required combination of cost, thermal efficiency, physical strength and quality of finish.

Acknowledgements

We thank Chris Meyer at Singleton Birch and Joe Orsi of Orsi Contini Consultants for supply of materials and helpful advice.

References

[1] IPCC, O. Edenhofer, R. Pichs-Madruga, Y. Sokona, E. Farahani, S. Kadner, K. Seyboth, A. Adler, I. Baum, S. Brunner, P. Eickemeier, B. Kriemann, J. Savolainen, S. Schlömer, C. von Stechow, T. Zwickel, J.C. Minx, Climate Change 2014: Mitigation of Climate Change. Contribution of Working Group III to the Fifth Assessment Report of the Intergovernmental Panel on Climate Change, Cambridge University Press, Cambridge, United Kingdom and New York NY, USA, 2014, p. 6.
[2] J. Edwards, A. Townsend, Buildings under Refurbishment. Carbon Action 2050 White Paper, Chartered Institute of Building: Englemere, 2011.
[3] S. Stahl, S. Brunner, M. Zimmermann, K. Ghazi Wakili, Thermo-hygric properties of a newly developed aerogel based insulation rendering for both exterior and interior applications, Energy. Build. 44 (2012) (2012) 114–117.
[4] C. Buratti, E. Moretti, E. Belloni, F. Agosti, Development of innovative aerogel based plasters: preliminary thermal and acoustic performance evaluation, Sustainability 6 (2014) 5839–5852.
[5] Fixit, Aerogel Insulating Plaster System [online] Available from: http://www.fixit.ch/aerogel/pdf/Fixit_222_Aerogel_Verarbeitungsrichtlinien_A4_EN.pdf 2016 accessed 7 August 2016.
[6] The Engineer, 2006, Thermal Conductivity, The Engineer, October 2006.
[7] S. Ng, B.P. Jelle, Y. Zhen, O. Wallevik, H., Effect of storage and curing conditions at elevated temperatures on aerogel-incorporated mortar samples based on UHPC recipe, Constr. Build. Mater. 106 (2016) (2016) 645.
[8] M.F. Julio, A. Soares, I.M. Ilharco, I. Flores-Colen, J. Brito, Aerogel-based renders with lightweight aggregates: correlation between molecular/pore structure and performance, Constr. Build. Mater. 124 (2016) (2016) 493.
[9] R. Baetens, B.P. Jelle, A. Gustavsen, Aerogel insulation for building applications: a state of the art review, Energ. Build. 43 (4) (2011) 764.
[10] M. Ayers, Science of aerogels [online], California: E. O. Lawrence Berkely National Laboratory, Available from: http://energy.lbl.gov/ecs/aerogels/sa-chemistry.html (accessed 9th May 2016), 2016.
[11] D. Hasanath, Aerogel the lightest solid known, Resonance (1996) 64.
[12] S.S. Kistler, Coherent expanded aerogels, J. Phy. Chem. 36 (1) (1931) 58.
[13] H. Canaday, Aerogels look promising for lightweight insulation. AviationWeek.com [online], Available from: http://aviationweek.com/advanced-machines-aerospace-manufacturing/aerogels-look-promising-light-weight-insulation [accessed 21 August 2017], 2016.
[14] R.D. Filho, Toledo, M.A. Sanjuan, Effect of low modulus sisal and polypropylene fibre on the free and restrained shrinkage of mortars at an early age, Cem. Concr. Res. 29 (10) (1999) 1587.
[15] R.S. Rajguru, A.R. Ghode, M.G. Pathan, M.K. Rathi, Effect of volume fraction of polypropylene fiber on the mechanical properties of concrete, Int. J. Eng. Res. Appl. 4 (6) (2014) 67–69.
[16] X. Yang, Y. Sun, D. Shi, J. Liu, Experimental investigation on mechanical properties of a fiber-reinforced silica aerogel composite, Mater. Sci. Eng. A 528 (2011) 4830–4836.
[17] J. Ingham, Laboratory investigation of lime mortars, plasters and renders, in: I. Brocklebank (Ed.), Building Limes in Conservation, Donhead Publishing, Shaftsbury, 2012, p. 155.
[18] Greenspec, 2017, Lime mortar, render and plaster [online], Available from: http://www.greenspec.co.uk/building-design/lime-mortar-render/ (accessed 18th January 2017).
[19] M.G. Margalha, A.S. Silva, M. Do Rosário Veiga, J. De Brito, R.J. Ball, G.C. Allen, Microstructural changes of lime putty during aging, J. Mater. Civ. Eng. 25 (10) (2013) 1524–1532.
[20] J. Straube, Moisture properties of plaster and stucco for strawbale buildings, Res. Highlight Tech. Series (2000) 3.
[21] A. El-Turki, R.J. Ball, S. Holmes, W.J. Allen, G.C. Allen, Environmental cycling and laboratory testing to evaluate the significance of moisture control for lime mortars, Constr. Build. Mater. 24 (8) (2010) 1392–1397.
[22] M. Ibrahim, E. Wurtz, P.H. Biwole, P. Achard, H. Sallee, Hygrothermal performance of exterior walls covered with aerogel-based insulating rendering, Energy Build. 84 (2014) (2014) 343.
[23] Q. Wang, H. Liu, The Experimental Research on the Water Vapour Permeability of Construction Gypsum Plaster Materials, International Conference on Materials for Renewable Energy & Environment, May 2011, vol. 1, pp. 854.
[24] M. Ibrahim, P.H. Biwole, P. Achard, E. Wurtz, Aerogel-based materials for improving the building envelope's thermal behaviour: a brief review with a focus on a new aerogel-based rendering, in: Energy Sustainability Through Green Energy, Springer, New Delhi Heidelberg New York Dordrecht London, 2015, p. 186.
[25] C.R. Iddon, S.K. Firth, Embodied and operational energy for new-build housing: a case study of construction methods in the UK, Energy Build. 67 (2013) (2013) 479.
[26] Adfil, Monofilament fibres [online] Available from: http://adfil.co.uk/products/micro-synthetic-fibres/monofilament-fibres/ 2016 accessed 12th May 2016.
[27] EN 1015-11:1999, Methods of test for mortar for masonry – Part 11: Determination of flexural and compressive strength of hardened mortar, BSI.
[28] P. Livesey, The use of lime mortars and renders in extreme weather conditions, J. Build. Limes Forum 17 (2010) (2010) 46–49.
[29] R. Singh, Simultaneous measurement of thermal conductivity and thermal diffusivity of some building materials using the transient hot strip method, J. Phys. D Appl. Phys. 18 (1984) 1.
[30] T. Gao, B.P. Jelle, A. Gustavsen, S. Jacobsen, Aerogel-incorporated concrete: An experimental study, Constr. Build. Mater. 52 (2014) (2014) 132.
[31] P. Innocenzi, Infrared spectroscopy of sol-gel derived silica-based films: a spectra-microstructure overview, J. Non-Cryst. Solids 316 (309–319) (2003) 311–313.
[32] G.E.A. Swann, S.V. Patwardhan, Application of Fourier Transform Infrared Spectroscopy (FTIR) for assessing biogenic silica sample purity in geochemical analyses and palaeoenvironmental research, Clim. Past 7 (65–74) (2011) 67.
[33] J.B. Lambert, Introduction to Organic Spectroscopy, Macmillan, USA, 1987, p. 176.
[34] NICODOM, 2012, FTIR Spectra of Polymers [online], Nicodom s.r.o.: Czech Republic. Available from: http://www.ftir-polymers.com/soon.htm [accessed: 15th May 2016

APPENDIX 2 – OLIVINE AS A REACTIVE AGGREGATE IN LIME MORTARS

Construction and Building Materials 195 (2019) 115–126

Contents lists available at ScienceDirect

Construction and Building Materials

journal homepage: www.elsevier.com/locate/conbuildmat

Olivine as a reactive aggregate in lime mortars

Paul Westgate *, Richard J. Ball, Kevin Paine

BRE Centre for Innovative Structural Materials, Department of Architecture and Civil Engineering, University of Bath, Bath BA2 7AY, UK

HIGHLIGHTS

- There is much interest in CO_2 sequestration using carbonate minerals.
- Calcium and magnesium carbonation is an effective method for permanent CO_2 storage.
- Olivine is highly suited to CO_2 sequestration due to its relatively high solubility.
- Olivine is widely available, being one of the most abundant minerals in the earth.
- Olivine mined for CO_2 sequestration could be used as an aggregate material.
- Olivine aggregate is effective in increasing strength in non-hydraulic lime mortars.
- Mortars containing olivine increase CO_2 absorption compared to traditional mortars.

ARTICLE INFO

Article history:
Received 28 May 2018
Received in revised form 24 October 2018
Accepted 7 November 2018

Keywords:
Olivine
Forsterite
Aggregate
Mortar
Carbon dioxide
Carbonate
CO_2 emissions

ABSTRACT

This paper presents the first investigation into the use of olivine as an aggregate material for calcium lime mortars. Lime binders provide many advantages when compared to cement binders such as higher vapour permeability and the ability to accommodate movement. They are undergoing a resurgence in their use in the conservation of historic buildings and in combination with environmentally friendly natural materials where these attributes are particularly important. Their ability to mitigate against global warming through the sequestration of CO_2 by carbonation is a further advantage which will bring impact.

The equilibrium reaction products between non-hydraulic lime and olivine were calculated using the thermodynamic software GEMS3 Selektor. Experimental mortar mixes were modelled with varying ratios of quartz sand aggregate and olivine sand aggregate. The software predicted phase assemblage at equilibrium comprising calcite, dolomite, magnesite and quartz, with mass percentages depending on the ratio of quartz to olivine.

The mortars morphological, chemical and mechanical properties were evaluated using Scanning electron microscopy, X-ray diffraction (XRD), Raman spectroscopy, thermogravimetric analysis (TGA) and compressive strength testing. Significantly, this study has shown that the use of olivine based aggregates in finely divided form can enhance carbonation, and hence the CO_2 absorption capacity of these mortars. Dolomite formed within the mortar from the reaction of olivine aggregate with lime and carbon dioxide in the presence of moisture is attributed to the superior mechanical properties observed increasing from 0.5 to 2.5 MPa.

1. Introduction

The continued high level of greenhouse gas emissions and its effect on the environment continues to be a major cause for concern. The International Panel on Climate Change (IPCC) has warned that continued emission of greenhouse gases will cause long-lasting changes to the climate system, increasing the likelihood of severe, pervasive and irreversible impacts for people and ecosystems [1]. One of the strategies being investigated to mitigate the effects of greenhouse gas emissions is the capture and storage of carbon dioxide, whereby carbon dioxide is captured from the atmosphere and stored in underground sites such as former gas and oil fields and in porous rock formations [2]. More recently, there has been much interest in capturing carbon dioxide by utilizing calcium and magnesium containing minerals to form carbonates [3]. This method of sequestration is very efficient because, unlike some other methods, it is safe and permanent; the bound CO_2 is chemically incorporated into the carbonate [4]. Furthermore, mineral deposits are larger than fossil resources, which

* Corresponding author.
E-mail address: pw4154@bath.ac.uk (P. Westgate).

https://doi.org/10.1016/j.conbuildmat.2018.11.062
0950-0618/

essentially provides an unlimited supply of the necessary cations (mainly magnesium and calcium) for the process. [5]. There has been much interest in recent years in the use of the mineral olivine for sequestration purposes [6,7]. This mineral is a good candidate for CO_2 sequestration due to its abundance in the earth's mantle, its lack of aluminium (which tends to produce clays, reducing the number of cations available for carbonation) and because it is a nesosilicate, the silicate group with the lowest ratio of silicon to cations [6].

Olivine is a naturally occurring silicate mineral having the composition $(Mg, Fe)_2SiO_4$. The name Olivine refers to a range of iron/-magnesium silicate minerals, with the composition varying from pure forsterite (Mg_2SiO_4) to pure fayalite (Fe_2SiO_4). Most Olivine falls somewhere between these two extremes, and the Mg and Fe content may occur in any ratio. The process by which olivine sequesters CO_2 is complex; however, it can be simplified as described by the three general reactions as shown in chemical Eqs. (1)–(3):

$$CO_2 + H_2O \leftrightarrow H_2CO_3 \leftrightarrow HCO_3^- + H^+ \leftrightarrow CO_3^{2-} + 2H^+ \quad (1)$$

$$Mg_2SiO_4 + 4H^+ \rightarrow 2Mg^{2+} + H_4SiO_4 \quad (2)$$

$$Mg^{2+} + CO_3^{2-} \leftrightarrow MgCO_3 \quad (3)$$

The first step involves the dissolution of atmospheric carbon dioxide in water, forming carbonic acid, which in turn dissociates and lowers the pH of the system (Eq. (1)). The next reaction (Eq. (2)) shows the dissolution of the magnesium-rich olivine by acid consumption. The third reaction is the precipitation of magnesium carbonate (Eq. (3)) [7]. Once this process is complete, CO_2 can be stored indefinitely within the magnesite rock. As magnesite is stable it is unlikely to release the bound CO_2 unless subjected to further heating. This process is exothermic and thermodynamically favourable and occurs naturally over geological timescales; however, to be of benefit in the current efforts to reduce the amount of CO_2 in the atmosphere, the process must be accelerated. This may be achieved by raising the reaction temperature, increasing pressure, using a catalyst or decreasing the particle size [8].

Decreasing the particle size of olivine is accomplished through 'mechanical activation' by high energy milling. This process modifies the properties of the olivine beyond merely reducing the particle size and increasing the surface area. It is noteworthy that, during and after activation, the crystal lattice is in a no equilibrium state and the excess energy attributed to disordering contributes to lowering the activation energy of any further reaction of the material [9].

Olivine that is being mined purely for CO_2 sequestration could potentially be made use of in the construction industry as a building material. A number of studies have previously been undertaken to assess the suitability of olivine as a method of solid stabilisation which exploit its ability to sequester CO_2 [10–13].

Here an investigation into the potential for olivine as either an aggregate or, in finely ground form, as a pozzolan in lime-based mortars is presented. An important advantage of olivine additions is increasing the amount of carbonation, and hence CO_2 absorption capacity of the mortar. The widespread use of olivine as an aggregate material has the potential not only to increase the quantity of CO_2 sequestered by lime-based construction materials but also to enhance physical properties. The choice of lime binder for this work is of particular interest because lime mortars have undergone a revival in recent years for conservation work and are now being actively promoted and used in new-build applications [14,15].

There are two potential reaction mechanisms to be investigated: firstly, the dissociation of olivine incorporated into a lime mortar could release Mg^{2+} cations to facilitate the formation of magnesium carbonates. This could potentially result in an increase in the amount of CO_2 absorbed during the hardening phase compared to quartz aggregate and possibly increased strength, as dolomitic limes have been shown to have higher mechanical strength compared to comparable calcitic mortars [16,17] secondly, if a pozzolanic reaction occurs, this could help reduce the quantity of lime binder used in a mortar mix.

The choice of binder is an important consideration for the optimal absorption of CO_2. Non-hydraulic lime is the most appropriate material for this type of investigation, as it not only has lower CO_2 emissions during production compared to hydraulic limes due to lower lower temperatures used during production, but it sets purely by carbonation, resulting in a higher quantity of CO_2 being absorbed during the setting phase. Hydraulic lime, by contrast, contains impurities and sets through a combination of carbonation and hydration reactions [18]. The process by which non-hydraulic lime carbonates is described in Eqs. (4) and (5).

Atmospheric carbon dioxide dissolving in water to form carbonic acid

$$CO_2 + H_2O \leftrightarrow H_2CO_3 \quad (4)$$

Calcium hydroxide reacts with carbonic acid to form calcium carbonate

$$Ca(OH)_2 + H_2CO_3 \rightarrow CaCO_3 + 2H_2O \quad (5)$$

Non-hydraulic lime is available as a lime hydrate or a lime putty. Lime hydrate is a powder, to which sand and water are added to produce the mortar. Lime putty is, as the name suggested, in the form of a soft putty, which is comprised of approximately 50% water and 50% lime by weight. Lime putty is mixed with sand to produce a mortar, but does not require the addition of more water.

2. Materials

2.1. Lime putty

The binder material used for this work was a calcium hydroxide ($Ca(OH)_2$) lime putty supplied by J J Sharpe which had matured for at least twelve months. Weight measurements of a representative sample of the lime putty were taken before and after water removal by drying in a furnace at 100 °C for twenty four hours to determine the solids content. This equated to a solids content of 51%, assumed to be calcium hydroxide. This allowed accurate batching of the mix constituents.

2.2. Olivine

The olivine used was supplied by Industrial Minerals & Refractories Olivine India based in Tamil Nadu, India. The olivine sand received had been derived from Dunite ore and had been processed using a Raymond three roller mill to grind raw olivine rocks into a sand at an output of approximately 1.25 tonnes per hour. Two different batches of the mineral were received: a fine sand and a coarse sand (Fig. 1). The coarse olivine sand was sieved to obtain particles with maximum size of 2 mm to match as closely as possible the standard sand. Chemical composition analysis data from the Material Safety Data Sheets as supplied with the olivine are shown in Table 1. The chemical composition confirms the mineral to be high magnesium, forsteritic olivine.

The particle size distribution of the fine olivine sand was determined using a Malvern Mastersizer particle size analyser (Fig. 2). With the 300 mm lens fitted to the Mastersizer, the maximum particle size measurable was 600 μm. The data shows that the quan-

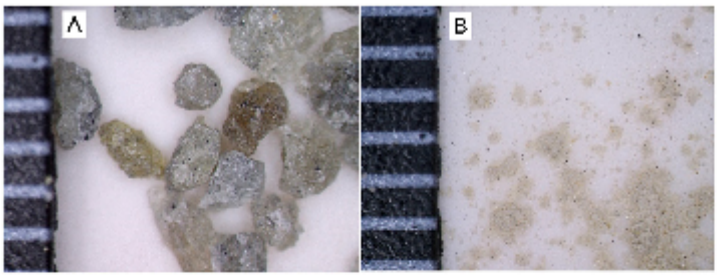

Fig. 1. Coarse olivine sand (A) and fine olivine sand (B) shown against a 1 mm scale.

Table 1
Chemical composition of olivine.

Material	MgO	SiO_2	Fe_2O_3	CaO	Al_2O_3
Coarse olivine sand	49%	21%	8%	1%	–
Fine olivine sand	48.7%	40.2%	8.5%	–	1.2%

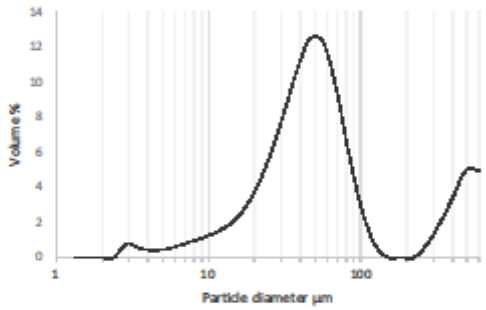

Fig. 2. Particle size distribution of the fine olivine sand obtained using the Malvern Mastersizer.

tity of particles increases with particle size, up to the limit of 600 µm.

The data sheet supplied with the olivine stated that the particles were of size mesh 200#–300#, which equates to approximately 50–74 µm. The majority of the particles do fall within this range; however, the peak at approximately 500 indicates some particle agglomeration.

2.3. Standard sand

The sand used in this investigation was a standard dry siliceous natural sand conforming to BS EN 196-1 and ISO 679: 2009. This grade of sand comprises particles that are generally isometric and rounded in shape with the particle size distribution shown in Fig. 3. This type of sand was specified for this investigation to facilitate consistency and repeatability of experimental conditions.

3. Methods

3.1. Sample preparation

Four different experimental mixes (Table 2) were prepared:

1. S0 – Lime putty binder and standard sand aggregate (2:1)
2. S1 – Lime putty binder and fine olivine sand aggregate (2:1)
3. S2 – Lime putty binder and fine olivine sand aggregate (3:1)
4. S3 – Lime putty binder aggregate and coarse olivine sand (2:1)

The lime and aggregate were prepared using a paddle mixer for a minimum of twenty minutes to ensure the mortar was suitably workable. The experimental mixes were then added to 18 × 38 mm cylindrical moulds in small quantities and tamped down as the material was added, to reduce the occurrence of trapped air bubbles within the specimens. After moulding, the specimens were stored in a climate chamber regulated at a constant temperature of 20 °C ± 2 °C and relative humidity of 65% ± 5% as specified in standard EN 1015-11:1999. The specimens were covered with a thin plastic wrap for the first week to maintain a high level of humidity, as exposure to ambient atmospheric conditions during this period can result in significant reduction in strength due to premature drying and subsequent cracking. The specimens were then left in the moulds for a further week to allow them to achieve sufficient rigidity to facilitate demoulding.

3.2. Thermodynamic modelling

The thermodynamic modelling software GEM-Selektor v.3 (GEMS3) was used to predict the phase assemblages resulting from lime/olivine mixes. The objective was to predict whether using olivine as an aggregate could theoretically consume more carbon dioxide, through the formation of carbonate phases when compared to a conventional mix of lime and standard sand. Also, the modelling was applied to predict whether the formation of hydration products such as C-S-H was thermodynamically favourable.

For the purposes of this modelling exercise it was necessary to make certain assumptions:

- The (open) thermodynamic system was considerd to comprise of mortar only.
- The small iron content of the olivine, approximately six percent, was not taken into account; the olivine was assumed to be pure fosterite.

The model assumes that the olivine sand completely dissociates and and equilibrium conditions are achieved.

The GEMS3 geochemical modelling programme uses an advanced convex programming method of Gibbs energy minimisation implemented as an efficient Interior Points Method. The software can be used to model a single reaction, or as a series of reactions in the form of a phase assemblage diagram [19–21].

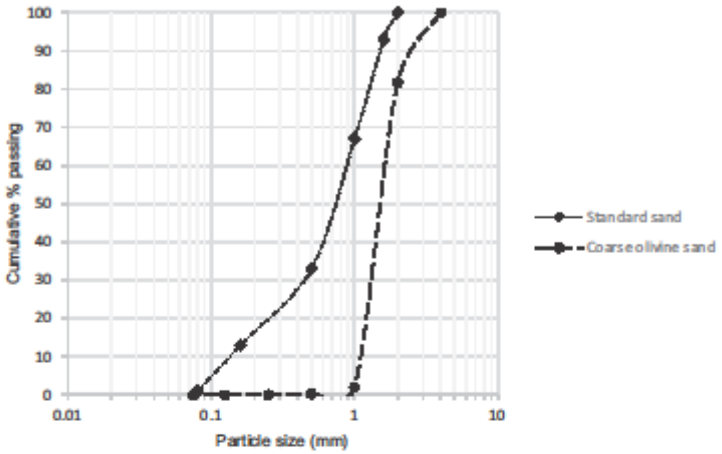

Fig. 3. Particle size distribution for stndard sand and large particle olivine obtained by sieve analysis.

Table 2
Composition of experimental mixes by volume.

Specimen	Nominal aggregate : binder ratio	Lime putty (cm^3)	Standard sand (cm^3)	Fine olivine sand (cm^3)	Coarse olivine sand (cm^3)	Bulk density Kg/m^3
S0	2:1	1000	1000	–	–	1504
S1	2:1	1000	–	1000	–	1309
S2	3:1	1000	–	2000	–	1325
S3	2:1	1000	–	–	1000	1515

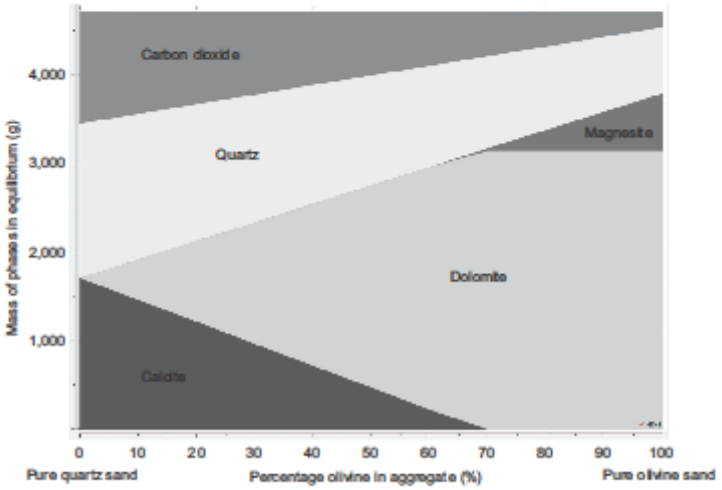

Fig. 4. Phase assemblage diagram calculated by the GEMS3 Selektor thermodynamic modelling software for the olivine – lime system.

3.3. X-ray diffraction

Powder X-ray diffraction was carried out using a BrukeraxsD8 Advance X-ray diffractometer equipped with a super speed PSD Vantec-1 detector and Cu K_α X-ray source of wavelength 1.5418 Å. Data was collected over the 2θ range from 5° to 60° at a step size of 0.016° and time per step of 424.8 s.

3.4. Raman spectroscopy

Raman Spectroscopy was carried out on specimen S2 at 28 days. A Renishaw InVia Raman Spectrometer was used employing a laser of wavelength 532 nm. Streamline image acquisition allowed a 1 × 6 mm scan of the surface to be obtained. 100% laser power of 80 mW was used for 10 s exposures with a slit of 65 μm and a 5x objective. The wavelength centre was 1000 giving a data range of 61 to 1835 cm^{-1}. The Raman data obtained from the scan were analysed using Renishaw WiRE 4.4 (Windows Raman Environment) software

3.5. Scanning electron microscopy (SEM)

Scanning electron microscopy was used to examine the physical condition of the specimens. Of particular interest was the occurrence of unreacted olivine particles and bonding between any olivine particles and carbonate phases. Specimens were analysed using a JEOL 6480 LV scanning electron microscope equipped with an Oxford Instruments INCA X-act X-ray detector (silicon drift detector offering a high count rate and reduced operation time).

3.6. Field emission scanning electron microscopy (FESEM)

Field emission scanning electron microscopy was used to examine the morphology of the binder and aggregate at high magnification. Specimens were coated with a 20 nm layer of chromium using a Quorum Q150TS machine. A JEOL JSM-6301F microscope was used with an accelerating voltage of 5 kV to obtain images with magnification ranging from 10,000x to 20,000x.

3.7. Thermogravimetric analysis (TGA)

TGA analysis was carried out on a sample of each of the two experimental lime/olivine mixes using a Setaram TG-92 with an open alumina crucible and nitrogen as the purge gas. The test was run over a temperature range of 0–1000 °C, in 20 °C steps and 2 min per step.

3.8. Mechanical strength testing

Mechanical strength testing was performed using a 50 kN Instron 3369 Universal motorised load frame based on BS EN 1015-11:1999 to test compressive strength. Bluehill 3 software monitored and recorded the load on the specimen as a function of extension throughout the test.

4. Results

4.1. Thermodynamic modelling

Fig. 4 shows the phase assemblage calculated by the thermodynamic modelling program. The program was used to model the mortar mix S1 as used in the physical tests. The x axis shows the composition of the aggregate, which was maintained at a constant mass of 1744 g, but varied from pure quartz sand to pure olivine sand.

The results shown are for the reactions at equilibrium when the forsterite will have completely dissociated into magnesium and silica ions; therefore forsterite does not appear in the diagram. The results show that as the proportion of olivine in the aggregate increases, the amount of dolomite increases, indicating that increasing amounts of magnesium ions become available from the dissociated olivine to undergo carbonation.

4.2. X-ray diffraction

XRD was carried out on the raw olivine as received and on the mortar mixes comprising olivine and lime binder in order to confirm the reactions taken place between the olivine aggregate and lime binder.

Fig. 5 shows the XRD spectra obtained for the fine olivine sand (A) and the coarse olivine sand (B). They both show high intensity peaks at 2θ values of approximately 23.0, 35.9 and 36.6°, confirming these to be high magnesium (fosteritic) olivine. The absence of a peak at 31.6 indicates the lack of any significant quantity of iron silicate.

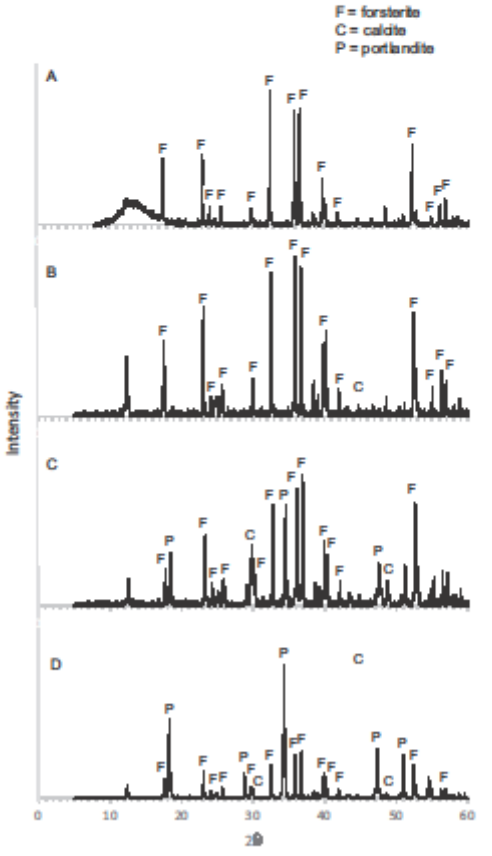

Fig. 5. X-ray diffraction (XRD) patterns for fine olivine sand (A), coarse olivine sand (B), mortar mix S2 (C) and mortar mix S3 (D).

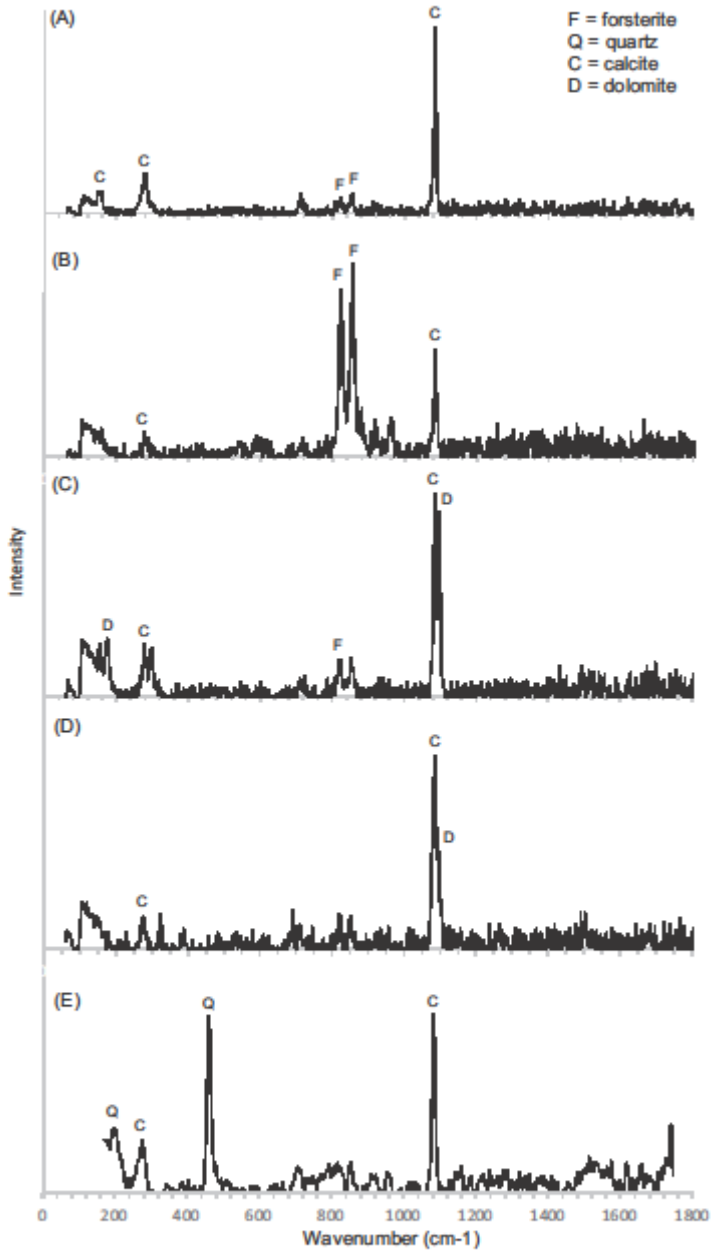

Fig. 6. Raman spectra obtained from surface scan of mortar specimen S2 confirming presence of calcite (A), forsterite (B), dolomite (C) magnesite (D) and Quartz (E).

The XRD patterns for the lime/olivine mortar mixes (S2 and S3) show peaks corresponding to the presence of forsterite, calcite and portlandite. The presence of portlandite indicated that the specimen had not completely carbonated, which also accounts for the low intensity peaks for calcite. Dolomite and magnesite could not be positively identified from the data due to having high intensity peaks at approximately 32.5° and 31° respectively, which overlap with strong forsterite peaks.

4.3. Raman spectroscopy

The S2 specimen was analysed to determine what reactions had taken place between the olivine and the lime and how closely they were in agreement with the results obtained using the thermodynamic software. The 1 × 6 mm Raman scan produced 35,478 spectra. These spectra were interrogated using the Renishaw Wire 4.4 program to search for instances of the phases predicted by the thermodynamic software: calcite ($CaCO_3$), dolomite ($CaMg(CO_3)_2$), magnesite ($MgCO_3$), and quartz (SiO_2). The data were also searched for instances of forsterite (Mg_2SiO_4), which would indicate incomplete dissolution of the olivine. The analysis did identify spectra for calcite, dolomite, magnesite, forsterite and quartz (Fig. 6). The data were also interrogated to try and identify the presence of any calcium silicate hydrates (C-S-H). Analysis failed to identify the presence of Tobermorite or Jennite phases, in agreement with the results obtained from the thermodynamic software.

The spectrum in Fig. 6(A) shows a spectrum that strongly correlates to calcite, with a strong peak at 1085 cm^{-1}, which is attributed to v_1 symmetric stretching of the CO_3 group and medium intensity peaks at 280, 157 cm^{-1}, which are assigned to v_2 lattice vibrations. Two low intensity peaks at 824 and 854 cm^{-1} indicate a small quantity of olivine in the specimen. Fig. 6(B) shows a spectrum from an area of the specimen comprising mainly unreacted olivine. The two high intensity peaks at 822 and 856 cm^{-1} are characteristic of forsteritic olivine and are assigned to the SiO_4 internal stretching vibrational modes. The lower intensity peaks at 1085 and 280 cm^{-1} indicate the presence of some calcite in this area. Fig. 6(C) shows the presence of dolomite and calcite together. The peaks at 1085 and 280 identify the calcite. The high intensity peak at 1098 cm^{-1} is a characteristic symmetrical stretching mode for dolomite, and the lower intensity peaks at 300 and 175 cm^{-1} are assigned to the dolomite lattice vibration mode. The spectrum shown in Fig. 6(D) is believed to show the presence of magnesite. The high intensity peak at 1095 cm^{-1} is characteristic of the symmetric stretching mode of the carbonate group in magnesite. The lower intensity peak at 325 cm^{-1} is assumed to be the lattice vibration mode peak for magnesite, which is somewhat shifted from its expected position of approximately 330 cm^{-1}. There were not found to be any alternative phases to which this peak could be assigned, given the chemical composition of the specimen under test. The peaks at 202 and 459 cm^{-1} in Fig. 6(E) indicate the presence of quartz. This is consistent with the thermodynamic software prediction that quartz should be produced from the dissociation of olivine.

The distribution of each of these minerals within the binder is shown in Fig. 7. The lighter areas of the image represent the highest concentration of the mineral being detected.

4.4. Scanning electron microscopy and field emission scanning electron microscopy

Lower magnification images (up to 5000X) were obtained using SEM, and FESEM was used to obtain higher resolution images. The images in Fig. 8 show the three different types of aggregate used.

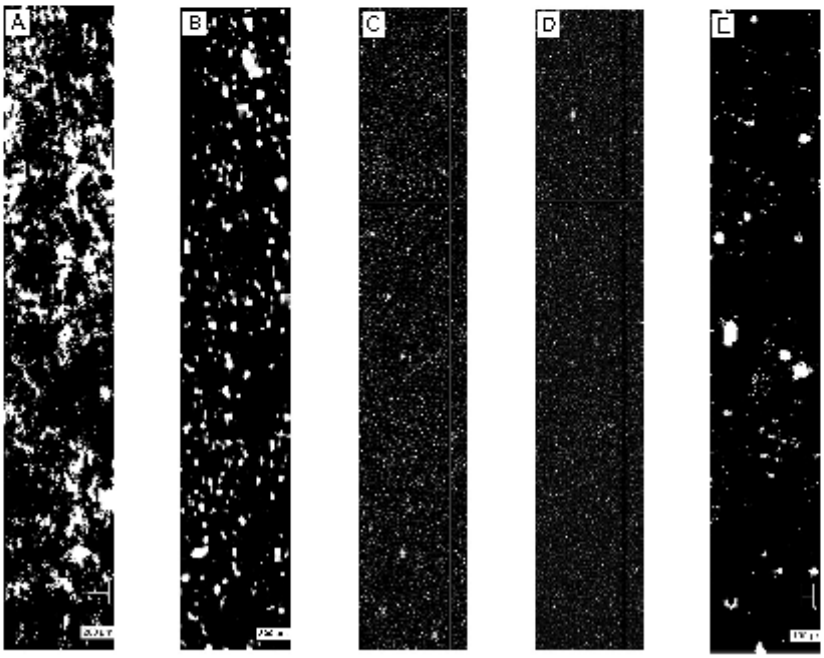

Fig. 7. 1 × 6 mm Raman scan of S2 specimen surface showing the phase distribution of calcite (A), forsterite (B), dolomite (C), magnesite (D) and quartz (E).

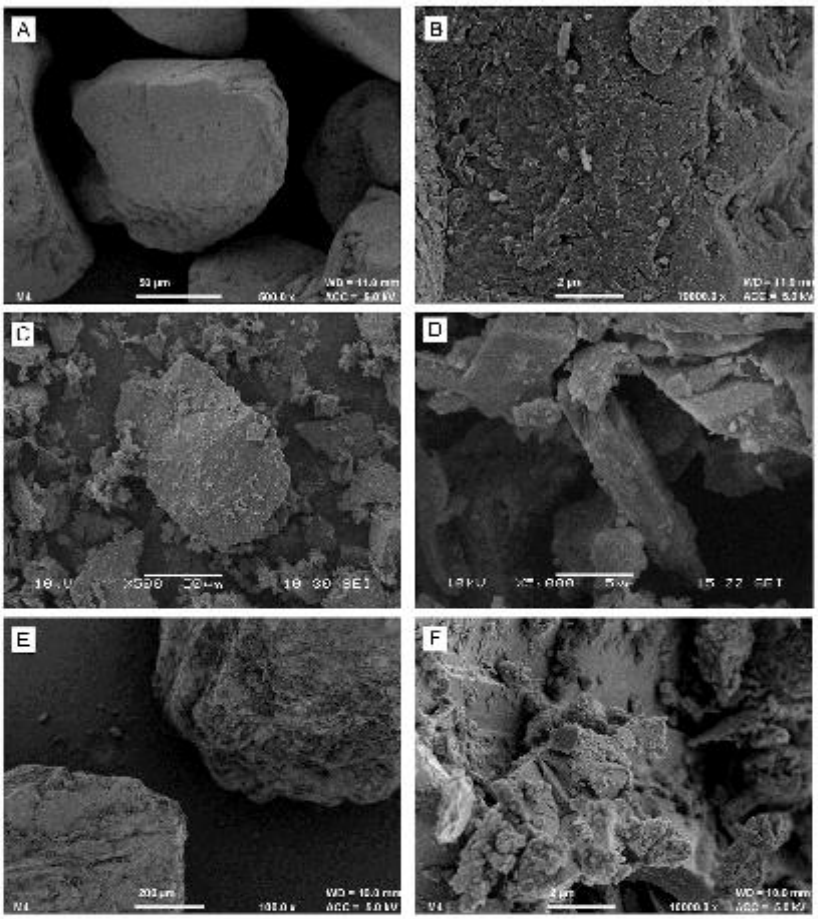

Fig. 8. Morphology of aggregate particles – standard sand (A) (B), fine olivine sand (C) (D) and coarse olivine sand (E) (F).

Images (A) and (B) are of standard sand and show the typical rounded shape of the particles. The fine olivine sand seen in images (C) and (D) shows a much more angular shape and rough surface condition, which is typical of the conchoidal fracture associated with olivine. Images (E) and (F) show the coarse olivine sand particles, which are also rounded in shape but show the typical conchoidal fracture faces.

The images in Fig. 9 show the widespread occurence of well-formed scalenohedral calcite crystals throughout the mortars containg the fine olivine sand aggregate (C)–(F). Images of the two mortars containing standard sand and large particle sand aggregates (A) (B) (G) (H) show more granular or massive calcite formations. In the images showing both fine and coarse olivine sand (E)–(H), unreacted olivine particles can be seen.

4.5. Thermogravimetric analysis

TGA analysis was carried out on all four mixes. Two distinct instances of mass loss (Fig. 10) were observed in each case. The smaller mass loss curve occurred between approximately 420 and 460 °C, and this was attributed to dehydration of portlandite. The largest mass loss occurred between approximately 700 and 800 °C, which is a result of the decomposition of carbonate material [22,23].

The equipment was not sufficiently accurate enough to distinguish between the different carbonate phases; however, it can be seen that the mortars containing olivine sand aggregate were shown to contain the highest proportion of carbonate material. In specimen S0 the percentage carbonate of the material that decomposed was 69.1%. In specimens S1, S2 and S3 it was 79.5%, 83.1% and 86% respectively.

4.6. Mechanical strength testing

Fig. 11 shows the compressive strength at twenty eight days for each of the four mortar mixes. The reference mortar comprising lime and sand (S0) achieved a level of strength that would be considered typical for a non-hydraulic mortar at twenty-eight days [24]. However, the specimens incorporating fine olivine sand as aggregate (S1 and S2) obtained compressive strength values that

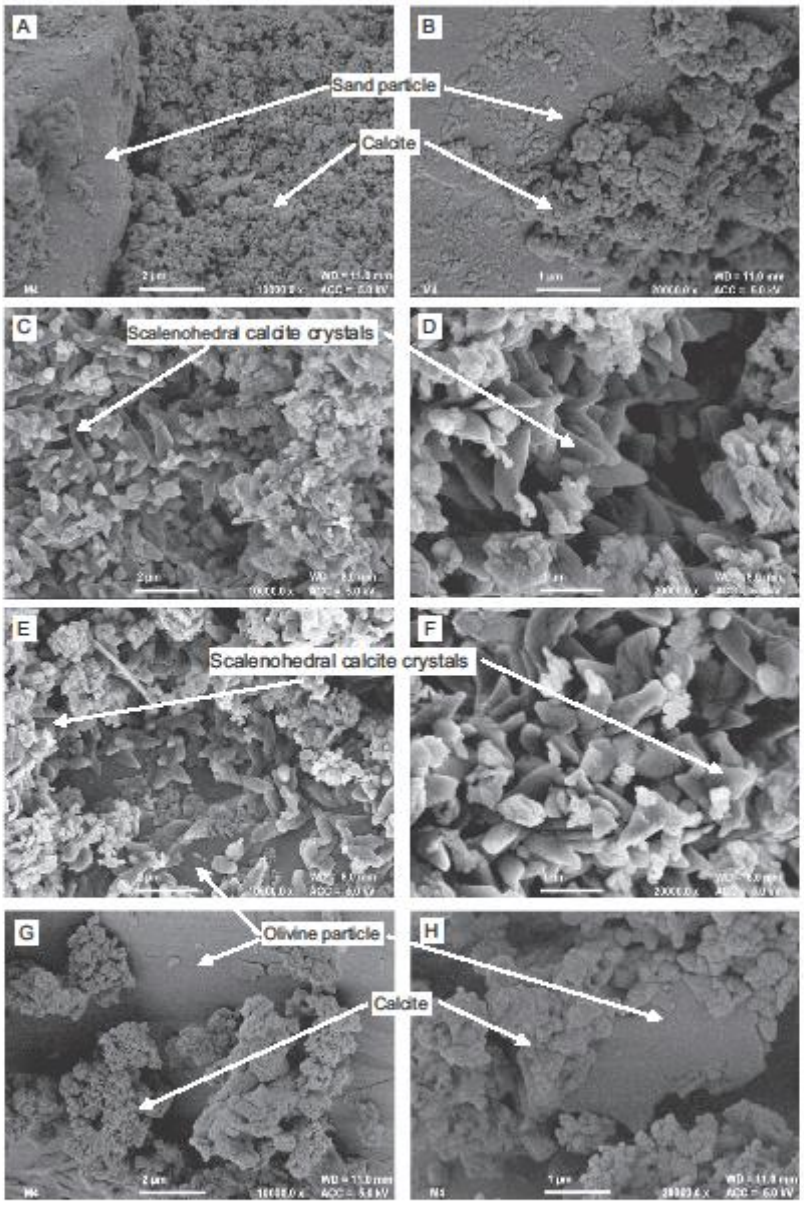

Fig. 9. Images of experimental mortar mixes S0 (A) (B), S1 (C) (D), S2 (E) (F) and S3 (G) (H).

were 278% and 370% higher than with conventional sand. Significantly, the specimen with the highest olivine content (S2) obtained the greatest strength. The specimen comprising lime and coarse olivine sand was the weakest of the mixes.

5. Discussion

The research described here has shown conclusively that olivine aggregate, in finely divided form, will react in the presence of lime

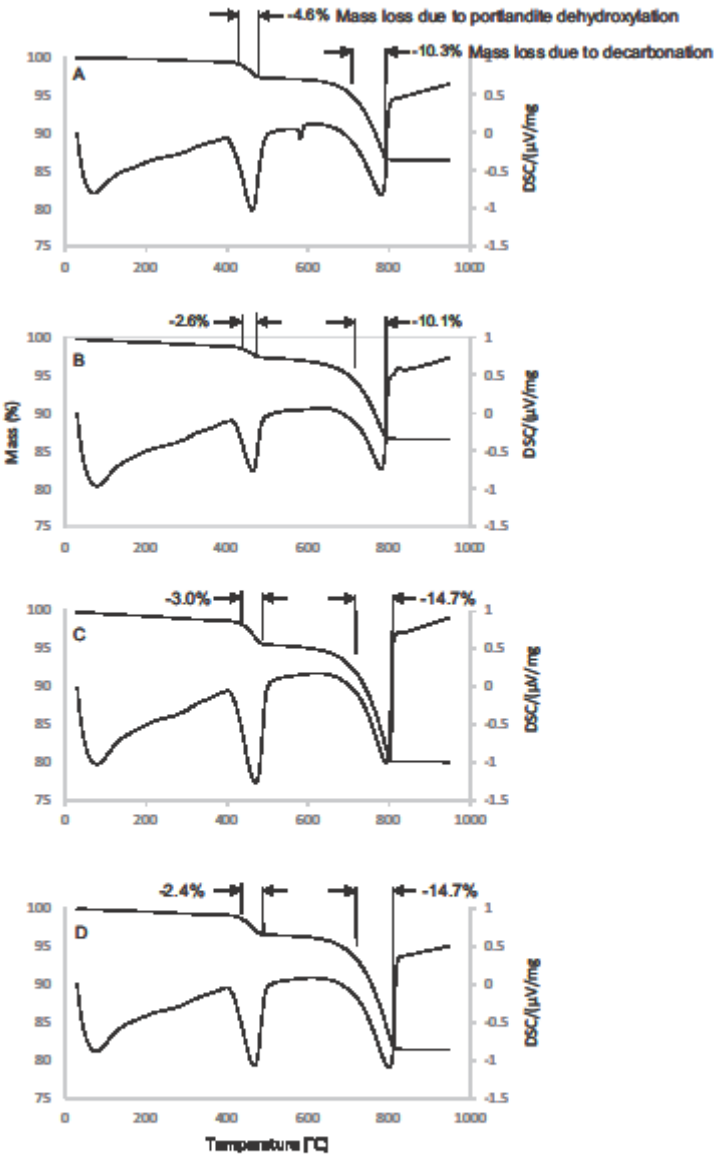

Fig. 10. TGA curves for each mortar mix: S0 (A), S1 (B), S2 (C) and S3 (D).

and water to produce magnesium carbonates, which not only increase the amount of CO_2 absorbed by the mortar during setting, but also provide a strength enhancing ability.

The thermodynamic model shows that, at equilibrium, when olivine is the sole aggregate, there should theoretically still be a significant amount of quartz within the system. This can be attributed to new quartz forming from the silica anions released by the dissolution of the olivine. In the experimental mixes, there is significantly less quartz present due to the fact that the system has not reached equilibrium and the olivine has not completely dissociated.

The diagram also shows that as the proportion of olivine aggregate is increased, the total mass of the carbonate phases (calcite, dolomite and magnesite) at equilibrium increases as the olivine

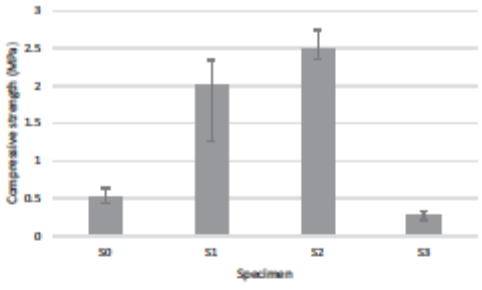

Fig. 11. 28 day compressive strength test results for the four experimental mixes; S0 = lime and standard sand, S1 = lime and fine olivine sand 2:1, S2 = lime and fine olivine sand 3:1, S3 = lime and coarse olivine sand.

dissociates to leave magnesium cations free to form increasing amounts of magnesium carbonates (dolomite and magnesite), and this in turn results in a corresponding increase in CO_2 consumption, as seen by the decreasing amount of CO_2 within the system as the proportion of olivine is increased. Magnesite is only shown to be formed when the aggregate comprises 75% or higher of olivine. The increase in carbonate products when olivine is present can be accounted for by the fact that olivine is a neosilicate and the most reactive mineral on the Goldich dissolution series, whereas quartz is the least reactive and can be considered inert [25]. The model did not predict the production of any hydration products.

The physical tests carried out during this investigation exhibited varying degrees of agreement with the thermodynamic modelling. Although the phases present agree with the thermodynamic software predictions, the quantities present were somewhat different. This is explained by the fact that the software calculated the minerals present at equilibrium, as if the olivine had completely dissociated and reacted with the lime. However, it can be seen from both the XRD and Raman data that there remains a significant quantity of unreacted olivine still present in the mortar. As the quantity of olivine that dissociated was small, the amount of magnesium carbonates (dolomite, magnesite) produced was correspondingly small, which left much of the portlandite free to carbonate and accounts for the large proportion of calcite detected.

The phases identified by Raman spectroscopy aligned more closely with those predicted by the thermodynamic software compared to phases identified from XRD studies. This may be due to the nature of the sample material under test. The XRD samples comprised small amounts of material (20–80 mg) which was ground into a powder. This sample, therefore, contained material both from the surface and from the bulk, which would account for the presence of unreacted lime (portlandite) from deeper within the specimen. In contrast, Raman spectra were obtained from the surface of the material only where the reactions initiated, which is consistent with the absence of portlandite. The dissociation of the olivine and the carbonation of the lime binder may continue as more water is added to the system over time.

In the absence of any hydration products such as C-S-H, the increased strength of the mixes incorporating olivine can be attributed to the creation of increased amounts of carbonates as shown by the model and by the XRD and Raman spectroscopy analysis. The specimen comprising lime binder to fine olivine aggregate at a ratio of 1:3 (S2) was significantly greater than the specimen comprising the same materials at 1:2 ratio (S1). As specimen S2 contained a higher proportion of carbonate material, this provides further support to the inference that higher compressive strength is correlated with higher carbonate content.

The higher carbonate content of the mortars containing fine olivine sand is consistent with the crystal structures identified with the electron microscopy images. The well-formed scalenohedral crystal structures in specimens S1 and S2 indicate that during carbonation there was room for these crystals to grow unconstrained, which would also have provided generous pathways for CO_2 and water vapour diffusion. Specimens S0 and S3, in contrast, consist of tightly packed granular carbonate crystals, which would be less condusive to carbonation.

Whether all of the strength increases obtained with olivine aggregate can be attributed to increased carbonation is uncertain. It is possible that there are physical effects too. For example, the shape and surface morphology of small particle olivine is substantially different from that of the large particle olivine and the normal silica sand. The small olivine particles are very angular in shape and have rough surfaces, both of which are conducive to higher strength due to bonding between the aggregate and the lime paste. The lower strength of the mix containing coarse olivine sand must be attributed to the larger particles of olivine possessing lower strength than the fine olivine sand, which could be due to the more intense milling that must be carried out to obtain the smaller particles.

6. Conclusions

This research has, for the first time, investigated the effect of using olivine as an aggregate in lime mortars. The following conclusions may be drawn:

- Olivine sand will dissociate in a lime mortar mix to facilitate the formation of magnesium carbonates, increasing CO_2 absorption.
- The total carbonate content of aged mortars containing fine olivine sand aggregate is greater than that found in a conventional silica sand lime mortar of similar mix proportions that contains a purely silica sand aggregate.
- The increased formation of carbonates when olivine aggregates are used promotes a greater compressive strength of 2.5 MPa compared to conventional mortar mixes 0.5 MPa incorporating quartz sand aggregate.
- The particle size of the olivine sand and corresponding surface area, is of significance in promoting the necessary dissociation and carbonation reactions.

Conflict of interest

None.

References

[1] IPCC, 2014, Climate Change 2014 Synthesis Report, Geneva, 2014
[2] L Papayianni, M. Papachristoforou, V. Patsiou, V. Petrohilos, Development of fire resistant shotcrete with olivine aggregates. IABSE Symposium, May 6 2013 Rotterdam 2013: Assessment, Upgrading and Refurbishment of Infrastructures (2013) 246–252.
[3] G.L. Fesce, I.W. Fletcher, R. Grant, M. Molinari, S.C. Parker, R.J. Ball, Carbonation of hydrous materials at the molecular level: a time of flight-secondary ion mass spectrometry, raman and density functional theory study, Cryst. Growth Des. 17 (3) (2017) 1036–1044.
[4] K.S. Lackner, C.H. Wendt, D.P. Butt, E.L. Joyce, D.H. Sharp, Carbon dioxide disposal in carbonate materials, Energy 20 (11) (1995) 1153–1170.
[5] S.J. Lackner, A guide to CO_2 sequestration, Science 300 (2003) 1677.
[6] M.H. Fasihnikoutlab, P. Westgate, B.B.K. Huat, A. Asadi, R.J. Ball, H. Nahazanan, P. Singh, New insights into potential capacity of olivine in ground improvement, Electron. J. Geotech. Eng. 20 (2015) (2015) 2137–2148.
[7] M.H. Fasihnikoutlab, A. Asadi, B.B.K. Huat, P. Westgate, R.J. Ball, S. Pouralthar, Laboratory-scale model of carbon dioxide deposition for soil stabilisation, J. Rock Mech. Geotech. Eng. 8 (2016) (2016) 178–186.
[8] J. Olsson, N. Bovet, E. Makovicky, K. Bechgaard, Z. Balogh, S.L.S. Stipp, Olivine reactivity with CO_2 and H_2O on a microscale: implications for carbon sequestration, Geochim. Cosmochim. Acta 77 (2012) (2011) 86–97.

[9] A.H. Tove, Dissolution and Carbonation of Mechanically Activated Olivine Thesis (PhD.), Norwegian University of Science and Technology, Trondheim, 2010.
[10] A. Demirbas, Carbon dioxide disposable via carbonation, Energy Sour. Part A: Recovery Util. Environ. Effects 29 (1) (2006) 59–65.
[11] K. Tkacova, Mechanical Activation of Minerals, Elsever Science Publishers, Amsterdam, 1989.
[12] M.H. Fasihnikoutalab, A. Asadi, C. Unuler, B.K. Huat, R.J. Ball, S. Pouralkbar, Utilization of alkali-activated olivine in soil stabilization and the effect of carbonation on unconfined compressive strength and microstructure, ASCE J. Mater. Civ. Eng. 29 (6) (2017) 06017002.
[13] M. Fasihnikoutalab, S. Pouralkbar, R. Ball, B. Huat, The Effect of olivine content and curing time on the strength of treated soil in presence of potassium hydroxide, Int. J. Geosynthetics Ground Eng. 3 (12) (2017).
[14] M. Fasihnikoutalab, A. Asadi, B. Huat, P. Westgate, R. Ball, S. Pouralkbar, Laboratory-scale model of carbon dioxide deposition for soil stabilisation, J. Rock Mech. Geotech. Eng. 8 (2) (2016) 1078–1186.
[15] M. Fasihnikoutalab, P. Westgate, B.B.K. Huat, A. Asadi, R. Ball, H. Nahazanan, P. Singh, New insights into potential capacity of olivine in ground improvement, Electron. J. Geotech. Eng. 20 (8) (2015) 2137–2148.
[16] K. Elert, C. Rodriguez-Navarro, E.S. Pardo, E. Hansen, O. Cazalla, Lime mortars for the conservation of historic buildings, Stud. Conserv. 47 (1) (2002) 62–75.
[17] T. Yates, A. Ferguson, The Use of Lime-Based Mortars in New Build, NHBC Foundation, Amersham, 2008.
[18] A. Arizzi, G. Cultrone, The difference in behaviour between calcitic and dolomitic lime mortars set under dry conditions: the relationship between textural and physical-mechanical properties, Cem. Concr. Res. 42 (2012) (2012) 818–826.
[19] J. Grant, G.L. Pesce, R.J. Ball, M. Molinari, S.C. Parker, An experimental and computational study to resolve the composition of dolomitic lime, RSC Adv. 6 (19) (2016) 16066–16072.
[20] I. Brocklebank (Ed.), Building Limes in Conservation, Donhead Publishing Ltd, Shaftsbury, 2012, p. 10.
[21] GEMS, Gibbs Energy Minimization Software for Geochemical Modelling, Paul Scherer Institut., Villingen, 2018. http://gems.web.psi.ch [Accessed 7 February 2018].
[22] D.A. Kulik, T. Wagner, S.V. Dmytrieva, G. Kosakowski, F.F. Hingerl, K.V. Chudnenko, U. Berner, GEM-Selektor geochemical modelling package: revised algorithm and GEMS3K numerical kernel for coupled simulation codes, Comput. Geosci. 17 (2013) 1–24.
[23] T. Wagner, D.A. Kulik, F.F. Hingerl, S.V. Dmytrieva, GEM-Selektor geochemical modelling package: TSolMod library and data interface for multicomponent phase models, Can. Mineral. 50 (2012) 1173–1195.
[24] J.M. Valverde, A. Perejon, S. Medina, L.A. Perez-Maqueda, Thermal decomposition of dolomite under CO2: insights from TGA and in situ XRD analysis, Phys. Chem. Chem. P 2015 (17) (2015) 30166.
[25] S.W. Wulandari, P.M. Adinata, A. Fajrin, Thermal decomposition of dolomite under CO_2–air atmosphere, AIP Conference Proceedings 1805, American Institute of Physics, 2017.